Dissertation

Labeled Multi-Bernoulli Filtering Methods for Efficient Multi-object Tracking

Ausgeführt zum Zwecke der Erlangung des akademischen Grades eines
Doktors der technischen Wissenschaften

unter der Leitung von
Ao. Univ.-Prof. Dr. Franz Hlawatsch
Institute of Telecommunications

von
Dipl.-Ing. Thomas Kropfreiter
[redacted]

Wien, im März 2022

Abstract

Multi-object tracking aims to estimate the time-dependent number and states of multiple objects from measurements provided by one or more sensors. Potential applications include surveillance, autonomous driving, indoor localization, robotics, and biomedical analytics. All these applications require accurate object state estimates computed by efficient and reliable multi-object tracking algorithms. The framework of labeled random finite sets (RFSs) provides a versatile mathematical tool for modeling the multi-object tracking problem and moreover enables track continuity, i.e., the consistent identification of objects over consecutive time steps. However, the practical application of many RFS-based multi-object tracking algorithms is limited by their high computational complexity. Therefore, to leverage the potential of labeled RFSs, there is a need for efficient yet accurate approximations and implementations.

This thesis presents three contributions to the field of RFS-based multi-object tracking. All of them involve a type of high-performing RFS-based multi-object tracking methods generically known as the labeled multi-Bernoulli (LMB) filter as well as the belief propagation (BP) algorithm for iterative Bayesian inference. First, we propose a new fast LMB filter that uses BP for probabilistic data association. The complexity of this filter is significantly smaller than that of existing LMB filters and scales only linearly in the number of Bernoulli components and the number of measurements. This scaling behavior is due to a new fast BP-based algorithm for probabilistic data association. The use of this algorithm within the LMB filter is enabled by a new derivation of the original LMB filter. In this derivation, the generalized LMB posterior probability density function (PDF) is reformulated in terms of a joint object-measurement association distribution, which is approximated by the product of its marginals. The new LMB filter is then obtained by an approximate marginalization using the proposed BP-based algorithm. Contrary to traditional LMB filter implementations based on a ranked assignment algorithm or a Gibbs sampler, our BP-based LMB filter does not prune any association information in the update step, which results in an improved tracking performance.

As a second contribution, we propose an efficient RFS-based algorithm for multi-object tracking, referred to as LMB/P filter, that exhibits an even better performance in challenging scenarios, e.g., in scenarios with a high number of objects and/or clutter measurements. The LMB/P filter is based on a new system model for tuples of labeled/unlabeled state RFSs as well as a description of the multi-object state by the tuple of an LMB RFS, i.e., a labeled RFS, and a Poisson RFS, i.e., an unlabeled RFS. The LMB/P filter tracks objects that are unlikely to exist within the less computationally demanding Poisson part and objects that are likely to exist within the more accurate but also more computationally demanding LMB part. Here, only if a quantity characterizing the plausibility of object existence is above a threshold, a new labeled Bernoulli component is created and the object is transferred from the Poisson part to the LMB part. Conversely, a labeled Bernoulli component is transferred back to the Poisson part if the corresponding existence probability falls below another threshold. The fact that unlikely objects are tracked within the less computationally demanding Poisson part combined with additional complexity-reducing approximations and modifications results in a low computational complexity of the LMB/P filter, especially in challenging scenarios.

Finally, we propose a distributed multi-sensor LMB filter that uses the generalized covariance intersection (GCI) technique to fuse the local LMB posterior PDFs. A critical aspect of such filters is to correctly associate labeled Bernoulli components describing the same object at different sensors. Instead of using a hard association of labeled Bernoulli components, which is done in current state-of-the-art distributed GCI-based LMB filters, we propose a soft (probabilistic) label association scheme. To develop this scheme, we first derive a formulation of the fused multi-object PDF that involves a label association distribution. We then show that approximating the label association distribution by the product of its marginals results in a fused multi-object PDF that is again of LMB form. We finally obtain an efficient implementation of the distributed LMB filter by using a BP-based algorithm for fast approximate marginalization and a Gaussian approximation of the spatial PDFs.

Abbreviations

2D Two-dimensional

BP Belief Propagation

CB-MeMBer Cardinality Balanced Multi-target Multi-Bernoulli

CPHD Cardinalized Probability Hypothesis Density

FISST Finite Set Statistics

GCI Generalized Covariance Intersection

GLMB Generalized Labeled Multi-Bernoulli

IPDA Integrated Probabilistic Data Association

JIPDA Joint Integrated Probabilistic Data Association

JPDA Joint Probabilistic Data Association

LMB Labeled Multi-Bernoulli

LMB/P Labeled Multi-Bernoulli/Poisson

LMBM Labeled Multi-Bernoulli Mixture

MAP Maximum A Posteriori

MeMBer Multi-target Multi-Bernoulli

MB Multi-Bernoulli

MBM Multi-Bernoulli Mixture

MHT Multiple Hypothesis Tracking

MMSE Minimum Mean Square Error

MOMB/P Measurement-oriented Marginal Multi-Bernoulli/Poisson

MOSPA Mean Optimal Subpattern Assignment

OSPA Optimal Subpattern Assignment

PDA Probabilistic Data Association

PDF Probability Density Function

PGFL Probability Generating Functional

PHD Probability Hypothesis Density

PMBM Poisson Multi-Bernoulli Mixture

PMF Probability Mass Function

PS Parameter Setting

RFS Random Finite Set

ROI Region of Interest

SC Simulation Scenario

TOMB/P Track-oriented Marginal Multi-Bernoulli/Poisson

TS Tracking Scenario

Contents

Chapter 1

Introduction

Multi-object tracking refers to the problem of estimating the time-dependent number and states of multiple objects from measurements provided by one or several sensors. The problem is complicated by randomly disturbed object motion, objects coming in close proximity, noisy and cluttered sensor measurements, low signal-to-noise ratios, and a data association uncertainty. Here, data association uncertainty refers to the problem that it is a priori unknown which measurement was generated by which object, or by clutter. All these issues make multi-object tracking a challenging task. Multi-object tracking has a long history, and first solutions [Kalman, 1960] can be traced back to the 1960s for aerospace surveillance applications [Vo et al., 2015]. Since then, the range of potential applications has expanded to a variety of areas, including further surveillance applications [Fortmann et al., 1983, Rasmussen and Hager, 2001, Lu et al., 2018, Gaglione et al., 2020], autonomous driving [Urmson et al., 2008, Patole et al., 2017, Levinson et al., 2011], indoor localization [Witrisal et al., 2016, Bartoletti et al., 2014, Shen and Molisch, 2014], robotics [Bullo et al., 2009, Hu et al., 2012, Ferri et al., 2017], and biomedical analytics [Adrian, 1991, Genovesio et al., 2006, Maška et al., 2014].

1.1 Multi-object Tracking

The multi-object tracking problem can be modeled in the framework of sequential Bayesian estimation. More specifically, the random object states are estimated recursively over time, relying on a statistical modeling of the object evolution process and the sensor measurement process. The state of an object usually includes its position, velocity, and possibly further quantities such as its extent. A sensor can be any measuring device that senses its environment such as RADAR, SONAR, or LIDAR sensors, infrared sensors, and cameras. In this thesis, we only consider methods that use point measurements. Point measurements are obtained by pre-processing the raw sensor data in order to reduce data flow and computational complexity. For linear/Gaussian system models and a Gaussian prior, the multi-object tracking problem without data association uncertainty can be solved in closed form. The resulting tracking algorithm is the well-known Kalman filter [Kalman, 1960, Anderson and Moore, 1979, Ho and Lee, 1964]. For nonlinear/non-Gaussian system models, computationally feasible approximations to the optimal Bayesian state estimator comprise the extended Kalman filter [Anderson and Moore, 1979], the unscented Kalman filter [Julier and Uhlmann, 2004], and the particle filter [Arulampalam et al., 2002].

The aforementioned algorithms are limited to problems with a known number of objects and without data association uncertainty, i.e., the correct association between objects and measurements is known. For the more realistic case with data association uncertainty, the state-of-the-art tracking approaches can be divided into "vector-type" and "set-type" algorithms.

1.1.1 Vector-type Algorithms

Vector-type filters model the multi-object state and measurements by random vectors. They are able to implicitly maintain track continuity (i.e., consistent identification of objects over consecutive time steps) by associating the object state estimates at the current time with the object state estimates at previous times. Vector-type algorithms can be further classified into methods based on the frameworks of probabilistic data association (PDA) and multiple hypothesis tracking (MHT).

PDA methods aim to compute the minimum mean square error (MMSE) estimate for each single object state at each single time step. More precisely, the PDA filter [Bar-Shalom et al., 2011, Sec. 3.4] models the data association by a nuisance variable that is "marginalized out." Whereas the PDA filter is able to track a single object under data association uncertainty, the joint PDA (JPDA) filter [Bar-Shalom, 1974] extends this principle to the tracking of multiple objects. The integrated PDA (IPDA) filter [Musicki et al., 1994] and the joint IPDA (JIDPA) filter [Musicki and Evans, 2004] extend the PDA filter and the JPDA filter, respectively, by modeling object existence as a Bernoulli random variable. All four filters model the kinematic object state as a Gaussian random variable, thus restricting them to linear/Gaussian system models. However, extensions to nonlinear/non-Gaussian system models are possible based on the principles of, e.g., the extended Kalman filter or the unscented Kalman filter, still assuming a Gaussian prior probability density function (PDF). Extensions based on particle representations of spatial PDFs, which do not require a Gaussian prior, were proposed in [Vermaak et al., 2005]. To lower the computational complexity of the JPDA and JIPDA filters, an efficient approximate belief propagation (BP) based algorithm for marginalization was proposed in [Williams and Lau, 2014]. Although the JPDA and JIPDA filters were proposed for a known number of objects, heuristic extensions allow them to be applied also when the number of objects is unknown.

MHT methods are based on the maximum a posteriori (MAP) estimator. More precisely, first the MAP estimator is used to find the most likely object-measurement association for a time window of a certain length [Reid, 1979]. Given this association, the MAP estimates of the object states are then calculated. Similar to traditional PDA methods, the kinematic object states are modeled by Gaussian PDFs. MHT can be formulated in two different forms, namely, hypothesis-oriented MHT [Reid, 1979, Cox and Hingorani, 1996] and track-oriented MHT [Kurien, 1990, Blackman, 2004, Morefield, 1977, Pattipati et al., 1992]. The original hypothesis-oriented MHT methods propagate a predefined number of the most likely object-measurement hypotheses. Each of these hypotheses is parametrized by a weight representing its plausibility and a sequence of object state PDFs. An efficient implementation is based on the m-best assignment algorithm for selecting the m-best hypotheses [Cox and Hingorani, 1996]. The more efficient track-oriented MHT methods represent object-measurement associations in the form of a series of tree structures [Kurien, 1990]. Each tree represents the possible measurement association history of a single object. The most likely hypothesis is then found by choosing a leaf node for each single-object tree in such a way that no measurement is used by more than one object. An enumeration of hypotheses is avoided through combinatorial optimization techniques [Pattipati et al., 1992].

1.1.2 Set-type Algorithms

A different approach underlies set-type algorithms. Here, the multi-object state and the measurements are modeled as random finite sets (RFSs) [Mahler, 2007b]. (An introduction to RFSs will be provided in Chapter 2.) The probability hypothesis density (PHD) filter [Mahler, 2003, Vo et al., 2005, Vo and Ma, 2006] approximates the posterior PDF by a Poisson PDF such that the PHD corresponding to the Poisson PDF is matched to the PHD corresponding to the true posterior PDF. This Poisson approximation leads to a low computational complexity of the PHD filter but results in only moderate tracking performance in more challenging tracking scenarios. An improved tracking performance is exhibited by the cardinalized PHD (CPHD) filter [Mahler, 2007a]. There, the posterior PDF is approximated by an independent and identically distributed (IID) cluster PDF such that the PHD and the cardinality distribution corresponding to the IID cluster PDF match the PHD and cardinality distribution corresponding to the true posterior PDF. The improved tracking performance of the CPHD filter comes at the expense of a higher computational complexity. Both the PHD filter and the CPHD filter do not maintain track continuity. The PHD filter will be reviewed in Section 3.3.

Another type of RFS filters is based on the multi-Bernoulli (MB) RFS. While the (single-) Bernoulli filter [Ristic et al., 2013] is only capable of tracking a single object, the so-called multi-target MB (MeMBer) filter [Mahler, 2007b, Sec. 17] is an extension to the tracking of multiple objects. In the MeMBer filter, the posterior PDF is approximated by an MB PDF by applying approximations to the posterior probability generating functional (PGFL), which expresses the same information as the posterior PDF but in a different form. The inherent cardinality bias caused by the applied approximations results in a rather poor tracking performance. However, an improved version, referred to as the cardinality-balanced MeMBer (CB-MeMBer) filter [Vo et al., 2009], compensates the cardinality bias and exhibits an improved tracking performance. Another instance of this class of filters is the Poisson Multi-Bernoulli Mixture (PMBM) filter [Williams, 2015], which models the posterior PDF as a combination of a Poisson PDF and an MB mixture (MBM) PDF. If the Poisson part is neglected, the PMBM filter simplifies to the MBM filter [Xia et al., 2019]. The Poisson part in the PMBM filter can improve the detection of newly appearing objects at the cost of a higher computational complexity. Low-complexity approximations of the PMBM filter include the track-oriented marginal MB-Poisson (TOMB/P) filter [Williams, 2015, Kropfreiter et al., 2016] and the measurement-oriented marginal MB-Poisson (MOMB/P) filter [Williams, 2015], which are based on the approximation of an inherent object-measurement association distribution by the product of its marginals. A modification proposed in [Williams, 2012] extends the conventional TOMB/P filter by *recycling*, which performs a transfer of Bernoulli components with a low existence probability to the Poisson part. All these set-based algorithms can be implemented using Gaussian PDFs, Gaussian mixture PDFs, or particle representations, thus making them suitable for both linear/Gaussian and nonlinear/non-Gaussian system models. With the exception of the (CB-)MeMBer filter and the MOMB/P filter, all algorithms mentioned in this paragraph can enable track continuity through the use of simple heuristic post-processing techniques.

A further, more recent type of set-based algorithms relies on labeled RFSs [Mahler, 2014, Vo and Vo, 2013, Vo et al., 2014]. The label explicitly models the identity of an object, thus enabling track continuity without any heuristic post-processing. Filters modeling the multi-object state by a labeled RFS are the labeled MB (LMB) filter [Reuter et al., 2014, Reuter et al., 2017] and the generalized LMB (GLMB) filter [Vo and Vo, 2013, Vo et al., 2014, Vo et al., 2017]. The GLMB filter is an exact solution to the multi-object tracking problem, while the LMB filter is an approximation with reduced computational complexity. Efficient implementations of the GLMB filter and the LMB filter are based on the Gibbs sampler [Vo et al., 2017, Reuter et al., 2017].

An even more recent approach to multi-object tracking models the entire sequences of multi-object states as an RFS of trajectories [García-Fernández et al., 2020b, García-Fernández and Svensson, 2019, Xia et al., 2019, Granström et al., 2018]. Each trajectory is characterized by the initial time, the trajectory length, and a sequence of object states. Algorithms based on this approach include the trajectory PHD and CPHD filters [García-Fernández and Svensson, 2019], the trajectory MBM filter [García-Fernández et al., 2020b], and the trajectory PMBM filter [Granström et al., 2018, Xia et al., 2019].

1.2 Outline and Contribution

In this thesis, we propose efficient LMB filtering algorithms for multi-object tracking. After a review of unlabeled and labeled RFSs in Chapter 2 and Bayesian RFS-based multi-object tracking in Chapter 3, we present in Chapter 4 an efficient LMB filter using BP for probabilistic data association. In Chapter 5, we augment the RFS description of the multi-object state used in Chapter 4 by a Poisson RFS, which yields a new description of the multi-object state as a combination of a labeled RFS, i.e., an LMB RFS, and an unlabeled RFS, i.e., a Poisson RFS. Using this description, we develop a multi-object tracking algorithm that, especially in challenging scenarios, has an even lower computational complexity than the LMB filter proposed in Chapter 4. In Chapter 6, we propose a distributed LMB filter for multi-sensor multi-object tracking based on the new concept of probabilistic label association. In the following, we provide a more detailed outline of the individual chapters of the thesis and a summary of the main contributions.

- In **Chapter 2**, we review basic concepts of unlabeled and labeled RFSs [Mahler, 2007b, Mahler, 2014], which form the foundation of the following chapters. More precisely, we introduce the multi-object PDF, the PGFL, and the PHD as descriptions of the statistics of an unlabeled RFS [Mahler, 2007b]. We furthermore present the Poisson, Bernoulli, and MB RFSs as important types of unlabeled RFSs. Next, we introduce labeled RFSs [Vo and Vo, 2013, Vo et al., 2014, Mahler, 2014] and the multi-object PDF, the PGFL, and the PHD for the labeled RFS case. Then, we introduce the LMB, labeled MBM RFS, and GLMB RFSs as important types of labeled RFSs. Throughout the chapter, useful conversion relationships between multi-object PDF, PGFL, and PHD are presented for both unlabeled and labeled RFSs.

- In **Chapter 3**, we review the Bayes multi-object filter for unlabeled and labeled RFSs [Mahler, 2007b, Mahler, 2014]. The Bayes multi-object filter recursively calculates the posterior multi-object PDF and consists of a prediction step and an update step. We furthermore present two common system models, each consisting of a state-transition model and a measurement model, that form the basis of many unlabeled and labeled RFS-based multi-object tracking algorithms. Three important RFS-based multi-object tracking algorithms, namely, the PHD filter, the TOMB/P filter, and the LMB filter, are finally discussed in detail.

- In **Chapter 4**, we propose a new fast LMB filter whose complexity scales only linearly in the number of Bernoulli components and the number of measurements. In addition to its low complexity, the proposed fast LMB filter can achieve improved tracking accuracy compared to other state-of-the-art tracking filters. The fast LMB filter is derived by reformulating the GLMB posterior PDF of the original LMB filter in terms of a joint object-measurement association distribution and approximating that distribution by the product of its marginals. A fast approximate marginalization is then achieved by an adaptation of a BP-based algorithm for probabilistic data association [Williams and Lau, 2014]. The proposed fast LMB filter also uses a novel efficient model for generating new Bernoulli components. After presenting a complexity analysis, we conclude the chapter with a simulation experiment comparing the results obtained by the proposed LMB filter with those obtained by the Gibbs sampler-based LMB filter [Reuter et al., 2017] and the BP-based implementation of the TOMB/P filter [Williams, 2015]. The results indicate that the proposed LMB filter significantly outperforms the Gibbs sampler-based LMB filter and performs similarly to the TOMB/P filter, but with a much lower computational complexity. Indeed, unlike our fast BP-based LMB filter, the Gibbs sampler-based LMB filter ignores valuable association information by pruning GLMB components, which results in a reduced tracking accuracy in more challenging tracking scenarios.

- In **Chapter 5**, we propose an RFS-based multi-object tracking method that improves on the fast LMB filter of Chapter 4 in challenging scenarios with, e.g., a high number of objects and/or clutter measurements. The proposed filter, termed LMB/P filter, combines the strengths of the LMB filter and the PHD filter in that it achieves track continuity and good tracking performance while requiring a relatively low computational complexity compared to other RFS-based tracking algorithms with track continuity. In the LMB/P filter, the multi-object state is modeled as a combination of an LMB RFS, i.e., a labeled RFS, and a Poisson RFS, i.e., an unlabeled RFS. We propose a new system model for labeled/unlabeled multi-object state RFSs and derive the prediction step and the exact update step based on this system model. An excellent accuracy-complexity compromise is achieved by a number of approximations and modifications of the exact update step, including the partitioning of label and measurement sets, the pruning of implausible object-measurement associations, and the transfer of certain unlabeled objects to labeled objects and vice versa. As a consequence of these approximations, objects that are likely to exist are tracked by the LMB RFS and objects that are unlikely to exist by the Poisson RFS. More specifically, only if a quantity characterizing the plausibility of object existence is above a predefined threshold, a new labeled Bernoulli component is generated based on the Poisson RFS, and the corresponding object is tracked within the more accurate but less efficient LMB part. Conversely, a labeled Bernoulli component is transferred to the Poisson RFS if its existence probability falls below another threshold. The fact that unlikely objects are tracked within the less computationally demanding Poisson part is the main reason for the low computational complexity of the LMB/P filter, especially in challenging scenarios with many objects and/or high clutter rates. We present simulation results demonstrating the advantages of the proposed LMB/P filter relative to the fast LMB filter of Chapter 4, the Gibbs sampler-based LMB filter [Reuter et al., 2017], and the BP-based TOMB/P filter using recycling [Williams, 2012]. Similar to the fast LMB filter of Chapter 4, our implementation of the proposed LMB/P filter uses BP to compute approximate marginal association probabilities and does not perform any pruning of GLMB components. This fact results in an improved tracking performance compared to the Gibbs sampler-based LMB filter. A comparison with the fast LMB filter and the BP-based TOMB/P filter with recycling shows that all three filters achieve a similar tracking accuracy while the proposed LMB/P filter has a significantly lower computational complexity than the fast LMB filter and the BP-based TOMB/P filter. The lower computational complexity is due to the fact that objects that are unlikely to exist are tracked within the less computationally demanding Poisson part of the filter. This is especially beneficial in scenarios with many objects and/or a high clutter rate, which tend to involve a high number of potentially existing objects. On the other hand, in scenarios with few objects and a low ore moderate clutter rate, the modeling of unlikely objects by a Poisson RFS may be unnecessarily complicated and result in an increased computational complexity. In such scenarios, the fast LMB filter proposed in Chapter 4 can achieve a lower computational complexity.

- In **Chapter 6**, we propose a distributed multi-sensor LMB filter based on the concepts of probabilistic label association, generalized covariance intersection (GCI), and BP. In distributed LMB filters based on GCI fusion, each sensor in a sensor network locally runs an LMB filter, e.g., the fast LMB filter of Chapter 4, and then fuses its local LMB posterior PDF with the local LMB posterior PDFs of its neighbors. A critical aspect of such filters is to correctly associate labeled Bernoulli components describing the same object at different sensors. Distributed LMB filters based on hard label association can result in a poor tracking performance, especially in more challenging tracking scenarios. We propose a GCI-based fusion method for LMB posterior PDFs that uses, for the first time, a soft (i.e., probabilistic) association of labeled Bernoulli components and thereby avoids a hard association. In the derivation of our distributed LMB filter, we first define a label association vector that describes the association of the labeled Bernoulli components of two sensors. Then, we perform GCI fusion of the two LMB posterior PDFs for a given association vector. However, since the correct label association is unknown, we model the label association vector by a random vector and derive the fused posterior PDF using soft label associations. It turns out that this PDF is no longer an LMB PDF but a GLMB PDF, which involves an inherent label association probability mass function (PMF). Therefore, we next approximate the fused GLMB posterior PDF by an LMB PDF, which is achieved by approximating the label association PMF by the product of its marginals. An efficient two-sensor distributed

LMB filter is finally obtained by incorporating a novel BP-based algorithm for fast approximate marginalization of the label association PMF and using a Gaussian approximation for the spatial PDFs involved in the LMB PDFs. Networkwide fusion with an arbitrary number of sensors is then obtained by iteratively applying the proposed pairwise fusion algorithm between each sensor and all its neighboring sensors. Our simulation results demonstrate that the proposed distributed LMB filter outperforms a state-of-the-art distributed LMB filter using hard label association [Li et al., 2019] and can perform close to the centralized multi-sensor LMB filter based on the iterated corrector approach [Reuter et al., 2014, Mahler, 2014].

- In **Chapter 7**, we summarize our contributions and suggest possible directions of future research.

Chapter 2

RFS Fundamentals

A random finite set (RFS), also known as a finite point process [Daley and Vere-Jones, 2002, Daley and Vere-Jones, 2007], is a mathematical object that captures the uncertainty of both the number of set elements and the specific values of the set elements. It was first considered by Mahler [Goodman et al., 1997, Mahler, 2007b] for modeling object states and measurements in a Bayesian multi-object tracking context. Mahler's "finite set statistics" (FISST) framework enables an elegant formulation of the Bayesian multi-object tracking problem and has facilitated the derivation of numerous novel multi-object tracking algorithms [Mahler, 2007b]. Initially, RFSs were considered as unlabeled quantities where all set elements are unordered and indistinguishable. As a consequence, multi-object tracking algorithms based on unlabeled RFSs are not able to model object identities and therefore do not support the estimation of entire object trajectories. This limitation was removed by Vo and Vo [Vo and Vo, 2013, Vo et al., 2014] with the introduction of labeled RFSs. Each element of a labeled RFS is augmented by a distinct identification variable referred to as a label. The concept of labeled RFSs led to a variety of new and powerful multi-object tracking algorithms that are capable of estimating entire object trajectories.[1]

The remainder of this chapter is structured as follows. Section 2.1 discusses some fundamentals of unlabeled RFSs, including the description of their statistics by means of the multi-object PDF, the PGFL, and the PHD. Furthermore, the Poisson, Bernoulli, and MB RFSs are presented. In Section 2.2, we discuss the concept of labeled RFSs and their statistical descriptions, and we finally present the LMB, LMBM, and GLMB RFSs. Throughout the chapter, we present important conversion relations between multi-object PDF, PGFL, and PHD for both unlabeled and labeled RFSs.

[1] An alternative approach to RFS-based multi-object tracking that also enables the estimation of object trajectories is based on RFSs of trajectories [García-Fernández et al., 2020b, Svensson and Morelande, 2014]. This approach tends to lead to a higher computational complexity and will not be considered in this work.

2.1 Unlabeled RFS

An unlabeled RFS X is a random variable whose realizations X are finite sets $\{\boldsymbol{x}^{(1)}, \ldots, \boldsymbol{x}^{(n)}\}$ of vectors $\boldsymbol{x}^{(i)} \in \mathbb{R}^{n_x}$. Both the vectors $\mathsf{x}^{(i)}$ and their number $\mathsf{n} = |\mathsf{X}|$ (the cardinality of X) are random quantities. Thus, X consists of a random number n of random vectors $\mathsf{x}^{(1)}, \ldots, \mathsf{x}^{(\mathsf{n})}$. Furthermore, the elements $\mathsf{x}^{(i)}$ of X are unordered, i.e., changing their order leaves the set X unchanged. While the conventional Riemann integral is not defined for sets, one can define the set integral of a real-valued set function $g(X)$ as [Mahler, 2007b]

$$\int g(X)\,\delta X \triangleq \sum_{n=0}^{\infty} \frac{1}{n!} \int_{\mathbb{R}^{n n_x}} g(\{\boldsymbol{x}^{(1)}, \ldots, \boldsymbol{x}^{(n)}\})\,\mathrm{d}\boldsymbol{x}^{(1)} \cdots \mathrm{d}\boldsymbol{x}^{(n)}. \tag{2.1}$$

Note that each term of the sum corresponds to one value of $n = |X|$.

2.1.1 Statistics of Unlabeled RFS

Adopting Mahler's FISST framework [Mahler, 2007b], the statistics of an RFS X can be described by its *multi-object PDF* $f_{\mathsf{X}}(X)$, briefly denoted $f(X)$. For any given realization $X = \{\boldsymbol{x}^{(1)}, \ldots, \boldsymbol{x}^{(n)}\}$ with cardinality $|X| = n$, the multi-object PDF is given by

$$f(X) = n!\,\rho(n)\,f_n(\boldsymbol{x}^{(1)}, \ldots, \boldsymbol{x}^{(n)}). \tag{2.2}$$

Here, $\rho(n) \triangleq \Pr\{|\mathsf{X}| = n\}$, $n \in \mathbb{N}_0$, is denoted as cardinality distribution and is the PMF of the random cardinality $\mathsf{n} = |\mathsf{X}|$, and $f_n(\boldsymbol{x}^{(1)}, \ldots, \boldsymbol{x}^{(n)})$ is a PDF of the random vectors $\mathsf{x}^{(1)}, \ldots, \mathsf{x}^{(n)}$ that is invariant to a permutation of the arguments $\boldsymbol{x}^{(i)}$. Note that $f(\emptyset) = \rho(0)$. The multi-object PDF (2.2) integrates to one using the set integral (2.1), i.e., $\int f(X)\,\delta X = 1$. Moreover, the cardinality distribution can be obtained from the multi-object PDF according to

$$\rho(n) = \frac{1}{n!} \int_{\mathbb{R}^{n n_x}} f(\{\boldsymbol{x}^{(1)}, \ldots, \boldsymbol{x}^{(n)}\})\,\mathrm{d}\boldsymbol{x}^{(1)} \cdots \mathrm{d}\boldsymbol{x}^{(n)}. \tag{2.3}$$

The multi-object PDF of the union of two statistically independent RFSs, X and Y, is given by the FISST convolution according to [Mahler, 2007b, Sec. 11.5.3]

$$f(X \cup Y) = \sum_{Y \subseteq X} f(Y)\,f(X \setminus Y). \tag{2.4}$$

In addition to the multi-object PDF (2.2), the statistics of an RFS X can also be described by the *probability generating functional* (PGFL) [Mahler, 2007b]. It is defined as the expectation of h^{X} with $h^{\mathsf{X}} \triangleq \prod_{\mathsf{x} \in \mathsf{X}} h(\mathsf{x})$ and where $h: \mathbb{R}^{n_x} \to [0, \infty)$ is any nonnegative vector function. Thus, we have

$$G_{\mathsf{X}}[h] \triangleq \mathrm{E}\{h^{\mathsf{X}}\} = \int h^X f(X)\,\delta X = \int \Big(\prod_{\boldsymbol{x} \in X} h(\boldsymbol{x}) \Big) f(X)\,\delta X. \tag{2.5}$$

Note that $\prod_{\boldsymbol{x}\in X} h(\boldsymbol{x}) = 1$ for $X = \emptyset$. It can be easily verified that $G_{\mathsf{X}}[1] = 1$ by setting $h(\boldsymbol{x}) = 1$ in (2.5). Let $\delta_{\boldsymbol{x}^{(i)}}(\boldsymbol{x}) \triangleq \delta(\boldsymbol{x} - \boldsymbol{x}^{(i)})$ denote the Dirac delta function at $\boldsymbol{x}^{(i)}$, and define the functional derivative of $G_{\mathsf{X}}[h]$ in direction $\delta_{\boldsymbol{x}^{(i)}}$ as $\frac{\delta}{\delta \boldsymbol{x}^{(i)}} G_{\mathsf{X}}[h] \triangleq \lim_{\epsilon\to 0} \frac{G_{\mathsf{X}}[h+\epsilon\delta_{\boldsymbol{x}^{(i)}}] - G_{\mathsf{X}}[h]}{\epsilon}$. Then, the multi-object PDF $f(X)$ can be recovered from $G_{\mathsf{X}}[h]$ with $X = \{\boldsymbol{x}^{(1)}, \dots, \boldsymbol{x}^{(n)}\}$ according to [Mahler, 2007b]

$$f(X) = \frac{\delta}{\delta X} G_{\mathsf{X}}[h]\bigg|_{h=0} \triangleq \frac{\delta^n}{\delta \boldsymbol{x}^{(1)} \cdots \delta \boldsymbol{x}^{(n)}} G_{\mathsf{X}}[h]\bigg|_{h=0}, \tag{2.6}$$

where in the last expression the functional derivative is applied iteratively.

One important property of PGFLS is the following [Mahler, 2007b]: The PGFL of the union $\mathsf{X} = \bigcup_{j=1}^{J} \mathsf{X}^{(j)}$ of statistically independent RFS $\mathsf{X}^{(j)}$, $j \in \{1, \dots, J\}$ is the product of the individual PGFLs $G_{\mathsf{X}^{(j)}}[h]$, i.e.,

$$G_{\mathsf{X}}[h] = \prod_{j=1}^{J} G_{\mathsf{X}^{(j)}}[h]. \tag{2.7}$$

Another important property of PGFLs is the product rule of functional derivatives [Mahler, 2007b]: For J PGFLs $G_{\mathsf{X}^{(j)}}[h]$ with $j \in \{1, \dots, J\}$ of statistically independent RFSs $\mathsf{X}^{(j)}$ and a finite set Y,

$$\frac{\delta}{\delta Y}\big(G_{\mathsf{X}^{(1)}}[h] \cdots G_{\mathsf{X}^{(J)}}[h]\big) = \sum_{W_1 \uplus \cdots \uplus W_J = Y} \frac{\delta G_{\mathsf{X}^{(1)}}[h]}{\delta W_1} \cdots \frac{\delta G_{\mathsf{X}^{(J)}}[h]}{\delta W_J}, \tag{2.8}$$

where the sum is over all configurations of disjoint subsets $W_1, \dots, W_J \subseteq Y$ such that $\bigcup_{j=1}^{J} W_j = Y$. Note that W_j can also comprise the empty set, i.e., $W_j = \emptyset$.

The ***probability hypothesis density*** (PHD) or intensity function $D_{\mathsf{X}}(\boldsymbol{x})\colon \mathbb{R}^{n_x} \to [0, \infty)$ of an RFS X is a probability function defined on $\mathbb{R}^{n_x}$ and can be considered as a first order moment of X. It is defined in terms of the multi-object PDF according to

$$D_{\mathsf{X}}(\boldsymbol{x}) \triangleq \mathrm{E}\{\delta_{\mathsf{X}}(\boldsymbol{x})\} = \int \delta_{X}(\boldsymbol{x})\, f(X)\, \delta X.$$

with

$$\delta_{X}(\boldsymbol{x}) \triangleq \begin{cases} 0, & X = \emptyset, \\ \sum_{i=1}^{n} \delta_{\boldsymbol{x}^{(i)}}(\boldsymbol{x}), & X = \{\boldsymbol{x}^{(1)}, \dots, \boldsymbol{x}^{(n)}\}, \end{cases}$$

where $\delta_{\boldsymbol{x}^{(i)}}(\boldsymbol{x}) = \delta(\boldsymbol{x} - \boldsymbol{x}^{(i)})$ is the Dirac delta function at $\boldsymbol{x}^{(i)}$ as defined previously. The PHD has the property that for any region $\mathcal{S} \subseteq \mathbb{R}^{n_x}$, the integral $\int_{\mathcal{S}} D_{\mathsf{X}}(\boldsymbol{x})\mathrm{d}\boldsymbol{x}$ yields the expected number of objects whose states are located in that region, i.e.,

$$\int_{\mathcal{S}} D_{\mathsf{X}}(\boldsymbol{x})\mathrm{d}\boldsymbol{x} = \mathrm{E}\{|\mathsf{X} \cap \mathcal{S}|\} = \int |X \cap \mathcal{S}|\, f(X)\, \delta X.$$

The PHD can be obtained from the corresponding PGFL by [Mahler, 2007b]

$$D_{\mathsf{X}}(\boldsymbol{x}) = \frac{\delta}{\delta \boldsymbol{x}} G_{\mathsf{X}}[h]\bigg|_{h=1}. \tag{2.9}$$

Next, we will review three types of unlabeled RFSs that are important for RFS-based multi-object tracking.

2.1.2 Poisson RFS

We start our review with the Poisson RFS. The cardinality $\mathsf{n} = |\mathsf{X}|$ of the Poisson RFS X is Poisson distributed with mean μ, i.e.,

$$\rho(n) = \frac{e^{-\mu}\mu^n}{n!},$$

for $n \in \mathbb{N}_0$, where the parameter μ is equal to both the mean and the variance of n. Given the cardinality $n = \mathsf{n}$, the elements $\mathbf{x}^{(1)}, \dots, \mathbf{x}^{(n)}$ of X are independent and identically distributed (iid) according to a spatial PDF $f(\boldsymbol{x})$, i.e., $f_n(\boldsymbol{x}^{(1)}, \dots, \boldsymbol{x}^{(n)}) = \prod_{i=1}^{n} f(\boldsymbol{x}^{(i)}) = \prod_{\boldsymbol{x} \in X} f(\boldsymbol{x})$. Inserting into (2.2) yields for the multi-object PDF

$$f(X) = e^{-\mu} \prod_{\boldsymbol{x} \in X} \mu f(\boldsymbol{x}) = e^{-\int \lambda(\boldsymbol{x}')\mathrm{d}\boldsymbol{x}'} \prod_{\boldsymbol{x} \in X} \lambda(\boldsymbol{x}), \tag{2.10}$$

where the product $\lambda(\boldsymbol{x}) = \mu f(\boldsymbol{x})$ is the PHD of the Poisson RFS X. The PGFL is obtained by inserting (2.10) in (2.5), which yields [Mahler, 2007b]

$$G_{\mathsf{X}}[h] = e^{\lambda[h-1]}, \tag{2.11}$$

with $\lambda[h-1] \triangleq \int (h(\boldsymbol{x}) - 1)\, \lambda(\boldsymbol{x})\, \mathrm{d}\boldsymbol{x}$. The Poisson RFS constitutes the basis of the PHD filter (cf. Section 3.3) and is also an essential component of the TOMB/P filter (cf. Section 3.4).

2.1.3 Bernoulli RFS

Next, we review the Bernoulli RFS. The Bernoulli RFS X is characterized by a probability of existence r and a spatial PDF $f(\boldsymbol{x})$. The Bernoulli RFS is empty with probability $1-r$ and contains one element $\mathbf{x} \sim f(\boldsymbol{x})$ with probability r. Hence, the multi-object PDF is given by

$$f(X) = \begin{cases} 1-r, & X = \emptyset, \\ r\, f(\boldsymbol{x}), & X = \{\boldsymbol{x}\}, \\ 0, & \text{otherwise.} \end{cases} \tag{2.12}$$

Inserting (2.12) in (2.5) yields for the PGFL

$$G_{\mathsf{X}}[h] = G^{\mathrm{Ber}}[h; r, f] \triangleq 1 - r + r\, f[h], \tag{2.13}$$

with $f[h] \triangleq \int h(\boldsymbol{x}) f(\boldsymbol{x}) \mathrm{d}\boldsymbol{x}$.

For later use, we note that a PGFL of the form $G_{\mathsf{X}}[h] = a + \int h(\boldsymbol{x}) b(\boldsymbol{x}) \mathrm{d}\boldsymbol{x}$ with $a \geq 0$, $b(\boldsymbol{x}) \geq 0$, and $\int b(\boldsymbol{x}) \mathrm{d}\boldsymbol{x} < \infty$ can be written as a weighted Bernoulli PGFL [Williams, 2015], i.e.,

$$G_{\mathsf{X}}[h] = a + \int h(\boldsymbol{x}) b(\boldsymbol{x}) \mathrm{d}\boldsymbol{x} = \beta\, G^{\mathrm{Ber}}[h; r, f], \tag{2.14}$$

with $\beta = a + \int b(\boldsymbol{x}) \mathrm{d}\boldsymbol{x}$, $r = \int b(\boldsymbol{x}) \mathrm{d}\boldsymbol{x} / \beta$, and $f(\boldsymbol{x}) = b(\boldsymbol{x}) / \int b(\boldsymbol{x}') \mathrm{d}\boldsymbol{x}'$. Furthermore, the linear combination of a certain number of Bernoulli pgfls is a Bernoulli pgfl, i.e., for weights γ_i satisfying $\gamma_i \geq 0$ and $\sum_i \gamma_i = 1$, we have

$$\sum_i \gamma_i G^{\mathrm{Ber}}\big[h; r^{(i)}, f^{(i)}\big] = G^{\mathrm{Ber}}[h; r, f], \tag{2.15}$$

where

$$r = \sum_i \gamma_i r^{(i)}, \quad f(\boldsymbol{x}) = \frac{1}{r} \sum_i \gamma_i r^{(i)} f^{(i)}(\boldsymbol{x}). \tag{2.16}$$

The Bernoulli RFS is the foundation of the Bernoulli filter [Ristic et al., 2013], which is a method for tracking a single object in the presence of sensor noise, missed detections, clutter and measurement origin uncertainty.

2.1.4 Multi-Bernoulli (MB) RFS

An MB RFS X is the union of a fixed number J of statistically independent Bernoulli RFSs $\mathsf{X}^{(j)}$, $j \in \{1, \ldots, J\}$ parametrized by J probabilities of existence $r^{(j)}$ and J spatial PDFs $f^{(j)}(\boldsymbol{x})$, i.e., by the parameter set $\big\{\big(r^{(j)}, f^{(j)}(\boldsymbol{x})\big)\big\}_{j \in \mathcal{J}}$ with $\mathcal{J} \triangleq \{1, \ldots, J\}$. Let $f^{(j)}(X)$ denote the multi-object PDF of Bernoulli component $\mathsf{X}^{(j)}$ (cf. (2.12)). The multi-object PDF $f(X)$ evaluated for a realization $X = \{\boldsymbol{x}^{(1)}, \ldots, \boldsymbol{x}^{(n)}\}$ of cardinality $n \leq J$ (note that $f(X) = 0$ for $n > J$) can be represented as follows. Consider a mapping α that maps an index $j \in \mathcal{J}$ to an index $\alpha(j) \in \{0, \ldots, n\}$. In our context, this means that n of the J Bernoulli component PDFs $f^{(j)}(X)$ are mapped to single-vector element sets $\{\boldsymbol{x}^{(\alpha(j))}\}$ and the other $J - n$ Bernoulli component PDFs are mapped to empty sets. It is assumed that for j_1, j_2 such that $\alpha(j_1), \alpha(j_2) \in \{1, \ldots, n\}$, $j_1 \neq j_2$ implies $\alpha(j_1) \neq \alpha(j_2)$, i.e., that two or more Bernoulli component PDFs are not mapped to the same set elements. Let $\mathcal{P}_{J,n}$ denote the set of all such mappings α (there are $|\mathcal{P}_{J,n}| = \frac{J!}{(J-n)!}$ of them). Then, the multi-object PDF evaluated for $X = \{\boldsymbol{x}^{(1)}, \ldots, \boldsymbol{x}^{(n)}\}$ is given by [Mahler, 2007b]

$$f(X) = f^{\mathrm{MB}}(X) = \sum_{\alpha \in \mathcal{P}_{J,n}} \prod_{j=1}^{J} f^{(j)}\big(X^{(\alpha(j))}\big), \tag{2.17}$$

where $n = |X|$ and $X^{(\alpha(j))}$ is given by $\emptyset$ for $\alpha(j) = 0$ and by $\{\boldsymbol{x}^{(\alpha(j))}\}$ for $\alpha(j) \in \{1, \ldots, n\}$. The multi-object PDF can also be represented according to (2.2) in terms of a cardinality distribution $\rho(n)$ and permutation-invariant vector PDFs $f_n(\boldsymbol{x}^{(1)}, \ldots, \boldsymbol{x}^{(n)})$. More precisely, by inserting (2.17) into (2.3), we get

$$\rho(n) = \frac{1}{n!} \sum_{\alpha \in \mathcal{P}_{J,n}} \prod_{j:\alpha(j)=0} \big(1 - r^{(j)}\big) \prod_{j':\alpha(j')>0} r^{(j')} \tag{2.18}$$

and

$$f_n(\boldsymbol{x}^{(1)}, \ldots, \boldsymbol{x}^{(n)}) = \sum_{\alpha \in \mathcal{P}_{J,n}} \prod_{j:\alpha(j)>0} f^{(j)}(\boldsymbol{x}^{(\alpha(j))}).$$

In the following, we illustrate the evaluation of (2.17) for $J = 3$ Bernoulli components and a realization X of cardinality $n = |X| = 2$, i.e., $X = \{\boldsymbol{x}^{(1)}, \boldsymbol{x}^{(2)}\}$. There are $|\mathcal{P}_{J,n}| = |\mathcal{P}_{3,2}| = 6$ different mappings $\alpha : \{1,2,3\} \to \{0,1,2\}$. Representing each mapping in the form $\alpha(1,2,3) = (\ell_1, \ell_2, \ell_3)$ with $\ell_j \in \{0,1,2\}$, the set of these mappings α is obtained as $\mathcal{P}_{3,2} = \{(1,2,0), (1,0,2), (0,1,2), (2,1,0), (0,2,1), (2,0,1)\}$. Hence, (2.17) combined with (2.12) gives

$$\begin{aligned} f(X) &= f(\{\boldsymbol{x}^{(1)}, \boldsymbol{x}^{(2)}\}) \\ &= r^{(1)} f^{(1)}(\boldsymbol{x}^{(1)}) r^{(2)} f^{(2)}(\boldsymbol{x}^{(2)}) \big(1 - r^{(3)}\big) + r^{(1)} f^{(1)}(\boldsymbol{x}^{(2)}) r^{(2)} f^{(2)}(\boldsymbol{x}^{(1)}) \big(1 - r^{(3)}\big) \\ &\quad + r^{(1)} f^{(1)}(\boldsymbol{x}^{(1)}) \big(1 - r^{(2)}\big) r^{(3)} f^{(3)}(\boldsymbol{x}^{(2)}) + r^{(1)} f^{(1)}(\boldsymbol{x}^{(2)}) \big(1 - r^{(2)}\big) r^{(3)} f^{(3)}(\boldsymbol{x}^{(1)}) \\ &\quad + \big(1 - r^{(1)}\big) r^{(2)} f^{(2)}(\boldsymbol{x}^{(2)}) r^{(3)} f^{(3)}(\boldsymbol{x}^{(1)}) + \big(1 - r^{(1)}\big) r^{(2)} f^{(2)}(\boldsymbol{x}^{(1)}) r^{(3)} f^{(3)}(\boldsymbol{x}^{(2)}). \end{aligned} \tag{2.19}$$

One can easily verify that this expression is invariant to a permutation of $\boldsymbol{x}^{(1)}, \boldsymbol{x}^{(2)}$. The cardinality distribution evaluated for $n = 2$ can be calculated by inserting (2.19) into (2.3) or by using (2.18), which yields in both cases

$$\rho(2) = r^{(1)} r^{(2)} \big(1 - r^{(3)}\big) + r^{(1)} \big(1 - r^{(2)}\big) r^{(3)} + \big(1 - r^{(1)}\big) r^{(2)} r^{(3)}.$$

Since an MB RFS is the union of J statistically independent Bernoulli RFSs, the MB PGFL is the product of the J corresponding Bernoulli PGFLs (cf. (2.7) and (2.13))

$$G_{\mathsf{X}}[h] = G_{\mathsf{X}}^{\mathrm{MB}}[h] = \prod_{j=1}^{J} G^{\mathrm{Ber}}[h; r^{(j)}, f^{(j)}], \tag{2.20}$$

where $f^{(j)}[h] \triangleq \int h(\boldsymbol{x}) f^{(j)}(\boldsymbol{x}) \mathrm{d}\boldsymbol{x}$.

A comparison of the expression of the MB PGFL (2.20) with the expression of the MB multi-object PDF (2.17) (and also with example (2.19)) shows that the statistics of the MB RFS can be represented much simpler in PGFL form. Consequently, many MB-based multi-object tracking filters are derived by means of PGFLs instead of multi-object

PDFs. The MB RFS is the foundation for the multi-target MB (MeMBer) filter [Mahler, 2007b, Sec. 17] and of its improved version, the cardinality balanced MeMBer (CB-MeMBer) filter [Vo et al., 2009]. In addition, the MB RFS is also an essential component of the TOMB/P filter, along with the Poisson RFS (cf. Section 2.1.2). Since the MeMBer filter and the CB-MeMBer filter are of minor importance in this work, they will not be considered further. The TOMB/P filter will be reviewed in Section 3.4.

2.2 Labeled RFS

In an unlabeled RFS, as considered previously, the set elements are indistinguishable. Hence, the use of an unlabeled RFS in multi-object tracking application does not allow object identification without any further post-processing. This shortcoming is addressed by the introduction of a labeled RFS, where the label can be used to identify different objects. In the following, we discuss some basics of labeled RFSs and introduce important types of labeled RFS that are relevant to multi-object tracking and, in particular, to this thesis.

In a labeled RFS $\tilde{\mathsf{X}}$, each element is a tuple of the form $(\mathsf{x}, \mathsf{l}) \in \mathbb{R}^{n_x} \times \mathbb{L}$. Here, the label space $\mathbb{L}$ is a countable set; we define $\mathbb{L}_n$ as the set of all possible sequences of n labels from $\mathbb{L}$, i.e., $\mathbb{L}_n \triangleq \{(l^{(1)}, l^{(2)}, \ldots, l^{(n)}) : l^{(j)} \in \mathbb{L}\}$. Furthermore, we will use the mapping $\mathcal{L} : \mathbb{R}^{n_x} \times \mathbb{L} \to \mathbb{L}$ that returns the label of a given element, i.e., $\mathcal{L}(\boldsymbol{x}, l) = l$. By extension, $\mathcal{L}(\tilde{X})$ denotes the set of all labels of $\tilde{X}$. Analogously to the unlabeled RFS case, a set integral of a real-valued function $g(\tilde{X})$ is defined as [Vo and Vo, 2013, Mahler, 2014]

$$\int g(\tilde{X})\delta\tilde{X} \triangleq \sum_{n=0}^{\infty} \frac{1}{n!} \int_{\mathbb{R}^{nn_x}} \sum_{(l^{(1)},\ldots,l^{(n)}) \in \mathbb{L}_n} g\big(\{(\boldsymbol{x}^{(1)}, l^{(1)}), \ldots, (\boldsymbol{x}^{(n)}, l^{(n)})\}\big)\, \mathrm{d}\boldsymbol{x}^{(1)} \cdots \mathrm{d}\boldsymbol{x}^{(n)}. \tag{2.21}$$

The set integral for labeled RFSs extends the set integral for unlabeled RFSs (cf. (2.1)) by the sum over all possible label sequences $\mathbb{L}_n$ for each cardinality n.

2.2.1 Statistics of Labeled RFS

The statistics of a labeled RFS $\tilde{\mathsf{X}}$ can be described by its multi-object PDF $f(\tilde{X})$ [Vo and Vo, 2013, Vo et al., 2014, Mahler, 2014]. The multi-object PDF integrates to one, i.e., $\int f(\tilde{X})\delta\tilde{X} = 1$ using the set integral for labeled RFSs in (2.21). The unlabeled RFS X corresponding to $\tilde{\mathsf{X}}$ can be obtained by simply discarding the labels from $\tilde{\mathsf{X}}$. The corresponding multi-object PDF can be calculated by marginalizing out the labels, i.e., for $\tilde{\mathsf{X}} \to \mathsf{X}$, the multi-object PDF of X evaluated for the realization $X = \{\boldsymbol{x}^{(1)}, \ldots, \boldsymbol{x}^{(n)}\}$ is given by

$$f(\{\boldsymbol{x}^{(1)}, \ldots, \boldsymbol{x}^{(n)}\}) = \sum_{(l^{(1)},\ldots,l^{(n)}) \in \mathbb{L}_n} f\big(\{(\boldsymbol{x}^{(1)}, l^{(1)}), \ldots, (\boldsymbol{x}^{(n)}, l^{(n)})\}\big). \tag{2.22}$$

Here, the sum is over all all possible label sequences $\mathbb{L}_n$. Note that operation (2.22) is also part of the set integral defined in (2.21).

The PGFL of a labeled RFS $\tilde{\mathsf{X}}$ is defined similarly to the PGFL of an unlabeled RFS (cf. (2.5)) as the expectation of $\tilde{h}^{\tilde{\mathsf{X}}}$, where $\tilde{h}^{\tilde{\mathsf{X}}} \triangleq \prod_{(\mathsf{x},\mathsf{l})\in\tilde{\mathsf{X}}} \tilde{h}(\mathsf{x},\mathsf{l}) = \prod_{\mathsf{l}\in\mathbb{L}} \tilde{h}(\mathsf{x},\mathsf{l})$ with $\tilde{h}\colon \mathbb{R}^{n_x} \times \mathbb{L} \to [0,\infty)$. More precisely, we get [Mahler, 2014, p. 449]

$$G_{\tilde{\mathsf{X}}}[\tilde{h}]$$
$$\triangleq \mathrm{E}\{\tilde{h}^{\tilde{\mathsf{X}}}\} = \int \tilde{h}^{\tilde{X}} f(\tilde{X})\delta\tilde{X} = \int \Big(\prod_{(\boldsymbol{x},l)\in\tilde{X}} \tilde{h}(\boldsymbol{x},l)\Big) f(\tilde{X})\delta\tilde{X} = \int \Big(\prod_{l\in\mathbb{L}} \tilde{h}(\boldsymbol{x},l)\Big) f(\tilde{X})\delta\tilde{X}\,. \tag{2.23}$$

Similarly to the PGFL of an unlabeled RFS (cf. Section 2.1.1), it can be easily verified that $G_{\tilde{\mathsf{X}}}[1] = 1$ by setting $\tilde{h}(\boldsymbol{x},l) = 1$ in (2.23). As was shown in [Mahler, 2014], the unlabeled PGFL $G_{\mathsf{X}}[h]$ (with argument $h(\boldsymbol{x})$) corresponding to the unlabeled RFS X obtained from $\tilde{\mathsf{X}}$ by discarding the labels, can be obtained from the labeled PGFL $G_{\tilde{\mathsf{X}}}[\tilde{h}]$ (with argument $\tilde{h}(\boldsymbol{x},l)$) by setting $\tilde{h}(\boldsymbol{x},l) = h(\boldsymbol{x})$, i.e.,

$$G_{\mathsf{X}}[h] = G_{\tilde{\mathsf{X}}}[\tilde{h}]\big|_{\tilde{h}(\boldsymbol{x},l)=h(\boldsymbol{x})}\,.$$

The PGFL of a labeled RFS and an unlabeled RFS (cf. Section 2.1.1) will be used to derive the RFS-based multi-object tracking algorithm proposed in Chapter 5.

Families of labeled RFSs relevant to multi-object tracking include the labeled MB (LMB) RFS, the LMB mixture (LMBM) RFS, and the GLMB RFS, which will be reviewed in the following.

2.2.2 Labeled Multi-Bernoulli (LMB) RFS

An LMB RFS $\tilde{\mathsf{X}}$ is an MB RFS (cf. Section 2.1.4) where for any realization $\tilde{X}$ each single-vector set $\{\boldsymbol{x}\}$ corresponding to Bernoulli component $\mathsf{X}^{(j)}$ is augmented by a distinct label $l \in \mathbb{L}^*$. Adopting the labeling procedure of [Mahler, 2014], the same label l is assigned to each state realization $\boldsymbol{x}$ of a given Bernoulli RFS $\mathsf{X}^{(j)}$. Here, $\mathbb{L}^* \subseteq \mathbb{L}$ denotes the finite set of assigned labels. To simplify the notation, we index the Bernoulli RFSs directly by their labels l, i.e., they are denoted $\mathsf{X}^{(l)}$, $l \in \mathbb{L}^*$ with corresponding existence probabilities $r^{(l)}$ and spatial distributions $f^{(l)}(\boldsymbol{x})$ [Reuter et al., 2014]. The LMB RFS $\tilde{\mathsf{X}}$ is completely specified by the parameter set $\big\{\big(r^{(l)}, f^{(l)}(\boldsymbol{x})\big)\big\}_{l\in\mathbb{L}^*}$.

The multi-object PDF of the LMB RFS $\tilde{\mathsf{X}}$ evaluated for a realization $\tilde{X} = \big\{(\boldsymbol{x}^{(1)}, l^{(1)}), \ldots, (\boldsymbol{x}^{(n)}, l^{(n)})\big\}$ with cardinality $n \leq J$ and label set $\mathcal{L}(\tilde{X}) = \{l^{(1)} \ldots, l^{(n)}\}$ is given by [Reuter et al., 2014]

$$f(\tilde{X}) = f^{\mathrm{LMB}}(\tilde{X}) \triangleq \Delta(\tilde{X})\, w(\mathcal{L}(\tilde{X})) \prod_{(\boldsymbol{x},l)\in\tilde{X}} 1_{\mathbb{L}^*}(l)\, f^{(l)}(\boldsymbol{x})\,. \tag{2.24}$$

Here, $\Delta(\tilde{X})$ is referred to as "distinct label indicator" [Vo and Vo, 2013, Vo et al., 2014]; $\Delta(\tilde{X}) = 1$ if the labels of $\tilde{X}$ are distinct and $\Delta(\tilde{X}) = 0$ otherwise. Furthermore, the indicator function $1_{\mathbb{L}^*}(l) = 1$ if $l \in \mathbb{L}^*$ and $1_{\mathbb{L}^*}(l) = 0$ otherwise. These two conditions guarantee that only realizations $\tilde{X} = \{(\boldsymbol{x}^{(1)}, l^{(1)}), \dots, (\boldsymbol{x}^{(n)}, l^{(n)})\}$ that have distinct labels and are from the set $\mathbb{L}^*$ have a nonzero probability mass, i.e., $f(\tilde{X}) > 0$. In a multi-object tracking context, this ensures that two different objects cannot be modeled by the same label (same identity). Finally, the weights are given by

$$w(L) \triangleq \left(\prod_{l \in L} 1_{\mathbb{L}^*}(l) r^{(l)}\right) \prod_{l' \in \mathbb{L}^* \setminus L} \left(1 - r^{(l')}\right), \tag{2.25}$$

for any $L \subseteq \mathbb{L}$.

The PGFL of the LMB RFS can be found by inserting (2.24) into (2.23), which yields [Mahler, 2014]

$$G_{\tilde{\mathsf{X}}}[\tilde{h}] = G_{\mathbb{L}^*}^{\mathrm{LMB}}[\tilde{h}] \triangleq \prod_{l \in \mathbb{L}^*} G^{\mathrm{Ber}}[\tilde{h}; r^{(l)}, f^{(l)}] = 1 - r^{(l)} + r^{(l)} f^{(l)}[\tilde{h}], \tag{2.26}$$

with $f^{(l)}[\tilde{h}] = \int \tilde{h}(\boldsymbol{x}, l) f^{(l)}(\boldsymbol{x}) \mathrm{d}\boldsymbol{x}$. Note that the LMB PGFL extends the MB PGFL (cf. (2.20)) in the sense that every Bernoulli PGFL is associated with one specific label.

Furthermore, its PHD is given by [Mahler, 2014]

$$\lambda(\boldsymbol{x}, l) = r^{(l)} f^{(l)}(\boldsymbol{x}). \tag{2.27}$$

As an example, we consider $J = 3$ Bernoulli components (and, hence, label set $\mathbb{L}^* = \{l^{(1)}, l^{(2)}, l^{(3)}\}$) and a realization $\tilde{X}$ of cardinality $n = |\tilde{X}| = 2$, i.e., $\tilde{X} = \{(\boldsymbol{x}^{(1)}, l^{(1)}), (\boldsymbol{x}^{(2)}, l^{(2)})\}$. We obtain from (2.24) and (2.25)

$$f(\tilde{X}) = r^{(l^{(1)})} f^{(l^{(1)})}(\boldsymbol{x}^{(1)}) r^{(l^{(2)})} f^{(l^{(2)})}(\boldsymbol{x}^{(2)}) (1 - r^{(l^{(3)})}). \tag{2.28}$$

Note the difference to (2.19): The introduction of labels reduces the six terms in (2.19) to just one term in (2.28). This is a consequence of the fact that the objects are now consistently identified by a distinct label, while objects are indistinguishable in the unlabeled case.

2.2.3 Labeled Multi-Bernoulli Mixture (LMBM) RFS

The LMBM RFS generalizes the LMB RFS in the sense that the multi-object PDF evaluated for a realization $\tilde{X} = \{(\boldsymbol{x}^{(1)}, l^{(1)}), \dots, (\boldsymbol{x}^{(n)}, l^{(n)})\}$, with cardinality $n \leq |\mathbb{L}^*|$ and labels $\mathcal{L}(\tilde{X})$, is a mixture of a finite number of LMB PDFs with identical label sets $\mathbb{L}^* = \{l^{(1)}, \dots, l^{(J)}\}$, i.e.,

$$f(\tilde{X}) = \sum_{b \in \mathcal{B}} w_b f_b^{\mathrm{LMB}}(\tilde{X}). \tag{2.29}$$

Here, $\mathcal{B} \subset \mathbb{N}$, the w_b are positive normalized weights, i.e., $\sum_{b \in \mathcal{B}} w_b = 1$, $f_b^{\mathrm{LMB}}(\tilde{X})$ are LMB PDFs (cf. (2.24)) parametrized by sets of existence probabilities $r_b^{(l)}$ and spatial PDFs $f_b^{(l)}(\boldsymbol{x})$. For cardinality $n > |\mathbb{L}^*|$, $f(\tilde{X}) = 0$. Note that the LMBM RFS $\tilde{\mathsf{X}}$ is completely specified by $|\mathcal{B}|$ weights w_b, $|\mathcal{B}||\mathbb{L}^*|$ existence probabilities $r_b^{(l)}$, and $|\mathcal{B}||\mathbb{L}^*|$ spatial PDFs $f_b^{(l)}(\boldsymbol{x})$. Its PGFL can be found by inserting (2.29) in (2.23), which yields [Mahler, 2014]

$$G_{\tilde{\mathsf{X}}}[\tilde{h}] = \sum_{b \in \mathcal{B}} w_b \prod_{l \in \mathbb{L}^*} G^{\mathrm{Ber}}[\tilde{h}; r_b^{(l)}, f_b^{(l)}],$$

with $f_b^{(l)}[\tilde{h}] = \int \tilde{h}(\boldsymbol{x}, l) f_b^{(l)}(\boldsymbol{x}) \mathrm{d}\boldsymbol{x}$. Furthermore, its PHD is given by [Mahler, 2014]

$$\lambda(\boldsymbol{x}, l) = \sum_{b \in \mathcal{B}} w_b \, r_b^{(l)} f_b^{(l)}(\boldsymbol{x}).$$

2.2.4 Generalized Labeled Multi-Bernoulli (GLMB) RFS

The GLMB RFS is another extension of the LMB RFS. Its multi-object PDF evaluated for a realization $\tilde{X} = \{(\boldsymbol{x}^{(1)}, l^{(1)}), \ldots, (\boldsymbol{x}^{(n)}, l^{(n)})\}$, with cardinality $n \leq |\mathbb{L}^*|$ and labels $\mathcal{L}(\tilde{X})$, is a mixture of a finite number of products of n spatial PDFs, i.e.,

$$f(\tilde{X}) = \Delta(\tilde{X}) \sum_{b \in \mathcal{B}} \omega_b(\mathcal{L}(\tilde{X})) \prod_{(\boldsymbol{x}, l) \in \tilde{X}} f_b^{(l)}(\boldsymbol{x}), \tag{2.30}$$

with $\mathcal{B} \subset \mathbb{N}$ and some weights $\omega_b(\mathcal{L}(\tilde{X})$. For cardinality $n > |\mathbb{L}^*|$, $f(\tilde{X}) = 0$. Note that each spatial PDF $f_b^{(l)}(\boldsymbol{x})$ in (2.30) is associated with a labeled state variable $(\boldsymbol{x}, l) \in \tilde{X}$. In contrast to the LMBM RFS, the weights ω_b depend on the labels of $\tilde{X}$, i.e., on $\mathcal{L}(\tilde{X})$, and also on the remaining labels in the label set $\mathbb{L}^*$, i.e., on $\mathbb{L}^* \setminus \mathcal{L}(\tilde{X})$. The weights are normalized in that $\sum_{b \in \mathcal{B}} \sum_{L \in \mathcal{F}(\mathbb{L}^*)} \omega_b(L) = 1$, where $\mathcal{F}(\mathbb{L}^*)$ is the power set of $\mathbb{L}^*$, i.e., the set of all subsets of $\mathbb{L}^*$. The GLMB RFS $\tilde{\mathsf{X}}$ is completely specified by $|\mathcal{B}||\mathcal{F}(\mathbb{L}^*)|$ weights $\omega_b(L)$, and $|\mathcal{B}||\mathbb{L}^*|$ spatial PDFs $f_b^{(l)}(\boldsymbol{x})$. The GLMB pdf can be rewritten according to [Vo and Vo, 2013, Vo et al., 2014]

$$f(\tilde{X}) = \Delta(\tilde{X}) \sum_{b \in \mathcal{B}} \sum_{L \in \mathcal{F}(\mathbb{L}^*)} \omega_b(L) \delta_L(\mathcal{L}(\tilde{X})) \prod_{(\boldsymbol{x}, l) \in \tilde{X}} f_b^{(l)}(\boldsymbol{x}). \tag{2.31}$$

Here, $\delta_L(\mathcal{L}(\tilde{X}))$ is one if $L = \mathcal{L}(\tilde{X})$ and zero otherwise. This form is often referred to as δ-GLMB form. By inserting (2.30) or (2.31) into (2.23), the PGFL can be found as [Mahler, 2014]

$$G_{\tilde{\mathsf{X}}}[\tilde{h}] = \sum_{b \in \mathcal{B}} \sum_{L \in \mathcal{F}(\mathbb{L}^*)} \omega_b(L) \prod_{l \in L} f_b^{(l)}[\tilde{h}],$$

with $f_b^{(l)}[\tilde{h}] = \int h(\boldsymbol{x}, l) f_b^{(l)}(\boldsymbol{x}) \mathrm{d}\boldsymbol{x}$. Furthermore, its PHD is given as [Mahler, 2014]

$$\lambda(\boldsymbol{x}, l) = \sum_{b \in \mathcal{B}} \sum_{L \in \mathcal{F}(\mathbb{L}^*)} 1_L(l)\omega_b(L) f_b^{(l)}(\boldsymbol{x}). \tag{2.32}$$

Finally, we review a close connection between the LMBM RFS and the GLMB RFS [García-Fernández et al., 2018]. In particular, any LMBM RFS can be formulated as a GLMB RFS. Indeed, let $\tilde{\mathbb{X}}$ be an LMBM RFS with existence probabilities $r_b^{(l)}$, spatial PDFs $f_b^{(l)}(\boldsymbol{x})$, and weights w_b with $b \in \mathcal{B} \subset \mathbb{N}$ and $l \in \mathbb{L}^*$. While the spatial PDFs $f_b^{(l)}(\boldsymbol{x})$ remain unchanged in GLMB form, the weights $\omega_b(L)$ of the GLMB RFS can be found from w_b and $r_b^{(l)}$ according to

$$\omega_b(L) = w_b \Bigg(\prod_{l' \in \mathbb{L}^* \setminus L} (1 - r_b^{(l')}) \Bigg) \prod_{l \in L} r_b^{(l)},$$

with $b \in \mathcal{B}$ and $L \in \mathcal{F}(\mathbb{L}^*)$. Note that the statistical description in LMBM form requires $|\mathcal{B}| + 2|\mathcal{B}||\mathbb{L}^*|$ parameters (consisting of $|\mathcal{B}|$ weights w_b, $|\mathcal{B}||\mathbb{L}^*|$ existence probabilities $r_b^{(l)}$, and $|\mathcal{B}||\mathbb{L}^*|$ spatial PDFs), whereas the description in GLMB form requires $|\mathcal{B}||\mathcal{F}(\mathbb{L}^*)| + |\mathcal{B}||\mathbb{L}^*|$ parameters (consisting of $|\mathcal{B}||\mathcal{F}(\mathbb{L}^*)|$ weights $\omega_b(L)$ and $|\mathcal{B}||\mathbb{L}^*|$ spatial PDFs). Because the number of parameters in GLMB form scales exponentially in $|\mathbb{L}^*|$ (since $|\mathcal{F}(\mathbb{L}^*)| = 2^{|\mathbb{L}^*|}$), but only linearly in $|\mathbb{L}^*|$ in LMBM form, the description in LMBM form is more efficient for large $|\mathbb{L}^*|$.

Chapter 3

Bayesian RFS-based Multi-object Tracking

The aim of Bayesian RFS-based multi-object tracking is to infer the time-dependent number and states of multiple objects from measurements provided by one or several sensors. The Bayes-optimal method for RFS-based multi-object tracking is known as the multi-object Bayes filter. This method consists of a prediction step and an update step; it calculates the posterior PDF recursively in time, taking into account newly acquired sensor measurements at each time step. However, a direct implementation of the general multi-object Bayes filter is usually infeasible, since it requires, e.g., the computation of complicated set integrals. A common approach then is to first assume a particular RFS type for the multi-object state (equivalently, for the posterior PDF), such as the Poisson RFS (PDF) or the LMB RFS (PDF), and then perform prediction and update steps for this RFS type [Mahler, 2007b, Mahler, 2014].

For some RFS types, the multi-object state RFS obtained after applying prediction and update steps is of the same type. The multi-object PDFs corresponding to these RFS types are referred to as conjugate priors, and the resulting tracking algorithms are instances of the multi-object Bayes filter and are therefore referred to as Bayes-optimal. The RFS types that are preserved by the prediction and update steps of the multi-object Bayes filter include the MB mixture (MBM) RFS, the union of a Poisson RFS and an MBM RFS, and the GLMB RFS. The corresponding filters are referred to as the MBM filter [Xia et al., 2019, García-Fernández et al., 2018], the Poisson-MB mixture (PMBM) filter [Williams, 2015, García-Fernández et al., 2018], and the GLMB filter [Vo and Vo, 2013, Vo et al., 2014, Mahler, 2014], respectively. However, all these filters are computationally demanding.

On the other hand, for many types of RFS, the multi-object state RFS obtained after applying the prediction and update steps is of a different (and, in most cases, more complicated) type. Here, a common strategy is to approximate the posterior PDF by a PDF of a simpler type. This strategy can also be applied to conjugate prior posterior

PDFs, i.e., to posterior PDFs that are of the same type after the prediction and update steps, in order to reduce the computational complexity. Filters based on this approach include the PHD filter [Mahler, 2003, Mahler, 2007b, Challa et al., 2011], the TOMB/P filter [Williams, 2015, Williams, 2011, Kropfreiter et al., 2016], and the LMB filter [Reuter et al., 2014, Reuter et al., 2017].

The remainder of this chapter is structured as follows. In Section 3.1, we review the multi-object Bayes filter for unlabeled and labeled RFSs. Two common system models used in multi-object tracking are presented in Section 3.2. The PHD filter is reviewed in Section 3.3, the TOMB/P filter in Section 3.4, and the LMB filter in Section 3.5.

3.1 The Multi-object Bayes Filter

In Bayesian RFS-based multi-object tracking, object states and measurements are modeled by RFSs. More precisely, the multi-object state at time k is either modeled as an unlabeled RFS $\mathsf{X}_k = \{\mathbf{x}_k^{(1)}, \dots, \mathbf{x}_k^{(\mathsf{N_k})}\}$ with $\mathbf{x}_k \in \mathbb{R}^{n_x}$ or as a labeled RFS $\tilde{\mathsf{X}}_k = \{(\mathbf{x}_k^{(1)}, \mathsf{l}^{(1)}), \dots, (\mathbf{x}_k^{(\mathsf{N_k})}, \mathsf{l}^{(\mathsf{N_k})})\}$ with $(\mathbf{x}_k, \mathsf{l}) \in \mathbb{R}^{n_x} \times \mathbb{L}_k^*$. Here, $\mathbb{L}_k^* \subseteq \mathbb{L}_k$ is a finite set containing the labels of $\tilde{\mathsf{X}}_k$; $\mathbb{L}_k$ is a countable set and is referred to as label space [Vo and Vo, 2013, Vo et al., 2014, Reuter et al., 2014]. Furthermore, the sensor measurements at time k are modeled as an unlabeled RFS $\mathsf{Z}_k = \{\mathbf{z}_k^{(1)}, \dots, \mathbf{z}_k^{(\mathsf{M_k})}\}$ with $\mathbf{z}_k \in \mathbb{R}^{n_z}$. Here, n_x is the dimension of the single-object state $\mathbf{x}_k$ and n_z of the measurement $\mathbf{z}_k$. The object state $\mathbf{x}_k$ typically consists of the object's position, the object's velocity and possible further parameters describing its extent, etc., whereas l is a label modeling the identity of the corresponding object. The measurement $\mathbf{z}_k$ might consist of Cartesian or polar coordinates. Note that the cardinalities of X_k or $\tilde{\mathsf{X}}_k$ and Z_k, i.e., $\mathsf{N_k}$ and $\mathsf{M_k}$, are random quantities as well.

The aim of Bayesian RFS-based multi-object tracking is to estimate the number of objects and their respective states at all times $k = 1, 2, \dots$. This task relies on the calculation of the posterior PDF $f(X_k|Z_{1:k})$, where $Z_{1:k} \triangleq (Z_1, \dots, Z_k)$ is the sequence of all acquired measurements up to time k, and is usually performed in a time-recursive manner. That is, the current posterior PDF $f(X_k|Z_{1:k})$ is computed from the previous posterior PDF $f(X_{k-1}|Z_{1:k-1})$ using the current measurement set Z_k.

This recursive calculation is performed in a two-step procedure consisting of a prediction step and an update step. In the prediction step, the previous posterior PDF $f(X_{k-1}|Z_{1:k-1})$ is converted into a "predicted posterior PDF" $f(X_k|Z_{1:k-1})$ according to

$$\begin{aligned} f\big(X_k|Z_{1:k-1}\big) &= \int f\big(X_k, X_{k-1}|Z_{1:k-1}\big)\, \delta X_{k-1} \\ &= \int f\big(X_k|X_{k-1}\big)\, f\big(X_{k-1}|Z_{1:k-1}\big)\, \delta X_{k-1}\,, \end{aligned} \tag{3.1}$$

where in the last step, it is assumed that the multi-object state at time k, i.e., X_k, given the multi-object state at time $k-1$, i.e., X_{k-1}, is independent of all measurements up to time $k-1$, i.e., $\mathsf{Z}_{1:k-1}$. Here, $f(X_k|X_{k-1})$ is referred to as (multi-object) state-transition PDF and models the temporal evolution of the multi-object state from one time step to the next. Note that according to the prediction relation (3.1), the state is assumed to evolve according to a Markov process, i.e., X_k, conditioned on X_{k-1}, is independent of all $\mathsf{X}_{k'}$ with $k' = 0, \ldots, k-2$ (in addition to $\mathsf{Z}_{1:k-1}$). Expression (3.1) is often referred to as Chapman-Kolmogorov equation [Mahler, 2007b, Bar-Shalom et al., 2011, Challa et al., 2011].

In the update step, the predicted posterior PDF $f(X_k|Z_{1:k-1})$ is converted into the current posterior PDF $f(X_k|Z_{1:k})$ according to

$$
\begin{aligned}
f\big(X_k|Z_{1:k}\big) &= \frac{f\big(Z_k, X_k|Z_{1:k-1}\big)}{f\big(Z_k|Z_{1:k-1}\big)} \\
&= \frac{f\big(Z_k|X_k\big) f\big(X_k|Z_{1:k-1}\big)}{f\big(Z_k|Z_{1:k-1}\big)},
\end{aligned} \tag{3.2}
$$

where in the last step, it is assumed that the measurements at time k, i.e., Z_k, given the multi-object state at time k, i.e., X_k, are independent of all measurements up to time $k-1$, i.e., $\mathsf{Z}_{1:k-1}$. Here, $f(Z_k|X_k)$ is referred to as (multi-object) likelihood function and models the statistical dependency of the measurements Z_k on the mulit-object state X_k. Note that according to the update relation (3.2), the measurements Z_k, conditioned on X_k, are assumed as independent of all object states $\mathsf{X}_{k'}$ with $k' = 0, \ldots, k-1$ (in addition to $\mathsf{Z}_{1:k-1}$). Note that expression (3.2) involves the current measurement set Z_k.

The prediction step (cf. (3.1)) in combination with the update step (cf. (3.2)) is often designated as multi-object Bayes filter [Mahler, 2007b]. In the presentation above, the multi-object state X_k is considered as an unlabeled RFS. However, the same formalism holds for labeled RFSs simply by replacing X_k by the labeled state RFS $\tilde{\mathsf{X}}_k$. Next, we present two common system models used in RFS-based multi-object tracking.

3.2 RFS-based System Models

3.2.1 System Model for Unlabeled RFS-based Multi-object Tracking

In the following, we present a common system model used in unlabeled multi-object tracking consisting of a state-transition model and a measurement model. Filters based on this model include the PHD filter [Mahler, 2003, Vo et al., 2005, Vo and Ma, 2006], the CPHD filter [Mahler, 2007a] and the TOMB/P filter [Williams, 2015]. The PHD filter and the TOMB/P filter will be reviewed in Section 3.3 and Section 3.4, respectively. Recap, that here the multi-object state and the measurements at time k are modeled by the unlabeled RFSs $\mathsf{X}_k = \{\mathbf{x}_k^{(1)}, \ldots, \mathbf{x}_k^{(\mathsf{N}_k)}\}$ and $\mathsf{Z}_k = \{\mathbf{z}_k^{(1)}, \ldots, \mathbf{z}_k^{(\mathsf{M}_k)}\}$, respectively.

The transition of the multi-object state from time $k-1$ to k, i.e., $\mathsf{X}_{k-1} \rightarrow \mathsf{X}_k$, is modeled as follows: An object with state $\mathsf{x}_{k-1} \in \mathsf{X}_{k-1}$ at time $k-1$ survives with probability $p_{\mathrm{S}}(\boldsymbol{x}_{k-1})$ or dies with probability $1-p_{\mathrm{S}}(\boldsymbol{x}_{k-1})$. If the object survives, its new state at time k is distributed according to the single-state transition PDF $f(\boldsymbol{x}_k|\boldsymbol{x}_{k-1})$. Thus, an object at time k that already existed at time $k-1$ is modeled by a Bernoulli RFS $\mathsf{S}_k(\boldsymbol{x}_{k-1})$ with existence probability $p_{\mathrm{S}}(\boldsymbol{x}_{k-1})$ and spatial PDF $f(\boldsymbol{x}_k|\boldsymbol{x}_{k-1})$ (cf. (2.12)). It is assumed that the states of different objects evolve independently, i.e., x_k is conditionally independent, given $\boldsymbol{x}_{k-1}$, of all the other x'_k. Hence, all objects at time k that already existed at time $k-1$ are modeled by an MB RFS $\bigcup_{\boldsymbol{x}_{k-1}\in X_{k-1}} \mathsf{S}_k(\boldsymbol{x}_{k-1})$ with parameter set $\big\{\big(p_{\mathrm{S}}(\boldsymbol{x}_{k-1}), f(\boldsymbol{x}_k|\boldsymbol{x}_{k-1})\big)\big\}_{\boldsymbol{x}_{k-1}\in X_{k-1}}$. In addition, it is possible that new objects appear at time k. These objects are referred as newborn objects and are modeled by a Poisson RFS $\mathsf{X}_k^{\mathrm{B}}$ with mean parameter μ_{B}, spatial PDF $f_{\mathrm{B}}(\boldsymbol{x}_k)$, and, thus, PHD $\lambda_{\mathrm{B}}(\boldsymbol{x}_k) = \mu_{\mathrm{B}} f_{\mathrm{B}}(\boldsymbol{x}_k)$ [Mahler, 2007b, Williams, 2015]. Here, $\mathsf{X}_k^{\mathrm{B}}$ is assumed to be conditionally independent, given the previous multi-object state RFS X_{k-1}, of $\bigcup_{\boldsymbol{x}_{k-1}\in X_{k-1}} \mathsf{S}_k(\boldsymbol{x}_{k-1})$. Summarizing, the overall multi-object state at time k, given the previous multi-object state X_{k-1}, is given by

$$\mathsf{X}_k = \Bigg(\bigcup_{\boldsymbol{x}_{k-1}\in X_{k-1}} \mathsf{S}_k(\boldsymbol{x}_{k-1})\Bigg) \cup \mathsf{X}_k^{\mathrm{B}}.$$

This model defines the state-transition PDF $f(X_k|X_{k-1})$ used in the derivation of the prediction step of the PHD and TOMB/P filter. The prediction step of the PHD and TOMB/P filter will be reviewed in Section 3.3.1 and Section 3.4.1, respectively.

The statistical dependency of the multi-object state on the measurement at time k, i.e., $\mathsf{Z}_k \to \mathsf{X}_k$, is modeled as follows: An object with state $\mathsf{x}_k \in \mathsf{X}_k$ is detected by the sensor with probability $p_{\mathrm{D}}(\boldsymbol{x}_k)$ or is missed with probability $1-p_{\mathrm{D}}(\boldsymbol{x}_k)$. If it is detected, it generates a measurement z_k according to the single-object likelihood function $f(\boldsymbol{z}_k|\boldsymbol{x}_k)$, and if it is not detected, it generates no measurement. Accordingly, the measurement originated from an object with state x_k is modeled as a Bernoulli RFS $\Theta_k(\boldsymbol{x}_k)$ with existence probability $p_{\mathrm{D}}(\boldsymbol{x}_k)$ and spatial PDF $f(\boldsymbol{z}_k|\boldsymbol{x}_k)$. It is assumed that each of these object-originated measurements z_k is conditionally independent, given the respective object state $\boldsymbol{x}_k$, of all the other measurements z'_k and all the other object states x'_k. Thus, these measurements form the MB RFS $\bigcup_{\boldsymbol{x}_k\in X_k} \Theta_k(\boldsymbol{x}_k)$ with parameter set $\big\{\big(p_{\mathrm{D}}(\boldsymbol{x}_k), f(\boldsymbol{z}_k|\boldsymbol{x}_k)\big)\big\}_{\boldsymbol{x}_k\in X_k}$. In addition, measurements may also be originated by clutter. Following [Mahler, 2007b, Williams, 2015], these clutter-originated measurements are modeled by the Poisson RFS $\mathsf{Z}_k^{\mathrm{C}}$ with mean parameter μ_{C}, spatial PDF $f_{\mathrm{C}}(\boldsymbol{z}_k)$, and, thus, corresponding PHD $\lambda_{\mathrm{C}}(\boldsymbol{z}_k) = \mu_{\mathrm{C}} f_{\mathrm{C}}(\boldsymbol{z}_k)$. Clutter-originated measurements are assumed conditionally independent, given X_k, of the object-originated measurements $\bigcup_{\boldsymbol{x}_k\in X_k} \Theta_k(\boldsymbol{x}_k)$. The overall measurement RFS at time k, given the multi-object state X_k, is given by

$$\mathsf{Z}_k = \Bigg(\bigcup_{\boldsymbol{x}_k\in X_k} \Theta_k(\boldsymbol{x}_k)\Bigg) \cup \mathsf{Z}_k^{\mathrm{C}}.$$

This model defines the likelihood function $f(Z_k|X_k)$ used in the derivation of the update step of the PHD and TOMB/P filter. The update step of the PHD and TOMB/P filter will be reviewed in Section 3.3.2 and Section 3.4.2, respectively.

3.2.2 System Model for Labeled RFS-based Multi-object Tracking

We now review a system model that is common in labeled RFS-based multi-object tracking. Similarly to the model for unlabeled multi-object tracking presented in the previous section, it consists of a state-transition model and a measurement model. Filters that are based on this model include the LMB filter [Reuter et al., 2014] and the GLMB filter [Vo and Vo, 2013, Vo et al., 2014]. The LMB filter will be reviewed in Section 3.5. Recap that in labeled RFS-based multi-object tracking, the multi-object state is modeled by the labeled RFS $\tilde{\mathsf{X}}_k = \{(\mathbf{x}_k^{(1)}, \mathsf{l}^{(1)}), \ldots, (\mathbf{x}_k^{(\mathsf{N}_k)}, \mathsf{l}^{(\mathsf{N}_k)})\}$ and the measurements by the unlabeled RFS $\mathsf{Z}_k = \{\mathbf{z}_k^{(1)}, \ldots, \mathbf{z}_k^{(\mathsf{M}_k)}\}$.

The transition of the multi-object state from time $k-1$ to time k, i.e., $\tilde{\mathsf{X}}_{k-1}$ to $\tilde{\mathsf{X}}_k$, is modeled as follows [Reuter et al., 2014, Mahler, 2014]: An object with state $(\mathbf{x}_{k-1}, \mathsf{l}) \in \tilde{\mathsf{X}}_{k-1}$ survives with probability $p_{\mathrm{S}}(\boldsymbol{x}_{k-1}, l)$ or dies with probability $1 - p_{\mathrm{S}}(\boldsymbol{x}_{k-1}, l)$. If it survives, its new state $\mathbf{x}_k$ (without the label) is distributed according to the single-state transition PDF $f(\boldsymbol{x}_k|\boldsymbol{x}_{k-1}, l)$ and the label l is preserved. Thus, an object at time k that already existed at time $k-1$ is modeled by a Bernoulli RFS $\tilde{\mathsf{S}}_k(\boldsymbol{x}_{k-1}, l)$ with existence probability $p_{\mathrm{S}}(\boldsymbol{x}_{k-1}, l)$ and spatial PDF $f(\boldsymbol{x}_k|\boldsymbol{x}_{k-1}, l)$. Note that the labels l do not change over time that is why they are denoted rather as l than l_k. The states of different objects evolve independently, i.e., $(\mathbf{x}_k, l)$ is conditionally independent, given $(\boldsymbol{x}_{k-1}, l)$, of all other $(\mathbf{x}_k, l')$ with $l' \neq l$. Accordingly, all objects at time k that already existed at time $k-1$ are modeled by an LMB RFS $\bigcup_{l \in \mathbb{L}_{k-1}^*} \tilde{\mathsf{S}}_k(\boldsymbol{x}_{k-1}, l)$ with parameters $\big\{\big(p_{\mathrm{S}}(\boldsymbol{x}_{k-1}, l), f(\boldsymbol{x}_k|\boldsymbol{x}_{k-1}, l)\big)\big\}_{l \in \mathbb{L}_{k-1}^*}$. There may also be newborn objects. They are modeled by an LMB RFS $\tilde{\mathsf{X}}_k^{\mathrm{B}}$, which is fully described by the parameter set $\big\{\big(r_{\mathrm{B},k}^{(l)}, f_{\mathrm{B}}^{(l)}(\boldsymbol{x}_k)\big)\big\}_{l \in \mathbb{L}_k^{\mathrm{B}*}}$, where $r_{\mathrm{B},k}^{(l)}$ and $f_{\mathrm{B}}^{(l)}(\boldsymbol{x}_k)$ are the existence probabilities and the spatial PDFs, respectively, of the newborn objects with labels $l \in \mathbb{L}_k^{\mathrm{B}*} \subseteq \mathbb{L}_k^{\mathrm{B}}$. Here, $\mathbb{L}_k^{\mathrm{B}}$ denotes the label space of newborn objects and is given by $\mathbb{L}_k^{\mathrm{B}} = \{k\} \times \mathbb{N}$. The overall label space $\mathbb{L}_k$ also evolves recursively according to $\mathbb{L}_k = \mathbb{L}_{k-1} \cup \mathbb{L}_k^{\mathrm{B}}$, where $\mathbb{L}_{k-1}$ is the label space at time $k-1$. Here, $\mathbb{L}_{k-1}$ and $\mathbb{L}_k^{\mathrm{B}}$ are disjoint, i.e., $\mathbb{L}_{k-1} \cap \mathbb{L}_k^{\mathrm{B}} = \emptyset$, which entails that $\mathbb{L}_{k-1}^* \cap \mathbb{L}_k^{\mathrm{B}*} = \emptyset$. We furthermore assume that the newborn objects $\tilde{\mathsf{X}}_k^{\mathrm{B}}$, given the previous multi-object state $\tilde{X}_{k-1}$, is independent of $\bigcup_{l \in \mathbb{L}_{k-1}^*} \tilde{\mathsf{S}}_k(\boldsymbol{x}_{k-1}, l)$. Summarizing, the overall multi-object state at time k, given the previous multi-object state $\tilde{X}_{k-1}$, is given by

$$\tilde{\mathsf{X}}_k = \left(\bigcup_{l \in \mathbb{L}_{k-1}^*} \tilde{\mathsf{S}}_k(\boldsymbol{x}_{k-1}, l) \right) \cup \tilde{\mathsf{X}}_k^{\mathrm{B}}. \tag{3.3}$$

This model specifies the state-transition PDF $f(\tilde{X}_k|\tilde{X}_{k-1})$ used in the derivation of the prediction step of the LMB filter. The prediction step of the LMB filter will be reviewed in Section 3.5.1.

Next, we will present the statistical dependency of the multi-object state on the measurements at time k, i.e., $\mathsf{Z}_k \rightarrow \tilde{\mathsf{X}}_k$. An object with state $(\mathbf{x}_k, \mathsf{l})$ at time k is detected by the sensor with probability $p_{\mathrm{D}}(\boldsymbol{x}_k, l)$, or missed with probability $1 - p_{\mathrm{D}}(\boldsymbol{x}_k, l)$. If it is detected, it generates a measurement $\mathbf{z}_k$ according to the single-state likelihood function $f(\boldsymbol{z}_k|\boldsymbol{x}_k, l)$ and if it is missed, it generates no measurement. Accordingly, the measurement originated by an object with state $(\boldsymbol{x}_k, l)$ is modeled by a Bernoulli RFS $\tilde{\Theta}_k(\boldsymbol{x}_k, l)$ with existence probability $p_{\mathrm{D}}(\boldsymbol{x}_k, l)$ and spatial PDF $f(\boldsymbol{z}_k|\boldsymbol{x}_k, l)$. It is assumed that each object-originated measurement $\mathbf{z}_k$ is conditionally independent, given the respective object state $(\boldsymbol{x}_k, l)$, of all the other measurements $\mathbf{z}'_k$ and all the other object states $(\mathbf{x}'_k, l')$. Hence, the object-originated measurements are modeled by an MB RFS[1] $\bigcup_{l\in\mathbb{L}^*_k} \tilde{\Theta}_k(\boldsymbol{x}_k, l)$ with parameter set $\big\{\big(p_{\mathrm{D}}(\boldsymbol{x}_k, l), f(\boldsymbol{z}_k|\boldsymbol{x}_k, l)\big)\big\}_{l\in\mathbb{L}^*_k}$. There may also be clutter-originated measurements; they are modeled by the Poisson RFS $\mathsf{Z}^{\mathrm{C}}_k$ parametrized by the mean parameter μ_{C}, the spatial PDF $f_{\mathrm{C}}(\boldsymbol{z}_k)$ and, thus, the PHD $\lambda_{\mathrm{C}}(\boldsymbol{z}_k) = \mu_{\mathrm{C}} f_{\mathrm{C}}(\boldsymbol{z}_k)$. This clutter model conforms the clutter model used in the unlabeled RFS-based system model of Section 3.2.1. It is assumed that $\mathsf{Z}^{\mathrm{C}}_k$ is conditionally independent of $\bigcup_{l\in\mathbb{L}^*_k} \tilde{\Theta}_k(\boldsymbol{x}_k, l)$, given the multi-object state $\tilde{X}_k$. The overall measurement RFS, given the multi-object state $\tilde{X}_k$, is given by

$$\mathsf{Z}_k = \left(\bigcup_{l\in\mathbb{L}^*_k} \tilde{\Theta}_k(\boldsymbol{x}_k, l)\right) \cup \mathsf{Z}^{\mathrm{C}}_k. \tag{3.4}$$

The measurement model specifies the likelihood function $f(Z_k|\tilde{X}_k)$ used in the derivation of the update step of the LMB filter. The update step of the LMB filter will be reviewed in Section 3.5.2.

In the next three subsections, we review the PHD filter, the TOMB/P filter, and the LMB filter.

3.3 The PHD Filter

The PHD filter is a low complexity approximation of the multi-object Bayes filter (cf. Section 3.1) and models the multi-object state X_k by a Poisson RFS. Thus, the posterior PDF at time $k-1$ is given by (cf. (2.10))

$$f(X_{k-1}|Z_{1:k-1}) = e^{-\int \lambda(\boldsymbol{x}'_{k-1})\mathrm{d}\boldsymbol{x}'_{k-1}} \prod_{\boldsymbol{x}_{k-1}\in X_{k-1}} \lambda(\boldsymbol{x}_{k-1}), \tag{3.5}$$

[1]Note that $\bigcup_{l\in\mathbb{L}^*_k} \tilde{\Theta}_k(\boldsymbol{x}_k, l)$ is an unlabeled RFS describing the statistics of the object-originated measurements and the label $l \in \mathbb{L}^*_k$ is purely used to index the Bernoulli RFSs $\tilde{\Theta}_k(\boldsymbol{x}_k, l)$.

where $\lambda(\boldsymbol{x}_{k-1})$ is the posterior PHD at time $k-1$. A detailed derivation of the PHD filter can be found in, e.g., [Mahler, 2003, Mahler, 2007b, Challa et al., 2011]. In the following, we will review the prediction and update step of the PHD filter.

3.3.1 Prediction Step of the PHD Filter

The predicted posterior PDF $f(X_k|Z_{1:k-1})$ can be obtained by inserting the previous posterior PDF $f(X_{k-1}|Z_{1:k-1})$ in (3.5) into the prediction relation (3.1). It turns out that the predicted posterior PDF is no longer of Poisson type, but can be approximated by the Poisson PDF $\tilde{f}(X_k|Z_{1:k-1})$ [Mahler, 2003, García-Fernández and Vo, 2015]. Here, $\tilde{f}(X_k|Z_{1:k-1})$ is chosen such that its corresponding PHD is equal to the PHD corresponding to the exact predicted posterior PDF $f(X_k|Z_{1:k-1})$. As was shown in [Mahler, 2003, Mahler, 2007b], this (approximated) predicted posterior PHD is given by

$$\lambda_{k|k-1}(\boldsymbol{x}_k) = \lambda_{\mathrm{B}}(\boldsymbol{x}_k) + \int f(\boldsymbol{x}_k|\boldsymbol{x}_{k-1}) p_{\mathrm{S}}(\boldsymbol{x}_{k-1}) \lambda(\boldsymbol{x}_{k-1}) \mathrm{d}\boldsymbol{x}_{k-1}. \tag{3.6}$$

Here, $\lambda_{\mathrm{B}}(\boldsymbol{x}_k)$, $f(\boldsymbol{x}_k|\boldsymbol{x}_{k-1})$, and $p_{\mathrm{S}}(\boldsymbol{x}_{k-1})$ are the birth PHD, the single-object state transition PDF, and the survival probability, respectively, introduced in Section 3.2.1, and $\lambda(\boldsymbol{x}_{k-1})$ is the posterior PHD at time $k-1$. The derivation of the prediction step of the PHD filter relies on the state transition PDF $f(X_k|X_{k-1})$ defined by the state transition model of Section 3.2.1. A specific expression of $f(X_k|X_{k-1})$ can be found in, e.g., [Mahler, 2007b]. Note that the prediction relation in (3.6) takes into account the birth/death of objects and the transition of survived objects from one time step to the next. The classical PHD prediction step presented here can be extended to object spawning [Mahler, 2003, Mahler, 2007b], where each object at time $k-1$ is a possible source of multiple objects at time k. However, object spawning is not considered in this work.

3.3.2 Update Step of the PHD Filter

The current posterior PDF $f(X_k|Z_{1:k})$ can be determined by applying the update relation in (3.2) and replacing the exact predicted posterior PDF $f(X_k|Z_{1:k-1})$ by its approximation $\tilde{f}(X_k|Z_{1:k-1})$ of Section 3.3.1. Similarly to the predicted posterior PDF, the new posterior PDF $f(X_k|Z_{1:k})$ is no longer of Poisson type and it is hence approximated by the Poisson PDF $\tilde{f}(X_k|Z_{1:k})$. Again, $\tilde{f}(X_k|Z_{1:k})$ is chosen such that its corresponding PHD is equal to the PHD corresponding to the exact posterior PDF $f(X_k|Z_{1:k})$. As shown in [Mahler, 2003, Mahler, 2007b], the (approximated) posterior PHD at time k is given by

$$\lambda(\boldsymbol{x}_k) = \big(1 - p_{\mathrm{D}}(\boldsymbol{x}_k)\big)\lambda_{k|k-1}(\boldsymbol{x}_k) + \sum_{\boldsymbol{z}_k \in Z_k} \frac{f(\boldsymbol{z}_k|\boldsymbol{x}_k) p_{\mathrm{D}}(\boldsymbol{x}_k) \lambda_{k|k-1}(\boldsymbol{x}_k)}{\lambda_{\mathrm{C}}(\boldsymbol{z}_k) + \int f(\boldsymbol{z}_k|\boldsymbol{x}_k) p_{\mathrm{D}}(\boldsymbol{x}_k) \lambda_{k|k-1}(\boldsymbol{x}_k) \mathrm{d}\boldsymbol{x}_k}. \tag{3.7}$$

Here, $p_{\mathrm{D}}(\boldsymbol{x}_k)$, $f(\boldsymbol{z}_k|\boldsymbol{x}_k)$, and $\lambda_{\mathrm{C}}(\boldsymbol{z}_k)$ are the detection probability, single-object likelihood function, and the clutter PHD, respectively, introduced in Section 3.2.1, and $\lambda_{k|k-1}(\boldsymbol{x}_k)$ is the predicted PHD in (3.6). The derivation of the update step of the PHD filter involves the likelihood function $f(Z_k|X_k)$ defined by the measurement model of Section 3.2.1. A specific expression of $f(Z_k|X_k)$ can be found in, e.g., [Mahler, 2007b]. Note that the update relation in (3.7) takes into account the detection/misdetection of objects, the noise corruption of detected objects, and clutter measurements.

The PHD filter is now obtained by recursively computing the prediction and update relations (3.6) and (3.7), where the update step incorporates the currently acquired sensor measurements Z_k. The filter equations (3.6) and (3.7) contain integrals; closed form solutions can only be obtained for linear/Gaussian state-transition PDFs $f(\boldsymbol{x}_k|\boldsymbol{x}_{k-1})$, Gaussian birth models, linear/Gaussian likelihood functions $f(\boldsymbol{z}_k|\boldsymbol{x}_k)$, and for a Gaussian mixture prior, i.e., the posterior PHD $\lambda(\boldsymbol{x}_k)$ at time $k = 0$ is modeled by a Gaussian mixture PDF. These assumptions result in a Gaussian mixture implementation of the PHD filter [Vo and Ma, 2006]. For non-linear/non-Gaussian models a particle implementation was proposed in [Vo et al., 2005].

The PHD filter provides a low complexity approximate solution to the multi-object tracking problem by recursively propagating the posterior PHD of a Poisson RFS over time. Recap from Section 2.1.1 that the PHD can generally be considered as first order moment of an RFS. Thus, the Poisson assumption in the PHD filter can equivalently be interpreted as first order moment approximation of an RFS of general type. While this first order moment approximation of $f(X_k|Z_{1:k})$ might be reasonable for some tracking scenarios, in more challenging scenarios, $f(X_k|Z_{1:k})$ may also comprise higher order moments that are non-zero. Here, the first order moment approximation might ignore valuable object state information. Hence, the PHD filter performs rather poorly in challenging scenarios with, e.g., a low detection probability and/or high clutter and/or a high number of objects [Mahler, 2003, Mahler, 2007b].

On the order hand, the PHD filter has very low computational requirements. In fact, the computational complexity scales according to $\mathcal{O}(N_k M_k)$, i.e., linearly in the number of objects and linearly in the number of measurements. Since the PHD filter only propagates the first order moment of the posterior PDF $f(X_k|Z_{1:k})$, one might consider to improve the tracking performance by additionally propagating higher order moments of the posterior PDF. Although, it is theoretically possible to derive a filter that also considers, e.g., the second order moment, it was noted in [Mahler, 2007b] that a practical implementation of such a filter seems to be infeasible. However, performance can be improved by modeling the cardinality distribution by a general cardinality PMF $\rho(n)$ rather than a Poisson PMF as in the PHD filter. This approach is pursued in the CPHD filter [Mahler, 2007a], which propagates the posterior cardinality distribution in addition to the posterior PHD. The CPHD filter was found to perform significantly better than the PHD filter, but at the expense of a higher computational complexity, which scales according to $\mathcal{O}(N_k M_k^3)$, i.e., linearly in the number of objects and cubically in the number of measurements. Recap that the PHD filter scales linearly in the number of objects and only linearly in the number of measurements. The CPHD filter will not be discussed further in this work.

3.4 The TOMB/P Filter

In this section, we review the TOMB/P filter introduced in [Williams, 2015, Williams, 2011]. A detailed derivation can be found in [Williams, 2015]. The TOMB/P filter is another approximation of the multi-object Bayes filter described in Section 3.1. It models the multi-object state RFS X_k by the union of a statistically independent MB RFS $\mathsf{X}_k^{\mathrm{D}}$ and a Poisson $\mathsf{X}_k^{\mathrm{U}}$, i.e., $\mathsf{X}_k = \mathsf{X}_k^{\mathrm{D}} \cup \mathsf{X}_k^{\mathrm{U}}$. Thus, the posterior PDF $f(X_{k-1}|Z_{1:k-1})$ at time $k-1$ is given using the FISST convolution (2.4) as

$$f(X_{k-1}|Z_{1:k-1}) = \sum_{Y \subseteq X_{k-1}} f^{\mathrm{U}}(Y) f^{\mathrm{D}}(X_{k-1} \backslash Y | Z_{1:k-1}), \tag{3.8}$$

where $f^{\mathrm{U}}(X_{k-1})$ is the posterior PDF describing $\mathsf{X}_{k-1}^{\mathrm{U}}$ (note that $\mathsf{X}_{k-1}^{\mathrm{U}}$ is independent of $\mathsf{Z}_{1:k-1}$) and $f^{\mathrm{D}}(X_{k-1}|Z_{1:k-1})$ is the posterior PDF describing $\mathsf{X}_{k-1}^{\mathrm{D}}$. The Poisson PDF $f^{\mathrm{U}}(X_{k-1})$ is represented by the posterior PHD $\lambda_{\mathrm{U}}(\boldsymbol{x}_{k-1})$ (cf. Section 2.1.2) and the MB PDF $f^{\mathrm{D}}(X_{k-1}|Z_{1:k-1})$ by J_{k-1} Bernoulli components with existence probabilities $r_{k-1}^{(j)}$ and spatial PDFs $f^{(j)}(\boldsymbol{x}_{k-1})$, $j \in \mathcal{J}_{k-1} \triangleq \{1, \ldots, J_{k-1}\}$ (cf. Section 2.1.4). Note that in the TOMB/P filter, the Poisson RFS models "undetected objects" and the MB RFS "detected objects". Undetected objects are objects that exist but have not yet been detected, while detected objects have already been detected and thus have already generated at least one measurement. The modeling of undetected objects can facilitate the generation of new Bernoulli components [Williams, 2015].

In the following, we will review the prediction and update step of the TOMB/P filter [Williams, 2015]. The derivation is based on the same system model for unlabeled RFS as the derivation of the PHD filter, i.e., the system model presented in Section 3.2.1.

3.4.1 Prediction Step of the TOMB/P Filter

The predicted posterior PDF $f(X_k|Z_{1:k-1})$ can be obtained by inserting the previous posterior PDF $f(X_{k-1}|Z_{1:k-1})$ (cf. (3.8)) into the prediction relation (3.1). It turns out that the predicted posterior PDF $f(X_k|Z_{1:k-1})$ preserves the convolutional form of (3.8), i.e., it can be decomposed again into a PDF $f_{k|k-1}^{\mathrm{D}}(X_k|Z_{1:k-1})$ describing detected objects and a PDF $f_{k|k-1}^{\mathrm{U}}(X_k)$ describing undetected objects [Williams, 2015]. Moreover, $f_{k|k-1}^{\mathrm{D}}(X_k|Z_{1:k-1})$ is again an MB PDF and $f_{k|k-1}^{\mathrm{U}}(X_k)$ is again a Poisson PDF.

More precisely, the predicted posterior PHD of undetected objects $\lambda_{k|k-1}^{\mathrm{U}}(\boldsymbol{x}_k)$ characterizing $f^{\mathrm{U}}_{k|k-1}(X_k)$ is calculated according to

$$\lambda^{\mathrm{U}}_{k|k-1}(\boldsymbol{x}_k) = \lambda_{\mathrm{B}}(\boldsymbol{x}_k) + \int f(\boldsymbol{x}_k|\boldsymbol{x}_{k-1})p_{\mathrm{S}}(\boldsymbol{x}_{k-1})\lambda_{\mathrm{U}}(\boldsymbol{x}_{k-1})\mathrm{d}\boldsymbol{x}_{k-1}. \tag{3.9}$$

Here, $\lambda_{\mathrm{B}}(\boldsymbol{x}_k)$, $f(\boldsymbol{x}_k|\boldsymbol{x}_{k-1})$ and $p_{\mathrm{S}}(\boldsymbol{x}_{k-1})$ are the birth PHD, the single-object state transition PDF, and the survival probability introduced in Section 3.2.1, respectively, and $\lambda_{\mathrm{U}}(\boldsymbol{x}_{k-1})$ is the posterior PHD of undetected objects at time $k-1$. Furthermore, the parameters $r^{(j)}_{k|k-1}$ and $f^{(j)}_{k|k-1}(\boldsymbol{x}_k)$, $j \in \mathcal{J}_{k-1}$ characterizing $f^{\mathrm{D}}_{k|k-1}(X_k|Z_{1:k-1})$ are calculated according to

$$r^{(j)}_{k|k-1} = r^{(j)}_{k-1}\int p_{\mathrm{S}}(\boldsymbol{x}_{k-1})f^{(j)}(\boldsymbol{x}_{k-1})\mathrm{d}\boldsymbol{x}_{k-1}, \tag{3.10}$$

$$f^{(j)}_{k|k-1}(\boldsymbol{x}_k) = \frac{\int f(\boldsymbol{x}_k|\boldsymbol{x}_{k-1})p_{\mathrm{S}}(\boldsymbol{x}_{k-1})f^{(j)}(\boldsymbol{x}_{k-1})\mathrm{d}\boldsymbol{x}_{k-1}}{\int p_{\mathrm{S}}(\boldsymbol{x}'_{k-1})f^{(j)}(\boldsymbol{x}'_{k-1})\mathrm{d}\boldsymbol{x}'_{k-1}}, \tag{3.11}$$

where $r^{(j)}_{k-1}$ and $f^{(j)}(\boldsymbol{x}_{k-1})$ are the existence probabilities and spatial pfds at time $k-1$, respectively. Here, the number of Bernoulli components J_{k-1} is not changed by the prediction step. Thus, no new Bernoulli components are generated in the prediction step. Object birth is modeled by the birth PHD $\lambda_{\mathrm{B}}(\boldsymbol{x}_k)$ entering the Poisson part via expression (3.9). The derivation of the prediction step here is based on the state transition PDF $f(X_k|X_{k-1})$ defined by the state transition model of Section 3.2.1. Note that the prediction relation of the undetected object component (3.9) is equal to the prediction relation of the PHD filter (3.6) and the prediction relations of the detected object component (3.10) and (3.11) are equal to those in the conventional MB filter (MeMBer filter) [Vo et al., 2009].

3.4.2 Update Step of the TOMB/P Filter

The current posterior PDF $f(X_k|Z_{1:k})$ can be determined by inserting the predicted posterior pdf $f(X_k|Z_{1:k-1})$ into the update relation (3.2). Although $\mathsf{X}^{\mathrm{U}}_k$ and $\mathsf{X}^{\mathrm{D}}_k$ are still independent, conditioned on $Z_{1:k}$, i.e., the convolutional form of (3.8) is preserved, the posterior PDF is not of Poisson/MB form anymore [Williams, 2015]. In fact, the posterior PDF $f^{\mathrm{U}}(X_k)$ is again a Poisson PDF, whose PHD $\lambda_{\mathrm{U}}(\boldsymbol{x}_k)$ is calculated according to

$$\lambda_{\mathrm{U}}(\boldsymbol{x}_k) = (1-p_{\mathrm{D}}(\boldsymbol{x}_k))\,\lambda^{\mathrm{U}}_{k|k-1}(\boldsymbol{x}_k). \tag{3.12}$$

Here, $p_{\mathrm{D}}(\boldsymbol{x}_k)$ is the detection probability introduced in Section 3.2.1 and $\lambda^{\mathrm{U}}_{k|k-1}(\boldsymbol{x}_k)$ is the predicted posterior PHD of undetected objects (cf. (3.9)). Note that the update step of the undetected object component in (3.12) does not include any measurements, i.e., $\lambda_{\mathrm{U}}(\boldsymbol{x}_k)$ represents previously undetected objects that remain undetected after applying the update step at time k.

However, the posterior PDF $f^{\mathrm{D}}(X_k|Z_{1:k})$ is no longer of MB form but of MBM form.

An expression of $f^{\mathrm{D}}(X_k|Z_{1:k})$ can be obtained by first introducing the (random) object-measurement association vector $\mathsf{a}_k = [\mathsf{a}_k^{(1)} \cdots \mathsf{a}_k^{(J_k)}]^{\mathrm{T}}$ with $J_k = J_{k-1} + M_k$ [Williams, 2015]. Here, $\mathsf{a}_k^{(j)} \in \{0, \dots, M_k\}$ for $j \in \mathcal{J}_{k-1}$ and $\mathsf{a}_k^{(j)} \in \{0, 1\}$ for $j \in \{J_{k-1}+1, \dots, J_k\}$. We call an association $\boldsymbol{a}_k$ admissible if at most one measurement is associated to the same object and no measurement is associated to more than one object. All admissible associations are collected in the association alphabet $\mathcal{A}_k$. Using a_k, the posterior PDF of detected objects can be written as

$$
\begin{aligned}
f^{\mathrm{D}}(X_k|Z_{1:k}) &= \sum_{\boldsymbol{a}_k \in \mathcal{A}_k} p(\boldsymbol{a}_k) \, f^{\mathrm{MB}}_{\boldsymbol{a}_k}(X_k) \\
&= \sum_{\boldsymbol{a}_k \in \mathcal{A}_k} p_k(\boldsymbol{a}_k) \sum_{\alpha \in \mathcal{P}_{J_k, n_k}} \prod_{j=1}^{J_k} f^{(j, a_k^{(j)})}\big(X_k^{(\alpha(j))}\big), \qquad (3.13)
\end{aligned}
$$

where $p(\boldsymbol{a}_k)$ is the probability of association $\boldsymbol{a}_k$, $n_k = |X_k|$, and $f^{\mathrm{MB}}_{\boldsymbol{a}_k}(X_k)$ is an MB PDF (cf. (2.17)) consisting of the Bernoulli PDFs $f^{(j,a_k^{(j)})}(X_k)$, where, in turn, the Bernoulli PDFs are parametrized by the existence probabilities $r_k^{(j,a_k^{(j)})}$ and the spatial PDFs $f^{(j,a_k^{(j)})}(\boldsymbol{x}_k)$. We refer to the Bernoulli components with index $j \in \mathcal{J}_{k-1}$ as legacy Bernoulli components and to those with index $j \in \{J_{k-1}+1, \dots, J_k\}$ as new Bernoulli components. Note that $f^{\mathrm{D}}(X_k|Z_{1:k})$ is an MBM PDF with one mixture component for each admissible object-measurement association vector $\boldsymbol{a}_k \in \mathcal{A}_k$ and the weight of the mixture component is given by the corresponding association probability $p(\boldsymbol{a}_k)$. The association PMF $p(\boldsymbol{a}_k)$ is given up to a normalization constant by

$$
p(\boldsymbol{a}_k) \propto \prod_{j=1}^{J_k} \beta_k^{(j,a_k^{(j)})}, \quad \boldsymbol{a}_k \in \mathcal{A}_k. \qquad (3.14)
$$

Here, the $\beta_k^{(j,a_k^{(j)})}$ are referred to as association weights. The calculation of the association weights $\beta_k^{(j,a_k^{(j)})}$, the existence probabilities $r_k^{(j,a_k^{(j)})}$, and spatial PDFs $f^{(j,a_k^{(j)})}(\boldsymbol{x}_k)$ will be discussed in the following.

For the legacy Bernoulli components, i.e, for $j \in \{1, \dots, J_{k-1}\}$, the association weights, existence probabilities, and spatial PDFs are given for $a_k^{(j)} = m \in \mathcal{M}_k \triangleq \{1, \dots, M_k\}$ by

$$
\beta_k^{(j,m)} = r_{k|k-1}^{(j)} \int f\big(\boldsymbol{z}_k^{(m)} \big| \boldsymbol{x}_k\big) \, p_{\mathrm{D}}(\boldsymbol{x}_k) \, f_{k|k-1}^{(j)}(\boldsymbol{x}_k) \, \mathrm{d}\boldsymbol{x}_k, \qquad (3.15)
$$

$$
r_k^{(j,m)} = 1, \qquad (3.16)
$$

$$
f^{(j,m)}(\boldsymbol{x}_k) = \frac{f\big(\boldsymbol{z}_k^{(m)} \big| \boldsymbol{x}_k\big) \, p_{\mathrm{D}}(\boldsymbol{x}_k) \, f_{k|k-1}^{(j)}(\boldsymbol{x}_k)}{\int f\big(\boldsymbol{z}_k^{(m)} \big| \boldsymbol{x}'_k\big) \, p_{\mathrm{D}}(\boldsymbol{x}'_k) \, f_{k|k-1}^{(j)}(\boldsymbol{x}'_k) \, \mathrm{d}\boldsymbol{x}'_k}. \qquad (3.17)
$$

Here, (3.16) indicates that the object x_k described by the Bernoulli component with index j exists and its state is distributed according to the spatial PDF $f^{(j,m)}(\boldsymbol{x}_k)$ in (3.17). The likelihood of this event is quantified by the association weight $\beta_k^{(j,m)}$ in (3.15). Furthermore, for $a_k^{(j)} = 0$

$$\beta_k^{(j,0)} = 1 - r_{k|k-1}^{(j)} + r_{k|k-1}^{(j)} \int (1 - p_{\mathrm{D}}(\boldsymbol{x}_k))\, f_{k|k-1}^{(j)}(\boldsymbol{x}_k)\,\mathrm{d}\boldsymbol{x}_k\,, \tag{3.18}$$

$$r_k^{(j,0)} = \frac{r_{k|k-1}^{(j)} \int (1 - p_{\mathrm{D}}(\boldsymbol{x}_k))\, f_{k|k-1}^{(j)}(\boldsymbol{x}_k)\,\mathrm{d}\boldsymbol{x}_k}{1 - r_{k|k-1}^{(j)} + r_{k|k-1}^{(j)} \int (1 - p_{\mathrm{D}}(\boldsymbol{x}'_k))\, f_{k|k-1}^{(j)}(\boldsymbol{x}'_k)\,\mathrm{d}\boldsymbol{x}'_k}\,, \tag{3.19}$$

$$f^{(j,0)}(\boldsymbol{x}_k) = \frac{(1 - p_{\mathrm{D}}(\boldsymbol{x}_k))\, f_{k|k-1}^{(j)}(\boldsymbol{x}_k)}{\int (1 - p_{\mathrm{D}}(\boldsymbol{x}'_k))\, f_{k|k-1}^{(j)}(\boldsymbol{x}'_k)\,\mathrm{d}\boldsymbol{x}'_k}\,. \tag{3.20}$$

Here, (3.19) is the probability that the object $\mathbf{x}_k$ described by the Bernoulli component with index j exists. Note that $r_k^{(j,0)} = 0$ would indicate that the corresponding object does not exist and $r_k^{(j,0)} = 1$ would indicate that the object exists but did not generate a measurement. If the object exists, its state $\mathbf{x}_k$ is distributed according to $f^{(j,0)}(\boldsymbol{x}_k)$ in (3.20). The likelihood of these two events (object nonexistence and object existence and misdetection) is quantified by the association weight $\beta_k^{(j,m)}$ in (3.18). There are also new Bernoulli components indexed by $j \in \{J_{k-1}+1, \dots, J_k\}$. We recall that here $a_k^{(j)} \in \{0, 1\}$. For $a_k^{(j)} = 1$, we have

$$\beta_k^{(j,1)} = \lambda_{\mathrm{C}}\big(\boldsymbol{z}_k^{(m)}\big) + \int f\big(\boldsymbol{z}_k^{(m)}|\boldsymbol{x}_k\big)\, p_{\mathrm{D}}(\boldsymbol{x}_k)\, \lambda_{k|k-1}^{\mathrm{U}}(\boldsymbol{x}_k)\,\mathrm{d}\boldsymbol{x}_k\,, \tag{3.21}$$

$$r_k^{(j,1)} = \frac{\int f\big(\boldsymbol{z}_k^{(m)}|\boldsymbol{x}_k\big)\, p_{\mathrm{D}}(\boldsymbol{x}_k)\, \lambda_{k|k-1}^{\mathrm{U}}(\boldsymbol{x}_k)\,\mathrm{d}\boldsymbol{x}_k}{\lambda_{\mathrm{C}}\big(\boldsymbol{z}_k^{(m)}\big) + \int f\big(\boldsymbol{z}_k^{(m)}|\boldsymbol{x}'_k\big)\, p_{\mathrm{D}}(\boldsymbol{x}'_k)\, \lambda_{k|k-1}^{\mathrm{U}}(\boldsymbol{x}'_k)\,\mathrm{d}\boldsymbol{x}'_k}\,, \tag{3.22}$$

$$f^{(j,1)}(\boldsymbol{x}_k) = \frac{f\big(\boldsymbol{z}_k^{(m)}|\boldsymbol{x}_k\big)\, p_{\mathrm{D}}(\boldsymbol{x}_k)\, \lambda_{k|k-1}^{\mathrm{U}}(\boldsymbol{x}_k)}{\int f\big(\boldsymbol{z}_k^{(m)}|\boldsymbol{x}'_k\big)\, p_{\mathrm{D}}(\boldsymbol{x}'_k)\, \lambda_{k|k-1}^{\mathrm{U}}(\boldsymbol{x}'_k)\,\mathrm{d}\boldsymbol{x}'_k}\,, \tag{3.23}$$

where the measurement index m is determined as $m = j - J_{k-1}$ with $j \in \{J_{k-1} + 1, \dots, J_k\}$. Here, $r_k^{(j,1)} = 0$ in (3.22) would indicate that the measurement $\mathbf{z}_k$ originated from clutter. On the other hand, $r_k^{(j,1)} = 1$ would indicate that the measurement $\mathbf{z}_k$ originated from an previously undetected object $\mathbf{x}_k$; its state is distributed according to $f^{(j,1)}(\boldsymbol{x}_k)$ in (3.23). The likelihood of these two events (originated by clutter or by an undetected object) is quantified by the association weight $\beta_k^{(j,1)}$ in (3.21). Finally, for $a_k^{(j)} = 0$, the association weights are $\beta_k^{(j,0)} = 1$, the existence probabilities are $r_k^{(j,0)} = 0$, and the spatial PDFs $f^{(j,0)}(\boldsymbol{x}_k)$ are not defined because $r_k^{(j,0)} = 0$ indicates that the corresponding object does not exist. Note that the derivation of the exact update step here is based on the likelihood function $f(Z_k|X_k)$ defined by the measurement model of Section 3.2.1.

The TOMB/P filter approximates the posterior MBM PDF $f^{\mathrm{D}}(X_k|Z_{1:k})$ in (3.13) by an MB PDF. This is achieved by first rewriting $p(\boldsymbol{a}_k)$ in (3.14) in terms of the extended association alphabet $\tilde{\mathcal{A}}_k$ that includes also inadmissible object-measurement associations $\boldsymbol{a}_k$ (i.e., a measurement may be associated with no object or with more than one object). In fact, for $\boldsymbol{a}_k \in \mathcal{A}_k$, $p(\boldsymbol{a}_k)$ is equal to (3.14) and for $\tilde{\mathcal{A}}_k \backslash \mathcal{A}_k$, $p(\boldsymbol{a}_k) = 0$. Next, the association PMF $p(\boldsymbol{a}_k)$ is approximated by the product of its marginals. That is,

$$p(\boldsymbol{a}_k) \approx \prod_{j=1}^{J_k} p(a_k^{(j)}), \quad \boldsymbol{a} \in \tilde{\mathcal{A}}_k, \tag{3.24}$$

with

$$p(a_k^{(j)}) \triangleq \sum_{\sim a_k^{(j)}} p(\boldsymbol{a}_k), \tag{3.25}$$

where the summation is over all $a_k^{(j')}$ with $j' \in \mathcal{J}_k \backslash \{j\}$ where $\mathcal{J}_k \triangleq \{1, \ldots, J_k\}$. The complexity of this summation is exponential in J_k and M_k; however, accurate approximations of $p(a_k^{(j)})$ can be efficiently calculated by using the belief propagation scheme of [Williams and Lau, 2014, Williams, 2015]. Substituting $\tilde{\mathcal{A}}_k$ for $\mathcal{A}_k$ in (3.13) and using (3.24) yields

$$\begin{aligned} f^{\mathrm{D}}(X_k|Z_{1:k}) &\approx \sum_{\boldsymbol{a}_k \in \tilde{\mathcal{A}}_k} \left(\prod_{j=1}^{J_k} p(a_k^{(j)}) \right) \sum_{\alpha \in \mathcal{P}_{J_k, n_k}} \prod_{j=1}^{J_k} f^{(j, a_k^{(j)})}(X_k^{(\alpha(j))}) \\ &\approx \sum_{\alpha \in \mathcal{P}_{J_k, n_k}} \prod_{j=1}^{J_k} \sum_{a_k^{(j)}=0}^{M_k} p(a_k^{(j)}) f^{(j, a_k^{(j)})}(X_k^{(\alpha(j))}) \\ &= \sum_{\alpha \in \mathcal{P}_{J_k, n_k}} \prod_{j=1}^{J_k} f^{(j)}(X_k^{(\alpha(j))}), \end{aligned} \tag{3.26}$$

where in the last step, the identity $\sum_{\boldsymbol{a}_k \in \tilde{\mathcal{A}}_k} \prod_{i=1}^{J_k} p(a_k^{(j)}) = \prod_{j=1}^{J_k} \sum_{a_k^{(j)}=0}^{M_k} p(a_k^{(j)})$ was used. Because $f^{(j)}(X_k^{(\alpha(j))}) \triangleq \sum_{a_k^{(j)}=0}^{M_k} p(a_k^{(j)}) f^{(j, a_k^{(j)})}(X_k^{(\alpha(j))})$ is a Bernoulli PDF, $f^{\mathrm{D}}(X_k|Z_{1:k})$ is approximated by an MB PDF (cf. (2.17)), consisting of $J_k = J_{k-1} + M_k$ Bernoulli components.

The approximate posterior MB PDF $f^{\mathrm{D}}(X_k|Z_{1:k})$ in (3.26) is characterized by the existence probabilities $r_k^{(j)}$ and spatial pdfs $f^{(j)}(\boldsymbol{x}_k)$, which are given for the legacy Bernoulli components, i.e., for $j \in \{1, \ldots, J_{k-1}\}$, by

$$r_k^{(j)} = \sum_{a_k^{(j)}=0}^{M_k} p(a_k^{(j)}) \, r_k^{(j, a_k^{(j)})}, \tag{3.27}$$

$$f^{(j)}(\boldsymbol{x}_k) = \frac{1}{r_k^{(j)}} \sum_{a_k^{(j)}=0}^{M_k} p(a_k^{(j)}) r_k^{(j,a_k^{(j)})} f^{(j,a_k^{(j)})}(\boldsymbol{x}_k), \tag{3.28}$$

and for the new Bernoulli components, i.e, for $j \in \{J_{k-1}+1, \dots, J_k\}$, by

$$r_k^{(j)} = p(a_k^{(j)} = 1)\, r_k^{(j,1)}, \tag{3.29}$$

$$f^{(j)}(\boldsymbol{x}_k) = f^{(j,1)}(\boldsymbol{x}_k). \tag{3.30}$$

In (3.27) and (3.28), the parameters $r_k^{(j,a_k^{(j)})}$ and $f^{(j,a_k^{(j)})}(\boldsymbol{x}_k)$ are given by (3.16), (3.17) and by (3.19), (3.20), respectively, and in (3.29) and (3.30), $r_k^{(j,1)}$ and $f^{(j,1)}(\boldsymbol{x}_k)$ are given by (3.22) and (3.23), respectively; $p(a_k^{(j)})$ are the marginal association probabilities given by (3.25).

The TOMB/P filter is now obtained by first applying the prediction step by computing the predicted posterior PHD of the undetected objects $\lambda^{\mathrm{U}}_{k|k-1}(\boldsymbol{x}_k)$ via (3.9) and, for the detected objects, the predicted existence probabilities $r_{k|k-1}^{(j)}$ via (3.10) and the predicted spatial PDFs $f_{k|k-1}^{(j)}(\boldsymbol{x}_k)$ via (3.11). The update step consists of calculating the posterior PHD of undetected objects $\lambda_{\mathrm{U}}(\boldsymbol{x}_k)$ via (3.12) and updating the detected object component as follows: first, the association weights, existence probabilities, and spatial PDFs are computed according to (3.15) – (3.23). Next, the marginal association probabilities are calculated according to (3.25). Note that an efficient (approximate) marginalization is enabled by the BP-based algorithm proposed in [Williams and Lau, 2014, Williams, 2015]. Finally, the updated existence probabilities $r_k^{(j)}$ and spatial PDFs $f^{(j)}(\boldsymbol{x}_k)$ are determined according to (3.27) – (3.30). An implementation of the TOMB/P filter for linear/Gaussian system models based on the representation of spatial distributions by Gaussian PDFs and/or Gaussian mixture PDFs was proposed in [Williams, 2015]. An extension to nonlinear/non-Gaussian system models using particle representations of spatial distributions was presented in [Kropfreiter et al., 2016].

The complexity of the TOMB/P filter is determined by the computation of the marginal association probabilities in (3.25), which is exponential in both the number of Bernoulli components J_k and the number of measurements M_k. However, an efficient approximate computation is enabled by BP-based algorithm [Williams, 2015]. With this modification, the complexity scaling of the TOMB/P filter can be lowered to $\mathcal{O}(IJ_kM_k)$, i.e., the complexity scales linearly in the number of BP iterations I, the number of Bernoulli components J_k, and the number of measurements M_k.

Since in each update step, M_k new Bernoulli components are generated, the number of Bernoulli components increases linearly with M_k over time. To reduce the complexity, a common strategy is to prune (discard) Bernoulli components with an existence probability below some defined threshold γ_{P}. However, the pruning can result in a reduced tracking accuracy. A remedy was proposed in [Williams, 2012], where Bernoulli components with a low existence probability are not pruned but instead transferred to the Poisson RFS. This transfer is referred to as recycling and the corresponding filter as TOMB/P with recycling (TOMB/P-R) filter. It was shown in [Williams, 2012] that the TOMB/P-R filter achieves a better tracking accuracy/complexity compromise than the conventional TOMB/P filter.

The TOMB/P filters presented here solely rely on unlabeled RFSs. Therefore, track continuity is theoretically impossible. However, trajectories can be formed by applying a simple, heuristic post-processing step. In addition, a label-augmented version of the TOMB/P filter was proposed in [Meyer et al., 2018] that avoids the post-processing step.

3.5 The LMB Filter

The LMB filter is an approximation of the (labeled) multi-object Bayes filter (cf. Section 3.1). In the LMB filter, the multi-object state at time k is modeled by an LMB RFS $\tilde{\mathsf{X}}_k$ (cf. Section 2.2.2). Thus, the posterior PDF at time $k-1$ is given by (cf. 2.24)

$$f(\tilde{X}_{k-1}|Z_{1:k-1}) = \Delta(\tilde{X}_{k-1})\, w\big(\mathcal{L}(\tilde{X}_{k-1})\big) \prod_{(\boldsymbol{x}_{k-1},l)\in\tilde{X}_{k-1}} 1_{\mathbb{L}^*_{k-1}}(l)\, f^{(l)}(\boldsymbol{x}_{k-1}). \tag{3.31}$$

Recap that $\Delta(\tilde{X}_{k-1})=1$ if the labels of $\tilde{X}_{k-1}$ are distinct and $\Delta(\tilde{X}_{k-1})=0$ otherwise, and $1_{\mathbb{L}^*_{k-1}}(l)=1$ if $l\in\mathbb{L}^*_{k-1}$ and $1_{\mathbb{L}^*_{k-1}}(l)=0$ otherwise. Here, the label set $\mathbb{L}^*_{k-1}\subset\mathbb{L}_{k-1}$ comprises the labels corresponding to $\tilde{\mathsf{X}}_{k-1}$ and is a subset of the underlying label space $\mathbb{L}_{k-1}$ (cf. Section 3.2.2). Furthermore, $f^{(l)}(\boldsymbol{x}_{k-1})$, $l\in\mathbb{L}^*_{k-1}$ denote the posterior spatial PDFs at time $k-1$ and the weights $w(L)$ are given according to (2.25) by

$$w(L) \triangleq \Bigg(\prod_{l\in L} 1_{\mathbb{L}^*_{k-1}}(l)\, r^{(l)}_{k-1}\Bigg) \prod_{l'\in\mathbb{L}^*_{k-1}\setminus L} \big(1-r^{(l')}_{k-1}\big), \tag{3.32}$$

for any $L\subseteq\mathbb{L}_{k-1}$. Here, $r^{(l)}_{k-1}$, $l\in\mathbb{L}^*_{k-1}$ denote the posterior existence probabilities at time $k-1$. By inserting (3.32) into (3.31), the LMB posterior PDF can be equivalently written as

$$\begin{aligned} &f(\tilde{X}_{k-1}|Z_{1:k-1}) \\ &\quad= \Delta(\tilde{X}_{k-1})\Bigg(\prod_{l'\in\mathbb{L}^*_{k-1}\setminus L} \big(1-r^{(l')}_{k-1}\big)\Bigg) \prod_{(\boldsymbol{x}_{k-1},l)\in\tilde{X}_{k-1}} 1_{\mathbb{L}^*_{k-1}}(l)\, r^{(l)}_{k-1} f^{(l)}(\boldsymbol{x}_{k-1}). \end{aligned} \tag{3.33}$$

Note that $f(\tilde{X}_{k-1}|Z_{1:k-1})$ is fully parametrized by $\{(r^{(l)}_{k-1}, f^{(l)}(\boldsymbol{x}_{k-1}))\}_{l\in\mathbb{L}^*_{k-1}}$. In the following, we review the prediction step and update step of the LMB filter [Reuter et al., 2014].

3.5.1 Prediction Step of the LMB Filter

In the prediction step, the previous posterior PDF $f(\tilde{X}_{k-1}|Z_{1:k-1})$ is converted into the predicted posterior PDF $f(\tilde{X}_k|Z_{1:k-1})$ according to (3.1). More precisely, as shown in [Reuter et al., 2014], the prediction step preserves the LMB form of $f(\tilde{X}_{k-1}|Z_{1:k-1})$ without applying any approximation. Hence, the predicted posterior PDF $f(\tilde{X}_k|Z_{1:k-1})$ is an LMB pdf and parametrized by the existence probabilities $r^{(l)}_{k|k-1}$ and spatial PDFs $f^{(l)}_{k|k-1}(\boldsymbol{x}_k)$, $l \in \mathbb{L}^*_{k-1}$, i.e, by the LMB parameter set $\big\{\big(r^{(l)}_{k|k-1}, f^{(l)}_{k|k-1}(\boldsymbol{x}_k)\big)\big\}_{l\in\mathbb{L}^*_k}$. Here, $\mathbb{L}^*_k = \mathbb{L}^*_{k-1} \cup \mathbb{L}^{\mathrm{B}*}_k$ is the label set corresponding to the predicted posterior LMB PDF $f(\tilde{X}_k|Z_{1:k-1})$. It is the union of the sets $\mathbb{L}^*_{k-1}$ and $\mathbb{L}^{\mathrm{B}*}_k$ containing the labels of the survived objects and the newborn objects, respectively (cf. Section 3.2.2). The existence probabilities and spatial PDFS can be found for $l \in \mathbb{L}^*_{k-1}$ as [Reuter et al., 2014]

$$r^{(l)}_{k|k-1} = r^{(l)}_{k-1} \int p_{\mathrm{S}}(\boldsymbol{x}_{k-1}, l)\, f^{(l)}(\boldsymbol{x}_{k-1})\, \mathrm{d}\boldsymbol{x}_{k-1}, \tag{3.34}$$

$$f^{(l)}_{k|k-1}(\boldsymbol{x}_k) = \frac{\int f(\boldsymbol{x}_k|\boldsymbol{x}_{k-1}, l)\, p_{\mathrm{S}}(\boldsymbol{x}_{k-1}, l)\, f^{(l)}(\boldsymbol{x}_{k-1})\, \mathrm{d}\boldsymbol{x}_{k-1}}{\int p_{\mathrm{S}}(\boldsymbol{x}'_{k-1}, l)\, f^{(l)}(\boldsymbol{x}'_{k-1})\, \mathrm{d}\boldsymbol{x}'_{k-1}}. \tag{3.35}$$

Here, $f(\boldsymbol{x}_k|\boldsymbol{x}_{k-1}, l)$ and $p_{\mathrm{S}}(\boldsymbol{x}_{k-1}, l)$ are the single-object state transition PDF and the survival probability introduced in Section 3.2.2, respectively, and $r^{(l)}_{k-1}$ and $f^{(l)}(\boldsymbol{x}_{k-1})$ are the posterior existence probabilities and spatial PDFs at time $k-1$. Furthermore, for $l \in \mathbb{L}^{\mathrm{B}*}_k$, we have

$$r^{(l)}_{k|k-1} = r^{(l)}_{\mathrm{B},k}, \tag{3.36}$$

$$f^{(l)}_{k|k-1}(\boldsymbol{x}_k) = f^{(l)}_{\mathrm{B}}(\boldsymbol{x}_k), \tag{3.37}$$

where the existence probabilities $r^{(l)}_{\mathrm{B},k}$ and spatial PDFs $f^{(l)}_{\mathrm{B}}(\boldsymbol{x}_k)$ were introduced in Section 3.2.2. Hence, the LMB filter generates new Bernoulli components according to the underlying LMB birth model described in Section 3.2.2. Note that the prediction relations of the survived objects in (3.34) and (3.35) are equal to the prediction relations of the detected objects in the TOMB/P filter (cf. (3.10) and (3.11)), with the extension that the labels allow object identification over time. The derivation of the prediction step of the LMB filter relies on the state transition PDF $f(\tilde{X}_k|\tilde{X}_{k-1})$ defined by the state transition model described in Section 3.2.2. An expression of $f(\tilde{X}_k|\tilde{X}_{k-1})$ can be found in [Mahler, 2014].

3.5.2 Update Step of the LMB Filter

The update step of the LMB filter converts the predicted posterior PDF $f(\tilde{X}_k|Z_{1:k-1})$ into the current posterior PDF $f(\tilde{X}_k|Z_{1:k})$. However, after applying the update step, the posterior PDF is no longer of LMB form but of GLBM form (cf. Section 2.2.4). To describe the posterior GLMB PDF, an object-measurement mapping is introduced first [Reuter et al., 2014]. More precisely, the mapping θ_k is defined as $\theta_k : L \to \{0, 1, \dots, M_k\}$ with $L \in \mathcal{F}(\mathbb{L}_k^*)$, where $\mathcal{F}(\mathbb{L}_k^*)$ is the power set of $\mathbb{L}_k^*$, i.e., the set of all subsets of $\mathbb{L}_k^*$. Here, $\theta_k(l) = m \in \mathcal{M}_k$ with $\mathcal{M}_k = \{1, \dots, M_k\}$ indicates that object state $(\mathbf{x}_k, l)$ is associated with measurement m and $\theta_k(l) = 0$ indicates that it is not associated with any measurement. Let Θ_L denote the set of all mappings θ_k that describe admissible associations, i.e., at most one measurement is associated to the same labeled object and no measurement is associated to more than one labeled object. Note that this definition of admissibility is similar to that one in the TOMB/P filter, where it is phrased in terms of an association vector associating (unlabeled) detected objects instead of labeled objects. Using θ_k, the posterior GLMB PDF $f(\tilde{X}_k|Z_{1:k})$ can be expressed as (cf. (2.31))

$$f(\tilde{X}_k|Z_{1:k}) = \Delta(\tilde{X}_k) \sum_{L\in\mathcal{F}(\mathbb{L}_k^*)} \sum_{\theta_k\in\Theta_L} w^{(L,\theta_k)}\, \delta_L(\mathcal{L}(\tilde{X}_k)) \prod_{(\boldsymbol{x}_k,l)\in\tilde{X}_k} f^{(l,\theta_k(l))}(\boldsymbol{x}_k)\,. \tag{3.38}$$

Recap that $\delta_L(\mathcal{L}(\tilde{X}_k))$ is one if $L = \mathcal{L}(\tilde{X}_k)$ and zero otherwise. Further, the weights $w^{(L,\theta_k)}$ are given up to a normalization constant by

$$w^{(L,\theta_k)} \propto \left(\prod_{l'\in\mathbb{L}_k^*\setminus L} \big(1 - r_{k|k-1}^{(l')}\big) \right) \prod_{l\in L} r_{k|k-1}^{(l)}\, \eta^{(l,\theta_k(l))}, \tag{3.39}$$

for $L \in \mathcal{F}(\mathbb{L}_k^*)$. Here, the weights $w^{(L,\theta_k)}$ are normalized, i.e., $\sum_{L\in\mathcal{F}(\mathbb{L}_k^*)} \sum_{\theta_k\in\Theta_L} w^{(L,\theta_k)} = 1$, $r_{k|k-1}^{(l)}$ is the predicted existence probabilities computed according to (3.34) and (3.36), and the factors $\eta^{(l,\theta_k(l))}$ are given by

$$\eta_k^{(l,m)} = \begin{cases} \int \big(1 - p_{\mathrm{D}}(\boldsymbol{x}_k, l)\big) f_{k|k-1}^{(l)}(\boldsymbol{x}_k)\, \mathrm{d}\boldsymbol{x}_k\,, & m = 0 \\ \int f(\boldsymbol{z}_k^{(m)}|\boldsymbol{x}_k, l)\, p_{\mathrm{D}}(\boldsymbol{x}_k, l)\, f_{k|k-1}^{(l)}(\boldsymbol{x}_k)\, \mathrm{d}\boldsymbol{x}_k / \lambda_{\mathrm{C}}(\boldsymbol{z}_k^{(m)}), & m \in \mathcal{M}_k\,. \end{cases} \tag{3.40}$$

Here, $p_{\mathrm{D}}(\boldsymbol{x}_k, l)$, $f(\boldsymbol{z}_k^{(m)}|\boldsymbol{x}_k, l)$, and $\lambda_{\mathrm{C}}(\boldsymbol{z}_k^{(m)})$ are the detection probability, the single-object likelihood function, and the clutter PHD, respectively, defined in Section 3.2.2, and $f_{k|k-1}^{(l)}(\boldsymbol{x}_k)$ is the predicted spatial PDF computed according to (3.35) and (3.37). Next, the spatial PDFs $f^{(l,m)}(\boldsymbol{x}_k)$ in (3.38) are given for $m = 0$ by

$$f^{(l,0)}(\boldsymbol{x}_k) = \frac{\big(1 - p_{\mathrm{D}}(\boldsymbol{x}_k, l)\big) f_{k|k-1}^{(l)}(\boldsymbol{x}_k)}{\int \big(1 - p_{\mathrm{D}}(\boldsymbol{x}'_k, l)\big) f_{k|k-1}^{(l)}(\boldsymbol{x}'_k)\, \mathrm{d}\boldsymbol{x}'_k}\,, \tag{3.41}$$

and for $m \in \mathcal{M}_k$ by

$$f^{(l,m)}(\boldsymbol{x}_k) = \frac{f(\boldsymbol{z}_k^{(m)}|\boldsymbol{x}_k, l)\, p_{\mathrm{D}}(\boldsymbol{x}_k, l)\, f_{k|k-1}^{(l)}(\boldsymbol{x}_k)}{\int f(\boldsymbol{z}_k^{(m)}|\boldsymbol{x}'_k, l)\, p_{\mathrm{D}}(\boldsymbol{x}'_k, l)\, f_{k|k-1}^{(l)}(\boldsymbol{x}'_k)\, \mathrm{d}\boldsymbol{x}'_k}\,. \tag{3.42}$$

Note that (3.41) is the spatial PDF describing the case that the object with state $(\mathbf{x}_k, l)$ generated no measurement (misdetection) and (3.42) that it generated measurement $m \in \mathcal{M}_k$. In fact, the two relations coincide with the spatial PDFs for detected objects (3.20) and (3.17) in the TOMB/P filter, with the extension that here the labels allow object identification over time. The derivation of the exact update step of the LMB filter relies on the likelihood function $f(Z_k|\tilde{X}_k)$ defined by the measurement model described in Section 3.2.2. A specific expression of $f(Z_k|\tilde{X}_k)$ can be found in [Mahler, 2014].

In the LMB filter [Reuter et al., 2014], the posterior GLMB PDF $f(\tilde{X}_k|Z_{1:k})$ in (3.38) is approximated by an LMB PDF such that the PHD corresponding to the exact posterior PDF (cf. (2.32)) matches the PHD corresponding to an LMB PDF (cf. (2.27)). This leads to a update relation for the existence probabilities

$$r_k^{(l)} = \sum_{L \in \mathcal{F}(\mathbb{L}_k^*)} \sum_{\theta_k \in \Theta_L} 1_L(l)\, w^{(L,\theta_k)}, \tag{3.43}$$

and for the spatial PDFs

$$f^{(l)}(\boldsymbol{x}_k) = \frac{1}{r_k^{(l)}} \sum_{L \in \mathcal{F}(\mathbb{L}_k^*)} \sum_{\theta_k \in \Theta_L} 1_L(l)\, w^{(L,\theta_k)} f^{(l,\theta_k(l))}(\boldsymbol{x}_k), \tag{3.44}$$

for $l \in \mathbb{L}_k^*$. Here, $1_L(l)$ is 1 if $l \in L$ and 0 otherwise.

The LMB filter is now obtained by first performing a prediction step in which the predicted existence probabilities $r_{k|k-1}^{(l)}$ are computed according to (3.34) and (3.36) and the predicted spatial PDFs $f_{k|k-1}^{(l)}(\boldsymbol{x}_k)$ according to (3.35) and (3.37) for $l \in \mathbb{L}_k^*$. Note that this involves both the prediction of already existing (legacy) Bernoulli components (representing survived objects with labels $l \in \mathbb{L}_{k-1}^*$) and the generation of new Bernoulli components (representing newborn objects with labels $l \in \mathbb{L}_k^{B*}$). Then, the update step is executed by first computing the weights $w^{(L,\theta_k)}$ in (3.39) and the spatial PDFs $f^{(l,\theta_k(l))}(\boldsymbol{x}_k)$ in (3.41) and (3.42), and then computing the updated existence probabilities $r_k^{(l)}$ and spatial PDFs $f^{(l)}(\boldsymbol{x}_k)$ according to (3.43) and (3.44). The LMB filter can be implemented for both linear/Gaussian system models using Gaussian or Gaussian mixture representations of the spatial PDFs and nonlinear/non-Gaussian system models using particle representations of the spatial PDFs [Reuter et al., 2014].

The complexity of the final update equations in (3.43) and (3.44) scales exponentially in the number of Bernoulli components $|\mathbb{L}_k^*|$ and the number of measurements M_k. By reducing the number of summation terms by means of a k-shortest path algorithm [Eppstein, 1998] and a ranked assignment algorithm [Jonker and A, 1987], a complexity of $\mathcal{O}(KC^3)$ with $C = \max\{|\mathbb{L}_k^*|, M_k\}$ can be obtained [Vo et al., 2014]. Here, K denotes the number of highest weights of the ranked assignment algorithm. The complexity can be further reduced by using a Gibbs sampler-based approach to reduce the number of summation terms [Reuter et al., 2017]. This leads to a complexity of $\mathcal{O}(P|\mathbb{L}_k^*|^2 M_k)$, where P

is the number of samples used in the Gibbs sampler and, as before, $|\mathbb{L}_k^*|$ and M_k are the numbers of Bernoulli components and measurements, respectively. An LMB filter with only linear complexity will be proposed in Chapter 4.

Chapter 4

A Fast LMB Filter Using Belief Propagation for Probabilistic Data Association

In this chapter, we propose a new LMB filter with low complexity yet excellent tracking accuracy. The derivation of the new LMB filter is based on a new derivation of the original LMB filter. More precisely, the GLMB posterior PDF arising in the original LMB filter is reformulated in terms of a joint object-measurement association PMF, and an LMB approximation to the GLMB posterior PDF is obtained by approximating this association PMF by the product of its marginals. Because an exact marginalization is only feasible for simple problems with a low number of Bernoulli components and measurements, we perform an efficient approximate marginalization by using a BP-based computation. The resulting BP-based LMB filter possesses a complexity scaling that is only linear in the number of Bernoulli components and the number of measurements (assuming a fixed number of BP iterations). Contrary to conventional LMB filter implementations using a ranked assignment algorithm or the Gibbs sampler, our BP-based LMB filter avoids the pruning of GLMB components in the update step. This preserves valuable association information that would otherwise be discarded. Since association information is especially helpful in more challenging tracking scenarios, the proposed LMB filter performs particularly well in scenarios with, e.g., a low detection probability.

The remainder of this chapter is structured as follows. In Section 4.1, we present a new derivation of the original LMB filter. A fast BP-based algorithm for computing approximate marginal object-measurement association probabilities is proposed in Section 4.2. In Section 4.3, we present the new fast LMB filter, including a scheme for the generation of new Bernoulli components, and we provide a complexity analysis. Finally, in Section 4.4, we present simulation results analyzing the accuracy of the BP-based marginalization and demonstrating the advantages of the proposed fast LMB filter compared to state-of-the-art multi-object tracking methods.

4.1 A New Derivation of the LMB Filter

In the following, we present a new derivation of the original LMB filter of [Reuter et al., 2014]. More precisely, we first show that the LMB filter can be derived by reformulating the GLMB posterior PDF in (3.38) in terms of a joint object-measurement association PMF and approximating this PMF by the product of its marginals. Note that a similar approach is used in the TOMB/P filter in order to approximate the (unlabeled) MBM posterior PDF by an MB PDF (cf. Section 3.4.2).

Recap from Section 3.5.2 that in the LMB filter, the GLMB posterior PDF is given according to (3.38) as

$$f(\tilde{X}_k|Z_{1:k}) = \Delta(\tilde{X}_k) \sum_{L\in\mathcal{F}(\mathbb{L}_k^*)} \sum_{\theta_k\in\Theta_L} w^{(L,\theta_k)}\, \delta_L(\mathcal{L}(\tilde{X}_k)) \prod_{(\boldsymbol{x}_k,l)\in\tilde{X}_k} f^{(l,\theta_k(l))}(\boldsymbol{x}_k), \tag{4.1}$$

where $\mathbb{L}_k^*$ is the set of labels underlying $\tilde{\mathsf{X}}_k$, $\mathcal{F}(\mathbb{L}_k^*)$ is the power set, i.e., the set of all subsets, of $\mathbb{L}_k^*$, θ_k and Θ_L are the association mapping and the set of all admissible association mappings with respect to the label set L, respectively, $w^{(L,\theta_k)}$ are the weights given by (3.39), and $f^{(l,\theta_k(l))}(\boldsymbol{x}_k)$ are the spatial PDFs given by (3.41) and (3.42). We can now rewrite the posterior PDF (4.1) as

$$f(\tilde{X}_k|Z_{1:k}) = \Delta(\tilde{X}_k) \sum_{\theta_k\in\Theta_{\mathcal{L}(\tilde{X}_k)}} w^{(\mathcal{L}(\tilde{X}_k),\theta_k)} \prod_{(\boldsymbol{x}_k,l)\in\tilde{X}_k} 1_{\mathbb{L}_k^*}(l)\, f^{(l,\theta_k(l))}(\boldsymbol{x}_k). \tag{4.2}$$

In (4.1), the factor $\delta_L(\mathcal{L}(\tilde{X}_k))$ with $L \in \mathcal{F}(\mathbb{L}_k^*)$ ensures that the labels of the realization $\tilde{X}_k$, i.e., $l \in \mathcal{L}(\tilde{X}_k)$, are from the set $\mathbb{L}_k^*$; this is now equivalently expressed by $\prod_{(\boldsymbol{x}_k,l)\in\tilde{X}_k} 1_{\mathbb{L}_k^*}(l)$. Next, instead of using the mapping θ_k to describe the object-measurement associations [Reuter et al., 2014,Reuter et al., 2017], we now introduce the fully equivalent association vector $\mathbf{c}_k$ and the corresponding association alphabet $\mathcal{C}_k$. The description in terms of association vectors can be leveraged to derive the LMB filter alternatively in terms of marginal association probabilities. In fact, we define the association vector $\mathbf{c}_k$ with elements $\mathsf{c}_k^{(l)} \in \{-1, 0, \ldots, M_k\}$, where $l \in \mathbb{L}_k^*$. Here, $\mathsf{c}_k^{(l)} = m \in \mathcal{M}_k$ indicates that object state $(\boldsymbol{x}_k, l)$ is associated with measurement m, $\mathsf{c}_k^{(l)} = 0$ indicates that it is not associated with any measurement (misdetection), and $\mathsf{c}_k^{(l)} = -1$ indicates that it does not exist, i.e., $(\boldsymbol{x}_k, l) \notin \tilde{X}_k$. Let $\mathcal{C}_k$ denote the set of admissible association vectors $\boldsymbol{c}_k$. Just as an admissible mapping θ_k in Section 3.5.2, an admissible association vector $\boldsymbol{c}_k$ assigns at most one measurement to the same object and no measurement to more than one object. We can now rewrite the GLMB PDF (4.2) in terms of the association vector $\mathbf{c}_k$ as

$$f(\tilde{X}_k|Z_{1:k}) = \Delta(\tilde{X}_k) \sum_{\boldsymbol{c}_k \in \mathcal{C}_k} \varphi(\boldsymbol{c}_k, \tilde{X}_k)\, w_{\boldsymbol{c}_k} \prod_{(\boldsymbol{x}_k,l)\in \tilde{X}_k} 1_{\mathbb{L}_k^*}(l)\, f^{(l,c_k^{(l)})}(\boldsymbol{x}_k)\,. \tag{4.3}$$

Here, $\varphi(\boldsymbol{c}_k, \tilde{X}_k) = 1$ for all $\boldsymbol{c}_k$ with $c_k^{(l)} = -1$ for $l \in \mathbb{L}_k^* \setminus \mathcal{L}(\tilde{X}_k)$ and $c_k^{(l)} \in \{0,\dots,M_k\}$ for $l \in \mathcal{L}(X_k)$, and $\varphi(\boldsymbol{c}_k, \tilde{X}_k) = 0$ otherwise; this factor reduces the sum over all $\boldsymbol{c}_k \in \mathcal{C}_k$ in (4.3) to the sum over all corresponding mappings $\theta_k \in \Theta_{\mathcal{L}(\tilde{X}_k)}$ in (4.2). Hence, both expressions are equivalent. Furthermore, the weights $w_{\boldsymbol{c}_k}$ in (4.3) can be expressed up to a normalization factor as (cf. (3.39))

$$w_{\boldsymbol{c}_k} \propto \prod_{l\in\mathbb{L}_k^*} \beta_k^{(l,c_k^{(l)})}, \quad \boldsymbol{c}_k \in \mathcal{C}_k\,, \tag{4.4}$$

where the association weights $\beta_k^{(l,m)}$ are defined as

$$\beta_k^{(l,m)} \triangleq \begin{cases} r_{k|k-1}^{(l)}\,\eta^{(l,m)}, & m \in \{0,\dots,M_k\} \\ 1 - r_{k|k-1}^{(l)}, & m = -1, \end{cases} \tag{4.5}$$

with $\eta^{(l,m)}$ given by (3.40). Finally, $f^{(l,c_k^{(l)})}(\boldsymbol{x}_k)$ in (4.3) equals $f^{(l,\theta_k(l))}(\boldsymbol{x}_k)$ in (3.41) and (3.42) (with $\theta_k(l)$ replaced by $c_k^{(l)}$) because $f^{(l,-1)}(\boldsymbol{x}_k)$ does not occur in (4.3) (recall that $c_k^{(l)} = -1$ implies $(\boldsymbol{x}_k, l) \notin \tilde{X}_k$). In contrast to the weights $w^{(L,\theta_k)}$ in (4.1), the weights $w_{\boldsymbol{c}_k}$ do not depend on the label set $\mathcal{L}(\tilde{X}_k)$. They are normalized in that $\sum_{\boldsymbol{c}_k\in\mathcal{C}_k} w_{\boldsymbol{c}_k} = 1$. Expressions (3.43) and (3.44) can now be reformulated in terms of $\boldsymbol{c}_k$ as

$$r_k^{(l)} = \sum_{\boldsymbol{c}_k \in \mathcal{C}_k^{(l)}} w_{\boldsymbol{c}_k}\,, \tag{4.6}$$

$$f^{(l)}(\boldsymbol{x}_k) = \frac{1}{r_k^{(l)}} \sum_{\boldsymbol{c}_k \in \mathcal{C}_k^{(l)}} w_{\boldsymbol{c}_k}\, f^{(l,c_k^{(l)})}(\boldsymbol{x}_k)\,, \tag{4.7}$$

where $\mathcal{C}_k^{(l)} \triangleq \{\boldsymbol{c}_k \in \mathcal{C}_k : c_k^{(l)} \in \{0,\dots,M_k\}\}$. This reformulation is possible because $r_k^{(l)}$ in (3.43) and $f^{(l)}(\boldsymbol{x}_k)$ in (3.44) contain only terms involving $w^{(L,\theta_k)}$ with L such that $l \in L$; this can be equivalently expressed via $\boldsymbol{c}_k$ by removing all $\boldsymbol{c}_k$ with $c_k^{(l)} = -1$ from $\mathcal{C}_k$, which results in $\mathcal{C}_k^{(l)}$.

With this reformulation, we can interpret the weights $w_{\boldsymbol{c}_k}$ as the PMF of the association vector $\mathbf{c}_k$. More precisely, we define the PMF of $\mathbf{c}_k$ as

$$p(\boldsymbol{c}_k) \triangleq \begin{cases} w_{\boldsymbol{c}_k}, & \boldsymbol{c}_k \in \mathcal{C}_k \\ 0, & \text{otherwise}. \end{cases} \tag{4.8}$$

We can then rewrite (4.3) as

$$f(\tilde{X}_k|Z_{1:k}) = \Delta(\tilde{X}_k) \sum_{\boldsymbol{c}_k \in \bar{\mathcal{M}}_k^{|\mathbb{L}_k^*|}} \varphi(\boldsymbol{c}_k, \tilde{X}_k)\, p(\boldsymbol{c}_k) \prod_{(\boldsymbol{x}_k, l) \in \tilde{X}_k} 1_{\mathbb{L}_k^*}(l)\, f^{(l, c_k^{(l)})}(\boldsymbol{x}_k), \tag{4.9}$$

with $\bar{\mathcal{M}}_k \triangleq \{-1, 0, \ldots, M_k\}$. Note that $\sum_{\boldsymbol{c}_k \in \mathcal{C}_k}$ in (4.3) can be replaced by $\sum_{\boldsymbol{c}_k \in \bar{\mathcal{M}}_k^{|\mathbb{L}_k^*|}}$, since $p(\boldsymbol{c}_k) = 0$ for $\boldsymbol{c}_k \in \bar{\mathcal{M}}_k^{|\mathbb{L}_k^*|} \setminus \mathcal{C}_k$. Next, we approximate the joint association PMF $p(\boldsymbol{c}_k)$ by the product of its marginals, i.e.,

$$p(\boldsymbol{c}_k) \approx \prod_{l \in \mathbb{L}_k^*} p(c_k^{(l)}), \quad \boldsymbol{c}_k \in \bar{\mathcal{M}}_k^{|\mathbb{L}_k^*|}, \tag{4.10}$$

where

$$p(c_k^{(l)}) = \sum_{\boldsymbol{c}_k^{\sim l} \in \bar{\mathcal{M}}_k^{|\mathbb{L}_k^*|-1}} p(\boldsymbol{c}_k). \tag{4.11}$$

(Here, $\boldsymbol{c}_k^{\sim l}$ denotes the vector $\boldsymbol{c}_k$ with the l^{th} component, i.e., $c_k^{(l)}$, removed.) Inserting (4.10) into (4.9) yields

$$f(\tilde{X}_k|Z_{1:k}) \approx \Delta(\tilde{X}_k) \sum_{\boldsymbol{c}_k \in \bar{\mathcal{M}}_k^{|\mathbb{L}_k^*|}} \left(\prod_{l' \in \mathbb{L}_k^*} p(c_k^{(l')}) \right) \varphi(\boldsymbol{c}_k, \tilde{X}_k) \prod_{(\boldsymbol{x}_k, l) \in \tilde{X}_k} 1_{\mathbb{L}_k^*}(l)\, f^{(l, c_k^{(l)})}(\boldsymbol{x}_k).$$

Next, splitting $\prod_{l' \in \mathbb{L}_k^*} p(c_k^{(l')})$ as $\left(\prod_{l' \in \mathbb{L}_k^* \setminus \mathcal{L}(\tilde{X}_k)} p(c_k^{(l')})\right) \prod_{l \in \mathcal{L}(\tilde{X}_k)} p(c_k^{(l)})$, using the identity $\sum_{\boldsymbol{c}_k \in \bar{\mathcal{M}}_k^{|\mathbb{L}_k^*|}} = \sum_{c_k^{(1)} \in \bar{\mathcal{M}}_k} \cdots \sum_{c_k^{(|\mathbb{L}_k^*|)} \in \bar{\mathcal{M}}_k}$, and evaluating $\varphi(\boldsymbol{c}_k, \tilde{X}_k)$ leads to

$$f(\tilde{X}_k|Z_{1:k}) \approx \Delta(\tilde{X}_k) \prod_{l' \in \mathbb{L}_k^* \setminus \mathcal{L}(\tilde{X}_k)} p(c_k^{(l')} = -1) \prod_{(\boldsymbol{x}_k, l) \in \tilde{X}_k} 1_{\mathbb{L}_k^*}(l) \sum_{c_k^{(l)}=0}^{M_k} p(c_k^{(l)})\, f^{(l, c_k^{(l)})}(\boldsymbol{x}_k). \tag{4.12}$$

Comparing expression (4.12) with (3.33), we conclude that the above approximation of $f(\tilde{X}_k|Z_{1:k})$ is an LMB PDF with existence probabilities

$$r_k^{(l)} = 1 - p(c_k^{(l)} = -1) = \sum_{c_k^{(l)}=0}^{M_k} p(c_k^{(l)}) \tag{4.13}$$

and spatial PDFs

$$f^{(l)}(\boldsymbol{x}_k) = \frac{1}{r_k^{(l)}} \sum_{c_k^{(l)}=0}^{M_k} p(c_k^{(l)})\, f^{(l, c_k^{(l)})}(\boldsymbol{x}_k). \tag{4.14}$$

Finally, we show that (4.13) and (4.14) are identical to (3.43) and (3.44), respectively. Inserting (4.11) into (4.13), we obtain

$$r_k^{(l)} = \sum_{c_k^{(l)}=0}^{M_k} \sum_{\boldsymbol{c}_k^{\sim l} \in \mathcal{M}_k^{|\mathbb{L}_k^*|-1}} p(\boldsymbol{c}_k) = \sum_{\boldsymbol{c}_k \in \mathcal{C}_k^{(l)}} w_{\boldsymbol{c}_k},$$

where the last expression follows because $p(\boldsymbol{c}_k)$ equals $w_{\boldsymbol{c}_k}$ for $\boldsymbol{c}_k \in \mathcal{C}_k$ and 0 otherwise. Thus, (4.13) is identical to (4.6) and, hence, to (3.43). Similarly, it can be verified that (4.14) is identical to (4.7) and, hence, to (3.44). This shows that our LMB approximation (4.12) of the GLMB posterior PDF $f(\tilde{X}_k|Z_{1:k})$ in (3.38) and (4.1) is equivalent to the LMB approximation underlying the original LMB filter [Reuter et al., 2014].

4.2 Fast BP-based Probabilistic Data Association

In the following section, we briefly review the general framework of factor graphs and BP [Kschischang et al., 2001] (Section 4.2.1) and derive a fast BP-based algorithm for computing approximations of the marginal association probabilities $p(c_k^{(l)})$ (Sections 4.2.2 and 4.2.3), which forms the basis for the fast BP-based LMB filter proposed in the next section.

4.2.1 Review of Belief Propagation

Consider J discrete random variables c_j, $j = 1, \dots, J$. We want to calculate the marginal PMFs $p(c_j)$ from the joint PMF $p(\boldsymbol{c})$ with $\mathbf{c} = [\mathsf{c}_1 \cdots \mathsf{c}_J]^{\mathrm{T}}$. However, often a direct marginalization is computationally infeasible.

Using BP (or, equivalently, the sum-product algorithm [Kschischang et al., 2001]), the marginalizations yielding the PMFs $p(c_j)$, $j = 1, \dots, J$ can be efficiently performed (at least approximately) if $p(\boldsymbol{c})$ factorizes according to

$$p(\boldsymbol{c}) \propto \prod_{q=1}^{Q} \psi_q(\boldsymbol{c}^{(q)}). \tag{4.15}$$

Here, each argument $\boldsymbol{c}^{(q)}$ comprises certain variables c_j. The factorization (4.15) can be represented by a factor graph, in which each variable c_j is represented by a variable node, each factor $\psi_q(\cdot)$ is represented by a factor node, and variable node "c_j" and factor node "ψ_q" are adjacent, i.e., connected by an edge, if the variable c_j is an argument of the factor $\psi_q(\cdot)$, i.e., part of $\boldsymbol{c}^{(q)}$. Figure 4.1 considers the case where $\mathbf{c} = [\mathsf{c}_1\ \mathsf{c}_2]^{\mathrm{T}}$ and shows the factor graph representing the factorization

$$p(\boldsymbol{c}) \propto \psi_1(c_1)\psi_2(c_1, c_2)\psi_3(c_2).$$

BP is a message passing algorithm where each node in the factor graph passes messages to the adjacent nodes. More specifically, consider a variable node "c_j" and an adjacent factor node "ψ_q", i.e., the variable c_j is part of the argument $\boldsymbol{c}^{(q)}$ of $\psi_q(\boldsymbol{c}^{(q)})$. Then, the

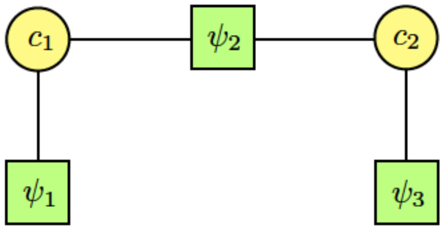

Figure 4.1: Factor graph representing the factorization of the PMF $p(\boldsymbol{c}) \propto \psi_1(c_1)\psi_2(c_1, c_2)\psi_3(c_2)$, with $\mathbf{c} = [c_1\ c_2]^{\mathrm{T}}$. Variable nodes are depicted as circles and factor nodes as squares.

message passed from factor node "ψ_q" to variable node "c_j" is given by

$$\phi^{(\psi_q \to c_j)}(c_j) = \sum_{\boldsymbol{c}^{\sim j}} \psi_q(\boldsymbol{c}^{(q)}) \prod_{j' \in \mathcal{J}_q \backslash \{j\}} \eta^{(c_{j'} \to \psi_q)}(c_{j'}), \tag{4.16}$$

where $\mathcal{J}_q$ denotes the neighborhood set of factor node "ψ_q", i.e., the set of indices j of all variable nodes "c_j" that are adjacent to factor node "ψ_q", $\sum_{\boldsymbol{c}^{\sim j}}$ denotes summation with respect to all variables $c_{j'}$, $j' \in \mathcal{J}_q$ except c_j, and $\eta^{(c_{j'} \to \psi_q)}(c_{j'})$ is the message passed from variable node "$c_{j'}$" to factor node "ψ_q" (to be explained presently). For example, the message passed from factor node "ψ_2" to variable node "c_2" in Figure 4.1 is $\phi^{(\psi_2 \to c_2)}(c_2) = \sum_{c_1} \psi_2(c_1, c_2)\eta^{(c_1 \to \psi_2)}(c_1)$. The message $\eta^{(c_j \to \psi_q)}(c_j)$ passed from variable node "c_j" to factor node "ψ_q" is given by the product of the messages passed to variable node "c_j" from all adjacent factor nodes except "ψ_q", i.e.,

$$\eta^{(c_j \to \psi_q)}(c_j) = \prod_{q' \in \mathcal{Q}_j \backslash \{q\}} \phi^{(\psi_{q'} \to c_j)}(c_j), \tag{4.17}$$

where the neighborhood set $\mathcal{Q}_j$ comprises the set of indices q of all factor nodes "ψ_q" that are adjacent to variable node "c_j". For example, in Figure 4.1, the message passed from variable node "c_2" to factor node "ψ_3" is $\eta^{(c_2 \to \psi_3)}(c_2) = \phi^{(\psi_2 \to c_2)}(c_2)$. This message passing process is started at variable nodes with only one edge, which pass a constant message, and/or factor nodes with only one edge, which pass the corresponding factor. We note that BP can also be applied problems with continuous random variables; the only difference is that in (4.16) the sum is replaced with an integration operator.

When all messages have been passed as described above, then for each variable node "c_j", a belief $\tilde{p}(c_j)$ is computed as the product of all incoming messages (passed from all adjacent factor nodes) followed by a normalization, i.e, $\sum_{c_j} \tilde{p}(c_j) = 1$. For example, in Figure 4.1,

$$\tilde{p}(c_2) \propto \phi^{(\psi_2 \to c_2)}(c_2)\phi^{(\psi_3 \to c_2)}(c_2).$$

If the factor graph is a tree, then the obtained belief $\tilde{p}(c_j)$ is exactly equal to the marginal PMF $p(c_j)$. On the other hand, if the factor graph contains cycles (loops), BP is usually applied in an iterative manner, and the beliefs $\tilde{p}(c_j)$ are only approximations of the respective marginal PMFs $p(c_j)$. In these iterative "loopy BP" schemes, there is no canonical order in which the messages should be calculated, and different orders may lead to different beliefs.

4.2.2 BP-based Computation of the Marginal Association Probabilities

We now derive a fast BP-based algorithm for calculating approximations of the marginal association probabilities $p(c_k^{(l)})$, $l \in \mathbb{L}_k^*$ involved in the update relations (4.13) and (4.14). This algorithm is a variant[1] of the BP scheme for probabilistic data association proposed in [Williams and Lau, 2014]. We recall that according to (4.8) $\boldsymbol{c}_k \in \bar{\mathcal{M}}_k^{|\mathbb{L}_k^*|}$ and, further, that $p(\boldsymbol{c}_k) = w_{\boldsymbol{c}_k}$ for $\boldsymbol{c}_k \in \mathcal{C}_k$ and $p(\boldsymbol{c}_k) = 0$ otherwise. Using (4.4), we can then express the joint association PMF $p(\boldsymbol{c}_k)$ as

$$p(\boldsymbol{c}_k) \propto \Psi(\boldsymbol{c}_k) \prod_{l \in \mathbb{L}_k^*} \beta_k^{(l, c_k^{(l)})}, \quad \boldsymbol{c}_k \in \bar{\mathcal{M}}_k^{|\mathbb{L}_k^*|}, \tag{4.18}$$

where $\Psi(\boldsymbol{c}_k)$ is defined as $\Psi(\boldsymbol{c}_k) = 1$ if $\boldsymbol{c}_k \in \mathcal{C}_k$ and $\Psi(\boldsymbol{c}_k) = 0$ otherwise, and enforces the validity of (4.8). Without $\Psi(\boldsymbol{c}_k)$, equation (4.18) would describe the probability of "independent" single-object associations, and in the resulting algorithm, each object would be tracked without taking into account the presence of other objects. This would produce track losses when objects are in close proximity.

Following [Williams and Lau, 2014], we introduce the alternative measurement-object association vector $\mathbf{b}_k$ with elements $\mathsf{b}_k^{(m)}$, $m \in \mathcal{M}_k$, where $\mathsf{b}_k^{(m)} = l \in \mathbb{L}_k^*$ indicates that measurement m is associated with object state $(\boldsymbol{x}_k, l)$ and $\mathsf{b}_k^{(m)} = 0$ indicates that measurement m is not associated with any object state. We can reformulate the joint association PMF $p(\boldsymbol{c}_k)$ in terms of both $\mathbf{c}_k$ and $\mathbf{b}_k$. Indeed, analogously to (4.18), we can express the joint association PMF $p(\boldsymbol{c}_k, \boldsymbol{b}_k)$ as

$$p(\boldsymbol{c}_k, \boldsymbol{b}_k) \propto \Psi(\boldsymbol{c}_k, \boldsymbol{b}_k) \prod_{l \in \mathbb{L}_k^*} \beta_k^{(l, c_k^{(l)})}. \tag{4.19}$$

Here, analogously to (4.18), the admissibility of the association vectors $\boldsymbol{c}_k$ and $\boldsymbol{b}_k$ is enforced by the indicator function

$$\Psi(\boldsymbol{c}_k, \boldsymbol{b}_k) = \prod_{l \in \mathbb{L}_k^*} \prod_{m=1}^{M_k} \Psi_{l,m}\big(c_k^{(l)}, b_k^{(m)}\big), \tag{4.20}$$

where $\Psi_{l,m}\big(c_k^{(l)}, b_k^{(m)}\big) = 0$ if either $c_k^{(l)} = m$ and $b_k^{(m)} \neq l$ or $c_k^{(l)} \neq m$ and $b_k^{(m)} = l$, and $\Psi_{l,m}\big(c_k^{(l)}, b_k^{(m)}\big) = 1$ otherwise.

In this reformulation, it should be noted that the vector $\mathbf{b}_k$ does not carry any addi-

[1] The algorithm in [Williams and Lau, 2014] is not suited in this context because it presupposes that the number of objects is known. The related algorithm in [Williams, 2015] used to compute approximate association probabilities in the TOMB/P filter is not suited either because it combines the association weights for object nonexistence, $\beta_k^{(l,-1)}$, and those for a missed detection, $\beta_k^{(l,0)}$, into common association weights (cf. (3.18)) and also includes association weights for objects that are detected for the first time (cf. (3.21)).

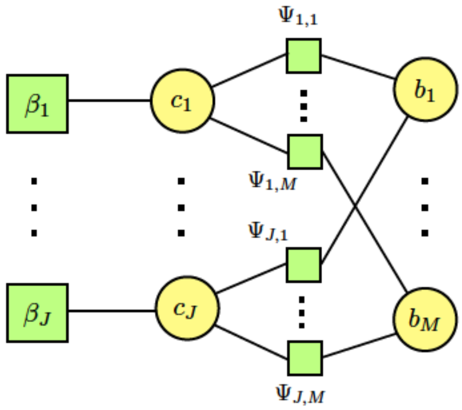

Figure 4.2: Factor graph representing the factorization (4.19), (4.20). The following short notations are used: $\beta_j \triangleq \beta_k^{(l',m')}$, $c_j \triangleq c_k^{(l')}$, $b_m \triangleq b_k^{(m)}$, $\Psi_{j,m} \triangleq \Psi_{l',m}\big(c_k^{(l')}, b_k^{(m)}\big)$, $M \triangleq M_k$, and $J = |\mathbb{L}_k^*|$, with $l' \triangleq l^{(j)}$ and $m' \triangleq c_k^{(l^{(j)})}$. Here, $l^{(j)} \in \mathbb{L}_k^* = \{l^{(1)}, \ldots, l^{(J)}\}$.

tional association information compared to the vector $\mathbf{c}_k$. However, as discussed in [Meyer et al., 2018] and [Williams and Lau, 2014], the redundant formulation of the joint association PMF using $\mathbf{c}_k$ and $\mathbf{b}_k$ in parallel, as given by (4.19) and (4.20), enables a fast method for BP-based probabilistic data association. On a more general level, the introduction of additional random variables that are redundant in that they deterministically depend on existing random variables (such as $\mathbf{b}_k$, which deterministically depends on $\mathbf{c}_k$) is a common means of expanding factor graphs [Kschischang et al., 2001]. In many cases, using BP on the expanded graph is more computationally efficient than using BP on the original graph. In our case, the introduction of the redundant association vector $\mathbf{b}_k$ results in the expression (4.20) of the admissibility constraint, which has the important property that it completely factorizes into individual components indexed by $(l, m) \in \mathbb{L}_k^* \times \mathcal{M}_k$. Based on this complete factorization, we next derive a fast algorithm for probabilistic data association. We want to emphazise again that the derivation is analogous to that in [Williams and Lau, 2014], where approximate marginal association probabilities are calculated for a slightly different association problem.

The factorization (4.19), (4.20) can be represented by the factor graph [Kschischang et al., 2001] shown in Figure 4.2. Then, still following [Williams and Lau, 2014], approximations of the marginal association PMFs $p\big(c_k^{(l)}\big)$ and $p\big(b_k^{(m)}\big)$ can be obtained via iterative BP message passing.[2] At message passing iteration $i \in \{1, \ldots, I\}$, first a message $\eta_k^{[i](c_k^{(l)} \to \Psi_{l,m})}\big(c_k^{(l)}\big)$ is passed from each variable node "$c_k^{(l)}$" to the adjacent factor node "$\Psi_{l,m}\big(c_k^{(l)}, b_k^{(m)}\big)$" in Figure 4.2. We now write $\nu_k^{[i-1](\Psi_{l,m} \to l)}\big(c_k^{(l)}\big)$ for $\phi_k^{[i-1](\Psi_{l,m} \to c_k^{(l)})}\big(c_k^{(l)}\big)$, i.e., for the message passed from factor node "$\Psi_{l,m}\big(c_k^{(l)}, b_k^{(m)}\big)$" to the adjacent variable

[2] We note that, as studied in [Williams and Lau, 2010], approximations of the $p\big(c_k^{(l)}\big)$ can also be calculated by running the BP algorithm on a factor graph containing only the variable nodes "$c_k^{(l)}$" and factor nodes representing the admissibility constraint factor $\psi(\mathbf{c}_k)$. However, these approximations are inferior to those obtained by running the BP algorithm on the factor graph of Figure 4.2 [Williams and Lau, 2010].

node "$c_k^{(l)}$" at message passing iteration $i-1$. According to (4.17), we obtain

$$\eta_k^{[i](c_k^{(l)} \to \Psi_{l,m})}\big(c_k^{(l)}\big) = \beta_k^{(l,c_k^{(l)})} \prod_{\substack{m'=1 \\ m' \neq m}}^{M_k} \nu_k^{[i-1](\Psi_{l,m'} \to l)}\big(c_k^{(l)}\big). \tag{4.21}$$

Then, a message $\phi_k^{[i](\Psi_{l,m} \to b_k^{(m)})}\big(b_k^{(m)}\big)$ is passed from each factor node "$\Psi_{l,m}\big(c_k^{(l)}, b_k^{(m)}\big)$" to the adjacent variable node "$b_k^{(m)}$". We now write $\zeta_k^{[i](\Psi_{l,m} \to m)}\big(b_k^{(m)}\big)$ for $\phi_k^{[i](\Psi_{l,m} \to b_k^{(m)})}\big(b_k^{(m)}\big)$. According to (4.16), this message is given by

$$\zeta_k^{[i](\Psi_{l,m} \to m)}\big(b_k^{(m)}\big) = \sum_{c_k^{(l)}=-1}^{M_k} \Psi_{l,m}\big(c_k^{(l)}, b_k^{(m)}\big) \eta_k^{[i](c_k^{(l)} \to \Psi_{l,m})}\big(c_k^{(l)}\big). \tag{4.22}$$

Inserting (4.21) in (4.22) results in

$$\zeta_k^{[i](\Psi_{l,m} \to m)}\big(b_k^{(m)}\big) = \sum_{c_k^{(l)}=-1}^{M_k} \beta_k^{(l,c_k^{(l)})} \Psi_{l,m}\big(c_k^{(l)}, b_k^{(m)}\big) \prod_{\substack{m'=1 \\ m' \neq m}}^{M_k} \nu_k^{[i-1](\Psi_{l,m'} \to l)}\big(c_k^{(l)}\big), \tag{4.23}$$

for $l \in \mathbb{L}_k^*$ and $m \in \mathcal{M}_k$. In a similar manner, we obtain the following expression of the message $\nu_k^{[i](\Psi_{l,m} \to l)}\big(c_k^{(l)}\big)$ that is passed from factor node "$\Psi_{l,m}\big(c_k^{(l)}, b_k^{(m)}\big)$" to the adjacent variable node "$c_k^{(l)}$":

$$\nu_k^{[i](\Psi_{l,m} \to l)}\big(c_k^{(l)}\big) = \sum_{b_k^{(m)} \in \{0\} \cup \mathbb{L}_k^*} \Psi_{l,m}\big(c_k^{(l)}, b_k^{(m)}\big) \prod_{l' \in \mathbb{L}_k^* \setminus \{l\}} \zeta_k^{[i](\Psi_{l',m} \to m)}\big(b_k^{(m)}\big), \tag{4.24}$$

for $l \in \mathbb{L}_k^*$ and $m \in \mathcal{M}_k$.

4.2.3 Efficient Formulation

Still following [Williams and Lau, 2014], the vector-valued messages (4.23) and (4.24) (vector-valued in the sense that there is one message value for each value of $b_k^{(m)}$ or $c_k^{(l)}$) can be simplified to scalar ones. Because of the admissibility constraint expressed by $\Psi_{l,m}\big(c_k^{(l)}, b_k^{(m)}\big)$, each message comprises actually only two different values. Indeed, for $\zeta_k^{[i](\Psi_{l,m} \to m)}\big(b_k^{(m)}\big)$, we have

$$\zeta_k^{[i](\Psi_{l,m} \to m)}\big(b_k^{(m)}\big) = \begin{cases} \zeta_{k,l,m}^{[i]}, & b_k^{(m)} = l \\ \zeta_{k,l,m}^{[i]\prime}, & b_k^{(m)} \neq l, \end{cases}$$

where

$$\zeta_{k,l,m}^{[i]} = \beta_k^{(l,m)} \prod_{\substack{m'=1 \\ m' \neq m}}^{M_k} \nu_k^{[i-1](\Psi_{l,m'} \to l)}(m), \tag{4.25}$$

$$\zeta_{k,l,m}^{[i]\prime} = \sum_{\substack{c_k^{(l)}=-1 \\ c_k^{(l)}\neq m}}^{M_k} \beta_k^{(l,c_k^{(l)})} \prod_{\substack{m'=1 \\ m'\neq m}}^{M_k} \nu_k^{[i-1](\Psi_{l,m'}\to l)}\big(c_k^{(l)}\big), \tag{4.26}$$

and similarly, for $\nu_k^{[i](\Psi_{l,m}\to l)}(c_k^{(l)})$, we have

$$\nu_k^{[i](\Psi_{l,m}\to l)}\big(c_k^{(l)}\big) = \begin{cases} \nu_{k,l,m}^{[i]}, & c_k^{(l)} = m \\ \nu_{k,l,m}^{[i]\prime}, & c_k^{(l)} \neq m, \end{cases}$$

where

$$\nu_{k,l,m}^{[i]} = \prod_{l'\in\mathbb{L}_k^*\setminus\{l\}} \zeta_k^{[i](\Psi_{l',m}\to m)}(l), \tag{4.27}$$

$$\nu_{k,l,m}^{[i]\prime} = \sum_{b_k^{(m)}\in(\{0\}\cup\mathbb{L}_k^*)\setminus\{l\}} \prod_{l'\in\mathbb{L}_k^*\setminus\{l\}} \zeta_k^{[i](\Psi_{l',m}\to m)}\big(b_k^{(m)}\big). \tag{4.28}$$

We next normalize the messages according to $\bar{\zeta}_k^{[i](\Psi_{l,m}\to m)}(b_k^{(m)}) \triangleq \zeta_k^{[i](\Psi_{l,m}\to m)}(b_k^{(m)})/\zeta_{k,l,m}^{[i]\prime}$ and $\bar{\nu}_k^{[i](\Psi_{l,m}\to l)}(c_k^{(l)}) \triangleq \nu_k^{[i](\Psi_{l,m}\to l)}(c_k^{(l)})/\nu_{k,l,m}^{[i]\prime}$, which yields

$$\bar{\zeta}_k^{[i](\Psi_{l,m}\to m)}\big(b_k^{(m)}\big) = \begin{cases} \zeta_{k,l,m}^{[i]}/\zeta_{k,l,m}^{[i]\prime}, & b_k^{(m)} = l \\ 1, & b_k^{(m)} \neq l, \end{cases} \tag{4.29}$$

and

$$\bar{\nu}_k^{[i](\Psi_{l,m}\to l)}\big(c_k^{(l)}\big) = \begin{cases} \nu_{k,l,m}^{[i]}/\nu_{k,l,m}^{[i]\prime}, & c_k^{(l)} = m \\ 1, & c_k^{(l)} \neq m. \end{cases} \tag{4.30}$$

Let us consider $\bar{\zeta}_k^{[i](\Psi_{l,m}\to m)}(b_k^{(m)})$ for $b_k^{(m)} = l$. Inserting (4.25) and (4.26) into (4.29) yields

$$\bar{\zeta}_k^{[i](\Psi_{l,m}\to m)}(l) = \frac{\beta_k^{(l,m)} \prod_{\substack{m'=1 \\ m'\neq m}}^{M_k} \nu_k^{[i-1](\Psi_{l,m'}\to l)}(m)}{\sum_{\substack{c_k^{(l)}=-1 \\ c_k^{(l)}\neq m}}^{M_k} \beta_k^{(l,c_k^{(l)})} \prod_{\substack{m'=1 \\ m'\neq m}}^{M_k} \nu_k^{[i-1](\Psi_{l,m'}\to l)}\big(c_k^{(l)}\big)}.$$

Substituting $\nu_k^{[i-1](\Psi_{l,m}\to l)}(c_k^{(l)}) = \bar{\nu}_k^{[i-1](\Psi_{l,m}\to l)}(c_k^{(l)})\, \nu_{k,l,m}^{[i-1]\prime}$, the above expression becomes

$$\bar{\zeta}_k^{[i](\Psi_{l,m}\to m)}(l) = \frac{\beta_k^{(l,m)} \prod_{\substack{m'=1 \\ m'\neq m}}^{M_k} \bar{\nu}_k^{[i-1](\Psi_{l,m'}\to l)}(m)}{\sum_{\substack{c_k^{(l)}=-1 \\ c_k^{(l)}\neq m}}^{M_k} \beta_k^{(l,c_k^{(l)})} \prod_{\substack{m'=1 \\ m'\neq m}}^{M_k} \bar{\nu}_k^{[i-1](\Psi_{l,m'}\to l)}\big(c_k^{(l)}\big)}. \tag{4.31}$$

Finally, using the fact that according to (4.30), $\bar{\nu}_k^{[i-1](\Psi_{l,m'}\to l)}(c_k^{(l)}) = 1$ for $c_k^{(l)} \neq m'$, expression (4.31) simplifies to

$$\bar{\zeta}_k^{[i](\Psi_{l,m}\to m)}(l) = \frac{\beta_k^{(l,m)}}{\beta_k^{(l,-1)} + \beta_k^{(l,0)} + \sum_{\substack{m'=1\\m'\neq m}}^{M_k} \beta_k^{(l,m')} \bar{\nu}_k^{[i-1](\Psi_{l,m'}\to l)}(m')} . \tag{4.32}$$

We also recall from (4.29) that $\bar{\zeta}_k^{[i](\Psi_{l,m}\to m)}(b_k^{(m)}) = 1$ for $b_k^{(m)} \neq l$.

Analogously, by inserting (4.27) and (4.28) into (4.30), we obtain for $\bar{\nu}_k^{[i](\Psi_{l,m}\to l)}(a_k^{(l)})$ with $a_k^{(l)} = m$

$$\bar{\nu}_k^{[i](\Psi_{l,m}\to l)}(m) = \frac{1}{1 + \sum_{l'\in\mathbb{L}_k^*\backslash\{l\}} \bar{\zeta}_k^{[i](\Psi_{l',m}\to m)}(l')} . \tag{4.33}$$

Furthermore, $\bar{\nu}_k^{[i](\Psi_{l,m}\to l)}(c_k^{(l)}) = 1$ for $c_k^{(l)} \neq m$. Finally, after introducing the shorthands $\zeta_k^{[i](l\to m)} \triangleq \bar{\zeta}_k^{[i](\Psi_{l,m}\to m)}(l)$ and $\nu_k^{[i](m\to l)} \triangleq \bar{\nu}_k^{[i](\Psi_{l,m}\to l)}(m)$, the two equations (4.32) and (4.33) become

$$\zeta_k^{[i](l\to m)} = \frac{\beta_k^{(l,m)}}{\beta_k^{(l,-1)} + \beta_k^{(l,0)} + \sum_{\substack{m'=1\\m'\neq m}}^{M_k} \beta_k^{(l,m')} \nu_k^{[i-1](m'\to l)}} , \tag{4.34}$$

$$\nu_k^{[i](m\to l)} = \frac{1}{1 + \sum_{l'\in\mathbb{L}_k^*\backslash\{l\}} \zeta_k^{[i](l'\to m)}} , \tag{4.35}$$

for $l \in \mathbb{L}_k^*$ and $\mathcal{M}_k$. The recursion established by these two equations is initialized by $\nu_k^{[0](m\to l)} = 1$.

After the final iteration $i = I$, approximations of the marginal association PMFs $p(c_k^{(l)})$, $l \in \mathbb{L}_k^*$ are provided by the beliefs at the respective variable nodes "$c_k^{(l)}$" in Figure 4.2. More precisely, the belief $\tilde{p}(c_k^{(l)})$ is obtained as the product of all the incoming messages at variable node "$c_k^{(l)}$" in Figure 4.2 and normalizaion of the resulting function (cf. Section 4.2.1). Thus,

$$\tilde{p}(c_k^{(l)} = m) \propto \beta_k^{(l,m)} \prod_{m'=1}^{M_k} \nu_k^{[I](\Psi_{l,m'}\to l)}(m),$$

for $m \in \bar{\mathcal{M}}_k$. Substituting $\nu_k^{[I](\Psi_{l,m'}\to l)}(c_k^{(l)}) = \bar{\nu}_k^{[I](\Psi_{l,m'}\to l)}(c_k^{(l)})\, \nu_{k,l,m'}^{[I]\prime}$, we obtain further

$$\begin{aligned}
\tilde{p}(c_k^{(l)} = m) &\propto \beta_k^{(l,m)} \left(\prod_{m''=1}^{M_k} \nu_{k,l,m''}^{[I]\prime} \right) \prod_{m'=1}^{M_k} \bar{\nu}_k^{[I](\Psi_{l,m'}\to l)}(m) \\
&\propto \beta_k^{(l,m)} \prod_{m'=1}^{M_k} \bar{\nu}_k^{[I](\Psi_{l,m'}\to l)}(m).
\end{aligned} \tag{4.36}$$

Since by (4.30) $\bar{\nu}_k^{[I](\Psi_{l,m'}\to l)}(m)=1$ for all $m'\neq m$, expression (4.36) simplifies to

$$\tilde{p}\big(c_k^{(l)}=m\big) \propto \begin{cases} \beta_k^{(l,m)}, & m\in\{-1,0\} \\ \beta_k^{(l,m)}\,\bar{\nu}_k^{[I](\Psi_{l,m}\to l)}(m), & m\in\{1,\ldots,M_k\}. \end{cases}$$

These expressions still need to be normalized, which amounts to division by $D_k^{(l)} \triangleq \beta_k^{(l,-1)} + \beta_k^{(l,0)} + \sum_{m=1}^{M_k}\beta_k^{(l,m)}\bar{\nu}^{[I](\Psi_{l,m}\to l)}(m)$. Finally, using the shorthand $\nu_k^{[I](m\to l)} \triangleq \bar{\nu}_k^{[I](\Psi_{l,m}\to l)}(m)$, we obtain

$$\tilde{p}\big(c_k^{(l)}=m\big) = \begin{cases} \beta_k^{(l,m)}/D_k^{(l)}, & m\in\{-1,0\} \\ \beta_k^{(l,m)}\nu_k^{[I](m\to l)}/D_k^{(l)}, & m\in\{1,\ldots,M_k\}, \end{cases} \tag{4.37}$$

Similarly, the belief $\tilde{p}\big(b_k^{(m)}\big)$ (to be used in Section 4.3) is obtained after the final iteration $i=I$ as the normalized product of all the incoming messages at variable node "$b_k^{(m)}$" in Figure 4.2. A analogous derivation to the one above leads to

$$\tilde{p}\big(b_k^{(m)}=l\big) = \begin{cases} 1/F_k^{(m)}, & l=0 \\ \zeta_k^{[I](l\to m)}/F_k^{(m)}, & l\in\mathbb{L}_k^*, \end{cases} \tag{4.38}$$

with $F_k^{(m)} \triangleq 1+\sum_{l\in\mathbb{L}_k^*}\zeta_k^{[I](l\to m)}$. This fast BP-based approximate calculation of the $p\big(c_k^{(l)}\big)$ according to (4.34), (4.35), and (4.37) constitutes the basis of the fast BP-based LMB filter proposed in next section.

4.3 The Proposed Fast LMB Filter

In the following, we propose a scheme for generating new Bernoulli components using the approximate marginal association probabilities and the set of measurements acquired at the previous time step. We furthermore present a summary of the resulting fast BP-based LMB filter and conclude the section with a brief complexity analysis of our proposed algorithm compared to two state-of-the-art LMB filter implementations.

We start by presenting a scheme for generating new Bernoulli components using the set of previous measurements Z_{k-1}. Recap that in the prediction step of the LMB filter (cf. Section 3.5.1), the existence probabilities and spatial pdfs of the Bernoulli components representing newborn objects, i.e., $\big\{\big(r_{\mathrm{B},k}^{(l)}, f_{\mathrm{B}}^{(l)}(\boldsymbol{x}_k)\big)\big\}_{l\in\mathbb{L}_k^{\mathrm{B}*}}$, are computed according to (3.36) and (3.37), respectively. We now present a scheme for choosing $\mathbb{L}_k^{\mathrm{B}*}$, $r_{\mathrm{B},k}^{(l)}$ and $f_{\mathrm{B}}^{(l)}(\boldsymbol{x}_k)$ using the previous set of measurements Z_{k-1}. Note that in the prediction step, the current set of measurements Z_k is not available yet. The belief $\tilde{p}\big(b_{k-1}^{(m)}=0\big)$ computed in (4.38) is an approximation of the probability that the measurement with index $m\in\mathcal{M}_{k-1}$ was not originated by an object modeled by any Bernoulli component. Hence, if

$\tilde{p}\big(b_{k-1}^{(m)}\!=0\big)$ is high, it is very likely that the corresponding measurement $\boldsymbol{z}_{k-1}^{(m)}$ originated either from clutter or from a newborn object that is not yet modeled by any Bernoulli component. It is therefore reasonable to generate a new Bernoulli component for all those measurements that have a high $\tilde{p}\big(b_{k-1}^{(m)}=0\big)$ value. We collect all measurement indices $m \in \mathcal{M}_{k-1}$ with $\tilde{p}\big(b_{k-1}^{(m)}\!=0\big) \geq \gamma_{\text{new}}$ in the set $\mathcal{M}_{k-1}^{\text{new}}$, where γ_{new} is a threshold between zero and one. We now define the label set of newborn objects $\mathbb{L}_k^{\text{B}*}$ as the set of all tuples $\{(k,m)\}$ with k being the current time step and $m \in \mathcal{M}_{k-1}^{\text{new}}$. Note that the number of newly generated Bernoulli components $|\mathbb{L}_k^{\text{B}*}| = |\mathcal{M}_{k-1}^{\text{new}}|$ is determined by the choice of γ_{new}. Next, we define the existence probabilities of newborn objects as

$$r_{\text{B},k}^{(l)} = \min\left\{ \frac{\mu_{\text{B}}\, \tilde{p}\big(b_{k-1}^{(m)}\!=0\big)}{|\mathcal{M}_{k-1}^{\text{new}}|}, 1 \right\}, \tag{4.39}$$

for $l = (k,m) \in \mathbb{L}_k^{\text{B}*}$. Consequently, $r_{\text{B},k}^{(l)}$ is equal to the expected number of newborn objects μ_{B} (cf. Section 3.2.1), divided by the total number of newly generated Bernoulli components $|\mathcal{M}_{k-1}^{\text{new}}|$, and weighted by $\tilde{p}\big(b_{k-1}^{(m)}\!=0\big)$, which is the (approximate) probability that the measurement with index m is not generated by an object already modeled by a Bernoulli component and thus already tracked by the LMB filter; this value is upper-bounded by one. Finally, the spatial PDFs of newborn objects are chosen according to

$$f_{\text{B}}^{(l)}(\boldsymbol{x}_k) = f\big(\boldsymbol{x}_k; \boldsymbol{z}_{k-1}^{(m)}\big), \tag{4.40}$$

where $l = (k,m) \in \mathbb{L}_k^{\text{B}*}$ and $m \in \mathcal{M}_{k-1}^{\text{new}}$. Here, $f\big(\boldsymbol{x}_k; \boldsymbol{z}_{k-1}^{(m)}\big)$ is a spatial PDF that is parametrized by the measurement $\boldsymbol{z}_{k-1}^{(m)}$; its exact definition strongly depends on the underlying tracking problem. A specific choice of $f\big(\boldsymbol{x}_k; \boldsymbol{z}_{k-1}^{(m)}\big)$ for the tracking scenario considered in Section 4.4 will be presented there.

The proposed fast LMB filter, termed BP-LMB filter, is finally obtained by executing a prediction step, where the predicted existence probabilities and spatial PDFs are computed according to (3.34) and (3.35) for $l \in \mathbb{L}_{k-1}^*$ and new Bernoulli components are generated according (4.39) and (4.40). Next, the association weights $\beta_k^{(l,m)}$ are computed according to (4.5) and the spatial PDFs $f^{(l,m)}(\boldsymbol{x}_k)$ for $m = 0$ according to (3.41) and for $m \in \mathcal{M}_k$ according to (3.42). Then, the BP algorithm for probabilistic data association is used to compute approximations of the marginal association probabilities by iteratively computing $\zeta_k^{[i](l\to m)}$ according to (4.34) and $\nu_k^{[i](m\to l)}$ according to (4.35) for $i = 1,\dots,I$. After the final iteration $i = I$, the approximate marginal association probabilities $\tilde{p}\big(c_k^{(l)}\big)$ are computed according to (4.37) and then the updated existence probabilities $r_k^{(l)}$ and spatial PDFs $f^{(l)}(\boldsymbol{x}_k)$ are determined according to (4.13) and (4.14), respectively. Finally, objects described by a high existence probability are declared to exist, estimates of their corresponding states are computed, and Bernoulli components with a low existence probability are pruned. It should be emphasized that the proposed BP-LMB filter is different from the LMB filters in [Reuter et al., 2014, Reuter et al., 2017] because the underlying

BP-based approximation is different from the approximations employed in [Reuter et al., 2014] and [Reuter et al., 2017]. A summary of the proposed BP-LMB filter is presented in Table 4.1.

Next, we analyze the complexity of our proposed BP-LMB filter and two state-of-the-art LMB filters. The original LMB filter implementation in [Reuter et al., 2014] uses a k-shortest path algorithm and a ranked assignment algorithm and has a complexity scaling of $\mathcal{O}(KC^3)$, where K is the number of highest weights in the ranked assignment algorithm and $C = \max\{|\mathbb{L}_k^*|, M_k\}$ [Vo et al., 2014]. Recap that $|\mathbb{L}_k^*|$ is the number of Bernoulli components and M_k is the number of measurements. The cubic scaling behavior was improved by the Gibbs sampler-based LMB filter proposed in [Reuter et al., 2017]. This filter achieves a scaling of $\mathcal{O}(P|\mathbb{L}_k^*|^2 M_k)$, where P is the number of samples used in the Gibbs sampler. By contrast, the complexity of our proposed LMB filter is $\mathcal{O}(I|\mathbb{L}_k^*|M_k)$, where I is the number of BP iterations. The linear scaling in $|\mathbb{L}_k^*|$ improves on the quadratic scaling exhibited by the Gibbs sampler-based LMB filter. The second difference is that P is replaced by I. A typical value of I is 20. As we will demonstrate in Section 4.4.3, for scenarios with a rather high clutter rate and/or a large number of objects, P has to be chosen much higher than 20 in order for the tracking performance of the Gibbs sampler-based LMB filter to be similar to that of our BP-LMB filter. Some algorithmic aspects affecting the complexity and performance of the BP-based and Gibbs sampler-based LMB filters are discussed in Section 4.4.3.

4.4 Numerical Study

In the following section, we present a simulation study in which we analyze the performance of the proposed fast BP-LMB filter. More precisely, in Section 4.4.1, we describe the underlying simulation scenario. A comparison of the exact and the approximate marginal association probabilities used in the BP-LMB filter is provided in Section 4.4.2. Finally, tracking results obtained by the proposed BP-LMB filter compared to those obtained by several state-of-the-art RFS-based tracking filters are reported in Section 4.4.3.

4.4.1 Simulation Setup

For evaluating the performance of the proposed BP-LMB filter, we consider a two-dimensional (2D) tracking scenario [Meyer et al., 2017], where a sensor is located at $\boldsymbol{p} = [p_1\ p_2]^{\mathrm{T}} = [0\ \ 150]^{\mathrm{T}}$. The sensor has a measurement range of 300 and the region of interest (ROI) corresponds to the sensor's field of view, i.e., the circular disk determined by the sensor's measurement range. We consider two different parameter settings PS1 and PS2. Ten (PS1) or twenty (PS2) objects appear before $k = 30$ and disappear after $k = 140$. The object states $\mathbf{x}_k$ consist of position and velocity, i.e., $\mathbf{x}_k = [\mathrm{x}_{1,k}\ \mathrm{x}_{2,k}\ \dot{\mathrm{x}}_{1,k}\ \dot{\mathrm{x}}_{2,k}]^{\mathrm{T}}$. They evolve according to the nearly constant velocity motion model [Bar-Shalom et al., 2002, Sec. 6.3.2]

Table 4.1: Proposed fast BP-LMB filter algorithm—recursion at time $k \geq 1$

Input: Previous existence probabilities $r_{k-1}^{(l)}$ and previous spatial PDFs $f^{(l)}(\boldsymbol{x}_{k-1})$ for $l \in \mathbb{L}_{k-1}^{*}$; measurements $\boldsymbol{z}_k^{(m)}$ for $m \in \mathcal{M}_k$ and $\boldsymbol{z}_{k-1}^{(m)}$ for $m \in \mathcal{M}_{k-1}^{\mathrm{new}}$; approximate marginal association probabilities $\tilde{p}(b_{k-1}^{(m)})$ for $m \in \mathcal{M}_{k-1}^{\mathrm{new}}$.

Output: Existence probabilities $r_k^{(l)}$ and spatial PDFs $f^{(l)}(\boldsymbol{x}_k)$ for $l \in \mathbb{L}_k^{*}$; approximate marginal association probabilities $\tilde{p}(b_k^{(m)})$ for $m \in \mathcal{M}_k^{\mathrm{new}}$; object state estimates $\hat{\boldsymbol{x}}_k^{(l)}$ for $l \in \mathbb{L}_k^{\mathrm{D}}$.

Operations:

Step 1 – Prediction Step:

1.1) For $l \in \mathbb{L}_{k-1}^{*}$, calculate the predicted existence probabilities $r_{k|k-1}^{(l)}$ and the predicted spatial PDFs $f_{k|k-1}^{(l)}(\boldsymbol{x}_k)$ according to (3.34) and (3.35).

1.2) if $k=1$, $\mathbb{L}_k^{\mathrm{B}*} = \emptyset$; else:
Determine $\mathbb{L}_k^{\mathrm{B}*}$ according to Section 4.3 and $r_{\mathrm{B},k}^{(l)}$ and $f_{\mathrm{B}}^{(l)}(\boldsymbol{x}_k)$ according to (4.39) and (4.40), respectively, using $\boldsymbol{z}_{k-1}$ and $\tilde{p}(b_{k-1}^{(m)})$ for $m \in \mathcal{M}_{k-1}^{\mathrm{new}}$.

1.3) Determine $\mathbb{L}_k^{*} = \mathbb{L}_{k-1}^{*} \cup \mathbb{L}_k^{\mathrm{B}*}$ and $\big\{\big(r_{k|k-1}^{(l)}, f_{k|k-1}^{(l)}(\boldsymbol{x}_k)\big)\big\}_{l \in \mathbb{L}_k^{*}}$ as $\big\{\big(r_{k|k-1}^{(l)}, f_{k|k-1}^{(l)}(\boldsymbol{x}_k)\big)\big\}_{l \in \mathbb{L}_{k-1}^{*}} \cup \big\{\big(r_{k|k-1}^{(l)}, f_{k|k-1}^{(l)}(\boldsymbol{x}_k)\big)\big\}_{l \in \mathbb{L}_k^{\mathrm{B}*}}$ with $r_{k|k-1}^{(l)} \triangleq r_{\mathrm{B},k}^{(l)}$ and $f_{k|k-1}^{(l)}(\boldsymbol{x}_k) \triangleq f_{\mathrm{B}}^{(l)}(\boldsymbol{x}_k)$ for $l \in \mathbb{L}_k^{\mathrm{B}*}$.

Step 2 – Update Step:

2.1) For $l \in \mathbb{L}_k^{*}$, calculate the association weights $\beta_k^{(l,m)}$ according to (4.5) and the spatial PDFs $f^{(l,m)}(\boldsymbol{x}_k)$ for $m=0$ according to (3.41) and for $m \in \mathcal{M}_k$ according to (3.42).

2.2) Initialize $\nu_k^{[0](m\to l)} = 1$, then iteratively calculate $\zeta_k^{[i](l\to m)}$ according to (4.34) and $\nu_k^{[i](m\to l)}$ according to (4.35) for $i=1,\ldots,I$.

2.3) For $l \in \mathbb{L}_k^{*}$ and $m \in \{0\} \cup \mathcal{M}_k$, determine the approximate marginal association probabilities $\tilde{p}(c_k^{(l)})$ and according to (4.37), and for $m \in \mathcal{M}_k^{\mathrm{new}}$, $\tilde{p}(b_k^{(m)} = 0)$ according to (4.38).

2.4) For $m \in \mathcal{M}_k$, compute the approximate marginal association probabilities $\tilde{p}(b_k^{(m)} = 0)$ according to (4.38) and determine $\mathcal{M}_k^{\mathrm{new}}$ according to Section 4.3.

2.5) For $l \in \mathbb{L}_k^{*}$, compute the updated existence probabilities $r_k^{(l)}$ and spatial PDFs $f^{(l)}(\boldsymbol{x}_k)$ according to (4.13) and (4.14), respectively.

Step 3 – Object Detection, State Estimation, Pruning:

3.1) Consider an object with $l \in \mathbb{L}_k^{*}$ to exist (to be detected) if $r_k^{(l)}$ is larger than a threshold γ_{D}. For each detected object, calculate a state estimate as $\hat{\boldsymbol{x}}_k = \int \boldsymbol{x}_k f_k^{(l)}(\boldsymbol{x}_k) \mathrm{d}\boldsymbol{x}_k$;

3.2) Prune (i.e., remove) the Bernoulli components $l \in \mathbb{L}_k^{*}$ with $r_k^{(l)} < \gamma_{\mathrm{P}}$;

Initialization at time $k=0$: $\big\{\big(r_0^{(l)}, f^{(l)}(\boldsymbol{x}_0)\big)\big\}_{l \in \mathbb{L}_0^{*}}$.

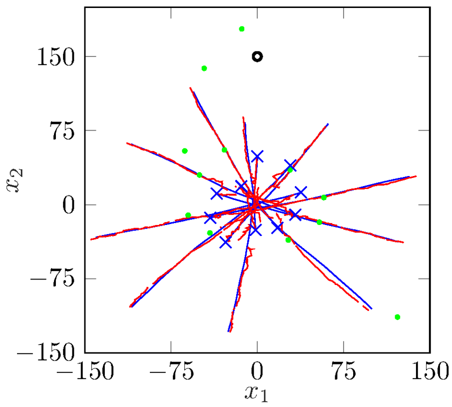

Figure 4.3: Example of true trajectories for parameter setting PS1 (blue lines; starting points indicated by blue crosses), as well as of trajectories estimated by the proposed BP-LMB filter (red lines) and measurements acquired at time $k = 100$ (green dots). The black circle indicates the sensor position.

$$\mathsf{x}_k = \boldsymbol{A}\mathsf{x}_{k-1} + \boldsymbol{W}\mathsf{u}_k \,,$$

where $\boldsymbol{A} \in \mathbb{R}^{4\times 4}$ and $\boldsymbol{W} \in \mathbb{R}^{4\times 2}$ are chosen as in [Bar-Shalom et al., 2002] and $\mathsf{u}_k \sim \mathcal{N}(\mathbf{0}, \sigma_u^2 \mathbf{I}_2)$ with $\sigma_u^2 = 0.01$ is an iid sequence of 2D Gaussian random vectors. We employ the trajectory generation scheme of [Meyer et al., 2017], according to which all objects move toward the point $(0, 0)$, come close to each other there around time $k = 60$, and separate again afterwards. A detailed description of this trajectory generation scheme can be found in [Meyer et al., 2017], and a realization of the object trajectories is shown in Figure 4.3. The sensor is characterized by the nonlinear range-bearing measurement model

$$\mathsf{z}_k = \big[\rho(\mathsf{x}_k) \;\; \phi(\mathsf{x}_k)\big]^{\mathrm{T}} + \mathsf{v}_k \,. \tag{4.41}$$

Here, $\rho(\mathsf{x}_k) \triangleq \|\mathsf{x}'_k - \boldsymbol{p}\|$, where $\mathsf{x}'_k \triangleq [\mathsf{x}_{1,k} \; \mathsf{x}_{2,k}]^{\mathrm{T}}$ denotes the position of an object, and $\phi(\mathsf{x}_k) \triangleq \tan^{-1}\big(\frac{\mathsf{x}_{2,k} - p_2}{\mathsf{x}_{1,k} - p_1}\big)$. Furthermore, v_k is iid Gaussian measurement noise with independent components and component standard deviations $\sigma_\rho = 2$ and $\sigma_\phi = 1°$. The clutter PDF $f_{\mathrm{C}}(\boldsymbol{z}_k)$ is uniform (in polar coordinates) on the ROI, and the mean parameter μ_{C} is 10 (PS1) or 50 (PS2). Objects are detected by the sensor with probability $p_{\mathrm{D}}(\boldsymbol{x}_k, l) = 0.5$.

We study the performance of the proposed BP-LMB filter in comparison to the Gibbs sampler-based LMB filter [Reuter et al., 2017] (briefly termed Gibbs-LMB filter) and the fast BP-based version of the label-augmented TOMB/P filter [Meyer et al., 2018, Williams, 2015, Williams and Lau, 2014] (briefly termed BP-TOMB/P filter). All filters use particle implementations [Reuter et al., 2014, Kropfreiter et al., 2016]. They represent the spatial PDF of each Bernoulli component by 1000 particles, prune components with an existence probability below $\gamma_{\mathrm{P}} = 10^{-4}$, declare an object as detected if its existence probability exceeds $\gamma_{\mathrm{D}} = 0.5$, and use $p_{\mathrm{S}}(\boldsymbol{x}_{k-1}, l) = p_{\mathrm{S}}(\boldsymbol{x}_{k-1}) = 0.99$ and $p_{\mathrm{D}}(\boldsymbol{x}_k, l) = p_{\mathrm{D}}(\boldsymbol{x}_k) = 0.5$. With regard to the newborn objects, the BP-LMB filter employs the Bernoulli generation scheme proposed in Section 4.3 with $\mu_{\mathrm{B}} = 0.1$ and spatial PDFs (cf. (4.40)) given by

$$f_{\mathrm{B}}^{(l)}(\boldsymbol{x}_k) \propto \int f(\boldsymbol{x}_k|\boldsymbol{x}_{k-1})\, f(\boldsymbol{z}_{k-1}|x_{1,k-1}, x_{2,k-1})\, f_{\mathrm{v}}(\dot{x}_{1,k-1}, \dot{x}_{2,k-1})\, \mathrm{d}\boldsymbol{x}_{k-1}\,, \tag{4.42}$$

for $l \in \mathbb{L}_k^{\mathrm{B}*}$. Here, $f(\boldsymbol{z}_{k-1}|x_{1,k-1}, x_{2,k-1})$ is the likelihood function corresponding to our measurement model (4.41) and $f_{\mathrm{v}}(\dot{x}_{1,k-1}, \dot{x}_{2,k-1})$ is the PDF of independent, zero-mean, Gaussian random variables $\dot{\mathrm{x}}_{1,k-1}$, $\dot{\mathrm{x}}_{2,k-1}$ with variance 0.25. By constrast, the Gibbs-LMB filter generates a new Bernoulli component for each measurement observed at the preceding time $k-1$; the existence probability of that Bernoulli component is initialized as μ_{B}/M_{k-1} with $\mu_{\mathrm{B}} = 0.1$ and the spatial PDFs are also initialized according to (4.42). The number P of samples used by the Gibbs sampler in the Gibbs-LMB filter is 100 or 1000; the resulting Gibbs-LMB filters are referred to as Gibbs-LMB-100 and Gibbs-LMB-1000, respectively. In the BP-TOMB/P filter (cf. Section 3.4), the PHD of newborn objects $\lambda_{\mathrm{B}}(\boldsymbol{x}_k) = \mu_{\mathrm{B}} f_{\mathrm{B}}(\boldsymbol{x}_k)$ has mean parameter $\mu_{\mathrm{B}} = 0.3$ and its spatial PDF $f_{\mathrm{B}}(\boldsymbol{x}_k)$ is uniform on the ROI; furthermore, the posterior PHD of undetected objects is chosen as a k-dependent constant on the ROI and initialized as $\lambda_{\mathrm{U}}(\boldsymbol{x}_0) = \mu_0^{\mathrm{U}} f_{\mathrm{U}}(\boldsymbol{x}_0)$ with $\mu_0^{\mathrm{U}} = 0.01$ and uniform $f_{\mathrm{U}}(\boldsymbol{x}_0)$. Recap, that the BP-TOMB/P filter generates a new Bernoulli component for each measurement at time k (cf. (3.29) and (3.30)). The BP-LMB and BP-TOMB/P filters use $I = 20$ BP iterations to calculate the approximate marginal probabilities.

4.4.2 Comparison of Exact and Approximate Marginal Association Probabilities

Next, we experimentally examine the accuracy of the approximate marginal association probabilities by comparing the exact marginal association probabilities $p\big(c_k^{(l)}\big)$ calculated according to (4.11) and used in the original LMB filter (cf. Section 4.1) with the approximate marginal probabilities $\tilde{p}\big(c_k^{(l)}\!=\!m\big)$ calculated according to (4.34), (4.35), and (4.37) and used in the proposed BP-LMB filter. For this comparison, we use a setup comprising seven Bernoulli components and five measurements. It was obtained by running the BP-LMB filter on the scenario described in the previous section and by extracting the sensor measurements and Bernoulli components arising in the BP-LMB filter after the prediction step at time $k = 60$. Thus, the Bernoulli components are parametrized by $\big\{\big(r_{k|k-1}^{(l)}, f_{k|k-1}^{(l)}(\boldsymbol{x}_k)\big)\big\}_{l \in \mathbb{L}_k^*}$ with label set $\mathbb{L}_k^* = \{l^{(1)}, \ldots, l^{(7)}\}$, where $k = 60$. Furthermore, the measurements are given by $Z_{60} = \{\boldsymbol{z}_{60}^{(1)}, \ldots, \boldsymbol{z}_{60}^{(5)}\}$. The simulation parameters and the parameters used in the BP-LMB filter were chosen as described in Section 4.4.1, except that the number of objects and the mean number of clutter measurements were both set to five. This was done because the calculation of the exact marginal probabilities of the LMB filter [Reuter et al., 2014] becomes infeasible for higher numbers of objects and clutter. However, the scenario is still challenging as the objects are in close proximity

m	$p(c_{60}^{(l^{(1)})}=m)$	$\tilde{p}(c_{60}^{(l^{(1)})}=m)$ for $I=1$	$\tilde{p}(c_{60}^{(l^{(1)})}=m)$ for $I=2$	$\tilde{p}(c_{60}^{(l^{(1)})}=m)$ for $I=5$
-1	0.5126	0.3637	0.5015	0.5126
0	0.0928	0.0659	0.0908	0.0928
1	1.87×10^{-5}	0.007	2.67×10^{-5}	1.87×10^{-5}
2	0	0	0	0
3	6.20×10^{-12}	2.77×10^{-9}	1.67×10^{-10}	6.20×10^{-12}
4	0.3945	0.5633	0.4077	0.3945
5	2.09×10^{-6}	1.6×10^{-4}	2.04×10^{-6}	2.08×10^{-6}

Table 4.2: Comparison of the exact marginal probabilities $p(c_{60}^{(l^{(1)})})$ and the approximate marginal probabilities $\tilde{p}(c_{60}^{(l^{(1)})})$ for 1, 2, and 5 BP iterations.

around time $k=60$.

Table 4.2 shows $p(c_k^{(l^{(1)})})$ and $\tilde{p}(c_k^{(l^{(1)})})$ at time $k=60$, for three different values of the number I of BP iterations. One can see that $\tilde{p}(c_{60}^{(l^{(1)})})$ deviates from $p(c_{60}^{(l^{(1)})})$ for $I=1$ and, somewhat less, for $I=2$. However, for $I=5$, $\tilde{p}(a_{60}^{(l^{(1)})})$ is effectively equal to $p(c_{60}^{(l^{(1)})})$. We observed a similar behavior for the remaining label values $l = l^{(2)}, \ldots, l^{(7)}$, and also for other times k. This shows that the approximate marginal association probabilities calculated by the proposed BP-LMB filter converge to the true association probabilities within a few BP iterations. However, if the association problem is more difficult, involving more (close) objects and clutter measurements, the BP algorithm needs a larger number of iterations to converge. This is the reason why we set $I = 20$ for our simulations in Section 4.4.1.

4.4.3 Analysis of Tracking Accuracy and Computational Complexity

In the following, we present the simulation results for the scenario described in Section 4.4.1. The example shown in Figure 4.3 suggests that the proposed BP-LMB filter has excellent detection and estimation performance. For a quantitative evaluation of the average performance of the three filters, we use the Euclidean distance-based optimal subpattern assignment (OSPA) metric with cutoff parameter $c = 20$ and order $p = 1$ [Schuhmacher et al., 2008]. The OSPA metric penalizes both a deviation between the estimated and true numbers of objects and deviations between the estimated and true object states [Schuhmacher et al., 2008].

Figure 4.4 shows the mean OSPA (MOSPA) error (averaged over 1000 simulation runs) versus time k for PS1 (10 objects, $\mu_{\mathrm{C}} = 10$) and PS2 (20 objects, $\mu_{\mathrm{C}} = 50$). For PS1, the BP-LMB, BP-TOMB/P, and Gibbs-LMB-1000 filters perform best and almost identically, closely followed by the Gibbs-LMB-100 filter. For the more challenging setting PS2, the BP-LMB and BP-TOMB/P filters perform best and almost identically, whereas both Gibbs-LMB filters perform substantially worse: already the Gibbs-LMB-1000 filter has a significantly larger MOSPA error during a long time interval, and the Gibbs-LMB-

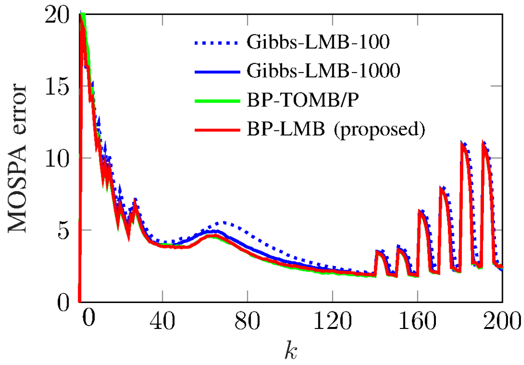

(a)

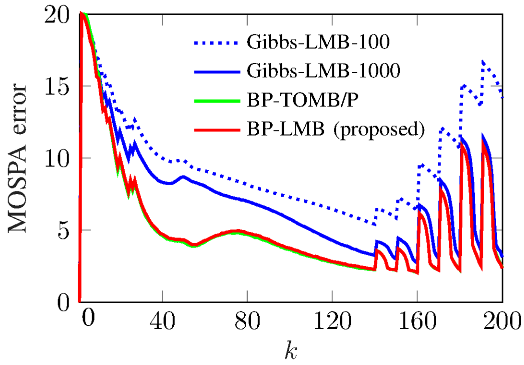

(b)

Figure 4.4: MOSPA error versus time for (a) PS1 and (b) PS2.

100 filter has an even larger MOSPA error at almost all times. If the number of samples is increased beyond 1000 (not shown in Figure 5.6), the MOSPA error of the Gibbs-LMB filter decreases, but this comes at the cost of a higher complexity.

The performance difference between the BP-LMB filter and the Gibbs-LMB filter for PS2 can be explained as follows. The Gibbs-LMB filter reduces complexity by pruning GLMB components with low weights in (3.38). As a consequence, the summations in the update equations (3.43) and (3.44) are performed only over the remaining (non-pruned) components. The pruning performed by the Gibbs-LMB filter can be equivalently formulated in terms of the association vector $\mathbf{c}_k$ introduced in Section 4.1. In this formulation, the pruning is based on drawing samples $\tilde{c}_k$ from the PMF $p(c_k)$, where each $\tilde{c}_k$ corresponds to one GLMB component. After sampling, all GLMB components that do not correspond to a sample $\tilde{c}_k$ are pruned. In PS2, the large numbers of objects and clutter measurements lead to a large number of relevant GLMB components with significant PMF values. As a consequence, if the number of samples is small, some of the relevant GLMB components are necessarily pruned, which means that relevant association information is ignored by the Gibbs-LMB filter. This results in a reduced tracking performance of the Gibbs-LMB filter in PS2. By contrast, in the BP-LMB filter, the approximate calculation of the marginal association probabilities is not based on any pruning of components (irrespectively of their weights).

We conclude from Figure 4.4 that for both PS1 and PS2, the proposed BP-LMB filter performs better than or similarly to the other filters. An interesting observation is the similarity of performance relative to the BP-TOMB/P filter. Indeed, a deeper analysis shows that despite the differences in the underlying state and system models, the BP-LMB and BP-TOMB/P filters are quite similar algorithmically. The BP-TOMB/P filter differs from the BP-LMB filter mainly in that it models undetected objects by a Poisson RFS. The modeling of undetected objects can facilitate the generation of new Bernoulli components resulting in improved tracking performance [Williams, 2015]. However, it did not show any performance improvements over our proposed Bernoulli generation

Filter	Total runtime	AP runtime
BP-LMB (proposed)	0.4435 s	$2.28\,10^{-7}$ s
Gibbs-LMB-100	0.4888 s	$2.98\,10^{-5}$ s
BP-TOMB/P	0.8189 s	$3.48\,10^{-7}$ s
Gibbs-LMB-1000	1.7318 s	$3.56\,10^{-4}$ s

Table 4.3: Total runtime and AP runtime for PS2.

scheme of Section 4.3, but resulted in a higher computational complexity in the considered scenarios. As we will show in Chapter 5, the use of the Poisson RFS can be extended from the modeling of undetected objects to the modeling of "unlikely" objects which are objects that are unlikely to exist. This extension is achieved by a flexible transfer of Bernoulli components between the Poisson and the LMB RFS. The modeling of unlikely objects can lead to a large reduction in computational complexity in challenging scenarios with a large number of objects and/or high clutter rate.

Table 4.3 lists the average runtimes of the different filters per time (k) step, referred to as "total runtimes," as well as the average runtimes used for calculating one approximate marginal association probability, referred to as "AP runtimes." The approximate marginal association probabilities are given by $\tilde{p}(c_k^{(l)}\!=\!m)$ in (4.37) for the proposed BP-LMB filter and similarly for the BP-TOMB/P filter, and analogous quantities are computed by the Gibbs-LMB filter using the Gibbs sampling algorithm. The runtimes were obtained for PS2, using a MATLAB implementation on an Intel quad-core i7-6600U CPU. The results for the total runtimes show that the proposed BP-LMB filter is here less complex than the BP-TOMB/P filter and the Gibbs-LMB-100 filter, and significantly less complex than the Gibbs-LMB-1000 filter. Furthermore, the AP runtimes of the BP-LMB and BP-TOMB/P filters are significantly lower than those of the Gibbs-LMB filter. Finally, as may be expected, the total and AP runtimes of the Gibbs-LMB filter increase with the number of Gibbs samples.

The observed lower runtimes of the BP-LMB filter compared to the Gibbs-LMB-1000 filter reflect also the linear scaling behavior of the BP algorithm compared to the quadratic scaling behavior of the Gibbs sampler-based calculation (cf. Section 4.3). On the other hand, the Gibbs-LMB filter employs a smaller number of Bernoulli components than the BP-LMB filter; this is a consequence of the reduction of the number of summation terms in (3.43) and (3.44) caused by the Gibbs sampling. However, this effect is counteracted by the fact that the complexity of the Gibbs-LMB filter scales quadratically in the number of Bernoulli components. This, together with the fact that the number P of samples used by the Gibbs sampler is considerably larger than the number I of BP iterations, causes the Gibbs-LMB filter to be more complex than the BP-LMB filter. Finally, the higher runtime of the BP-TOMB/P filter results from additional operations related to an explicit modeling of undetected objects and a different strategy for generating Bernoulli components.

The proposed BP-LMB filter achieves an excellent tracking accuracy/complexity compromise for the considered tracking scenarios. However, in scenarios with many objects and/or a high clutter rate, the sensor generates a large number of measurements. The large number of measurements results in a large number of newly generated Bernoulli components according to the scheme proposed in Section 4.3, which in turn results in a high computational complexity. In the next chapter, we augment the LMB state RFS by a Poisson RFS. The Poisson RFS will be used to track objects that are unlikely to exist and the LMB RFS to track objects that are likely to exist. The tracking of some part of the multi-object state within the less computationally demanding Poisson part, results in a reduced computational complexity, especially in scenarios of a high clutter rate.

Chapter 5

An Efficient LMB/Poisson Filter

In this chapter, we propose an RFS-based multi-object tracking method with track continuity that improves on the fast LMB filter of Chapter 4. The proposed method combines the strengths of the LMB filter (cf. Section 3.5 and Chapter 4) and the PHD filter (cf. Section 3.3) in that it achieves track continuity and good tracking performance while requiring a relatively low computational complexity. In our method, the multi-object state is modeled as a combination of an LMB RFS, i.e., a labeled RFS, and a Poisson RFS, i.e., an unlabeled RFS. After proposing a system model for labeled/unlabeled multi-object state RFSs, we derive the exact prediction and update steps for this system model. Then, we apply several approximations and modifications including the partitioning of label and measurement sets, the pruning of implausible object-measurement associations, and the transfer of certain unlabeled objects to labeled objects and vice versa.

The resulting algorithm, referred to as LMB/P filter, achieves an excellent compromise between tracking accuracy and computational complexity. This is due to the fact that the LMB/P filter uses the LMB RFS to track objects that are likely to exist and the Poisson RFS to track objects that are unlikely to exist. More specifically, only if a quantity characterizing the plausibility of object existence is above a predefined threshold, the LMB/P filter generates a new labeled Bernoulli component based on the Poisson RFS, and the corresponding object is tracked within the more accurate but less efficient LMB part. Conversely, the LMB/P filter transfers labeled Bernoulli components to the Poisson RFS if the corresponding existence probability falls below another threshold.

In scenarios with many objects and/or a high clutter rate, LMB filters have to generate and maintain a large number of Bernoulli components in order to ensure satisfactory tracking performance. Since the proposed LMB/P filter tracks potential objects within the less computationally demanding Poisson part until their existence is sufficiently plausible, the LMB/P filter achieves a low complexity and a good accuracy/complexity compromise in challenging scenarios. This advantage is demonstrated by simulation experiments comparing the performance and complexity of the proposed filter to those of two state-of-the-art filters and the BP-LMB filter of Chapter 4. On the other hand, in scenarios with few objects and a low or moderate clutter rate, the modeling of unlikely objects by a Poisson RFS may be unnecessarily complicated and result in an increased computational complexity. In such scenarios, the fast LMB filter proposed in Chapter 4 can achieve a lower computational complexity.

The remainder of this chapter is structured as follows. In Section 5.1, we present the system model underlying the LMB/P filter. The prediction step and the exact update step are derived in Sections 5.2 and 5.3, respectively. In Sections 5.4 and 5.5, we present the approximations introduced in the update step of the proposed LMB/P filter. A summary of the LMB/P filter algorithm is provided in Section 5.6. Finally, a simulation study assessing the performance of the proposed algorithm in comparison to the fast LMB filter of Chapter 4 and two state-of-the art filters is presented in Section 5.7.

5.1 System Model

In this section, we describe the system model underlying the proposed LMB/P filter. We present the state-transition model in Section 5.1.1, the measurement model in Section 5.1.2, and the multi-object state model in Section 5.1.3.

In general, we model the multi-object state at time $k-1$ by the tuple $(\tilde{\mathsf{X}}_{k-1}, \mathsf{X}_{k-1})$, where $\tilde{\mathsf{X}}_{k-1}$ is a labeled RFS (cf. Section 2.2) and X_{k-1} an unlabeled RFS (cf. Section 2.1), respectively. The elements of $\tilde{\mathsf{X}}_{k-1}$ are random tuples of the form $(\mathbf{x}_{k-1}, \mathsf{l}) \in \mathbb{R}^{n_x} \times \mathbb{L}^*_{k-1}$, while the elements of X_{k-1} are random vectors $\mathbf{x}_{k-1} \in \mathbb{R}^{n_x}$. Here, $\mathbf{x}_{k-1}$ describes the kinematic part of the state and typically consists of the object's position, the object's velocity and possibly further parameters and l is the label that models the object's identity. The finite set $\mathbb{L}^*_{k-1} \subset \mathbb{L}_{k-1}$ contains the labels corresponding to $\tilde{\mathsf{X}}_{k-1}$, which is a subset of the label space $\mathbb{L}_{k-1} = \{1, \ldots, k-1\} \times \mathbb{N}$. Each label $l \in \mathbb{L}_{k-1}$ is a tuple of the form $l = (k', \nu)$, where $k' \in \{1, \ldots, k-1\}$ represents the object's time of birth and $\nu \in \mathbb{N}$ distinguishes objects born at the same time. We next present the state-transition model underlying the LMB/P filter.

5.1.1 State-transition Model

The state-transition of object state $(\tilde{\mathsf{X}}_{k-1}, \mathsf{X}_{k-1})$ to object state $(\tilde{\mathsf{X}}_k, \mathsf{X}_k)$ can be described by the (multi-object) state-transition pdf $f(\tilde{X}_k, X_k | \tilde{X}_{k-1}, X_{k-1})$. We assume that $\tilde{\mathsf{X}}_k$ and X_k evolve independently in the sense that $\tilde{\mathsf{X}}_k$ and X_k are independent given $(\tilde{X}_{k-1}, X_{k-1})$. Thus, the joint state-transition PDF can be decomposed according to $f(\tilde{X}_k, X_k | \tilde{X}_{k-1}, X_{k-1}) = f(\tilde{X}_k | \tilde{X}_{k-1}, X_{k-1}) f(X_k | \tilde{X}_{k-1}, X_{k-1})$; by further assuming that $f(\tilde{X}_k | \tilde{X}_{k-1}, X_{k-1}) = f(\tilde{X}_k | \tilde{X}_{k-1})$ and $f(X_k | \tilde{X}_{k-1}, X_{k-1}) = f(X_k | X_{k-1})$, i.e., that the labeled objects at time k are independent of the unlabeled objects at time $k-1$ and that the unlabeled objects at time k are independent of the labeled objects at time $k-1$, we get $f(\tilde{X}_k, X_k | \tilde{X}_{k-1}, X_{k-1}) = f(\tilde{X}_k | \tilde{X}_{k-1}) f(X_k | X_{k-1})$. Alternatively, the state-transition statistics can be described by the joint "state-transition PGFL," which is defined as[1]

$$G_{\tilde{\mathsf{X}}_k,\mathsf{X}_k}[\tilde{h},h|\tilde{X}_{k-1},X_{k-1}] \triangleq \int\!\!\int \tilde{h}^{\tilde{X}_k} h^{X_k} f(\tilde{X}_k, X_k|\tilde{X}_{k-1}, X_{k-1})\,\delta X_k\,\delta\tilde{X}_k. \tag{5.1}$$

By inserting $f(\tilde{X}_k, X_k|\tilde{X}_{k-1}, X_{k-1}) = f(\tilde{X}_k|\tilde{X}_{k-1})\,f(X_k|X_{k-1})$ into (5.1), we get

$$G_{\tilde{\mathsf{X}}_k,\mathsf{X}_k}[\tilde{h},h|\tilde{X}_{k-1},X_{k-1}] = G_{\tilde{\mathsf{X}}_k}[\tilde{h}|\tilde{X}_{k-1}]\,G_{\mathsf{X}_k}[h|X_{k-1}], \tag{5.2}$$

with

$$G_{\tilde{\mathsf{X}}_k}[\tilde{h}|\tilde{X}_{k-1}] \triangleq \int \tilde{h}^{\tilde{X}_k} f(\tilde{X}_k|\tilde{X}_{k-1})\,\delta\tilde{X}_k, \tag{5.3}$$

$$G_{\mathsf{X}_k}[h|X_{k-1}] \triangleq \int h^{X_k} f(X_k|X_{k-1})\,\delta X_k. \tag{5.4}$$

Next, we will develop expressions for (5.3) and (5.4).

At time $k-1$, an object with labeled state $(\mathsf{x}_{k-1},\mathsf{l}) \in \tilde{\mathsf{X}}_{k-1}$ either survives with probability $p_{\mathrm{S}}(\boldsymbol{x}_{k-1},l)$ or dies with probability $1-p_{\mathrm{S}}(\boldsymbol{x}_{k-1},l)$. If it survives, its new state x_k (without the label l) is distributed according to the transition PDF $f(\boldsymbol{x}_k|\boldsymbol{x}_{k-1},l)$, and the label is preserved. We assume that the states of different objects evolve independently, i.e., $(\mathsf{x}_k,\mathsf{l})$ is conditionally independent, given $(\boldsymbol{x}_{k-1},l)$, of all the other $(\mathsf{x}'_k,\mathsf{l}') \in \tilde{\mathsf{X}}_k$ and of all the $\mathsf{x}'_k \in \mathsf{X}_k$. Due to these assumptions, the multi-object state of the labeled objects at time k, given $\tilde{X}_{k-1}$, is described by an LMB RFS (cf. Section 2.2.2)

$$\tilde{\mathsf{X}}_k = \bigcup_{l\in\mathbb{L}^*_{k-1}} \tilde{\mathsf{S}}_k(\boldsymbol{x}_{k-1},l), \tag{5.5}$$

where $\tilde{\mathsf{S}}_k(\boldsymbol{x}_{k-1},l)$ is a labeled Bernoulli RFS parametrized by the existence probability $p_{\mathrm{S}}(\boldsymbol{x}_{k-1},l)$ and the spatial PDF $f(\boldsymbol{x}_k|\boldsymbol{x}_{k-1},l)$. The LMB RFS $\tilde{\mathsf{X}}_k$, given $\tilde{X}_{k-1}$, is thus fully characterized by $\big\{\big(p_{\mathrm{S}}(\boldsymbol{x}_{k-1},l), f(\boldsymbol{x}_k|\boldsymbol{x}_{k-1},l)\big)\big\}_{l\in\mathbb{L}^*_{k-1}}$. The state-transition model (5.5) defines the state-transition PDF of labeled objects $f(\tilde{X}_k|\tilde{X}_{k-1})$ and, thus, also the corresponding state-transition PGFL of labeled objects $G_{\tilde{\mathsf{X}}_k}[\tilde{h}|\tilde{X}_{k-1}]$ in (5.3), which is of LMB type and given by

$$G_{\tilde{\mathsf{X}}_k}[\tilde{h}|\tilde{X}_{k-1}] = \prod_{l\in\mathbb{L}^*_{k-1}} G^{\mathrm{Ber}}\big[\tilde{h}; p_{\mathrm{S}}(\boldsymbol{x}_{k-1},l), f\big(\,\cdot\,\big|\boldsymbol{x}_{k-1},l\big)\big], \tag{5.6}$$

where $f\big[\tilde{h}\big|\boldsymbol{x}_{k-1},l\big] \triangleq \int \tilde{h}(\boldsymbol{x}_k,l)\,f\big(\boldsymbol{x}_k\big|\boldsymbol{x}_{k-1},l\big)\,\mathrm{d}\boldsymbol{x}_k$.

Furthermore, at time $k-1$, an unlabeled object with state $\mathsf{x}_{k-1} \in \mathsf{X}_{k-1}$ either survives with probability[2] $p_{\mathrm{S}}(\boldsymbol{x}_{k-1})$ or dies with probability $1-p_{\mathrm{S}}(\boldsymbol{x}_{k-1})$. If it survives, its new

[1] This mixed labeled/unlabeled integral is defined as an iterated integral, e.g., $\int\Big(\int h^{X_k} f(\tilde{X}_k, X_k|Z_{1:k})\,\delta X_k\Big)\tilde{h}^{\tilde{X}_k}\,\delta\tilde{X}_k$, using first (2.1) for the inner integral and then (2.21) for the outer integral.

[2] With an abuse of notation, $p_{\mathrm{S}}(\cdot)$ is used to denote both the survival probability of labeled objects (with argument $(\boldsymbol{x}_{k-1},l)$) and of unlabeled objects (with argument $\boldsymbol{x}_{k-1}$). A similar remark applies to the detection probability $p_{\mathrm{D}}(\cdot)$ considered in Section 5.1.2.

state x_k is distributed according to the transition PDF $f(\boldsymbol{x}_k|\boldsymbol{x}_{k-1})$. We assume that the states of different unlabeled objects evolve independently, i.e., x_k is conditionally independent, given $\boldsymbol{x}_{k-1}$, of all the other $\mathsf{x}'_k \in \mathsf{X}_k$ and of all $(\mathsf{x}'_k, \mathsf{l}') \in \tilde{\mathsf{X}}_k$. Accordingly, the multi-object state of the survived unlabeled objects at time k, given X_{k-1}, is modeled as an MB RFS (cf. Section 2.1.4) $\mathsf{X}_k^{\mathrm{S}} = \bigcup_{\boldsymbol{x}_{k-1} \in X_{k-1}} \mathsf{S}_k(\boldsymbol{x}_{k-1})$, where $\mathsf{S}_k(\boldsymbol{x}_{k-1})$ is a Bernoulli RFS with existence probability $p_{\mathrm{S}}(\boldsymbol{x}_{k-1})$ and spatial PDF $f(\boldsymbol{x}_k|\boldsymbol{x}_{k-1})$. The MB RFS $\mathsf{X}_k^{\mathrm{S}}$ is thus fully characterized by $\big\{\big(p_{\mathrm{S}}(\boldsymbol{x}_{k-1}), f(\boldsymbol{x}_k|\boldsymbol{x}_{k-1})\big)\big\}_{\boldsymbol{x}_{k-1} \in X_{k-1}}$.

There may also be newborn unlabeled objects.[3] Their multi-object state is modeled by a Poisson RFS $\mathsf{X}_k^{\mathrm{B}}$ with mean parameter μ_{B} and spatial PDF $f_{\mathrm{B}}(\boldsymbol{x}_k)$ and, hence, PHD $\lambda_{\mathrm{B}}(\boldsymbol{x}_k) = \mu_{\mathrm{B}} f_{\mathrm{B}}(\boldsymbol{x}_k)$ (cf. Section 2.1.2). We furthermore assume that the newborn objects $\mathsf{X}_k^{\mathrm{B}}$ are conditionally independent, given $\tilde{X}_{k-1}$, of the survived objects $\mathsf{X}_k^{\mathrm{S}}$. The entirety of unlabeled objects at time k, given X_{k-1}, is modeled by the RFS

$$\mathsf{X}_k = \mathsf{X}_k^{\mathrm{S}} \cup \mathsf{X}_k^{\mathrm{B}} = \left(\bigcup_{\boldsymbol{x}_{k-1} \in X_{k-1}} \mathsf{S}_k(\boldsymbol{x}_{k-1}) \right) \cup \mathsf{X}_k^{\mathrm{B}}. \tag{5.7}$$

The state-transition model (5.7) defines the state-transition PDF of unlabeled objects $f(X_k|X_{k-1})$ and, thus, also the corresponding state-transition PGFL of unlabeled objects $G_{\mathsf{X}_k}[h|X_{k-1}]$ in (5.4). Given our model assumptions described above, it follows that $\mathsf{X}_k^{\mathrm{S}}$ and $\mathsf{X}_k^{\mathrm{B}}$ in (5.7) are conditionally independent given X_{k-1}; thus, the PGFL $G_{\mathsf{X}_k}[h|X_{k-1}]$ factorizes according to (2.7) as

$$G_{\mathsf{X}_k}[h|X_{k-1}] = G_{\mathsf{X}_k^{\mathrm{S}}}[h|X_{k-1}]\, G_{\mathsf{X}_k^{\mathrm{B}}}[h]. \tag{5.8}$$

According to our model, $G_{\mathsf{X}_k^{\mathrm{S}}}[h|X_{k-1}]$ is of MB type (cf. (2.20)), i.e.,

$$G_{\mathsf{X}_k^{\mathrm{S}}}[h|X_{k-1}] = \prod_{\boldsymbol{x}_{k-1} \in X_{k-1}} G^{\mathrm{Ber}}\big[h; p_{\mathrm{S}}(\boldsymbol{x}_{k-1}), f(\cdot|\boldsymbol{x}_{k-1})\big], \tag{5.9}$$

with $f[h|\boldsymbol{x}_{k-1}] \triangleq \int h(\boldsymbol{x}_k) f(\boldsymbol{x}_k|\boldsymbol{x}_{k-1}) \mathrm{d}\boldsymbol{x}_k$, and $G_{\mathsf{X}_k^{\mathrm{B}}}[h]$ is of Poisson type (cf. (2.11)), i.e.,

$$G_{\mathsf{X}_k^{\mathrm{B}}}[h] = e^{\lambda_k^{\mathrm{B}}[h-1]}, \tag{5.10}$$

with $\lambda_k^{\mathrm{B}}[h-1] \triangleq \int (h(\boldsymbol{x}_k) - 1) \lambda_{\mathrm{B}}(\boldsymbol{x}_k) \mathrm{d}\boldsymbol{x}_k$. Next, we describe the measurement model underlying the proposed LMB/P filter.

[3] In our system model, newborn objects may not be labeled objects. As we will explain in Section 5.3, there do exist “new” labeled objects, which are previously unlabeled objects that are augmented by a new distinct label and thereby are transferred from the unlabeled RFS to the labeled RFS. Thus, this creation of new labeled objects is not modeled by a birth process as in the LMB filter [Reuter et al., 2014]; it is considered as part of the tracking algorithm, rather than of the system model.

5.1.2 Measurement Model

At time k, a sensor produces M_k measurements $\mathbf{z}_k^{(1)}, \dots, \mathbf{z}_k^{(\mathsf{M}_k)}$, which are modeled as an (unlabeled) RFS $\mathsf{Z}_k \triangleq \{\mathbf{z}_k^{(1)}, \dots, \mathbf{z}_k^{(\mathsf{M}_k)}\}$[4]. The measurements may originate from a labeled object, an unlabeled object, or clutter. The statistics of the measurements can be described by the likelihood function $f(Z_k|\tilde{X}_k, X_k)$ or, equivalently, by the "likelihood PGFL," which is defined as

$$G_{\mathsf{Z}_k}[g|\tilde{X}_k, X_k] \triangleq \int g^{Z_k} f(Z_k|\tilde{X}_k, X_k)\, \delta Z_k . \tag{5.11}$$

In the following, we develop an expression for (5.11).

A labeled object with state $(\mathbf{x}_k, \mathsf{l}) \in \tilde{\mathsf{X}}_k$ is detected (i.e., it generates a measurement) with probability $p_{\mathrm{D}}(\boldsymbol{x}_k, l)$ or is missed (i.e., it does not generate a measurement) with probability $1 - p_{\mathrm{D}}(\boldsymbol{x}_k, l)$. In the first case, the object generates exactly one measurement $\mathbf{z}_k$, which is distributed according to the single-object likelihood function $f(\boldsymbol{z}_k|\boldsymbol{x}_k, l)$. We assume that $\mathbf{z}_k$ is conditionally independent, given $(\boldsymbol{x}_k, l)$, of all the other $\mathbf{z}'_k \in \mathsf{Z}_k$, all the other $(\mathbf{x}'_k, \mathsf{l}') \in \tilde{\mathsf{X}}_k$, and all the $\mathbf{x}'_k \in \mathsf{X}_k$. Accordingly, the measurements originating from labeled objects, given $\tilde{X}_k$, are modeled by an MB $\mathsf{Z}_k^{\mathrm{L}} = \bigcup_{l \in \mathbb{L}_{k-1}^*} \Theta_k^{\mathrm{L}}(\boldsymbol{x}_k, l)$, where $\Theta_k^{\mathrm{L}}(\boldsymbol{x}_k, l)$ is a Bernoulli RFS with existence probability $p_{\mathrm{D}}(\boldsymbol{x}_k, l)$ and spatial PDF $f(\boldsymbol{z}_k|\boldsymbol{x}_k, l)$. Thus, $\mathsf{Z}_k^{\mathrm{L}}$ is characterized by the parameter set $\{(p_{\mathrm{D}}(\boldsymbol{x}_k, l), f(\boldsymbol{z}_k|\boldsymbol{x}_k, l))\}_{l \in \mathbb{L}_{k-1}^*}$.

An unlabeled object with state $\mathbf{x}_k \in \mathsf{X}_k$ is detected with probability $p_{\mathrm{D}}(\boldsymbol{x}_k)$ or is missed with probability $1 - p_{\mathrm{D}}(\boldsymbol{x}_k)$. In the first case, it generates exactly one measurement $\mathbf{z}_k$, which is distributed according to the single-object likelihood function $f(\boldsymbol{z}_k|\boldsymbol{x}_k)$. We assume that $\mathbf{z}_k$ is conditionally independent, given $\boldsymbol{x}_k$, of all the other $\mathbf{z}'_k \in \mathsf{Z}_k$, all the other $\mathbf{x}'_k \in \mathsf{X}_k$, and all the $(\mathbf{x}'_k, \mathsf{l}') \in \tilde{\mathsf{X}}_k$. Thus, the measurements originating from unlabeled objects, given X_k, are modeled by an MB RFS $\mathsf{Z}_k^{\mathrm{U}} = \bigcup_{\boldsymbol{x}_k \in X_k} \Theta_k^{\mathrm{U}}(\boldsymbol{x}_k)$, where $\Theta_k^{\mathrm{U}}(\boldsymbol{x}_k)$ is a Bernoulli RFS with existence probability $p_{\mathrm{D}}(\boldsymbol{x}_k)$ and spatial PDF $f(\boldsymbol{z}_k|\boldsymbol{x}_k)$. Thus, $\mathsf{Z}_k^{\mathrm{U}}$ is characterized by the parameter set $\{(p_{\mathrm{D}}(\boldsymbol{x}_k), f(\boldsymbol{z}_k|\boldsymbol{x}_k))\}_{\boldsymbol{x}_k \in X_k}$.

Finally, the clutter-originated measurements are modeled by a Poisson RFS $\mathsf{Z}_k^{\mathrm{C}}$ with mean parameter μ_{C} and spatial PDF $f_{\mathrm{C}}(\boldsymbol{z}_k)$ and, hence, PHD $\lambda_{\mathrm{C}}(\boldsymbol{z}_k) = \mu_{\mathrm{C}} f_{\mathrm{C}}(\boldsymbol{z}_k)$. We furthermore assume that the clutter-orginated measurements are conditionally independent, given $(\tilde{X}_k, X_k)$, of the measurements originated by labeled and unlabeled objects, i.e., of $\mathsf{Z}_k^{\mathrm{L}}$ and $\mathsf{Z}_k^{\mathrm{U}}$. The overall measurement RFS at time k, given the multi-object state $(\tilde{X}_k, X_k)$, is

$$\mathsf{Z}_k = \mathsf{Z}_k^{\mathrm{L}} \cup \mathsf{Z}_k^{\mathrm{U}} \cup \mathsf{Z}_k^{\mathrm{C}} = \Bigg(\bigcup_{l \in \mathbb{L}_{k-1}^*} \Theta_k^{\mathrm{L}}(\boldsymbol{x}_k, l) \Bigg) \cup \Bigg(\bigcup_{\boldsymbol{x}_k \in X_k} \Theta_k^{\mathrm{U}}(\boldsymbol{x}_k) \Bigg) \cup \mathsf{Z}_k^{\mathrm{C}} . \tag{5.12}$$

[4]The measurement model describes the statistical dependency of the random (unobserved) measurements on the multiobject state. Accordingly, at this point, the measurements are considered random and thus denoted as $\mathsf{Z}_k = \{\mathbf{z}_k^{(1)}, \dots, \mathbf{z}_k^{(\mathsf{M}_k)}\}$. However, in the context of the proposed tracking algorithm (see Sections 5.1.3–5.6), the measurements will be considered as deterministic (observed) and will thus be denoted as $Z_k = \{\boldsymbol{z}_k^{(1)}, \dots, \boldsymbol{z}_k^{(M_k)}\}$.

The measurement model (5.12) defines the multi-object likelihood function $f(Z_k|\tilde{X}_k, X_k)$ and, thus, also the likelihood PGFL $G_{\mathsf{Z}_k}[g|\tilde{X}_k, X_k]$ in (5.11). Due to our model assumptions described above, the measurements $\mathsf{Z}_k^{\mathrm{L}}$, $\mathsf{Z}_k^{\mathrm{U}}$, and $\mathsf{Z}_k^{\mathrm{C}}$ are conditionally independent given $(\tilde{X}_k, X_k)$. Thus, $G_{\mathsf{Z}_k}[g|\tilde{X}_k, X_k]$ factorizes according to

$$G_{\mathsf{Z}_k}[g|\tilde{X}_k, X_k] = G_{\mathsf{Z}_k^{\mathrm{L}}}[g|\tilde{X}_k]\, G_{\mathsf{Z}_k^{\mathrm{U}}}[g|X_k]\, G_{\mathsf{Z}_k^{\mathrm{C}}}[g]\,. \tag{5.13}$$

Here, $G_{\mathsf{Z}_k^{\mathrm{L}}}[g|\tilde{X}_k]$ and $G_{\mathsf{Z}_k^{\mathrm{U}}}[g|X_k]$ are both of MB type, i.e.,

$$G_{\mathsf{Z}_k^{\mathrm{L}}}[g|\tilde{X}_k] = \prod_{l \in \mathbb{L}_{k-1}^*} G^{\mathrm{Ber}}\big[g; p_{\mathrm{D}}(\boldsymbol{x}_k, l), f(\,\cdot\,|\boldsymbol{x}_k, l)\big]\,, \tag{5.14}$$

$$G_{\mathsf{Z}_k^{\mathrm{U}}}[g|X_k] = \prod_{\boldsymbol{x}_k \in X_k} G^{\mathrm{Ber}}\big[g; p_{\mathrm{D}}(\boldsymbol{x}_k), f(\cdot|\boldsymbol{x}_k)\big]\,, \tag{5.15}$$

where $f[g|\boldsymbol{x}_k, l] \triangleq \int g(\boldsymbol{z}_k) f(\boldsymbol{z}_k|\boldsymbol{x}_k, l)\mathrm{d}\boldsymbol{z}_k$ and $f[g|\boldsymbol{x}_k] \triangleq \int g(\boldsymbol{z}_k) f(\boldsymbol{z}_k|\boldsymbol{x}_k)\mathrm{d}\boldsymbol{z}_k$. Further, $G_{\mathsf{Z}_k^{\mathrm{C}}}[g]$ is of Poisson type, i.e.,

$$G_{\mathsf{Z}_k^{\mathrm{C}}}[g] = e^{\lambda_k^{\mathrm{C}}[g-1]}\,, \tag{5.16}$$

where $\lambda_k^{\mathrm{C}}[g-1] \triangleq \int (g(\boldsymbol{z}_k)-1)\,\lambda_{\mathrm{C}}(\boldsymbol{z}_k)\mathrm{d}\boldsymbol{z}_k$. Next, we will specify the model of the multi-object state.

5.1.3 Multi-object State Model

In a Bayesian sequential inference framework, the fundamental quantity to be calculated recursively is the joint posterior multi-object PDF of $\tilde{\mathsf{X}}_k$ and X_k, i.e., $f(\tilde{X}_k, X_k|Z_{1:k})$, with $Z_{1:k} \triangleq (Z_1, \dots, Z_k)$. We assume that at time $k-1$, $\tilde{\mathsf{X}}_{k-1}$ and X_{k-1} are conditionally independent given $Z_{1:k-1}$, so that

$$f(\tilde{X}_{k-1}, X_{k-1}|Z_{1:k-1}) = f(\tilde{X}_{k-1}|Z_{1:k-1})\, f(X_{k-1}|Z_{1:k-1})\,. \tag{5.17}$$

Alternatively, we can describe the posterior statistics in form of the joint posterior PGFL, which is defined at time $k-1$ as

$$G_{\tilde{\mathsf{X}}_{k-1},\mathsf{X}_{k-1}}[\tilde{h}, h|Z_{1:k-1}] \triangleq \int\!\!\int \tilde{h}^{\tilde{X}_{k-1}} h^{X_{k-1}} f(\tilde{X}_{k-1}, X_{k-1}|Z_{1:k-1})\, \delta\tilde{X}_{k-1}\delta X_{k-1}\,. \tag{5.18}$$

Inserting (5.17) into (5.18) yields

$$G_{\tilde{\mathsf{X}}_{k-1},\mathsf{X}_{k-1}}[\tilde{h}, h|Z_{1:k-1}] = G_{\tilde{\mathsf{X}}_{k-1}}[\tilde{h}|Z_{1:k-1}]\, G_{\mathsf{X}_{k-1}}[h|Z_{1:k-1}]\,, \tag{5.19}$$

where

$$G_{\tilde{\mathsf{X}}_{k-1}}[\tilde{h}|Z_{1:k-1}] \triangleq \int \tilde{h}^{\tilde{X}_{k-1}} f(\tilde{X}_{k-1}|Z_{1:k-1})\,\delta\tilde{X}_{k-1}\,, \tag{5.20}$$

$$G_{\mathsf{X}_{k-1}}[h|Z_{1:k-1}] \triangleq \int h^{X_{k-1}} f(X_{k-1}|Z_{1:k-1})\,\delta X_{k-1}\,. \tag{5.21}$$

The posterior PGFLs $G_{\tilde{\mathsf{X}}_{k-1}}[\tilde{h}|Z_{1:k-1}]$ and $G_{\mathsf{X}_{k-1}}[h|Z_{1:k-1}]$ are defined as follows. We model $\tilde{\mathsf{X}}_{k-1}$ as an LMB RFS consisting of $|\mathbb{L}^*_{k-1}|$ labeled Bernoulli RFSs with existence probabilities $r^{(l)}_{k-1}$ and spatial PDFs $f^{(l)}(\boldsymbol{x}_{k-1})$, $l \in \mathbb{L}^*_{k-1}$. Here, $\mathbb{L}^*_{k-1} \subseteq \mathbb{L}_{k-1}$ is the set of labels underlying the LMB state RFS $\tilde{\mathsf{X}}_{k-1}$. Thus, according to (2.26), the posterior PGFL of the labeled objects at time $k-1$ is

$$G_{\tilde{\mathsf{X}}_{k-1}}[\tilde{h}|Z_{1:k-1}] = \prod_{l \in \mathbb{L}^*_{k-1}} G^{\text{Ber}}[\tilde{h}; r^{(l)}_{k-1}, f^{(l)}_{k-1}], \tag{5.22}$$

where $f^{(l)}_{k-1}[\tilde{h}] = \int \tilde{h}(\boldsymbol{x}_{k-1}, l)\, f^{(l)}(\boldsymbol{x}_{k-1})\mathrm{d}\boldsymbol{x}_{k-1}$. Note that each Bernoulli component in (5.22) represents a potentially existing object. Furthermore, we model X_{k-1} as a Poisson RFS with PHD $\lambda(\boldsymbol{x}_{k-1})$. Thus, according to (2.11), the posterior PGFL of the unlabeled objects at time $k-1$ is given by

$$G_{\mathsf{X}_{k-1}}[h|Z_{1:k-1}] = e^{\lambda_{k-1}[h-1]}, \tag{5.23}$$

with $\lambda_{k-1}[h-1] = \int (h(\boldsymbol{x}_{k-1}) - 1)\, \lambda(\boldsymbol{x}_{k-1})\mathrm{d}\boldsymbol{x}_{k-1}$.

The labeled state RFS, i.e, the LMB RFS $\tilde{\mathsf{X}}_{k-1}$, allows the corresponding objects to be distinguished, whereas the objects modeled by the unlabeled state RFS, i.e., the Poisson RFS X_{k-1}, are indistinguishable. On the other hand, the Poisson RFS is parametrized by a single function, i.e., its PHD, and it enables a much more efficient representation and processing of a large number of potentially existing objects. Therefore, we will model objects that are likely to exist by the computationally more demanding LMB part and objects that are unlikely to exist by the computationally less demanding Poisson part. The LMB part guarantees track continuity and thereby allows the consistent tracking of distinguishable objects over consecutive time steps.

5.2 Prediction Step

The proposed LMB/P filter propagates the posterior multi-object PDF $f(\tilde{X}_k, X_k|Z_{1:k})$, equivalently the posterior PGFL $G_{\tilde{\mathsf{X}}_k,\mathsf{X}_k}[\tilde{h}, h|Z_{1:k}]$, from one time step to the next. This propagation consists of a prediction step and an update step.

We start with the derivation of the prediction step, which converts the previous posterior PGFL $G_{\tilde{\mathsf{X}}_{k-1},\mathsf{X}_{k-1}}[\tilde{h}, h|Z_{1:k-1}]$ in (5.18), into the predicted posterior PGFL $G_{\tilde{\mathsf{X}}_k,\mathsf{X}_k}[\tilde{h}, h|Z_{1:k-1}]$. It is defined according to

$$G_{\tilde{\mathsf{X}}_k,\mathsf{X}_k}[\tilde{h}, h|Z_{1:k-1}] \triangleq \int\!\!\int \tilde{h}^{\tilde{X}_k} h^{X_k} f(\tilde{X}_k, X_k|Z_{1:k-1})\, \delta\tilde{X}_k \delta X_k\,, \tag{5.24}$$

where $f(\tilde{X}_k, X_k|Z_{1:k-1})$ is the predicted posterior multi-object PDF. This conversion is based on the multi-object state-transition model described in Section 5.1.1. The derivation of the prediction step is similar to that in [Williams, 2015] but extends it from an unlabeled object state to a labeled/unlabeled object state.

Recap that the prediction step is given by the Chapman-Kolmogorov equation according to (3.1) as

$$f(\tilde{X}_k, X_k|Z_{1:k-1}) = \iint f(\tilde{X}_k, X_k|\tilde{X}_{k-1}, X_{k-1}) f(\tilde{X}_{k-1}, X_{k-1}|Z_{1:k-1}) \delta\tilde{X}_{k-1} \delta X_{k-1} . \tag{5.25}$$

Here, expression (5.25) extends (3.1) from PDFs describing unlabeled RFSs to PDFs describing tuples of labeled/unlabeled RFSs. Inserting (5.25) into (5.24) and grouping terms, yields

$$\begin{aligned} &G_{\tilde{\mathsf{X}}_k,\mathsf{X}_k}[\tilde{h}, h|Z_{1:k-1}] \\ &= \iint \left(\iint \tilde{h}^{\tilde{X}_k} h^{X_k} f(\tilde{X}_k, X_k|\tilde{X}_{k-1}, X_{k-1}) \delta\tilde{X}_k \delta X_k \right) f(\tilde{X}_{k-1}, X_{k-1}|Z_{1:k-1}) \delta\tilde{X}_{k-1} \delta X_{k-1} \\ &= \iint G_{\tilde{\mathsf{X}}_k,\mathsf{X}_k}[\tilde{h}, h|\tilde{X}_{k-1}, X_{k-1}]\, f(\tilde{X}_{k-1}, X_{k-1}|Z_{1:k-1}) \delta\tilde{X}_{k-1} \delta X_{k-1} , \end{aligned} \tag{5.26}$$

where we have used the definition of the state-transition PGFL $G_{\tilde{\mathsf{X}}_k,\mathsf{X}_k}[\tilde{h}, h|\tilde{X}_{k-1}, X_{k-1}]$ in (5.1). Further using (5.2) and (5.17) yields

$$\begin{aligned} G_{\tilde{\mathsf{X}}_k,\mathsf{X}_k}[\tilde{h}, h|Z_{1:k-1}] = &\int G_{\tilde{\mathsf{X}}_k}[\tilde{h}|\tilde{X}_{k-1}]\, f(\tilde{X}_{k-1}|Z_{1:k-1}) \delta\tilde{X}_{k-1} \\ &\times \int G_{\mathsf{X}_k}[h|X_{k-1}]\, f(X_{k-1}|Z_{1:k-1}) \delta X_{k-1} . \end{aligned}$$

After introducing the short notations

$$G_{\tilde{\mathsf{X}}_k}[\tilde{h}|Z_{1:k-1}] \triangleq \int G_{\tilde{\mathsf{X}}_k}[\tilde{h}|\tilde{X}_{k-1}]\, f(\tilde{X}_{k-1}|Z_{1:k-1}) \delta\tilde{X}_{k-1} , \tag{5.27}$$

$$G_{\mathsf{X}_k}[h|Z_{1:k-1}] \triangleq \int G_{\mathsf{X}_k}[h|X_{k-1}]\, f(X_{k-1}|Z_{1:k-1}) \delta X_{k-1} , \tag{5.28}$$

expression (5.26) becomes

$$G_{\tilde{\mathsf{X}}_k,\mathsf{X}_k}[\tilde{h}, h|Z_{1:k-1}] = G_{\tilde{\mathsf{X}}_k}[\tilde{h}|Z_{1:k-1}]\, G_{\mathsf{X}_k}[h|Z_{1:k-1}] . \tag{5.29}$$

Analogously to the previous joint posterior PGFL (5.19), the predicted joint posterior PGFL (5.29) factorizes into a labeled and an unlabeled part. Hence, the prediction step can be performed separately for the labeled and unlabeled objects. This is a direct consequence of the model assumptions (5.17) and (5.2). Next, we derive expressions of the predicted posterior pgfl of labeled objects $G_{\tilde{\mathsf{X}}_k}[\tilde{h}|Z_{1:k-1}]$ in (5.27) and the predicted posterior pgfl of unlabeled objects $G_{\mathsf{X}_k}[h|Z_{1:k-1}]$ in (5.28) based on the state-transition model proposed in Section 5.1.1.

5.2.1 Expression of the Predicted Posterior PGFL of Labeled Objects $G_{\tilde{\mathsf{X}}_k}[\tilde{h}|Z_{1:k-1}]$

We now derive a specific expression of $G_{\tilde{\mathsf{X}}_k}[\tilde{h}|Z_{1:k-1}]$ in (5.29) by first inserting (5.6) into (5.27), which yields

$$G_{\tilde{\mathsf{X}}_k}[\tilde{h}|Z_{1:k-1}] = \int \bigg(\prod_{l \in \mathbb{L}^*_{k-1}} G^{\mathrm{Ber}}\big[\tilde{h}; p_{\mathrm{S}}(\boldsymbol{x}_{k-1}, l), f(\,\cdot\,|\boldsymbol{x}_{k-1}, l)\big] \bigg) f(\tilde{X}_{k-1}|Z_{1:k-1})\,\delta\tilde{X}_{k-1}$$
$$= G_{\tilde{\mathsf{X}}_{k-1}}[\tilde{h}'|Z_{1:k-1}]. \tag{5.30}$$

Here, we have used the definition of the PGFL of a labeled RFS in (2.23) and introduced the short notation

$$\tilde{h}'(\boldsymbol{x}_k, l) \triangleq G^{\mathrm{Ber}}\big[\tilde{h}; p_{\mathrm{S}}(\boldsymbol{x}_{k-1}, l), f(\,\cdot\,|\boldsymbol{x}_{k-1}, l)\big]$$
$$= 1 - p_{\mathrm{S}}(\boldsymbol{x}_{k-1}, l) + p_{\mathrm{S}}(\boldsymbol{x}_{k-1}, l) \int \tilde{h}(\boldsymbol{x}_k, l) f(\boldsymbol{x}_k|\boldsymbol{x}_{k-1}, l)\,\mathrm{d}\boldsymbol{x}_k.$$

The PGFL $G_{\tilde{\mathsf{X}}_{k-1}}[\tilde{h}'|Z_{1:k-1}]$ in (5.30) is the previous posterior PGFL of labeled objects (5.20) but with $\tilde{h}(\boldsymbol{x}_{k-1}, l)$ replaced by $\tilde{h}'(\boldsymbol{x}_k, l)$. Since, according to (5.22), $G_{\tilde{\mathsf{X}}_{k-1}}[\tilde{h}|Z_{1:k-1}]$ is an LMB pgfl parametrized by $\big\{(r^{(l)}_{k-1}, f^{(l)}(\boldsymbol{x}_{k-1}))\big\}_{l \in \mathbb{L}^*_{k-1}}$, the predicted posterior PGFL of labeled objects (5.30) can be rewritten according to (2.26) as

$$G_{\tilde{\mathsf{X}}_k}[h|Z_{1:k-1}] = \prod_{l \in \mathbb{L}^*_{k-1}} 1 - r^{(l)}_{k-1} + r^{(l)}_{k-1} \int \tilde{h}'(\boldsymbol{x}_{k-1}, l)\, f^{(l)}(\boldsymbol{x}_{k-1})\mathrm{d}\boldsymbol{x}_{k-1}.$$

Note that the same expression appears in the derivation of the LMB filter [Reuter et al., 2014]. There it was shown that it corresponds to an LMB pgfl and can thus be rewritten according to

$$G_{\tilde{\mathsf{X}}_k}[h|Z_{1:k-1}] = \prod_{l \in \mathbb{L}^*_{k-1}} 1 - r^{(l)}_{k|k-1} + r^{(l)}_{k|k-1} \int \tilde{h}(\boldsymbol{x}_k, l)\, f^{(l)}_{k|k-1}(\boldsymbol{x}_k)\mathrm{d}\boldsymbol{x}_k$$
$$= \prod_{l \in \mathbb{L}^*_{k-1}} G^{\mathrm{Ber}}[\tilde{h}; r^{(l)}_{k|k-1}, f^{(l)}_{k|k-1}], \tag{5.31}$$

with the existence probabilities and spatial PDFs given by

$$r^{(l)}_{k|k-1} = r^{(l)}_{k-1} \int p_{\mathrm{S}}(\boldsymbol{x}_{k-1}, l) f^{(l)}(\boldsymbol{x}_{k-1})\mathrm{d}\boldsymbol{x}_{k-1}, \tag{5.32}$$

$$f^{(l)}_{k|k-1}(\boldsymbol{x}_k) = \frac{\int f(\boldsymbol{x}_k|\boldsymbol{x}_{k-1}, l) p_{\mathrm{S}}(\boldsymbol{x}_{k-1}, l) f^{(l)}(\boldsymbol{x}_{k-1})\mathrm{d}\boldsymbol{x}_{k-1}}{\int p_{\mathrm{S}}(\boldsymbol{x}'_{k-1}, l) f^{(l)}(\boldsymbol{x}'_{k-1})\mathrm{d}\boldsymbol{x}'_{k-1}}, \tag{5.33}$$

for $l \in \mathbb{L}^*_{k-1}$. Here, $p_{\mathrm{S}}(\boldsymbol{x}_{k-1}, l)$ and $f(\boldsymbol{x}_k|\boldsymbol{x}_{k-1}, l)$ are the survival probability and state-transition PDF, respectively, introduced in Section 5.1.1, and $r^{(l)}_{k-1}$ and $f^{(l)}(\boldsymbol{x}_{k-1})$ are the posterior existence probabilities and posterior spatial PDFs, respectively, describing the labeled objects at time $k-1$ (cf. (5.22)). Note that the relations (5.32) and (5.33) are equal to the prediction relations in the LMB filter (cf. (3.34) and (3.35)).

5.2.2 Expression of the Predicted Posterior PGFL of Unlabeled Objects $G_{\mathsf{X}_k}[h|Z_{1:k-1}]$

Next, we derive a specific expression of the PGFL $G_{\mathsf{X}_k}[h|Z_{1:k-1}]$ in (5.28). We therefore insert (5.8)–(5.10) into (5.28), which yields

$$\begin{aligned} &G_{\mathsf{X}_k}[h|Z_{1:k-1}] \\ &\quad = \int \Bigg(\prod_{\boldsymbol{x}_{k-1} \in X_{k-1}} G^{\mathrm{Ber}}\big[h; p_{\mathrm{S}}(\boldsymbol{x}_{k-1}), f(\cdot|\boldsymbol{x}_{k-1})\big] \Bigg) e^{\lambda_k^{\mathrm{B}}[h-1]} f(X_{k-1}|Z_{1:k-1})\, \delta X_{k-1} \\ &\quad = G_{\mathsf{X}_{k-1}}[h'|Z_{1:k-1}]\, e^{\lambda_k^{\mathrm{B}}[h-1]}. \end{aligned} \tag{5.34}$$

Here, we have used the definition of the PGFL of an unlabeled RFS (2.5) and introduced the short notation

$$\begin{aligned} h'(\boldsymbol{x}_k) &\triangleq G^{\mathrm{Ber}}\big[h; p_{\mathrm{S}}(\boldsymbol{x}_{k-1}), f(\,\cdot\,|\boldsymbol{x}_{k-1})\big] \\ &= 1 - p_{\mathrm{S}}(\boldsymbol{x}_{k-1}) + p_{\mathrm{S}}(\boldsymbol{x}_{k-1}) \int h(\boldsymbol{x}_k) f(\boldsymbol{x}_k|\boldsymbol{x}_{k-1}) \mathrm{d}\boldsymbol{x}_k. \end{aligned}$$

The PGFL $G_{\mathsf{X}_{k-1}}[h'|Z_{1:k-1}]$ in (5.34) is the previous posterior PGFL of unlabeled objects (5.21) but with $h(\boldsymbol{x}_{k-1})$ replaced by $h'(\boldsymbol{x}_k)$. Note that $G_{\mathsf{X}_{k-1}}[h|Z_{1:k-1}]$ is of Poisson type according to (5.23) parametrized by the posterior PHD $\lambda(\boldsymbol{x}_{k-1})$. Hence, the predicted posterior PGFL of unlabeled objects in (5.34) can be rewritten as

$$G_{\mathsf{X}_k}[h|Z_{1:k-1}] = e^{\lambda_{k-1}[h'-1] + \lambda_k^{\mathrm{B}}[h-1]}, \tag{5.35}$$

where $\lambda_{k-1}[h'-1] = \int (h'(\boldsymbol{x}_k) - 1) \lambda(\boldsymbol{x}_{k-1}) \mathrm{d}\boldsymbol{x}_k$. An analysis of (5.35) shows that it is equal to the predicted posterior PGFL in the PHD filter [Mahler, 2003]. Since (5.35) is no longer of Poisson type, we approximate it as in the PHD filter by a Poisson RFS whose PHD equals the PHD corresponding to $G_{\mathsf{X}_k}[h|Z_{1:k-1}]$. This yields [Mahler, 2003]

$$G_{\mathsf{X}_k}[h|Z_{1:k-1}] \approx e^{\lambda_{k|k-1}[h-1]}, \tag{5.36}$$

where $\lambda_{k|k-1}[h-1] = \int (h(\boldsymbol{x}_k) - 1)\, \lambda_{k|k-1}(\boldsymbol{x}_k) \mathrm{d}\boldsymbol{x}_k$ with

$$\lambda_{k|k-1}(\boldsymbol{x}_k) = \lambda_{\mathrm{B}}(\boldsymbol{x}_k) + \int f(\boldsymbol{x}_k|\boldsymbol{x}_{k-1}) p_{\mathrm{S}}(\boldsymbol{x}_{k-1}) \lambda(\boldsymbol{x}_{k-1}) \mathrm{d}\boldsymbol{x}_{k-1}. \tag{5.37}$$

Here, $p_{\mathrm{S}}(\boldsymbol{x}_{k-1})$, $f(\boldsymbol{x}_k|\boldsymbol{x}_{k-1})$, and $\lambda_{\mathrm{B}}(\boldsymbol{x}_k)$ are the survival probability, the state-transition PDF, and the birth PHD, respectively, introduced in Section 5.1.1, and $\lambda(\boldsymbol{x}_{k-1})$ is the posterior PHD of unlabeled objects at time $k-1$ (cf. (5.23)). Expression (5.37) equals the prediction relation of the PHD filter (cf. (3.6)).

Note that the labeled state RFS, i.e, the LMB RFS $\tilde{\mathsf{X}}_{k-1}$, allows the corresponding objects to be distinguished, whereas the objects modeled by the unlabeled state RFS, i.e., the Poisson RFS $\tilde{\mathsf{X}}_{k-1}$, are indistinguishable. On the other hand, the Poisson RFS is parametrized by a single function, i.e., its PHD, and it enables a much more efficient representation and processing of a large number of potentially existing objects. Therefore, we aim to model objects that are likely to exist by the computationally more demanding LMB part and objects that are rather unlikely to exist by the computationally less demanding Poisson part. The LMB part moreover guarantees track continuity and thereby allows the consistent tracking of distinguishable objects over consecutive time steps.

We conclude that when applying approximation (5.36), the prediction step preserves the LMB-Poisson form of the previous posterior PGFL $G_{\tilde{\mathsf{X}}_{k-1},\mathsf{X}_{k-1}}[\tilde{h},h|Z_{1:k-1}]$. Summarizing, the prediction step of the proposed LMB/P filter now consists of computing the predicted posterior existence probabilities $r^{(l)}_{k|k-1}$ and the predicted spatial PDFs $f^{(l)}_{k|k-1}(\boldsymbol{x}_k)$ according to (5.32) and (5.33), respectively, for the labeled objects and the predicted posterior PHD $\lambda_{k|k-1}(\boldsymbol{x}_k)$ according to (5.37) for the unlabeled objects.

5.3 Exact Update Step

In the update step, the predicted posterior PGFL $G_{\tilde{\mathsf{X}}_k,\mathsf{X}_k}[\tilde{h},h|Z_{1:k-1}]$ is converted into the current posterior PGFL $G_{\tilde{\mathsf{X}}_k,\mathsf{X}_k}[\tilde{h},h|Z_{1:k}]$, which is defined as

$$G_{\tilde{\mathsf{X}}_k,\mathsf{X}_k}[\tilde{h},h|Z_{1:k}] = \iint \tilde{h}^{\tilde{X}_k} h^{X_k} f(\tilde{X}_k, X_k|Z_{1:k})\,\delta\tilde{X}_k\,\delta X_k\,. \tag{5.38}$$

Here, $f(\tilde{X}_k, X_k|Z_{1:k})$ is the posterior PDF at time k. This conversion is based on the measurement model described in Section 5.1.2 and involves the current measurement set Z_k. It turns out that the posterior PGFL $G_{\tilde{\mathsf{X}}_k,\mathsf{X}_k}[\tilde{h},h|Z_{1:k}]$ factors according to

$$G_{\tilde{\mathsf{X}}_k,\mathsf{X}_k}[\tilde{h},h|Z_{1:k}] = G'_{\tilde{\mathsf{X}}_k,\mathsf{X}_k}[\tilde{h},h|Z_{1:k}]\,G_{\mathsf{X}_k}[h], \tag{5.39}$$

where $G'_{\tilde{\mathsf{X}}_k,\mathsf{X}_k}[\tilde{h},h|Z_{1:k}]$ is a joint labeled/unlabeled PGFL and $G_{\mathsf{X}_k}[h]$ is a solely unlabeled PGFL. The factor $G'_{\tilde{\mathsf{X}}_k,\mathsf{X}_k}[\tilde{h},h]$ represents objects – either likely to exist or not – that generated a measurement in the current or a previous update step, while the factor $G_{\mathsf{X}_k}[h]$ represents objects that are unlikely to exist and did not generate a measurement in the current update step. Hence, we call $G'_{\tilde{\mathsf{X}}_k,\mathsf{X}_k}[\tilde{h},h]$ the pgfl of detected objects and $G_{\mathsf{X}_k}[h]$ the pgfl of undetected objects.

The derivation of the exact update step is an extension of that in [Williams, 2015] from an unlabeled to a labeled/unlabeled case. Similar results, but without derivation and in terms of multi-object PDFs, were reported in [Meyer et al., 2018]. We emphasize that the update step of the proposed LMB/P filter is different in that it involves several modifications and approximations, to be described in Section 5.4 and Section 5.5. In the following subsections, we derive (5.39), i.e., we first show that $G_{\tilde{\mathsf{X}}_k,\mathsf{X}_k}[\tilde{h},h|Z_{1:k}]$ factorizes in $G'_{\tilde{\mathsf{X}}_k,\mathsf{X}_k}[\tilde{h},h|Z_{1:k}]$ and $G_{\mathsf{X}_k}[h]$, and we then derive specific expressions of these PGFLs.

5.3.1 Expression of the Posterior PGFL $G_{\tilde{\mathsf{X}}_k,\mathsf{X}_k}[\tilde{h},h|Z_{1:k}]$

Analogously to the prediction step, we now derive the update step using PGFLs. In addition to PGFLs $G[h]$ (which satisfy $G[1]=1$ (cf. Section 2.1.1 and Section 2.2.1)), we will also use conventional functionals $F[h]$ (for which $F[1]\neq 1$ in general) in the following. A functional is defined equivalently to a PGFL (cf. (2.5) and (2.23)) with the difference that the function $f(X)$ in (2.5) and $f(\tilde{X})$ in (2.23) is a general set function and not a valid multi-object PDF, i.e., the function does not necessarily integrate to one $\big(\int f(X)\delta X \neq 1$ and $\int f(\tilde{X})\delta\tilde{X} \neq 1\big)$.

We start by formulating the update step of the multi-object Bayes filter in (3.2) in terms of jointly labeled/unlabeled multi-object PDFs, i.e.,

$$f(\tilde{X}_k, X_k|Z_{1:k}) = \frac{f(Z_k,\tilde{X}_k,X_k|Z_{1:k-1})}{f(Z_k|Z_{1:k-1})}. \tag{5.40}$$

By inserting (5.40) into (5.38), we get for the posterior PGFL

$$G_{\tilde{\mathsf{X}}_k,\mathsf{X}_k}[\tilde{h},h|Z_{1:k}] = \frac{\iint \tilde{h}^{\tilde{X}_k} h^{X_k} f(Z_k,\tilde{X}_k,X_k|Z_{1:k-1})\delta\tilde{X}_k\delta X_k}{f(Z_k|Z_{1:k-1})}. \tag{5.41}$$

Note that Z_k is considered deterministic here and represents the actual measurements generated by the sensor. Thus, $f(Z_k,\tilde{X}_k,X_k|Z_{1:k-1})$ is only a function of $\tilde{X}_k$ and X_k and not of Z_k and consequently $G_{\tilde{\mathsf{X}}_k,\mathsf{X}_k}[\tilde{h},h|Z_{1:k}]$ is also only a PGFL with respect to $\tilde{\mathsf{X}}_k$ and X_k and not with respect to Z_k. Note that the denominator of (5.41) is only a normalization factor (since Z_k is observed and deterministic) that ensures that $G_{\tilde{\mathsf{X}}_k,\mathsf{X}_k}[\tilde{h},h|Z_{1:k}]$ is a valid PGFL, i.e., $G[1]=1$. Next, we define the functional given by the numerator of (5.41) according to

$$F_{\tilde{\mathsf{X}}_k,\mathsf{X}_k}[\tilde{h},h|Z_{1:k}] \triangleq \iint \tilde{h}^{\tilde{X}_k} h^{X_k} f(Z_k,\tilde{X}_k,X_k|Z_{1:k-1})\delta\tilde{X}_k\delta X_k. \tag{5.42}$$

We further note that the denominator of (5.41) can be computed from (5.42) by setting $\tilde{h}=1$ and $h=1$, i.e.,

$$\begin{aligned} f(Z_k|Z_{1:k-1}) &= \iint f(Z_k,\tilde{X}_k,X_k|Z_{1:k-1})\delta\tilde{X}_k\delta X_k \\ &= F_{\tilde{\mathsf{X}}_k,\mathsf{X}_k}[\tilde{h},h|Z_{1:k}]\big|_{\tilde{h}=1,h=1}. \end{aligned} \tag{5.43}$$

After replacing the numerator and the denominator of (5.41) by (5.42) and (5.43), respectively, we get for the joint posterior PGFL of labeled and unlabeled objects

$$G_{\tilde{\mathsf{X}}_k,\mathsf{X}_k}[\tilde{h}, h|Z_{1:k}] = \frac{F_{\tilde{\mathsf{X}}_k,\mathsf{X}_k}[\tilde{h}, h|Z_{1:k}]}{F_{\tilde{\mathsf{X}}_k,\mathsf{X}_k}[\tilde{h}, h|Z_{1:k}]\big|_{\tilde{h}=1,h=1}}. \tag{5.44}$$

Note that (5.44) constitutes the update step of the multi-object Bayes filter for labeled/unlabeled state RFSs in PGFL form. A similar result for purely unlabeled RFS was presented in [Mahler, 2007b]. Next, we derive an expression of $F_{\tilde{\mathsf{X}}_k,\mathsf{X}_k}[\tilde{h}, h|Z_{1:k}]$ in (5.44).

5.3.2 Expression of $F_{\tilde{\mathsf{X}}_k,\mathsf{X}_k}[\tilde{h}, h|Z_{1:k}]$

We start by introducing the joint functional of measurements Z_k, labeled objects $\tilde{\mathsf{X}}_k$, and unlabeled objects X_k according to

$$F_{\mathsf{Z}_k,\tilde{\mathsf{X}}_k,\mathsf{X}_k}[g, \tilde{h}, h|Z_{1:k-1}] \triangleq \iiint g^{Z_k}\tilde{h}^{\tilde{X}_k}h^{X_k} f(Z_k, \tilde{X}_k, X_k|Z_{1:k-1})\,\delta Z_k\,\delta\tilde{X}_k\,\delta X_k, \tag{5.45}$$

where, contrary to (5.42), the measurements Z_k are considered as random. From this expression, the functional $F_{\tilde{\mathsf{X}}_k,\mathsf{X}_k}[\tilde{h}, h|Z_{1:k}]$ in (5.42) can be obtained according to (2.6) as

$$F_{\tilde{\mathsf{X}}_k,\mathsf{X}_k}[\tilde{h}, h|Z_{1:k}] = \frac{\delta F_{\mathsf{Z}_k,\tilde{\mathsf{X}}_k,\mathsf{X}_k}[g, \tilde{h}, h|Z_{1:k-1}]}{\delta Z'_k}\bigg|_{\substack{g=0\\ Z'_k=Z_k}}, \tag{5.46}$$

where $\frac{\delta}{\delta Z'_k} = \frac{\delta^{M_k}}{\delta \boldsymbol{z}_k'^{(1)}\cdots\delta \boldsymbol{z}_k'^{(M_k)}}$. Note that here $F_{\tilde{\mathsf{X}}_k,\mathsf{X}_k}[\tilde{h}, h|Z_{1:k}]$ is computed by first taking the functional derivative with respect to $\boldsymbol{z}_k'^{(1)}\cdots\boldsymbol{z}_k'^{(M_k)}$ and then setting $g = 0$. As a result of these two operations, the measurement-related part of the joint PGFL $F_{\mathsf{Z}_k,\tilde{\mathsf{X}}_k,\mathsf{X}_k}[g, \tilde{h}, h|Z_{1:k-1}]$ is transformed into the "multi-object PDF domain". Finally, inserting (conditioning on) the observed measurements Z_k, we obtain $F_{\tilde{\mathsf{X}}_k,\mathsf{X}_k}[\tilde{h}, h|Z_{1:k}]$.

Next, we develop a specific expression of the functional $F_{\mathsf{Z}_k,\tilde{\mathsf{X}}_k,\mathsf{X}_k}[g, \tilde{h}, h|Z_{1:k-1}]$ in (5.45) based on the measurement model proposed in Section 5.1.2. We first use the factorization $f(Z_k, \tilde{X}_k, X_k|Z_{1:k-1}) = f(Z_k|\tilde{X}_k, X_k, Z_{1:k-1})\,f(\tilde{X}_k, X_k|Z_{1:k-1})$ and the assumption that the current measurements Z_k are conditionally independent of all measurements up to time $k-1$, $\mathsf{Z}_{1:k-1}$, given the current object state $(\tilde{X}_k, X_k)$, i.e., $f(Z_k|\tilde{X}_k, X_k, Z_{1:k-1}) = f(Z_k|\tilde{X}_k, X_k)$ (cf. Section 3.1). This leads to (cf. (5.45))

$$\begin{aligned} F_{\mathsf{Z}_k,\tilde{\mathsf{X}}_k,\mathsf{X}_k}[g, \tilde{h}, h|Z_{1:k-1}] &= \iiint g^{Z_k}\tilde{h}^{\tilde{X}_k}h^{X_k} f(Z_k|\tilde{X}_k, X_k)\,f(\tilde{X}_k, X_k|Z_{1:k-1})\,\delta Z_k\,\delta\tilde{X}_k\,\delta X_k \\ &= \iint \tilde{h}^{\tilde{X}_k}h^{X_k}G_{\mathsf{Z}_k}[g|\tilde{X}_k, X_k]\,f(\tilde{X}_k, X_k|Z_{1:k-1})\,\delta\tilde{X}_k\,\delta X_k, \end{aligned}$$

where we have used the definition of the likelihood PGFL in (5.11), i.e., $G_{\mathsf{Z}_k}[g|\tilde{X}_k, X_k] \triangleq \int g^{Z_k} f(Z_k|\tilde{X}_k, X_k)\,\delta Z_k$. Using next factorizations (5.13) and (5.17), we obtain

$$F_{\mathsf{Z}_k,\tilde{\mathsf{X}}_k,\mathsf{X}_k}[g,\tilde{h},h|Z_{1:k-1}] = \left(\int \tilde{h}^{\tilde{X}_k}\, G_{\mathsf{Z}_k^{\mathrm{L}}}[g|\tilde{X}_k]\, f(\tilde{X}_k|Z_{1:k-1})\,\delta\tilde{X}_k\right) \times \left(\int h^{X_k}\, G_{\mathsf{Z}_k^{\mathrm{U}}}[g|X_k]\, f(X_k|Z_{1:k-1})\,\delta X_k\right) G_{\mathsf{Z}_k^{\mathrm{C}}}[g]. \tag{5.47}$$

After introducing the short notations

$$F_{\mathsf{Z}_k,\tilde{\mathsf{X}}_k}[g,\tilde{h}|Z_{1:k-1}] \triangleq \int \tilde{h}^{\tilde{X}_k}\, G_{\mathsf{Z}_k^{\mathrm{L}}}[g|\tilde{X}_k]\, f(\tilde{X}_k|Z_{1:k-1})\,\delta\tilde{X}_k, \tag{5.48}$$

$$F_{\mathsf{Z}_k,\mathsf{X}_k}[g,h|Z_{1:k-1}] \triangleq \left(\int h^{X_k}\, G_{\mathsf{Z}_k^{\mathrm{U}}}[g|X_k]\, f(X_k|Z_{1:k-1})\,\delta X_k\right) G_{\mathsf{Z}_k^{\mathrm{C}}}[g], \tag{5.49}$$

expression (5.47) can be rewritten according to

$$F_{\mathsf{Z}_k,\tilde{\mathsf{X}}_k,\mathsf{X}_k}[g,\tilde{h},h|Z_{1:k-1}] = F_{\mathsf{Z}_k,\tilde{\mathsf{X}}_k}[g,\tilde{h}|Z_{1:k-1}]\, F_{\mathsf{Z}_k,\mathsf{X}_k}[g,h|Z_{1:k-1}]. \tag{5.50}$$

Finally, inserting (5.50) into (5.46) yields

$$F_{\tilde{\mathsf{X}}_k,\mathsf{X}_k}[\tilde{h},h|Z_{1:k}] = \frac{\delta}{\delta Z'_k}\left(F_{\mathsf{Z}_k,\tilde{\mathsf{X}}_k}[g,\tilde{h}|Z_{1:k-1}]\, F_{\mathsf{Z}_k,\mathsf{X}_k}[g,h|Z_{1:k-1}]\right)\Bigg|_{\substack{g=0\\ Z'_k=Z_k}}. \tag{5.51}$$

In the next subsection, we take the functional derivatives occurring in (5.51).

5.3.3 Functional Derivatives of $F_{\tilde{\mathsf{X}}_k,\mathsf{X}_k}[\tilde{h},h|Z_{1:k}]$

In the following, we will develop specific expressions of the functionals $F_{\mathsf{Z}_k,\tilde{\mathsf{X}}_k}[g,\tilde{h}|Z_{1:k-1}]$ and $F_{\mathsf{Z}_k,\mathsf{X}_k}[g,h|Z_{1:k-1}]$ defined in (5.48) and (5.49), respectively, based on the measurement model proposed in Section 5.1.2. For this purpose, we insert $G_{\mathsf{Z}_k^{\mathrm{L}}}[g|\tilde{X}_k]$ in (5.14) into (5.48) and use $\tilde{h}^{\tilde{X}_k} = \prod_{l\in\mathbb{L}^*_{k-1}} \tilde{h}(\boldsymbol{x}_k,l)$, which yields

$$F_{\mathsf{Z}_k,\tilde{\mathsf{X}}_k}[g,\tilde{h}|Z_{1:k-1}] = \int \left(\prod_{l\in\mathbb{L}^*_{k-1}} \tilde{h}(\boldsymbol{x}_k,l)\, G^{\mathrm{Ber}}\big[g;p_{\mathrm{D}}(\boldsymbol{x}_k,l),f(\cdot|\boldsymbol{x}_k,l)\big]\right) f(\tilde{X}_k|Z_{1:k-1})\,\delta\tilde{X}_k. \tag{5.52}$$

By furthermore introducing the short notation

$$\tilde{h}''(\boldsymbol{x}_k,l) \triangleq \tilde{h}(\boldsymbol{x}_k,l)\, G^{\mathrm{Ber}}\big[g;p_{\mathrm{D}}(\boldsymbol{x}_k,l),f(\,\cdot\,|\boldsymbol{x}_k,l)\big], \tag{5.53}$$

and using the definition of the PGFL of labeled RFS in (2.23), expression (5.52) can be rewritten as

$$F_{\mathsf{Z}_k,\tilde{\mathsf{X}}_k}[g,\tilde{h}|Z_{1:k-1}] = G_{\tilde{\mathsf{X}}_k}[\tilde{h}''|Z_{1:k-1}]. \tag{5.54}$$

Note that $G_{\tilde{\mathsf{X}}_k}[\tilde{h}''|Z_{1:k-1}]$ here is the predicted posterior LMB PGFL of labeled objects in (5.31), but where $\tilde{h}(\boldsymbol{x}_k, l)$ is replaced by $\tilde{h}''(\boldsymbol{x}_k, l)$, and (5.54) can thus be rewritten as

$$F_{\mathsf{Z}_k,\tilde{\mathsf{X}}_k}[g,\tilde{h}|Z_{1:k-1}] = \prod_{l\in\mathbb{L}^*_{k-1}} G^{\mathrm{Ber}}[\tilde{h}''; r^{(l)}_{k|k-1}, f^{(l)}_{k|k-1}]. \tag{5.55}$$

Analogously, we insert $G_{\mathsf{Z}^{\mathrm{U}}_k}[g|X_k]$ in (5.15) into (5.49) and use $h^{X_k} = \prod_{\boldsymbol{x}_k\in X_k} h(\boldsymbol{x}_k)$, which yields

$$\begin{aligned} &F_{\mathsf{Z}_k,\mathsf{X}_k}[g,h|Z_{1:k-1}] \\ &\quad= \left(\int\left(\prod_{\boldsymbol{x}_k\in X_k} h(\boldsymbol{x}_k)\, G^{\mathrm{Ber}}\big[g; p_{\mathrm{D}}(\boldsymbol{x}_k), f(\cdot|\boldsymbol{x}_k)\big]\right) f(X_k|Z_{1:k-1})\,\delta X_k\right) G_{\mathsf{Z}^{\mathrm{C}}_k}[g]. \end{aligned} \tag{5.56}$$

Next, we introduce the short notation

$$h''(\boldsymbol{x}_k) \triangleq h(\boldsymbol{x}_k)\, G^{\mathrm{Ber}}\big[g; p_{\mathrm{D}}(\boldsymbol{x}_k), f(\cdot|\boldsymbol{x}_k)\big], \tag{5.57}$$

and use the definition of the PGFL of unlabeled objects in (2.5) to rewrite expression (5.56) according to

$$F_{\mathsf{Z}_k,\mathsf{X}_k}[g,h|Z_{1:k-1}] = G_{\mathsf{X}_k}[h''|Z_{1:k-1}]\, G_{\mathsf{Z}^{\mathrm{C}}_k}[g]. \tag{5.58}$$

Note that $G_{\mathsf{X}_k}[h''|Z_{1:k-1}]$ here is the predicted posterior Poisson PGFL of unlabeled objects in (5.36), but where $h(\boldsymbol{x}_k)$ is replaced by $h''(\boldsymbol{x}_k)$, $G_{\mathsf{Z}^{\mathrm{C}}_k}[g]$ is the PGFL given by (5.16), and (5.58) can thus be rewritten as

$$F_{\mathsf{Z}_k,\mathsf{X}_k}[g,h|Z_{1:k-1}] = e^{\lambda_{k|k-1}[h''-1]+\lambda^{\mathrm{C}}_k[g-1]}. \tag{5.59}$$

Finally, inserting (5.55) and (5.59) into (5.51) leads to

$$F_{\tilde{\mathsf{X}}_k,\mathsf{X}_k}[\tilde{h},h|Z_{1:k}] = \frac{\delta}{\delta Z'_k}\left(\left(\prod_{l\in\mathbb{L}^*_{k-1}} G^{\mathrm{Ber}}[\tilde{h}''; r^{(l)}_{k|k-1}, f^{(l)}_{k|k-1}]\right) e^{\lambda_{k|k-1}[h''-1]+\lambda^{\mathrm{C}}_k[g-1]}\right)\Bigg|_{\substack{g=0\\ Z'_k=Z_k}}. \tag{5.60}$$

Next, we apply the product rule of functional derivatives (cf. (2.8)) to (5.60), which yields (analogous to [Williams, 2015])

$$\begin{aligned} &F_{\tilde{\mathsf{X}}_k,\mathsf{X}_k}[\tilde{h},h|Z_{1:k}] \\ &\quad= \sum_{\boldsymbol{d}_k\in\mathcal{D}_k}\left(\prod_{l\in\mathbb{L}^*_{k-1}} \frac{\delta G^{\mathrm{Ber}}[\tilde{h}''; r^{(l)}_{k|k-1}, f^{(l)}_{k|k-1}]}{\delta \boldsymbol{z}^{(d^{(l)}_k)}_k}\right)\prod_{m\in\mathcal{M}_{\boldsymbol{d}_k}} \frac{\delta e^{\lambda_{k|k-1}[h''-1]+\lambda^{\mathrm{C}}_k[g-1]}}{\delta \boldsymbol{z}^{(m)}_k}\Bigg|_{\substack{g=0\\ Z'_k=Z_k}}, \end{aligned} \tag{5.61}$$

where we have introduced the index vector $\boldsymbol{d}_k$ of length $|\mathbb{L}^*_{k-1}|$ with entries $d^{(l)}_k = m \in$

$\{0\} \cup \mathcal{M}_k$ for $l \in \mathbb{L}^*_{k-1}$ (recap that $\mathcal{M}_k = \{1, \ldots, M_k\}$). Here, the set $\mathcal{D}_k$ comprises all those vectors $\boldsymbol{d}_k$, whose nonzero entries are different. An interpretation of $\boldsymbol{d}_k$ and $d_k^{(l)}$ in the context of object-measurement associations will be given in Section 5.3.7. Further, $\mathcal{M}_{\boldsymbol{d}_k} \subseteq \mathcal{M}_k$ comprises all (nonzero) measurement indices that are not involved in the index vector $\boldsymbol{d}_k$. Next, we will take the functional derivatives of $G^{\mathrm{Ber}}[\tilde{h}''; r^{(l)}_{k|k-1}, f^{(l)}_{k|k-1}]$ and $e^{\lambda_{k|k-1}[h''-1]+\lambda^{\mathrm{C}}_k[g-1]}$ with respect to $\boldsymbol{z}^{(m)}_k$, $m \in \mathcal{M}_k$.

We first consider the functionals $G^{\mathrm{Ber}}[\tilde{h}''; r^{(l)}_{k|k-1}, f^{(l)}_{k|k-1}]$ in (5.61) and rewrite them by using (2.13) and (5.53) according to

$$G^{\mathrm{Ber}}[\tilde{h}''; r^{(l)}_{k|k-1}, f^{(l)}_{k|k-1}] = 1 - r^{(l)}_{k|k-1} + r^{(l)}_{k|k-1} \int \tilde{h}(\boldsymbol{x}_k, l)\Big(1 - p_{\mathrm{D}}(\boldsymbol{x}_k, l) + p_{\mathrm{D}}(\boldsymbol{x}_k, l) \int g(\boldsymbol{z}_k)\, f(\boldsymbol{z}_k|\boldsymbol{x}_k, l)\,\mathrm{d}\boldsymbol{z}_k\Big)\, f^{(l)}_{k|k-1}(\boldsymbol{x}_k)\,\mathrm{d}\boldsymbol{x}_k . \quad (5.62)$$

Let $\Delta^{(l,m)}[\tilde{h}]$ denote the functional derivative $\delta G^{\mathrm{Ber}}\big[\tilde{h}''; r^{(l)}_{k|k-1}, f^{(l)}_{k|k-1}\big]/\delta \boldsymbol{z}^{(m)}_k$, $m \in \{0\} \cup \mathcal{M}_k$. We get

$$\Delta^{(l,m)}[\tilde{h}] = r^{(l)}_{k|k-1} \int \tilde{h}(\boldsymbol{x}_k, l)\, p_{\mathrm{D}}(\boldsymbol{x}_k, l)\, f(\boldsymbol{z}^{(m)}_k|\boldsymbol{x}_k, l)\, f^{(l)}_{k|k-1}(\boldsymbol{x}_k)\,\mathrm{d}\boldsymbol{x}_k , \quad (5.63)$$

for $m \in \mathcal{M}_k$. Note that for $m = 0$, the functional derivative operation is not applied. Hence, we have

$$\Delta^{(l,0)}[\tilde{h}] = G^{\mathrm{Ber}}[\tilde{h}''; r^{(l)}_{k|k-1}, f^{(l)}_{k|k-1}], \quad (5.64)$$

with $G^{\mathrm{Ber}}[\tilde{h}''; r^{(l)}_{k|k-1}, f^{(l)}_{k|k-1}]$ given by (5.62).

Next, we consider the functional $e^{\lambda_{k|k-1}[h''-1]+\lambda^{\mathrm{C}}_k[g-1]}$ in (5.61). By using $\lambda_{k|k-1}[h''-1] = \int (h''(\boldsymbol{x}_k) - 1)\, \lambda_{k|k-1}(\boldsymbol{x}_k)\,\mathrm{d}\boldsymbol{x}_k$, $\lambda^{\mathrm{C}}_k[g-1] = \int (g(\boldsymbol{z}_k) - 1)\, \lambda_{\mathrm{C}}(\boldsymbol{z}_k)\,\mathrm{d}\boldsymbol{z}_k$, and furthermore (2.13) and (5.57), we get

$$\lambda_{k|k-1}[h'' - 1] + \lambda^{\mathrm{C}}_k[g - 1] = \int \Big(h(\boldsymbol{x}_k)\big(1 - p_{\mathrm{D}}(\boldsymbol{x}_k) + p_{\mathrm{D}}(\boldsymbol{x}_k) \int g(\boldsymbol{z}_k)\, f(\boldsymbol{z}_k|\boldsymbol{x}_k)\,\mathrm{d}\boldsymbol{z}_k\big) - 1\Big) \times \lambda_{k|k-1}(\boldsymbol{x}_k)\,\mathrm{d}\boldsymbol{x}_k + \int \big(g(\boldsymbol{z}_k) - 1\big)\, \lambda_{\mathrm{C}}(\boldsymbol{z}_k)\,\mathrm{d}\,\boldsymbol{z}_k .$$

Let $\Delta_{\mathsf{X}_k}[h]$ denote $\prod_{m \in \mathcal{M}_{\boldsymbol{d}_k}} \frac{\delta}{\delta \boldsymbol{z}^{(m)}_k}\, e^{\lambda_{k|k-1}[h''-1]+\lambda^{\mathrm{C}}_k[g-1]}$, which can be found as

$$\Delta_{\mathsf{X}_k}[h] = F_{\mathsf{X}_k}[h]\, \bar{F}_{\mathsf{X}_k}[h] \prod_{m \in \mathcal{M}_{\boldsymbol{d}_k}} \Delta^{(m)}[h] . \quad (5.65)$$

Here, the functionals $F_{\mathsf{X}_k}[h]$, $\bar{F}_{\mathsf{X}_k}[h]$ and $\Delta^{(m)}[h]$ are given by

$$F_{\mathsf{X}_k}[h] \triangleq e^{\int (h(\boldsymbol{x}_k)(1 - p_{\mathrm{D}}(\boldsymbol{x}_k)) - 1)\, \lambda_{k|k-1}(\boldsymbol{x}_k)\,\mathrm{d}\boldsymbol{x}_k} \quad (5.66)$$

$$\bar{F}_{\mathsf{X}_k}[h] \triangleq e^{\int (\bar{h}(\boldsymbol{x}_k) - 1) \lambda_{k|k-1}(\boldsymbol{x}_k)\,\mathrm{d}\boldsymbol{x}_k + \int (g(\boldsymbol{z}_k) - 1)\, \lambda_{\mathrm{C}}(\boldsymbol{z}_k)\,\mathrm{d}\boldsymbol{z}_k}$$

$$\Delta^{(m)}[h] \triangleq \lambda_{\mathrm{C}}(\boldsymbol{z}_k^{(m)}) + \int h(\boldsymbol{x}_k)\lambda_{k|k-1}(\boldsymbol{x}_k)p_{\mathrm{D}}(\boldsymbol{x}_k)f(\boldsymbol{z}_k^{(m)}|\boldsymbol{x}_k)\mathrm{d}\boldsymbol{x}_k\,, \tag{5.67}$$

respectively, with $\bar{h}(\boldsymbol{x}_k) \triangleq h(\boldsymbol{x}_k)(p_{\mathrm{D}}(\boldsymbol{x}_k)\int g(\boldsymbol{z}_k)f(\boldsymbol{z}_k|\boldsymbol{x}_k)\mathrm{d}\boldsymbol{z}_k)$. We are now ready to insert the obtained results into (5.61).

5.3.4 Final Expression of $F_{\tilde{\mathsf{X}}_k,\mathsf{X}_k}[\tilde{h},h|Z_{1:k}]$

We insert expressions (5.63), (5.64), and (5.65) into (5.61), which yields

$$F_{\tilde{\mathsf{X}}_k,\mathsf{X}_k}[\tilde{h},h|Z_{1:k}] = \sum_{\boldsymbol{d}_k\in\mathcal{D}_k}\left(\prod_{l\in\mathbb{L}^*_{k-1}}\Delta^{(l,d_k^{(l)})}[\tilde{h}]\right)F_{\mathsf{X}_k}[h]\,\bar{F}_{\mathsf{X}_k}[h]\prod_{m\in\mathcal{M}_{\boldsymbol{d}_k}}\Delta^{(m)}[h]\bigg|_{g=0},$$

Next, we set $g(\boldsymbol{z}_k) = 0$, which leads to

$$F_{\tilde{\mathsf{X}}_k,\mathsf{X}_k}[\tilde{h},h|Z_{1:k}] = \sum_{\boldsymbol{d}_k\in\mathcal{D}_k}\left(\prod_{l\in\mathbb{L}^*_{k-1}}\bar{\Delta}^{(l,d_k^{(l)})}[\tilde{h}]\right)\left(\prod_{m\in\mathcal{M}_{\boldsymbol{d}_k}}\Delta^{(m)}[h]\right)F_{\mathsf{X}_k}[h],$$

where $\bar{\Delta}^{(l,d_k^{(l)})}[\tilde{h}]$ is given for $m\in\mathcal{M}_k$ by $\Delta^{(l,d_k^{(l)})}[\tilde{h}]$ in (5.63) and for $m=0$ by

$$\bar{\Delta}^{(l,0)}[\tilde{h}] = 1 - r^{(l)}_{k|k-1} + r^{(l)}_{k|k-1}\int\tilde{h}(\boldsymbol{x}_k,l)\big(1-p_{\mathrm{D}}(\boldsymbol{x}_k,l)\big)f^{(l)}_{k|k-1}(\boldsymbol{x}_k)\mathrm{d}\boldsymbol{x}_k\,. \tag{5.68}$$

Since the functional $F_{\mathsf{X}_k}[h]$ is independent of $\boldsymbol{d}_k$, $F_{\tilde{\mathsf{X}}_k,\mathsf{X}_k}[\tilde{h},h|Z_{1:k}]$ can be grouped according to

$$F_{\tilde{\mathsf{X}}_k,\mathsf{X}_k}[\tilde{h},h|Z_{1:k}] = F'_{\tilde{\mathsf{X}}_k,\mathsf{X}_k}[\tilde{h},h|Z_{1:k}]\,F_{\mathsf{X}_k}[h], \tag{5.69}$$

with

$$F'_{\tilde{\mathsf{X}}_k,\mathsf{X}_k}[\tilde{h},h|Z_{1:k}] = \sum_{\boldsymbol{d}_k\in\mathcal{D}_k}\left(\prod_{l\in\mathbb{L}^*_{k-1}}\bar{\Delta}^{(l,d_k^{(l)})}[\tilde{h}]\right)\prod_{m\in\mathcal{M}_{\boldsymbol{d}_k}}\Delta^{(m)}[h]\,. \tag{5.70}$$

Finally, to obtain the posterior PGFL $G_{\tilde{\mathsf{X}}_k,\mathsf{X}_k}[\tilde{h},h|Z_{1:k}]$, the functional $F_{\tilde{\mathsf{X}}_k,\mathsf{X}_k}[\tilde{h},h|Z_{1:k}]$ has to be normalized according to (5.44). Since it is composed of two separate functionals (cf. (5.69)), the normalization can be performed separately for each functional. More precisely, inserting (5.69) into (5.44) yields

$$G_{\tilde{\mathsf{X}}_k,\mathsf{X}_k}[\tilde{h},h|Z_{1:k}] = \frac{F'_{\tilde{\mathsf{X}}_k,\mathsf{X}_k}[\tilde{h},h|Z_{1:k}]}{F'_{\tilde{\mathsf{X}}_k,\mathsf{X}_k}[\tilde{h},h|Z_{1:k}]\big|_{\tilde{h}=1,h=1}}\,\frac{F_{\mathsf{X}_k}[h]}{F_{\mathsf{X}_k}[h|Z_{1:k}]\big|_{h=1}}\,. \tag{5.71}$$

After introducing the short notations

$$G'_{\tilde{\mathsf{X}}_k,\mathsf{X}_k}[\tilde{h},h|Z_{1:k}] \triangleq \frac{F'_{\tilde{\mathsf{X}}_k,\mathsf{X}_k}[\tilde{h},h|Z_{1:k}]}{F'_{\tilde{\mathsf{X}}_k,\mathsf{X}_k}[\tilde{h},h|Z_{1:k}]\big|_{\tilde{h}=1,h=1}}, \tag{5.72}$$

$$G_{\mathsf{X}_k}[h|Z_{1:k}] \triangleq \frac{F_{\mathsf{X}_k}[h]}{F_{\mathsf{X}_k}[h|Z_{1:k}]\big|_{h=1}}, \tag{5.73}$$

expression (5.71) becomes (5.39). In the next two subsections, we develop specific expressions of $G'_{\tilde{\mathsf{X}}_k,\mathsf{X}_k}[\tilde{h},h|Z_{1:k}]$ and $G_{\mathsf{X}_k}[h|Z_{1:k}]$ by performing the normalizations according to (5.72) and (5.73), respectively. Note that the factor $G'_{\tilde{\mathsf{X}}_k,\mathsf{X}_k}[\tilde{h},h]$ represents objects – either likely to exist or not – that generated a measurement in the current or a previous update step, while the factor $G_{\mathsf{X}_k}[h]$ represents objects that are unlikely to exist and did not generate a measurement in the current update step. Hence, we call $G'_{\tilde{\mathsf{X}}_k,\mathsf{X}_k}[\tilde{h},h]$ the PGFL of detected objects and $G_{\mathsf{X}_k}[h]$ the PGFL of undetected objects.

5.3.5 Expression of the PGFL of Detected Objects $G'_{\tilde{\mathsf{X}}_k,\mathsf{X}_k}[\tilde{h},h]$

We start with the normalization of $F'_{\tilde{\mathsf{X}}_k,\mathsf{X}_k}[\tilde{h},h|Z_{1:k}]$ in (5.70) according to (5.72). We notice that the functionals $\bar{\Delta}^{(l,m)}[\tilde{h}]$ (cf. (5.63) with $\bar{\Delta}^{(l,d_k^{(l)})}[\tilde{h}] = \Delta^{(l,d_k^{(l)})}[\tilde{h}]$ and (5.68)) and $\Delta^{(m)}[h]$ (cf. (5.67)) in (5.70) can be represented as weighted Bernoulli PGFLs by using identity (2.14). More precisely, $\bar{\Delta}^{(l,m)}[\tilde{h}]$ can be rewritten as $\beta_k^{(l,m)} G^{\mathrm{Ber}}[\tilde{h}; r_k^{(l,m)}, f_k^{(l,m)}]$, where for $l \in \mathbb{L}^*_{k-1}$ and $m \in \mathcal{M}_k$ (cf. (5.63)), the parameters are given by

$$\beta_k^{(l,m)} = r_{k|k-1}^{(l)} \int p_{\mathrm{D}}(\boldsymbol{x}_k, l)\, f\big(\boldsymbol{z}_k^{(m)}\big|\boldsymbol{x}_k, l\big)\, f_{k|k-1}^{(l)}(\boldsymbol{x}_k)\, \mathrm{d}\boldsymbol{x}_k, \tag{5.74}$$

$$r_k^{(l,m)} = 1, \tag{5.75}$$

$$f^{(l,m)}(\boldsymbol{x}_k) = \frac{p_{\mathrm{D}}(\boldsymbol{x}_k, l)\, f\big(\boldsymbol{z}_k^{(m)}\big|\boldsymbol{x}_k, l\big)\, f_{k|k-1}^{(l)}(\boldsymbol{x}_k)}{\int p_{\mathrm{D}}(\boldsymbol{x}'_k, l)\, f\big(\boldsymbol{z}_k^{(m)}\big|\boldsymbol{x}'_k, l\big)\, f_{k|k-1}^{(l)}(\boldsymbol{x}'_k)\, \mathrm{d}\boldsymbol{x}'_k}, \tag{5.76}$$

and for $l \in \mathbb{L}^*_{k-1}$ and $m = 0$ (cf. (5.68)) by

$$\beta_k^{(l,0)} = 1 - r_{k|k-1}^{(l)} + r_{k|k-1}^{(l)} \int \big(1 - p_{\mathrm{D}}(\boldsymbol{x}_k, l)\big)\, f_{k|k-1}^{(l)}(\boldsymbol{x}_k)\, \mathrm{d}\boldsymbol{x}_k, \tag{5.77}$$

$$r_k^{(l,0)} = \frac{r_{k|k-1}^{(l)} \int \big(1 - p_{\mathrm{D}}(\boldsymbol{x}_k, l)\big)\, f_{k|k-1}^{(l)}(\boldsymbol{x}_k)\, \mathrm{d}\boldsymbol{x}_k}{1 - r_{k|k-1}^{(l)} + r_{k|k-1}^{(l)} \int \big(1 - p_{\mathrm{D}}(\boldsymbol{x}'_k, l)\big)\, f_{k|k-1}^{(l)}(\boldsymbol{x}'_k)\, \mathrm{d}\boldsymbol{x}'_k}, \tag{5.78}$$

$$f^{(l,0)}(\boldsymbol{x}_k) = \frac{\big(1 - p_{\mathrm{D}}(\boldsymbol{x}_k, l)\big)\, f_{k|k-1}^{(l)}(\boldsymbol{x}_k)}{\int \big(1 - p_{\mathrm{D}}(\boldsymbol{x}'_k, l)\big)\, f_{k|k-1}^{(l)}(\boldsymbol{x}'_k)\, \mathrm{d}\boldsymbol{x}'_k}. \tag{5.79}$$

Analogously, the functionals $\Delta^{(m)}[h]$ can be represented as $\beta_k^{(m)} G^{\mathrm{Ber}}[h; \bar{r}_k^{(m)}, \bar{f}_k^{(m)}]$, where for $m \in \mathcal{M}_{\boldsymbol{d}_k} \subseteq \mathcal{M}_k$ (cf. (5.70)), the parameters are given by

$$\beta_k^{(m)} = \lambda_{\mathrm{C}}(\boldsymbol{z}_k^{(m)}) + \int p_{\mathrm{D}}(\boldsymbol{x}_k)\, f\big(\boldsymbol{z}_k^{(m)}\big|\boldsymbol{x}_k\big)\, \lambda_{k|k-1}(\boldsymbol{x}_k)\, \mathrm{d}\boldsymbol{x}_k, \tag{5.80}$$

$$\bar{r}_k^{(m)} = \frac{\int p_{\mathrm{D}}(\boldsymbol{x}_k)\, f\big(\boldsymbol{z}_k^{(m)}\big|\boldsymbol{x}_k\big)\, \lambda_{k|k-1}(\boldsymbol{x}_k)\, \mathrm{d}\boldsymbol{x}_k}{\lambda_{\mathrm{C}}(\boldsymbol{z}_k^{(m)}) + \int p_{\mathrm{D}}(\boldsymbol{x}'_k)\, f\big(\boldsymbol{z}_k^{(m)}\big|\boldsymbol{x}'_k\big)\, \lambda_{k|k-1}(\boldsymbol{x}'_k)\, \mathrm{d}\boldsymbol{x}'_k}, \tag{5.81}$$

$$\bar{f}^{(m)}(\boldsymbol{x}_k) = \frac{p_{\mathrm{D}}(\boldsymbol{x}_k)\, f\big(\boldsymbol{z}_k^{(m)}\big|\boldsymbol{x}_k\big)\, \lambda_{k|k-1}(\boldsymbol{x}_k)}{\int p_{\mathrm{D}}(\boldsymbol{x}'_k)\, f\big(\boldsymbol{z}_k^{(m)}\big|\boldsymbol{x}'_k\big)\, \lambda_{k|k-1}(\boldsymbol{x}'_k)\, \mathrm{d}\boldsymbol{x}'_k}. \tag{5.82}$$

Expression (5.70) now reads:

$$\begin{aligned} &F'_{\tilde{\mathsf{X}}_k,\mathsf{X}_k}[\tilde{h}, h|Z_{1:k}] \\ &\quad = \sum_{\boldsymbol{d}_k \in \mathcal{D}_k} \Bigg(\prod_{l \in \mathbb{L}^*_{k-1}} \beta_k^{(l,d_k^{(l)})} G^{\mathrm{Ber}}[\tilde{h}; r_k^{(l,d_k^{(l)})}, f_k^{(l,d_k^{(l)})}] \Bigg) \prod_{m \in \mathcal{M}_{\boldsymbol{d}_k}} \beta_k^{(m)} G^{\mathrm{Ber}}[h; \bar{r}_k^{(m)}, \bar{f}_k^{(m)}] \\ &\quad = \sum_{\boldsymbol{d}_k \in \mathcal{D}_k} w'_{\boldsymbol{d}_k}\, G^{\mathrm{LMB},\boldsymbol{d}_k}_{\mathbb{L}^*_{k-1}}[\tilde{h}]\, G^{\mathrm{MB}}_{\mathcal{M}_{\boldsymbol{d}_k}}[h]. \end{aligned} \tag{5.83}$$

Here, we have introduced the (unnormalized) weights $w'_{\boldsymbol{d}_k}$ according to

$$w'_{\boldsymbol{d}_k} \triangleq \Bigg(\prod_{l \in \mathbb{L}^*_{k-1}} \beta_k^{(l,d_k^{(l)})} \Bigg) \prod_{m \in \mathcal{M}_{\boldsymbol{d}_k}} \beta_k^{(m)}, \tag{5.84}$$

and the LMB PGFL (cf. (2.26)) and the MB PGFL (cf. (2.20)) according to

$$G^{\mathrm{LMB},\boldsymbol{d}_k}_{\mathbb{L}^*_{k-1}}[\tilde{h}] \triangleq \prod_{l \in \mathbb{L}^*_{k-1}} G^{\mathrm{Ber}}\big[\tilde{h}; r_k^{(l,d_k^{(l)})}, f_k^{(l,d_k^{(l)})}\big], \tag{5.85}$$

$$G^{\mathrm{MB}}_{\mathcal{M}_{\boldsymbol{d}_k}}[h] \triangleq \prod_{m \in \mathcal{M}_{\boldsymbol{d}_k}} G^{\mathrm{Ber}}\big[h; \bar{r}_k^{(m)}, \bar{f}_k^{(m)}\big]. \tag{5.86}$$

To finally obtain $G'_{\tilde{\mathsf{X}}_k,\mathsf{X}_k}[\tilde{h}, h|Z_{1:k}]$ according to (5.72), we first have to compute the denominator $B_k \triangleq F'_{\tilde{\mathsf{X}}_k,\mathsf{X}_k}[\tilde{h}, h|Z_{1:k}]\big|_{\tilde{h}=1,h=1}$, which can be found as

$$B_k = \sum_{\boldsymbol{d}_k \in \mathcal{D}_k} w'_{\boldsymbol{d}_k} = \sum_{\boldsymbol{d}_k \in \mathcal{D}_k} \Bigg(\prod_{l \in \mathbb{L}^*_{k-1}} \beta_k^{(l,d_k^{(l)})} \Bigg) \prod_{m \in \mathcal{M}_{\boldsymbol{d}_k}} \beta_k^{(m)}. \tag{5.87}$$

Here, we have used (5.84). Inserting (5.83) and (5.87) into (5.72), we get after some reformulation

$$G'_{\tilde{\mathsf{X}}_k,\mathsf{X}_k}[\tilde{h}, h] = \sum_{\boldsymbol{d}_k \in \mathcal{D}_k} w_{\boldsymbol{d}_k}\, G^{\mathrm{LMB},\boldsymbol{d}_k}_{\mathbb{L}^*_{k-1}}[\tilde{h}]\, G^{\mathrm{MB}}_{\mathcal{M}_{\boldsymbol{d}_k}}[h], \tag{5.88}$$

where we have defined the (normalized) weights $w_{\boldsymbol{d}_k}$ as

$$w_{\boldsymbol{d}_k} = \frac{1}{B_k} \Bigg(\prod_{l \in \mathbb{L}^*_{k-1}} \beta_k^{(l,d_k^{(l)})} \Bigg) \prod_{m \in \mathcal{M}_{\boldsymbol{d}_k}} \beta_k^{(m)}. \tag{5.89}$$

An interpretation of the posterior PGFL of detected objects in (5.88) in terms of object-measurement associations will be presented in Section 5.3.7. In the next subsection, we compute $G_{\mathsf{X}_k}[h|Z_{1:k}]$ according to (5.73).

5.3.6 Expression of the PGFL of Undetected Objects $G_{\mathsf{X}_k}[h]$

We continue with the normalization of $F_{\mathsf{X}_k}[h]$ (cf. (5.66)) in (5.69) according to (5.73). More precisely, by setting $h=1$ in (5.66), we get for the normalization factor

$$F_{\mathsf{X}_k}[h]\big|_{h=1} = e^{-\int p_{\mathrm{D}}(\boldsymbol{x}_k)\,\lambda_{k|k-1}(\boldsymbol{x}_k)\mathrm{d}\boldsymbol{x}_k}. \tag{5.90}$$

Inserting (5.66) and (5.90) into (5.73) yields

$$\begin{aligned} G_{\mathsf{X}_k}[h] &= \frac{e^{\int \big(h(\boldsymbol{x}_k)(1-p_{\mathrm{D}}(\boldsymbol{x}_k))-1\big)\,\lambda_{k|k-1}(\boldsymbol{x}_k)\mathrm{d}\boldsymbol{x}_k}}{e^{-\int p_{\mathrm{D}}(\boldsymbol{x}_k)\,\lambda_{k|k-1}(\boldsymbol{x}_k)\mathrm{d}\boldsymbol{x}_k}} \\ &= e^{\int (h(\boldsymbol{x}_k)-1)\,(1-p_{\mathrm{D}}(\boldsymbol{x}_k))\lambda_{k|k-1}(\boldsymbol{x}_k)\,\mathrm{d}\boldsymbol{x}_k} \\ &= e^{\lambda_k[h-1]}, \end{aligned} \tag{5.91}$$

with $\lambda_k[h-1] = \int (h(\boldsymbol{x}_k)-1)\lambda(\boldsymbol{x}_k)\mathrm{d}\boldsymbol{x}_k$, and where the posterior PHD of undetected objects $\lambda(\boldsymbol{x}_k)$ is given according to

$$\lambda(\boldsymbol{x}_k) = (1-p_{\mathrm{D}}(\boldsymbol{x}_k))\,\lambda_{k|k-1}(\boldsymbol{x}_k). \tag{5.92}$$

Note that $G_{\mathsf{X}_k}[h]$ in (5.91) is a Poisson PGFL with PHD (5.92). In the next subsection, we will discuss some important facts about the derived exact update step.

5.3.7 Discussion of Results

In the following, we summarize the results obtained after applying the update step to the predicted posterior PGFL in (5.29). As we showed, the updated posterior PGFL $G_{\tilde{\mathsf{X}}_k,\mathsf{X}_k}[\tilde{h},h]$ is a product of a joint labeled/unlabeled PGFL $G'_{\tilde{\mathsf{X}}_k,\mathsf{X}_k}[\tilde{h},h]$ representing objects that already generated a measurement in the current or a previous update step and an unlabeled PGFL $G_{\mathsf{X}_k}[h]$ that did not generate a measurement in the current time step k. More precisely, the labeled/unlabeled PGFL is given by (5.88) according to

$$G'_{\tilde{\mathsf{X}}_k,\mathsf{X}_k}[\tilde{h},h] = \sum_{\boldsymbol{d}_k\in\mathcal{D}_k} w_{\boldsymbol{d}_k} G^{\mathrm{LMB},\boldsymbol{d}_k}_{\mathbb{L}^*_{k-1}}[\tilde{h}]\, G^{\mathrm{MB}}_{\mathcal{M}_{\boldsymbol{d}_k}}[h].$$

Thus, $G'_{\tilde{\mathsf{X}}_k,\mathsf{X}_k}[\tilde{h},h]$ is a mixture of PGFLs, each of which is the product of an LMB PGFL $G^{\mathrm{LMB},\boldsymbol{d}_k}_{\mathbb{L}^*_{k-1}}[\tilde{h}]$ (cf. (5.85)) and an MB PGFL $G^{\mathrm{MB}}_{\mathcal{M}_{\boldsymbol{d}_k}}[h]$ (cf. (5.86)). There are $|\mathcal{D}_k|$ mixture components, where each component is indexed by a vector $\boldsymbol{d}_k \in \mathcal{D}_k$. The vector $\boldsymbol{d}_k$ allows for an interesting interpretation in terms of object-measurement associations, which is why $\boldsymbol{d}_k$ will be referred to as (object-measurement) association vector in what follows. More precisely, each $\boldsymbol{d}_k \in \mathcal{D}_k$ corresponds to an admissible object-measurement association. We call an association hypothesis $\boldsymbol{d}_k$ admissible if all the nonzero entries $d_k^{(l)}$ are different, which implies that at most one measurement is assigned to the same labeled object and no measurement is assigned to more than one labeled object. In fact, $d_k^{(l)} \in \mathcal{M}_k$ describes the case where the labeled object with state (x_k, l) generates measurement $\boldsymbol{z}_k^{(m)}$ and $d_k^{(l)} = 0$ the case where the object does not generate any measurement. The set $\mathcal{M}_{\boldsymbol{d}_k} \subseteq \mathcal{M}_k$ comprises all measurement indices that are not associated with any labeled object and are thus generated either by an unlabeled object or by clutter. The statistics of each labeled object is described by a labeled Bernoulli component (cf. (5.85)) and the statistics of each unlabeled object by a (unlabeled) Bernoulli component (cf. (5.86)). The likelihood of each object-measurement association is quantified by the weight in (5.89). Furthermore, the likelihood of the event that the labeled object with state (x_k, l) generated measurement $m \in \mathcal{M}_k$ is quantified by the association weight $\beta_k^{(l,m)}$ in (5.74) and of the event that it did not generate a measurement by $\beta_k^{(l,0)}$ in (5.77). In the first case, the object is described by a labeled Bernoulli component, whose existence probability $r_k^{(l,m)}$ in (5.75) indicates that the object exists and its state is distributed according to $f^{(l,m)}(\boldsymbol{x}_k)$ in (5.76). In the second case, the object is also described by a labeled Bernoulli component. Here, the object existence is uncertain and quantified by the existence probability $r_k^{(l,0)}$ in (5.78). Note that $r_k^{(l,0)} = 0$ would indicate that the labeled object with state (x_k, l) does not exist and $r_k^{(l,0)} = 1$ would indicate that the object exists but did not generate a measurement. If the object exists, its state (x_k, l) is distributed according to $f^{(l,0)}(\boldsymbol{x}_k)$ in (5.79). Finally, the likelihood of the event that the measurement with index $m \in \mathcal{M}_{\boldsymbol{d}_k}$ is either originated by an unlabeled object or by clutter is quantified by $\beta_k^{(m)}$ in (5.80). The statistics of the object associated with this measurement is described by an (unlabeled) Bernoulli component. Object existence is modeled by $\bar{r}_k^{(m)}$ in (5.81). Here, $\bar{r}_k^{(m)} = 1$ would indicate that measurement $\boldsymbol{z}_k^{(m)}$ originated from an unlabeled object; its state x_k is distributed according to $\bar{f}^{(m)}(\boldsymbol{x}_k)$ in (5.82). On the other hand, $\bar{r}_k^{(m)} = 0$ would indicate that $\boldsymbol{z}_k^{(m)}$ originates from clutter.

The unlabeled PGFL $G_{\mathsf{X}_k}[h]$ is given by (5.91) according to

$$G_{\mathsf{X}_k}[h] = e^{\lambda_k[h-1]},$$

where the posterior PHD $\lambda(\boldsymbol{x}_k)$ is given by (5.92). Here, $G_{\mathsf{X}_k}[h]$ models all objects that did not give rise to a measurement at time step k.

5.4 Update Step: First Approximation Stage

The proposed LMB/P filter is now obtained by two successive approximations of the exact update step presented above, which result in a significant reduction of complexity. The first approximation stage results in a transformation of certain unlabeled objects into labeled objects. More concretely, to reduce the complexity of data association, we first cluster the LMB–MB mixture pgfl $G'_{\tilde{\mathsf{X}}_k,\mathsf{X}_k}[\tilde{h},h]$ in (5.88) into C LMB–MB mixture PGFLs. Then we transfer unlabeled objects that were previously unlikely to exist but satisfy a suitable threshold criterion to the labeled object part, which means that they are now considered as objects that are likely to exist.

5.4.1 Partitioning of Label and Measurement Sets

The clustering of $G'_{\tilde{\mathsf{X}}_k,\mathsf{X}_k}[\tilde{h},h]$ is based on a partitioning of the label set $\mathbb{L}^*_{k-1}$ and of the measurement set $\mathcal{M}_k = \{1,\ldots,M_k\}$. More precisely, we partition the label set $\mathbb{L}^*_{k-1}$ into $C \in \mathbb{N}$ disjoint subsets, i.e.,

$$\mathbb{L}^*_{k-1} = \bigcup_{c\in\mathcal{C}} \mathbb{L}^{(c)}_{k-1}, \tag{5.93}$$

where $\mathcal{C} \triangleq \{1,\ldots,C\}$, and we partition the measurement index set $\mathcal{M}_k = \{1,\ldots,M_k\}$ into $C+1$ disjoint subsets, i.e.,

$$\mathcal{M}_k = \left(\bigcup_{c\in\mathcal{C}} \mathcal{M}^{(c)}_k\right) \cup \mathcal{M}^{\mathrm{res}}_k. \tag{5.94}$$

Each measurement index subset $\mathcal{M}^{(c)}_k \subseteq \mathcal{M}_k$ is associated with a corresponding label subset $\mathbb{L}^{(c)}_{k-1} \subseteq \mathbb{L}^*_{k-1}$, whereas the residual measurement index subset $\mathcal{M}^{\mathrm{res}}_k = \mathcal{M}_k \setminus \bigcup_{c\in\mathcal{C}} \mathcal{M}^{(c)}_k$ is not associated with any label set. More specifically, the partitionings (5.93) and (5.94) are chosen such that for any $c \in \mathcal{C}$, the association (described by $d^{(l)}_k$) of an object with state $(\mathbf{x}_k, l)$, $l \in \mathbb{L}^{(c)}_{k-1}$ with a measurement with index m is plausible for $m \in \mathcal{M}^{(c)}_k$ and implausible for $m \in \mathcal{M}^{(c')}_k$ with $c' \neq c$. Here, the plausibility of an association is quantified by the association weight $\beta^{(l,m)}_k$ in (5.74). An algorithm for constructing the partitionings (5.93) and (5.94) is presented in the appendix of the thesis. This algorithm uses a nonnegative threshold γ_{C} that determines $\mathbb{L}^{(c)}_{k-1}$, $\mathcal{M}^{(c)}_k$, and $\mathcal{M}^{\mathrm{res}}_k$.

The above-described partitionings of $\mathbb{L}^*_{k-1}$ and $\mathcal{M}_k$ are illustrated in Figures 5.1 and 5.2, respectively. The proposed overall partitioning scheme is similar in spirit to the classical gating procedure used, e.g., in the JPDA filter [Bar-Shalom et al., 2011]. However, it is different in that it considers also the (non)existence of objects, it uses the association weights $\beta^{(l,m)}_k$ as plausibility measures, it does not rely on any Gaussian assumptions, and it collects all the residual measurement indices in $\mathcal{M}^{\mathrm{res}}_k$.

5.4.2 Pruning

According to our partitioning scheme, only the associations between objects with labeled state $(\mathbf{x}_k, l)$, $l \in \mathbb{L}^{(c)}_{k-1}$ and measurements with index $m \in \mathcal{M}^{(c)}_k$ are plausible. Thus, by pruning all the implausible association hypotheses $\boldsymbol{d}_k \in \mathcal{D}_k$ that associate some object label $l \in \mathbb{L}^{(c)}_{k-1}$ with some measurement index $m \in \mathcal{M}_k \setminus \mathcal{M}^{(c)}_k$, we obtain a more efficient representation of the relevant association information with fewer association hypotheses.

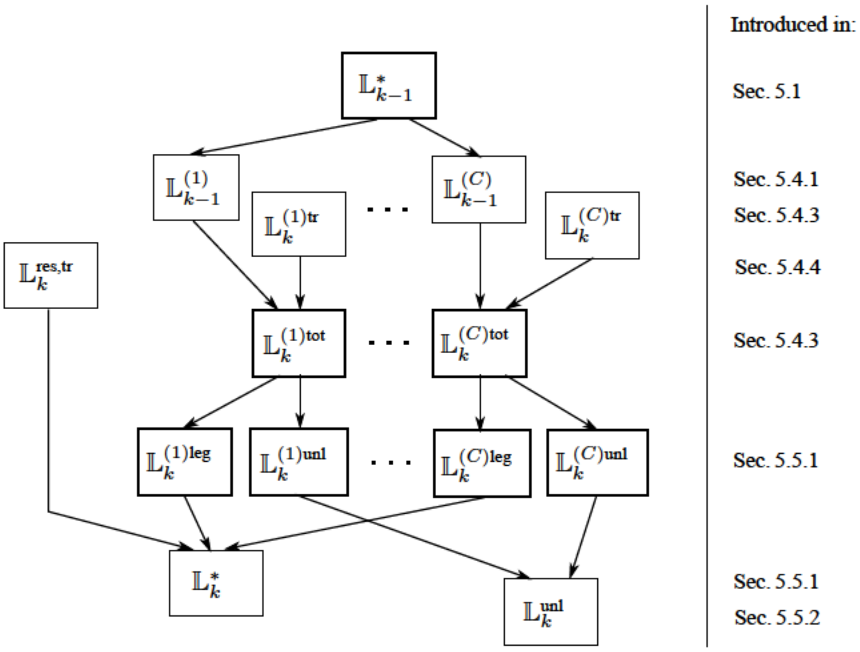

Figure 5.1: Some label sets involved in the approximations described in Sections 5.4 and 5.5.

Let $\mathcal{D}_k^{\text{rem}} \subseteq \mathcal{D}_k$ denote the set of the remaining (nonpruned) association hypotheses $\boldsymbol{d}_k$. Note that our pruning does not include missed detections (described by $d_k^{(l)} = 0$), i.e., association vectors $\boldsymbol{d}_k$ with $d_k^{(l)} = 0$, $l \in \mathbb{L}_{k-1}^{(c)}$ are part of $\mathcal{D}_k^{\text{rem}}$. Therefore, each $\boldsymbol{d}_k \in \mathcal{D}_k^{\text{rem}}$ associates each object label $l \in \mathbb{L}_{k-1}^{(c)}$ with some measurement index $m \in \{0\} \cup \mathcal{M}_k^{(c)}$.

The pruning yields the following approximation of $G'_{\tilde{\mathsf{X}}_k,\mathsf{X}_k}[\tilde{h}, h]$ in (5.88):

$$G'_{\tilde{\mathsf{X}}_k,\mathsf{X}_k}[\tilde{h}, h] \approx \sum_{\boldsymbol{d}_k \in \mathcal{D}_k^{\text{rem}}} \bar{w}_{\boldsymbol{d}_k} G^{\text{LMB},\boldsymbol{d}_k}_{\mathbb{L}^*_{k-1}}[\tilde{h}]\, G^{\text{MB}}_{\mathcal{M}_{\boldsymbol{d}_k}}[h]. \tag{5.95}$$

Here, the weights $\bar{w}_{\boldsymbol{d}_k}$ are given by expression (5.89) but with B_k replaced by $\bar{B}_k \triangleq \sum_{\boldsymbol{d}_k \in \mathcal{D}_k^{\text{rem}}} \Big(\prod_{l \in \mathbb{L}^*_{k-1}} \beta_k^{(l, d_k^{(l)})} \Big) \prod_{m \in \mathcal{M}_{\boldsymbol{d}_k}} \beta_k^{(m)}$. This ensures that $\sum_{\boldsymbol{d}_k \in \mathcal{D}_k^{\text{rem}}} \bar{w}_{\boldsymbol{d}_k} = 1$ and, thus, that (5.96) remains a valid PGFL. Furthermore, the LMB PGFL $G^{\text{LMB},\boldsymbol{d}_k}_{\mathbb{L}^*_{k-1}}[\tilde{h}]$ and the MB PGFL $G^{\text{MB}}_{\mathcal{M}_{\boldsymbol{d}_k}}[h]$ are given by (5.85) and (5.86), respectively. Using the fact that the Bernoulli component factors $G^{\text{MB}}_{\mathcal{M}_{\boldsymbol{d}_k}}[h]$ with $m \in \mathcal{M}_k^{\text{res}} \subseteq \mathcal{M}_{\boldsymbol{a}_k}$ appear in each one of the summation terms in (5.95), we obtain

$$G'_{\tilde{\mathsf{X}}_k,\mathsf{X}_k}[\tilde{h}, h] \approx G^{\text{MB}}_{\mathcal{M}_k^{\text{res}}}[h] \sum_{\boldsymbol{d}_k \in \mathcal{D}_k^{\text{rem}}} \bar{w}_{\boldsymbol{d}_k} G^{\text{LMB},\boldsymbol{d}_k}_{\mathbb{L}^*_{k-1}}[\tilde{h}]\, G^{\text{MB}}_{\mathcal{M}_{\boldsymbol{d}_k} \setminus \mathcal{M}_k^{\text{res}}}[h]. \tag{5.96}$$

Here, the MB PGFLs $G^{\text{MB}}_{\mathcal{M}_k^{\text{res}}}[h]$ and $G^{\text{MB}}_{\mathcal{M}_{\boldsymbol{d}_k} \setminus \mathcal{M}_k^{\text{res}}}[h]$ are given by (5.86) with $\mathcal{M}_{\boldsymbol{d}_k}$ replaced by $\mathcal{M}_k^{\text{res}}$ and $\mathcal{M}_{\boldsymbol{d}_k} \setminus \mathcal{M}_k^{\text{res}}$, respectively.

As a consequence of the pruning, all objects with labels $l \in \mathbb{L}_{k-1}^{(c)}$, i.e., corresponding to cluster c, are now associated only with measurements of the same cluster c, $m \in$

$\{0\} \cup \mathcal{M}_k^{(c)}$, and not with any other measurements $m \in \mathcal{M}_k \setminus \mathcal{M}_k^{(c)}$. This implies that each entry $d_k^{(l)}$ of $\boldsymbol{d}_k \in \mathcal{D}_k^{\mathrm{rem}}$ associates labels $l \in \mathbb{L}_{k-1}^{(c)}$ of cluster c only with measurements $m \in \{0\} \cup \mathcal{M}_k^{(c)}$ of cluster c. Therefore, the association vector $\boldsymbol{d}_k$ (of dimension $|\mathbb{L}_{k-1}^{*}|$) can be split into C subvectors $\boldsymbol{d}_k^{(c)} \in \big(\{0\} \cup \mathcal{M}_k^{(c)}\big)^{|\mathbb{L}_{k-1}^{(c)}|}$, $c \in \mathcal{C}$ of lower dimensions $|\mathbb{L}_{k-1}^{(c)}|$. Here, for each $c \in \mathcal{C}$, the entry $d_k^{(c,l)}$ of $\boldsymbol{d}_k^{(c)}$, with $l \in \mathbb{L}_{k-1}^{(c)}$, is defined similarly to $d_k^{(l)}$ in Section 5.3.5 as $d_k^{(c,l)} \triangleq m \in \mathcal{M}_k^{(c)}$ if the labeled object with state $(\mathbf{x}_k, l)$ generates measurement $\boldsymbol{z}_k^{(m)}$ and $d_k^{(c,l)} \triangleq 0$ if it does not generate a measurement. The admissible association vectors $\boldsymbol{d}_k^{(c)}$ (where admissibility was defined in Section 5.3.5) are collected in the association alphabet $\mathcal{D}_k^{(c)}$. We can now factor the weights as

$$\bar{w}_{\boldsymbol{d}_k} = \prod_{c \in \mathcal{C}} w_{\boldsymbol{d}_k^{(c)}}, \tag{5.97}$$

where (cf. (5.89))

$$w_{\boldsymbol{d}_k^{(c)}} = \frac{1}{B_k^{(c)}} \Bigg(\prod_{l \in \mathbb{L}_{k-1}^{(c)}} \beta_k^{(l, d_k^{(c,l)})} \Bigg) \prod_{m \in \mathcal{M}_{\boldsymbol{d}_k^{(c)}}} \beta_k^{(m)}, \tag{5.98}$$

with $B_k^{(c)} \triangleq \sum_{\boldsymbol{d}_k^{(c)} \in \mathcal{D}_k^{(c)}} \Big(\prod_{l \in \mathbb{L}_{k-1}^{(c)}} \beta_k^{(l, d_k^{(c,l)})} \Big) \prod_{m \in \mathcal{M}_{\boldsymbol{d}_k^{(c)}}} \beta_k^{(m)}$. Here, $\mathcal{M}_{\boldsymbol{d}_k^{(c)}} \subseteq \mathcal{M}_k^{(c)}$ comprises all measurement indices $m \in \mathcal{M}_k^{(c)}$ that are not associated with any labeled object via $\boldsymbol{d}_k^{(c)} \in \mathcal{D}_k^{(c)}$ and, thus, originate from an unlabeled object or from clutter. In particular, $\mathcal{M}_{\boldsymbol{d}_k^{(c)}} = \emptyset$ indicates that all measurement indices $m \in \mathcal{M}_k^{(c)}$ are associated with an object with label $l \in \mathbb{L}_{k-1}^{(c)}$. Furthermore, we have (cf. (5.85) and (5.86))

$$G_{\mathbb{L}_{k-1}^{*}}^{\mathrm{LMB}, \boldsymbol{d}_k}[\tilde{h}] = \prod_{c \in \mathcal{C}} G_{\mathbb{L}_{k-1}^{(c)}}^{\mathrm{LMB}, \boldsymbol{d}_k^{(c)}}[\tilde{h}], \tag{5.99}$$

$$G_{\mathcal{M}_{\boldsymbol{d}_k} \setminus \mathcal{M}_k^{\mathrm{res}}}^{\mathrm{MB}}[h] = \prod_{c \in \mathcal{C}} G_{\mathcal{M}_{\boldsymbol{d}_k^{(c)}}}^{\mathrm{MB}}[h], \tag{5.100}$$

with

$$G_{\mathbb{L}_{k-1}^{(c)}}^{\mathrm{LMB}, \boldsymbol{d}_k^{(c)}}[\tilde{h}] \triangleq \prod_{l \in \mathbb{L}_{k-1}^{(c)}} G^{\mathrm{Ber}}\big[\tilde{h}; r_k^{(l, d_k^{(l,c)})}, f_k^{(l, d_k^{(l,c)})}\big],$$

$$G_{\mathcal{M}_{\boldsymbol{d}_k^{(c)}}}^{\mathrm{MB}}[h] \triangleq \prod_{m \in \mathcal{M}_{\boldsymbol{d}_k^{(c)}}} G^{\mathrm{Ber}}\big[h; \bar{r}_k^{(m)}, \bar{f}_k^{(m)}\big].$$

Using the factorizations (5.97), (5.99), and (5.100) as well as the identity $\sum_{\boldsymbol{d}_k \in \mathcal{D}_k^{\mathrm{rem}}} = \sum_{\boldsymbol{d}_k^{(1)} \in \mathcal{D}_k^{(1)}} \cdots \sum_{\boldsymbol{d}_k^{(C)} \in \mathcal{D}_k^{(C)}}$, we can rewrite the approximation (5.96) in terms of $\boldsymbol{d}_k^{(c)}$ as

$$G'_{\tilde{\mathsf{X}}_k, \mathsf{X}_k}[\tilde{h}, h] \approx G_{\mathcal{M}_k^{\mathrm{res}}}^{\mathrm{MB}}[h] \prod_{c \in \mathcal{C}} G^{(c)}[\tilde{h}, h], \tag{5.101}$$

where

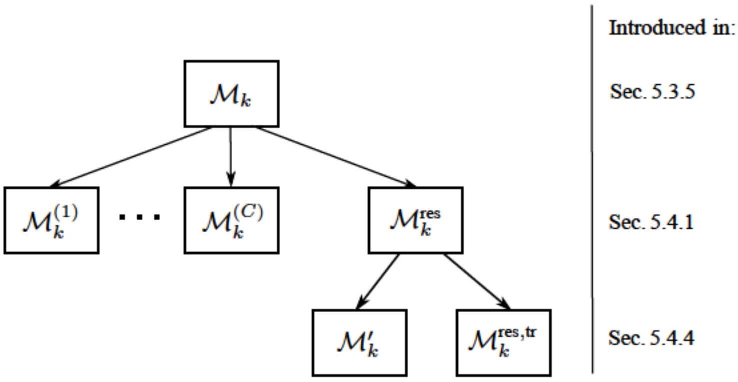

Figure 5.2: Some measurement index sets involved in the approximations described in Sections 5.4 and 5.5.

$$G^{(c)}[\tilde{h}, h] \triangleq \sum_{\boldsymbol{d}_k^{(c)} \in \mathcal{D}_k^{(c)}} w_{\boldsymbol{d}_k^{(c)}} G^{\mathrm{LMB}, \boldsymbol{d}_k^{(c)}}_{\mathbb{L}_{k-1}^{(c)}}[\tilde{h}] G^{\mathrm{MB}}_{\mathcal{M}_{\boldsymbol{d}_k^{(c)}}}[h]. \tag{5.102}$$

We note that $G^{(c)}[\tilde{h}, h]$ and $G^{\mathrm{MB}}_{\mathcal{M}_k^{\mathrm{res}}}[h]$ represent clustered objects and nonclustered objects, respectively, which, in both cases, may be likely or unlikely to exist. So far, we approximated $G'_{\tilde{\mathsf{X}}_k, \mathsf{X}_k}[\tilde{h}, h]$ in (5.88) by expression (5.101), which is the product of the C LMB–MB mixture PGFLs $G^{(c)}[\tilde{h}, h]$ in (5.102) and the MB PGFL $G^{\mathrm{MB}}_{\mathcal{M}_k^{\mathrm{res}}}[h]$. As visualized in Figure 5.3, this is the first stage in a series of PGFL approximations or modifications that are used in the development of the proposed LMB/P filter. Next, we will develop approximations of $G^{(c)}[\tilde{h}, h]$ and $G^{\mathrm{MB}}_{\mathcal{M}_k^{\mathrm{res}}}[h]$.

5.4.3 Approximation of the PGFL of Clustered Objects $G^{(c)}[\tilde{h}, h]$

We approximate the PGFL of clustered objects, $G^{(c)}[\tilde{h}, h]$, by an LMBM PGFL. To this end, we recall from Section 5.4.2 that the MB PGFL $G^{\mathrm{MB}}_{\mathcal{M}_{\boldsymbol{d}_k^{(c)}}}[h]$ involved in $G^{(c)}[\tilde{h}, h]$ in (5.102) corresponds to measurements $m \in \mathcal{M}_k^{(c)}$ that originate from an unlabeled object or from clutter. We want to transfer unlabeled objects that are very likely to exist, or more specifically, (unlabeled) Bernoulli components $G^{\mathrm{Ber}}\big[h; \bar{r}_k^{(m)}, \bar{f}_k^{(m)}\big]$, $m \in \mathcal{M}_{\boldsymbol{d}_k^{(c)}}$ with $\bar{r}_k^{(m)} \geq \gamma_{\mathrm{tr}}$, to the labeled RFS part. Here, $\bar{r}_k^{(m)}$ is given by (5.81) and γ_{tr} is a positive threshold. This transfer is motivated by the fact that the labeled RFS part guarantees track continuity and, in addition, after further modifications to be described in Section 5.5, achieves a higher tracking accuracy than the unlabeled RFS part. The transfer is accomplished by formally replacing the measurement index m arising in $G^{\mathrm{Ber}}\big[h; \bar{r}_k^{(m)}, \bar{f}_k^{(m)}\big]$ by the label $l = (k, m)$. Let $\mathbb{L}_k^{(c)\mathrm{tr}}$ collect the labels of the transferred Bernoulli components (cf. also Figure 5.1). We note that a higher threshold γ_{tr} tends to imply a smaller number of transferred Bernoulli components, $|\mathbb{L}_k^{(c)\mathrm{tr}}|$. Furthermore, since the other Bernoulli components $G^{\mathrm{Ber}}\big[h; \bar{r}_k^{(m)}, \bar{f}_k^{(m)}\big]$ (with $\bar{r}_k^{(m)} < \gamma_{\mathrm{tr}}$), $m \in \mathcal{M}_{\boldsymbol{d}_k^{(c)}}$ model objects that are unlikely to exist, we prune them. This is done by setting $h = 1$ because $G^{\mathrm{Ber}}\big[1; \bar{r}_k^{(m)}, \bar{f}_k^{(m)}\big] = 1$.

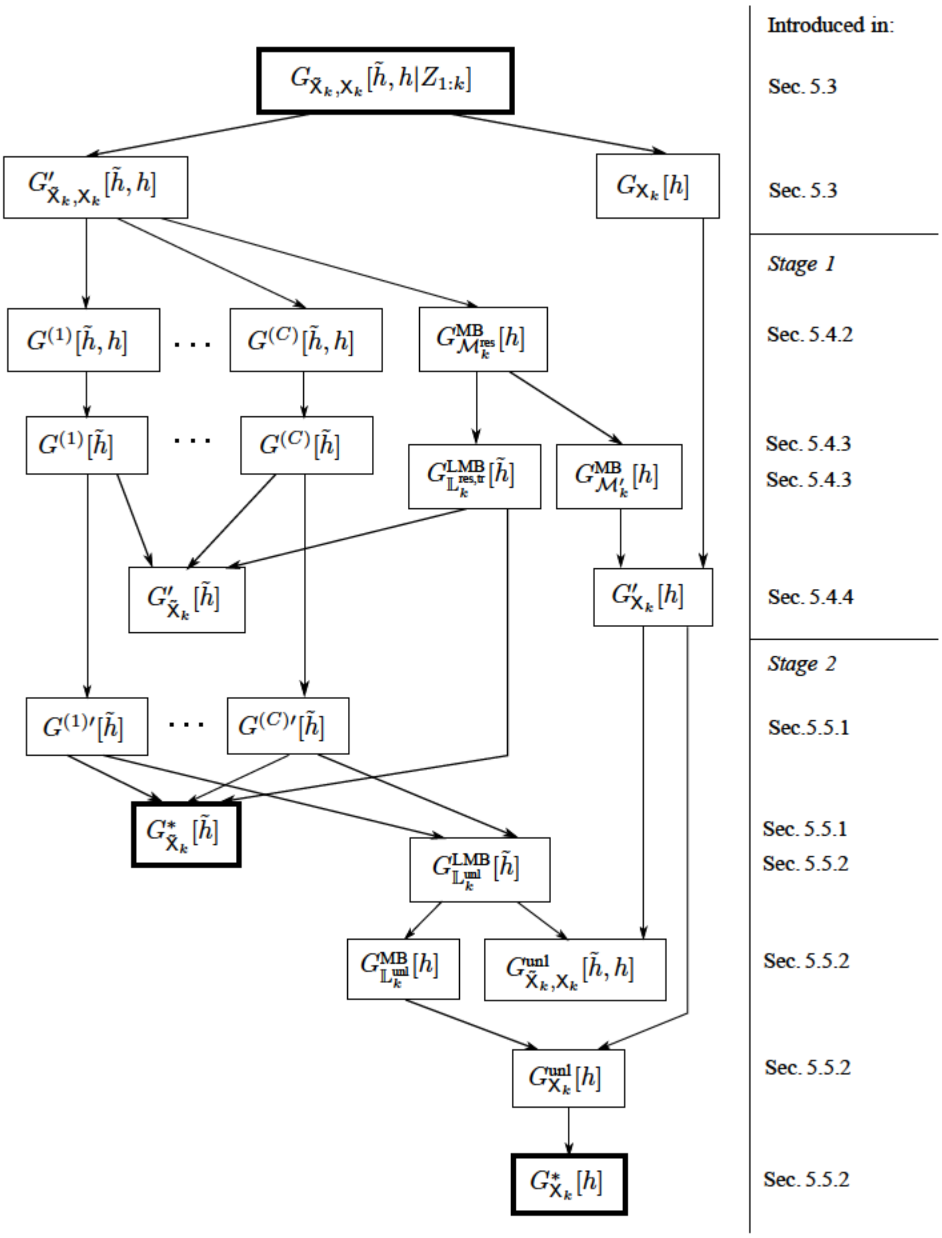

Figure 5.3: Some PGFLs involved in the approximations described in Sections 5.4 and 5.5.

With these modifications, $G^{(c)}[\tilde{h}, h]$ in (5.102) is replaced by (cf. Figure 5.3)

$$G^{(c)}[\tilde{h}] \triangleq \sum_{\boldsymbol{d}_k^{\prime(c)} \in \mathcal{D}_k^{\prime(c)}} w_{\boldsymbol{d}_k^{\prime(c)}} G_{\mathbb{L}_k^{(c)\text{tot}}}^{\text{LMB},\boldsymbol{d}_k^{\prime(c)}}[\tilde{h}], \tag{5.103}$$

with the LMB PGFL

$$G_{\mathbb{L}_k^{(c)\text{tot}}}^{\text{LMB},\boldsymbol{d}_k^{\prime(c)}}[\tilde{h}] \triangleq \prod_{l \in \mathbb{L}_k^{(c)\text{tot}}} G^{\text{Ber}}\big[\tilde{h}; r_k^{(l,d_k^{\prime(c,l)})}, f_k^{(l,d_k^{\prime(c,l)})}\big]. \tag{5.104}$$

Here, the label set $\mathbb{L}_k^{(c)\text{tot}}$ is given as (see Figure 5.1)

$$\mathbb{L}_k^{(c)\text{tot}} \triangleq \mathbb{L}_{k-1}^{(c)} \cup \mathbb{L}_k^{(c)\text{tr}}, \tag{5.105}$$

where $\mathbb{L}_{k-1}^{(c)} \cap \mathbb{L}_k^{(c)\text{tr}} = \emptyset$. Furthermore, the entries $d_k^{\prime(c,l)}$ of the association vector $\boldsymbol{d}_k^{\prime(c)} \in \tilde{\mathcal{D}}_k^{(c)} \subseteq \big(\{0\} \cup \mathcal{M}_k^{(c)}\big)^{|\mathbb{L}_{k-1}^{(c)}|} \times \{0,1\}^{|\mathbb{L}_k^{(c)\text{tr}}|}$ are defined as follows: for $l \in \mathbb{L}_{k-1}^{(c)}$, $d_k^{\prime(c,l)}$ is equal to $d_k^{(c,l)}$ (as defined in Section 5.4.2), and for $l \in \mathbb{L}_k^{(c)\text{tr}}$, $d_k^{\prime(c,l)}$ is 1 if the labeled object with state $(\mathbf{x}_k, l)$ generates measurement $\boldsymbol{z}_k^{(m)}$ and 0 if it does not generate a measurement. Next, the association alphabet $\mathcal{D}_k^{\prime(c)} \subseteq \boldsymbol{d}_k^{\prime(c)} \in \tilde{\mathcal{D}}_k^{(c)}$ collects all the admissible association vectors $\boldsymbol{d}_k^{\prime(c)}$ (we recall that admissibility was defined in Section 5.3.5). The LMB PGFL $G_{\mathbb{L}_k^{(c)\text{tot}}}^{\text{LMB},\boldsymbol{d}_k^{\prime(c)}}[\tilde{h}]$ in (5.103) comprise Bernoulli PGFLs for $l \in \mathbb{L}_{k-1}^{(c)}$ and for $l \in \mathbb{L}_k^{(c)\text{tr}}$. In the first case, the parameters $r_k^{(l,m)}$ and $f_k^{(l,m)}(\boldsymbol{x}_k)$ of these Bernoulli components (cf. (5.85)) are given for $m \in \mathcal{M}_k^{(c)}$ by (5.75) and (5.76), respectively and for $m = 0$ by (5.78) and (5.79), respectively. In the second case, i.e., $l = (k, m) \in \mathbb{L}_k^{(c)\text{tr}}$, the parameters $r_k^{(l,1)}$ and $f_k^{(l,1)}(\boldsymbol{x}_k)$ are given for by $\bar{r}_k^{(m)}$ in (5.81) and $\bar{f}_k^{(m)}(\boldsymbol{x}_k)$ in (5.82), respectively; furthermore $r_k^{(l,0)} = 0$ whereas $f_k^{(l,0)}(\boldsymbol{x}_k)$ is not defined since the object does not exist. Finally, the weights $w_{\boldsymbol{d}_k^{\prime(c)}}$ are given by (cf. (5.98))

$$w_{\boldsymbol{d}_k^{\prime(c)}} = \frac{1}{B_k^{\prime(c)}} \left(\prod_{l \in \mathbb{L}_k^{(c)\text{tot}}} \beta_k^{(l,d_k^{\prime(c,l)})} \right) \prod_{m \in \mathcal{M}_{\boldsymbol{d}_k^{\prime(c)}}} \beta_k^{(m)}, \tag{5.106}$$

where $\mathcal{M}_{\boldsymbol{d}_k^{\prime(c)}} \subseteq \mathcal{M}_{\boldsymbol{d}_k^{(c)}}$ comprises all measurement indices $m \in \mathcal{M}_{\boldsymbol{d}_k^{(c)}}$ that are not associated with any object label $l \in \mathbb{L}_k^{(c)\text{tot}}$. For $l \in \mathbb{L}_{k-1}^{(c)}$, the association weights $\beta_k^{(l,m)}$ are given for $m \in \mathcal{M}_k^{(c)}$ by (5.74) and for $m = 0$ by (5.77), and for $l \in \mathbb{L}_k^{(c)\text{tr}}$, the $\beta_k^{(l,m)}$ are given for $m = 1$ by (5.80) and for $m = 0$ by 1. Furthermore, the $\beta_k^{(m)}$ are given by (5.80). The normalization constant $B_k^{\prime(c)}$ is given by $B_k^{\prime(c)} \triangleq \sum_{\boldsymbol{d}_k^{\prime(c)} \in \mathcal{D}_k^{\prime(c)}} \Big(\prod_{l \in \mathbb{L}_k^{(c)\text{tot}}} \beta_k^{(l,d_k^{\prime(c,l)})} \Big) \prod_{m \in \mathcal{M}_{\boldsymbol{d}_k^{\prime(c)}}} \beta_k^{(m)}$.

To summarize, we approximated the PGFL of clustered objects $G^{(c)}[\tilde{h}, h]$ in (5.102), which is an LMB–MB mixture PGFL, by the LMBM PGFL $G^{(c)}[\tilde{h}]$ in (5.103). This approximation involved the transfer of unlabeled Bernoulli components to the labeled RFS part. Finally, replacing in (5.101) $G^{(c)}[\tilde{h}, h]$ with $G^{(c)}[\tilde{h}]$, we obtain

$$G'_{\tilde{\mathsf{X}}_k,\mathsf{X}_k}[\tilde{h},h] \approx G^{\mathrm{MB}}_{\mathcal{M}_k^{\mathbf{res}}}[h]\prod_{c\in\mathcal{C}} G^{(c)}[\tilde{h}]. \tag{5.107}$$

5.4.4 Approximation of the PGFL of Nonclustered Objects $G^{\mathrm{MB}}_{\mathcal{M}_k^{\mathbf{res}}}[h]$

Next, we consider the MB PGFL $G^{\mathrm{MB}}_{\mathcal{M}_k^{\mathbf{res}}}[h]$ of nonclustered objects in (5.107). We recall from Section 5.4.2 that

$$G^{\mathrm{MB}}_{\mathcal{M}_k^{\mathbf{res}}}[h] = \prod_{m\in\mathcal{M}_k^{\mathbf{res}}} G^{\mathrm{Ber}}\big[h;\bar{r}_k^{(m)},\bar{f}_k^{(m)}\big].$$

Similarly to the measurements $m\in\mathcal{M}_{\boldsymbol{d}_k^{(c)}}$ involved in $G^{\mathrm{MB}}_{\mathcal{M}_{\boldsymbol{d}_k^{(c)}}}[h]$ in (5.102), the measurements $m\in\mathcal{M}_k^{\mathbf{res}}$ involved in $G^{\mathrm{MB}}_{\mathcal{M}_k^{\mathbf{res}}}[h]$ originate from an unlabeled object or from clutter. Analogously to Section 5.4.3, we transfer objects that are likely to exist to the labeled RFS part, and thus we formally replace the measurement index m in each Bernoulli component $G^{\mathrm{Ber}}\big[h;\bar{r}_k^{(m)},\bar{f}_k^{(m)}\big]$, $m\in\mathcal{M}_k^{\mathbf{res}}$ of $G^{\mathrm{MB}}_{\mathcal{M}_k^{\mathbf{res}}}[h]$ with $\bar{r}_k^{(m)}\geq\gamma_{\mathrm{tr}}$ by the label $l=(k,m)$. These labels are collected in the set $\mathbb{L}_k^{\mathbf{res,tr}}$ (see Figure 5.1), and the corresponding measurement indices are collected in the set $\mathcal{M}_k^{\mathbf{res,tr}}\subseteq\mathcal{M}_k^{\mathbf{res}}$ (see Figure 5.2). The remaining measurement indices are collected in the set $\mathcal{M}'_k=\mathcal{M}_k^{\mathbf{res}}\setminus\mathcal{M}_k^{\mathbf{res,tr}}$ (again see Figure 5.2). As before, a higher threshold γ_{tr} tends to imply a smaller number of transferred Bernoulli components, $|\mathbb{L}_k^{\mathbf{res,tr}}|$. Using these modifications, $G^{\mathrm{MB}}_{\mathcal{M}_k^{\mathbf{res}}}[h]$ is approximated according to (see Figure 5.3)

$$G^{\mathrm{MB}}_{\mathcal{M}_k^{\mathbf{res}}}[h] \approx G^{\mathrm{LMB}}_{\mathbb{L}_k^{\mathbf{res,tr}}}[\tilde{h}]\,G^{\mathrm{MB}}_{\mathcal{M}'_k}[h], \tag{5.108}$$

where the PGFLs are defined as

$$G^{\mathrm{LMB}}_{\mathbb{L}_k^{\mathbf{res,tr}}}[\tilde{h}] \triangleq \prod_{l\in\mathbb{L}_k^{\mathbf{res,tr}}} G^{\mathrm{Ber}}[\tilde{h};\bar{r}_k^{(l)},\bar{f}_k^{(l)}], \tag{5.109}$$

with $l=(k,m)$ and $G^{\mathrm{MB}}_{\mathcal{M}'_k}[h]\triangleq\prod_{m\in\mathcal{M}'_k}G^{\mathrm{Ber}}\big[h;\bar{r}_k^{(m)},\bar{f}_k^{(m)}\big]$; here the existence probabilities and spatial PDFs are given by (5.81) and (5.82), respectively. Inserting (5.108) into (5.107) yields

$$G'_{\tilde{\mathsf{X}}_k,\mathsf{X}_k}[\tilde{h},h|Z_{1:k}] \approx G^{\mathrm{LMB}}_{\mathbb{L}_k^{\mathbf{res,tr}}}[\tilde{h}]\,G^{\mathrm{MB}}_{\mathcal{M}'_k}[h]\prod_{c\in\mathcal{C}} G^{(c)}[\tilde{h}]. \tag{5.110}$$

Finally, inserting approximation (5.110) into (5.39) and grouping terms, we obtain (again see Figure 5.3)

$$G_{\tilde{\mathsf{X}}_k,\mathsf{X}_k}[\tilde{h},h|Z_{1:k}] \approx G'_{\tilde{\mathsf{X}}_k}[\tilde{h}]\,G'_{\mathsf{X}_k}[h], \tag{5.111}$$

with the labeled part

$$G'_{\tilde{\mathsf{X}}_k}[\tilde{h}] \triangleq G^{\mathrm{LMB}}_{\mathbb{L}_k^{\mathbf{res,tr}}}[\tilde{h}]\prod_{c\in\mathcal{C}} G^{(c)}[\tilde{h}] \tag{5.112}$$

and the unlabeled part

$$G'_{\mathsf{X}_k}[h] \triangleq G^{\mathrm{MB}}_{\mathcal{M}'_k}[h]\,G_{\mathsf{X}_k}[h]. \tag{5.113}$$

Here, $G_{\mathsf{X}_k}[h]$ is the Poisson PGFL given by (5.91) and (5.92). Note that $G'_{\mathsf{X}_k}[h]$ is an MB–Poisson PGFL representing unlabeled objects, which are objects that are unlikely to exist.

In summary, in the first approximation stage, the exact joint posterior PGFL $G_{\tilde{\mathsf{X}}_k,\mathsf{X}_k}[\tilde{h},h|Z_{1:k}] = G'_{\tilde{\mathsf{X}}_k,\mathsf{X}_k}[\tilde{h},h]G_{\mathsf{X}_k}[h]$ in (5.39) is approximated by $G'_{\tilde{\mathsf{X}}_k}[\tilde{h}]G'_{\mathsf{X}_k}[h]$ in (5.111). Here, $G'_{\tilde{\mathsf{X}}_k}[\tilde{h}]$ is the PGFL of a labeled RFS, more precisely, the product of the LMB PGFL $G^{\mathrm{LMB}}_{\mathbb{L}_k^{\mathbf{res,tr}}}[\tilde{h}]$ and the LMBM PGFLs $G^{(c)}[\tilde{h}]$, $c = 1, \dots, C$. Furthermore, $G'_{\mathsf{X}_k}[h]$ is the PGFL of an unlabeled RFS, more specifically, the product of the MB PGFL $G^{\mathrm{MB}}_{\mathcal{M}'_k}[h]$ and the Poisson PGFL $G_{\mathsf{X}_k}[h]$. The overall effect of the first approximation stage is on the one hand (i) to reduce the overall complexity (via the clustering and pruning described in Section 5.4.1 and Section 5.4.2, respectively) and on the other hand (ii) to transfer the part of the unlabeled RFS representing likely unlabeled objects to the labeled RFS (see Sections 5.4.3 and 5.4.4). As a result of this transfer, some objects that were previously modeled as unlabeled objects are now considered as labeled objects. This transfer can be viewed as the creation of "new" labeled objects. Note that this creation is an inherent part of our tracking algorithm, and not due to a birth process in our system model (cf. Section 5.1.1).

5.5 Update Step: Second Approximation Stage

In the second approximation stage, we approximate $G'_{\tilde{\mathsf{X}}_k}[\tilde{h}]$ in (5.111) and (5.112), which is the product of an LMB PGFL and C LMBM PGFLs, by an LMB PGFL. Furthermore, we modify $G'_{\mathsf{X}_k}[h]$ in (5.111) and (5.113), which is the product of an MB PGFL and a Poisson PGFL. This modification consists of first combining $G'_{\mathsf{X}_k}[h]$ with the "unlikely" legacy Bernoulli components of the LMB PGFL approximating $G'_{\tilde{\mathsf{X}}_k}[\tilde{h}]$ and then approximating the resulting PGFL by a Poisson PGFL.

5.5.1 Labeled Objects

We first approximate the PGFL of labeled objects, $G'_{\tilde{\mathsf{X}}_k}[\tilde{h}]$, by an LMB pgfl, and then we transfer labeled objects that are unlikely to exist to the unlabeled RFS part. This transfer is known as recycling [Williams, 2012].

According to (5.112), $G'_{\tilde{\mathsf{X}}_k}[\tilde{h}] = G^{\mathrm{LMB}}_{\mathbb{L}_k^{\mathbf{res,tr}}}[\tilde{h}] \prod_{c\in\mathcal{C}} G^{(c)}[\tilde{h}]$. To approximate $G'_{\tilde{\mathsf{X}}_k}[\tilde{h}]$ by an LMB PGFL, we first note that the product of LMB PGFLs is again an LMB PGFL, and that $G^{\mathrm{LMB}}_{\mathbb{L}_k^{\mathbf{res,tr}}}[\tilde{h}]$ is already an LMB PGFL. Therefore, we now approximate the LMBM PGFLs $G^{(c)}[\tilde{h}]$, $c \in \mathcal{C}$ by LMB PGFLs. For this, we start from expression (5.103) and exploit the fact that the weights $w_{\boldsymbol{d}_k'^{(c)}}$, $\boldsymbol{d}_k'^{(c)} \in \mathcal{D}_k'^{(c)}$ in (5.106) satisfy $\sum_{\boldsymbol{d}_k'^{(c)}\in\mathcal{D}_k'^{(c)}} w_{\boldsymbol{d}_k'^{(c)}} = 1$. Thus, we are able to formally interpret them as the PMF of the *random* association vector $\mathbf{d}_k'^{(c)}$, i.e., we set

$$p\big(\boldsymbol{d}_k'^{(c)}\big) \triangleq \begin{cases} w_{\boldsymbol{d}_k'^{(c)}}, & \boldsymbol{d}_k'^{(c)} \in \mathcal{D}_k'^{(c)}, \\ 0, & \text{otherwise.} \end{cases} \tag{5.114}$$

Expression (5.103) can then be rewritten as

$$G^{(c)}[\tilde{h}] = \sum_{\boldsymbol{d}_k'^{(c)} \in \tilde{\mathcal{D}}_k^{(c)}} p\big(\boldsymbol{d}_k'^{(c)}\big)\, G^{\mathrm{LMB},\boldsymbol{d}_k'^{(c)}}_{\mathbb{L}_k^{(c)\mathbf{tot}}}[\tilde{h}], \tag{5.115}$$

Here, the summation over the larger set $\tilde{\mathcal{D}}_k^{(c)}$ (i.e., larger than $\mathcal{D}_k'^{(c)}$ in (5.103)) is possible because $p\big(\boldsymbol{d}_k'^{(c)}\big) = 0$ for $\boldsymbol{d}_k'^{(c)} \in \tilde{\mathcal{D}}_k^{(c)} \setminus \mathcal{D}_k'^{(c)}$. Note that $\tilde{\mathcal{D}}_k^{(c)}$ also includes inadmissible associations.

Following the approach taken in [Williams, 2015] and our proposed fast LMB filter of Chapter 4, we now approximate $p\big(\boldsymbol{d}_k'^{(c)}\big)$ by the product of the marginal PMFs $p\big(d_k'^{(c,l)}\big)$, i.e.,

$$p\big(\boldsymbol{d}_k'^{(c)}\big) \approx \prod_{l \in \mathbb{L}_k^{(c)\mathbf{tot}}} p\big(d_k'^{(c,l)}\big), \quad \boldsymbol{d}_k'^{(c)} \in \tilde{\mathcal{D}}_k^{(c)}. \tag{5.116}$$

Here,

$$p\big(d_k'^{(c,l)}\big) \triangleq \begin{cases} \sum_{\boldsymbol{d}_k'^{(c)\sim l} \in \tilde{\mathcal{D}}_k^{(c)\mathbf{leg}}} p\big(\boldsymbol{d}_k'^{(c)}\big), & l \in \mathbb{L}_{k-1}^{(c)}, \\ \sum_{\boldsymbol{d}_k'^{(c)\sim l} \in \tilde{\mathcal{D}}_k^{(c)\mathbf{tr}}} p\big(\boldsymbol{d}_k'^{(c)}\big), & l \in \mathbb{L}_k^{(c)\mathbf{tr}} \end{cases} \tag{5.117}$$

(recall that $\mathbb{L}_k^{(c)\mathbf{tot}} = \mathbb{L}_{k-1}^{(c)} \cup \mathbb{L}_k^{(c)\mathbf{tr}}$), where $\boldsymbol{d}_k'^{(c)\sim l}$ denotes the vector $\boldsymbol{d}_k'^{(c)}$ without entry $d_k'^{(c,l)}$, and the summation sets are defined as $\tilde{\mathcal{D}}_k^{(c)\mathbf{leg}} \triangleq \big(\{0\} \cup \mathcal{M}_k^{(c)}\big)^{|\mathbb{L}_{k-1}^{(c)}|-1} \times \{0,1\}^{|\mathbb{L}_k^{(c)\mathbf{tr}}|}$, and $\tilde{\mathcal{D}}_k^{(c)\mathbf{tr}} \triangleq \big(\{0\} \cup \mathcal{M}_k^{(c)}\big)^{|\mathbb{L}_{k-1}^{(c)}|} \times \{0,1\}^{|\mathbb{L}_k^{(c)\mathbf{tr}}|-1}$. We note that an efficient and scalable approximate implementation of the marginalization in (5.117) is provided by the belief propagation algorithm proposed in [Williams, 2015]. Inserting approximation (5.116) in (5.115) and using (5.104) yields the following approximation of $G^{(c)}[\tilde{h}]$:

$$G^{(c)\prime}[\tilde{h}] \triangleq \sum_{\boldsymbol{d}_k'^{(c)} \in \tilde{\mathcal{D}}_k^{(c)}} \prod_{l \in \mathbb{L}_k^{(c)\mathbf{tot}}} p\big(d_k'^{(c,l)}\big)\, G^{\mathrm{Ber}}\big[\tilde{h}; r_k^{(l,d_k'^{(c,l)})}, f_k^{(l,d_k'^{(c,l)})}\big]$$

Using $\sum_{\boldsymbol{d}_k^{(c)} \in \tilde{\mathcal{D}}_k^{(c)}} = \sum_{d_k^{(c,1)} \in \{0\} \cup \mathcal{M}_k^{(c)}} \cdots \sum_{d_k^{(c,|\mathbb{L}_{k-1}^{(c)}|)} \in \{0\} \cup \mathcal{M}_k^{(c)}} \sum_{d_k^{(c,|\mathbb{L}_{k-1}^{(c)}|+1)} \in \{0,1\}} \cdots \times \sum_{d_k^{(c,|\mathbb{L}_{k-1}^{(c)}|+|\mathbb{L}_k^{(c)\mathbf{tr}}|)} \in \{0,1\}}$ and $\prod_{l \in \mathbb{L}_k^{(c)\mathbf{tot}}} = \prod_{l \in \mathbb{L}_{k-1}^{(c)}} \prod_{l \in \mathbb{L}_k^{(c)\mathbf{tr}}}$, this becomes

$$G^{(c)\prime}[\tilde{h}] = \Bigg(\prod_{l \in \mathbb{L}_{k-1}^{(c)}} \sum_{d_k'^{(c,l)} \in \{0\} \cup \mathcal{M}_k^{(c)}} p\big(d_k'^{(c,l)}\big)\, G^{\mathrm{Ber}}\big[\tilde{h}; r_k^{(l,d_k'^{(c,l)})}, f_k^{(l,d_k'^{(c,l)})}\big] \Bigg) \\ \times \prod_{l \in \mathbb{L}_k^{(c)\mathbf{tr}}} \sum_{d_k'^{(c,l)} \in \{0,1\}} p\big(d_k'^{(c,l)}\big)\, G^{\mathrm{Ber}}\big[\tilde{h}; r_k^{(l,d_k'^{(c,l)})}, f_k^{(l,d_k'^{(c,l)})}\big].$$

Using (2.15), this can be written as the LMB PGFL

$$G^{(c)\prime}[\tilde{h}] = \prod_{l \in \mathbb{L}_k^{(c)\mathrm{tot}}} G^{\mathrm{Ber}}\big[\tilde{h}; r_k^{(l)}, f_k^{(l)}\big], \tag{5.118}$$

where, according to (2.16), $r_k^{(l)}$ and $f^{(l)}(\boldsymbol{x}_k)$ are given for $l \in \mathbb{L}_{k-1}^{(c)}$ by

$$r_k^{(l)} = \sum_{d_k^{\prime(c,l)} \in \{0\} \cup \mathcal{M}_k^{(c)}} p\big(d_k^{\prime(c,l)}\big)\, r_k^{(l,d_k^{\prime(c,l)})}, \tag{5.119}$$

$$f^{(l)}(\boldsymbol{x}_k) = \frac{1}{r_k^{(l)}} \sum_{d_k^{\prime(c,l)} \in \{0\} \cup \mathcal{M}_k^{(c)}} p\big(d_k^{\prime(c,l)}\big)\, r_k^{(l,d_k^{\prime(c,l)})} f^{(l,d_k^{\prime(c,l)})}(\boldsymbol{x}_k), \tag{5.120}$$

and for $l \in \mathbb{L}_k^{(c)\mathrm{tr}}$ by

$$r_k^{(l)} = p\big(d_k^{\prime(c,l)} = 1\big)\, r_k^{(l,d_k^{\prime(c,l)}=1)}, \tag{5.121}$$

$$f^{(l)}(\boldsymbol{x}_k) = f^{(l,d_k^{\prime(c,l)}=1)}(\boldsymbol{x}_k). \tag{5.122}$$

(To obtain (5.121) and (5.122), we used the fact that $r_k^{(l,a_k^{(c,l)}=0)} = 0$ for $l \in \mathbb{L}_k^{(c)\mathrm{tr}}$, as mentioned in Section 5.4.3.) Note that (5.119)–(5.122) are the update equations for the labeled objects; more specifically, (5.119) and (5.120) are the update equations for the legacy Bernoulli components and (5.121) and (5.122) are the update equations for the transferred Bernoulli components. Analogously to Section 4.1, it can furthermore be shown that our LMB approximation of the LMBM PGFLs—which is based on interpreting the weights $w_{\boldsymbol{d}_k^{\prime(c)}}$ as the joint association PMF $p\big(\boldsymbol{d}_k^{\prime(c)}\big)$ and approximating that PMF by the product of its marginals—is fully equivalent to the LMB approximation of the LMBM PGFLs that is obtained by matching the PHD of an LMB PGFL to that of the corresponding LMBM PGFL.

Let $\mathbb{L}_k^{(c)\mathrm{leg}} \subseteq \mathbb{L}_{k-1}^{(c)}$ collect the labels $l \in \mathbb{L}_{k-1}^{(c)}$ of those legacy Bernoulli components that are "likely" in the sense that their existence probability $r_k^{(l)}$ in (5.119) satisfies $r_k^{(l)} \geq \gamma_{\mathrm{leg}}$, where γ_{leg} is another positive threshold. The total label set of all "likely" legacy Bernoulli components and transferred Bernoulli components is then given by (see Figure 5.1)

$$\mathbb{L}_k^{*} = \Big(\bigcup_{c \in \mathcal{C}} \mathbb{L}_k^{(c)\mathrm{leg}} \cup \mathbb{L}_k^{(c)\mathrm{tr}}\Big) \cup \mathbb{L}_k^{\mathrm{res,tr}}, \tag{5.123}$$

where $\mathbb{L}_k^{\mathrm{res,tr}}$ was introduced in Section 5.4.4. The LMB pgfl corresponding to $\mathbb{L}_k^{*}$ is now given by

$$G_{\tilde{\mathsf{X}}_k}^{*}[\tilde{h}] \triangleq \prod_{l \in \mathbb{L}_k^{*}} G^{\mathrm{Ber}}\big[\tilde{h}; r_k^{(l)}, f_k^{(l)}\big] \tag{5.124}$$

(see Figure 5.3), which equals the product of the LMB pgfl $G_{\mathbb{L}_k^{\mathrm{res,tr}}}^{\mathrm{LMB}}[\tilde{h}]$ involved in (5.112) and the C LMB pgfls obtained by restricting the LMB pgfls in (5.118) to the label sets $\mathbb{L}_k^{(c)\mathrm{leg}}$, for all $c \in \mathcal{C}$. This is our final approximation of the labeled object part, i.e., of the PGFL $G'_{\tilde{\mathsf{X}}_k}[\tilde{h}]$ in (5.112). That is, we have

$$G'_{\tilde{\mathsf{X}}_k}[\tilde{h}] \approx G^*_{\tilde{\mathsf{X}}_k}[\tilde{h}].$$

The "unlikely" legacy Bernoulli components correspond to the labels $l \in \mathbb{L}_{k-1}^{(c)}$ with $r_k^{(l)} < \gamma_{\mathrm{leg}}$, or equivalently to $l \in \mathbb{L}_k^{(c)\mathrm{unl}} \triangleq \mathbb{L}_{k-1}^{(c)} \setminus \mathbb{L}_k^{(c)\mathrm{leg}}$. Instead of discarding them, as is done, e.g., in the LMB filter [Reuter et al., 2014], we transfer them to the unlabeled RFS part. As a consequence, these unlikely objects are still being tracked but with a smaller computational cost. A higher threshold γ_{leg} tends to imply that fewer Bernoulli components remain in the labeled RFS part and more are transferred to the unlabeled RFS part. We note that the Bernoulli components transferred to the unlabeled RFS part comprise only *legacy* Bernoulli components and do not include Bernoulli components that were previously transferred from the unlabeled RFS part to the labeled RFS part. This is due to the fact that the corresponding label sets $\mathbb{L}_{k-1}^{(c)}$ and $\mathbb{L}_k^{(c)\mathrm{tr}}$ are disjoint (cf. (5.105)) and, thus, Bernoulli components that were transferred from the unlabeled RFS part to the labeled RFS part are not transferred back in the current time step.

5.5.2 Unlabeled Objects

We proceed by representing unlabeled and currently labeled objects that are unlikely to exist by a Poisson RFS. Compared to our previous use of an LMB RFS to represent objects that are likely to exist, using a Poisson RFS reduces the computational complexity at the expense of a decreased tracking accuracy and the loss of track continuity for the respective objects.

According to our discussion above, the labeled PGFL comprising all the unlikely legacy Bernoulli components is (cf. Figure 5.3)

$$G^{\mathrm{LMB}}_{\mathbb{L}_k^{\mathrm{unl}}}[\tilde{h}] \triangleq \prod_{l \in \mathbb{L}_k^{\mathrm{unl}}} G^{\mathrm{Ber}}[\tilde{h}; r_k^{(l)}, f_k^{(l)}], \tag{5.125}$$

with (see Figure 5.1)

$$\mathbb{L}_k^{\mathrm{unl}} \triangleq \bigcup_{c \in \mathcal{C}} \mathbb{L}_k^{(c)\mathrm{unl}}. \tag{5.126}$$

We now combine the labeled (LMB) PGFL $G^{\mathrm{LMB}}_{\mathbb{L}_k^{\mathrm{unl}}}[\tilde{h}]$ with the unlabeled PGFL $G'_{\mathsf{X}_k}[h]$ in (5.113) by defining

$$G^{\mathrm{unl}}_{\tilde{\mathsf{X}}_k,\mathsf{X}_k}[\tilde{h}, h] \triangleq G^{\mathrm{LMB}}_{\mathbb{L}_k^{\mathrm{unl}}}[\tilde{h}]\, G'_{\mathsf{X}_k}[h]. \tag{5.127}$$

We recall that $G'_{\mathsf{X}_k}[h]$ is the product of an MB PGFL and a Poisson PGFL (cf. (5.113)), and it represents unlabeled objects that are unlikely to exist. Thus, the LMB–MB–Poisson PGFL $G^{\mathrm{unl}}_{\tilde{\mathsf{X}}_k,\mathsf{X}_k}[\tilde{h}, h]$ represents both the labeled and unlabeled objects that are unlikely to exist.

In order to further reduce the complexity of the update step, we next approximate $G^{\text{unl}}_{\tilde{\mathsf{X}}_k,\mathsf{X}_k}[\tilde{h},h]$ by a Poisson PGFL, i.e. (cf. Figure 5.3)

$$G^{\text{unl}}_{\tilde{\mathsf{X}}_k,\mathsf{X}_k}[\tilde{h},h] \approx G^{*}_{\mathsf{X}_k}[h] \triangleq e^{\lambda^*_k[h-1]}, \tag{5.128}$$

To find the PHD $\lambda^*(\boldsymbol{x}_k)$, we first "unlabel" the LMB PGFL of (5.125). This results in the MB PGFL $G^{\text{MB}}_{\mathbb{L}^{\text{unl}}_k}[h] \triangleq \prod_{l\in\mathbb{L}^{\text{unl}}_k} G^{\text{Ber}}\big[h; r^{(l)}_k, f^{(l)}_k\big]$, wherein $l \in \mathbb{L}^{\text{unl}}_k$ is used solely to index the Bernoulli components, and not as the label of a labeled state $(\mathbf{x}_k, l)$ in an LMB RFS. Through this unlabeling, the mixed labeled/unlabeled PGFL $G^{\text{unl}}_{\tilde{\mathsf{X}}_k,\mathsf{X}_k}[\tilde{h},h]$ in (5.127) is converted into the unlabeled (MB–Poisson) PGFL

$$G^{\text{unl}}_{\mathsf{X}_k}[h] \triangleq G^{\text{MB}}_{\mathbb{L}^{\text{unl}}_k}[h]\, G'_{\mathsf{X}_k}[h].$$

The PHD $\lambda^*(\boldsymbol{x}_k)$ is now chosen as the PHD corresponding to $G^{\text{unl}}_{\mathsf{X}_k}[h]$. That is, invoking (2.9), we set $\lambda^*(\boldsymbol{x}_k) = \delta G^{\text{unl}}_{\mathsf{X}_k}[h]/\delta \boldsymbol{x}_k\big|_{h=1}$. Using (5.113), (5.91), and (5.92), this can be shown to yield

$$\lambda^*(\boldsymbol{x}_k) = \sum_{l\in\mathbb{L}^{\text{unl}}_k} r^{(l)}_k f^{(l)}(\boldsymbol{x}_k) + \sum_{m\in\mathcal{M}'_k} \bar{r}^{(m)}_k \bar{f}^{(m)}(\boldsymbol{x}_k) + \big(1 - p_{\text{D}}(\boldsymbol{x}_k)\big)\lambda_{k|k-1}(\boldsymbol{x}_k), \tag{5.129}$$

where $r^{(l)}_k$ and $f^{(l)}(\boldsymbol{x}_k)$ are given by (5.119) and (5.120), respectively, $\bar{r}^{(m)}_k$ and $\bar{f}^{(m)}(\boldsymbol{x}_k)$ are given by (5.81) and (5.82), respectively, and $\lambda_{k|k-1}(\boldsymbol{x}_k)$ is given by (5.37). The first term in (5.129), $\sum_{l\in\mathbb{L}^{\text{unl}}_k} r^{(l)}_k f^{(l)}(\boldsymbol{x}_k)$, corresponds to originally labeled objects that are unlikely ot exist—either because the objects already disappeared or because no measurement was associated with them for some time. The second term, $\sum_{m\in\mathcal{M}'_k} \bar{r}^{(m)}_k \bar{f}^{(m)}(\boldsymbol{x}_k)$, corresponds to measurements that are not likely to originate from any labeled objects. The third term, $\big(1 - p_{\text{D}}(\boldsymbol{x}_k)\big)\lambda_{k|k-1}(\boldsymbol{x}_k)$, corresponds to unlabeled objects that are undetected. The Poisson PGFL $G^{*}_{\mathsf{X}_k}[h]$ defined in (5.128) is our final approximation of the unlabeled object part.

5.6 The Proposed LMB/P Filter

The core of the proposed LMB/P filter algorithm is the approximate update step developed in Section 5.4 and Section 5.5, which transforms the predicted posterior PGFL $G_{\tilde{\mathsf{X}}_k,\mathsf{X}_k}[\tilde{h},h|Z_{1:k-1}] = G_{\tilde{\mathsf{X}}_k}[\tilde{h}]G_{\mathsf{X}_k}[h]$ in (5.29) into the following approximation of the new posterior PGFL $G_{\tilde{\mathsf{X}}_k,\mathsf{X}_k}[\tilde{h},h|Z_{1:k}]$ in (5.39):

$$G_{\tilde{\mathsf{X}}_k,\mathsf{X}_k}[\tilde{h},h|Z_{1:k}] \approx G^{*}_{\tilde{\mathsf{X}}_k}[\tilde{h}]\, G^{*}_{\mathsf{X}_k}[h].$$

This is the product of the LMB PGFL $G^{*}_{\tilde{\mathsf{X}}_k}[\tilde{h}]$, which is given by (5.124), (5.109) and (5.119)–(5.122), and the Poisson PGFL $G^{*}_{\mathsf{X}_k}[h]$, which is given by (5.128) and (5.129). The update relations are (5.119)–(5.122) for the LMB parameters (existence probabilities and spatial PDFs) and (5.129) for the Poisson parameter (PHD). Note that in the approximate update step, implausible object-measurement associations are pruned. Furthermore, a part of the unlabeled RFS is transferred to the labeled RFS and a part of the labeled RFS is transferred to the unlabeled RFS. These transfers are controlled by the thresholds γ_{C}, γ_{tr}, and γ_{leg}.

The proposed LMB/P filter algorithm is finally obtained by cascading the prediction step (Section 5.2) and the approximate update step (Sections 5.4 and 5.5), and by adding a detection-estimation step. Since the unlabeled RFS part represents objects that are unlikely to exist, object detection and state estimation are based solely on the labeled RFS part. An object with label $l \in \mathbb{L}_k^*$ is detected—i.e., declared to exist—if its existence probability $r_k^{(l)}$ is larger than a positive detection threshold γ_{D}; the label l is then included in the set $\mathbb{L}_k^{\mathrm{D}} \subseteq \mathbb{L}_k^*$. Subsequently, for each detected object $l \in \mathbb{L}_k^{\mathrm{D}}$, an MMSE state estimate is calculated according to

$$\hat{\boldsymbol{x}}_k^{(l)} = \int \boldsymbol{x}_k f^{(l)}(\boldsymbol{x}_k) \mathrm{d}\boldsymbol{x}_k . \tag{5.130}$$

Table 5.1 summarizes the proposed LMB/P filter algorithm.

5.7 Numerical Study

In the following, we analyze the performance of the proposed LMB/P filter by means of simulation experiments. More precisely, in Section 5.7.1, we describe the underlying simulation scenario, and, in Section 5.7.2, we present the obtained tracking results of the LMB/P filter compared to those obtained by several state-of-the-art RFS-based tracking filters.

5.7.1 Simulation Setup

We evaluate the performance of the proposed LMB/P filter in two two-dimensional (2D) tracking scenarios, termed TS1 and TS2. In TS1, ten objects appear at randomly chosen positions in the region of interest (ROI) before time $k=40$ and disappear after $k=150$. In TS2, 20 objects appear before $k=100$ and disappear after $k=140$; they conform to the object generation scheme of [Meyer et al., 2017], according to which all objects move toward the point $(0,0)$ and simultaneously come in close proximity around that point at $k=120$. The object states consist of 2D position and velocity, i.e, $\mathbf{x}_k = [\mathrm{x}_{1,k}\ \mathrm{x}_{2,k}\ \dot{\mathrm{x}}_{1,k}\ \dot{\mathrm{x}}_{2,k}]^{\mathrm{T}}$. They evolve according to the nearly constant velocity motion model, i.e., $\mathbf{x}_k = \mathbf{A}\mathbf{x}_{k-1} + \mathbf{W}\mathbf{u}_k$, where $\mathbf{A} \in \mathbb{R}^{4\times 4}$ and $\mathbf{W} \in \mathbb{R}^{4\times 2}$ are chosen as in [Bar-Shalom et al., 2002, Sec. 6.3.2] and $\mathbf{u}_k$ is an iid sequence of 2D zero-mean Gaussian random vectors with independent components and component variance $\sigma_u^2 = 10^{-4}$. The sensor is located at position $\boldsymbol{p} =$

Table 5.1: Proposed LMB/P filter algorithm—recursion at time $k \geq 1$

Input: Previous existence probabilities $r^{(l)}$ and previous spatial PDFs $f^{(l)}(\boldsymbol{x}_{k-1})$ for $l \in \mathbb{L}^*_{k-1}$; previous PHD $\lambda(\boldsymbol{x}_{k-1})$ (in practice, this is replaced by the previously calculated approximation $\lambda^*(\boldsymbol{x}_{k-1})$); measurements $\boldsymbol{z}_k^{(m)}$ for $m \in \mathcal{M}_k$.

Output: Existence probabilities $r_k^{(l)}$ and spatial PDFs $f^{(l)}(\boldsymbol{x}_k)$ for $l \in \mathbb{L}^*_k$; approximate PHD $\lambda^*(\boldsymbol{x}_k)$; object state estimates $\hat{\boldsymbol{x}}_k^{(l)}$ for $l \in \mathbb{L}^{\mathrm{D}}_k$.

Operations:

Step 1 – Prediction:

1.1) For $l \in \mathbb{L}^*_{k-1}$, calculate the predicted existence probabilities $r_{k|k-1}^{(l)}$ and the predicted spatial PDFs $f_{k|k-1}^{(l)}(\boldsymbol{x}_k)$ according to (5.32) and (5.33), respectively.

1.2) Calculate the predicted posterior PHD $\lambda_{k|k-1}(\boldsymbol{x}_k)$ according to (5.37).

Step 2 – Preparations for Update:

2.1) For $l \in \mathbb{L}^*_{k-1}$, calculate the association weights $\beta_k^{(l,m)}$, existence probabilities $r_k^{(l,m)}$, and spatial PDFs $f^{(l,m)}(\boldsymbol{x}_k)$ according to (5.74)–(5.76) (for $m \in \mathcal{M}_k$) and (5.77)–(5.79) (for $m = 0$).

2.2) For $m \in \mathcal{M}_k$, calculate $\beta_k^{(m)}$, $\bar{r}_k^{(m)}$, and $\bar{f}_k^{(m)}(\boldsymbol{x}_k)$ according to (5.80)–(5.82).

2.3) Partition the label set $\mathbb{L}^*_{k-1}$ and the measurement index set $\mathcal{M}_k$ as described in Section 5.4.1. This yields $\mathbb{L}^{(c)}_{k-1}$ and $\mathcal{M}_k^{(c)}$ for $c \in \mathcal{C}$ as well as $\mathcal{M}_k^{\mathbf{res}}$.

2.4) Determine $\mathbb{L}_k^{(c)\mathbf{tr}}$ for $c \in \mathcal{C}$ as described in Section 5.4.3, and $\mathbb{L}_k^{\mathbf{res,tr}}$ (corresponding to $\mathcal{M}_k^{\mathbf{res,tr}}$) and $\mathcal{M}'_k$ as described in Section 5.4.4.

Step 3 – Update for Labeled Objects:

3.1) For $c \in \mathcal{C}$, calculate the weights $w_{\boldsymbol{d}_k'^{(c)}}$ according to (5.106) and the joint association pmf $p(\boldsymbol{d}_k'^{(c)})$ according to (5.114).

3.2) For $c \in \mathcal{C}$ and $l \in \mathbb{L}_k^{(c)\mathbf{tot}} = \mathbb{L}^{(c)}_{k-1} \cup \mathbb{L}_k^{(c)\mathbf{tr}}$, calculate the marginal association PMF $p(d_k'^{(c,l)})$ according to (5.117). (An efficient BP algorithm for computing $p(d_k'^{(c,l)})$ is presented in [Williams, 2015].)

3.3) For $c \in \mathcal{C}$, calculate the updated existence probabilities $r_k^{(l)}$ and spatial PDFs $f^{(l)}(\boldsymbol{x}_k)$ according to (5.119) and (5.120) (for $l \in \mathbb{L}^{(c)}_{k-1}$) and (5.121) and (5.122) (for $l \in \mathbb{L}_k^{(c)\mathbf{tr}}$).

3.4) For $c \in \mathcal{C}$, determine $\mathbb{L}_k^{(c)\mathbf{leg}}$ and $\mathbb{L}_k^{(c)\mathbf{unl}}$ as described in Section 5.5.1 and Section 5.5.2, respectively.

3.5) Determine $\mathbb{L}^*_k$ according to (5.123) and $\mathbb{L}_k^{\mathbf{unl}}$ according to (5.126).

Step 4 – Update for Unlabeled Objects: Calculate the approximate updated posterior PHD $\lambda^*(\boldsymbol{x}_k)$ according to (5.129).

Step 5 – Object Detection and State Estimation:

5.1) Determine $\mathbb{L}^{\mathrm{D}}_k$ as described in Section 5.

5.2) For $l \in \mathbb{L}^{\mathrm{D}}_k$, calculate an object state estimate $\hat{\boldsymbol{x}}_k^{(l)}$ according to (5.130).

Initialization at time $k = 0$: $\mathbb{L}^*_0 = \emptyset$, $\lambda_0(\boldsymbol{x}_0)$.

$[p_1\ p_2]^{\mathrm{T}} = [0\ \ {-50}]^{\mathrm{T}}$ and has a measurement range of 300. The ROI is equal to the disk determined by the sensor's measurement range.

The object-originated measurements conform to the nonlinear range-bearing model $\mathbf{z}_k = \big[\rho(\mathbf{x}_k)\ \ \theta(\mathbf{x}_k)\big]^{\mathrm{T}} + \mathbf{v}_k$. Here, $\rho(\mathbf{x}_k) \triangleq \|\mathbf{x}'_k - \boldsymbol{p}\|$, where $\mathbf{x}'_k \triangleq [\mathrm{x}_{1,k}\ \mathrm{x}_{2,k}]^{\mathrm{T}}$ is the object position, and $\theta(\mathbf{x}_k) \triangleq \tan^{-1}\big(\frac{\mathrm{x}_{2,k}-p_2}{\mathrm{x}_{1,k}-p_1}\big)$. Furthermore, $\mathbf{v}_k$ is 2D white Gaussian measurement noise with independent components and component standard deviations $\sigma_\rho = 2$ and $\sigma_\theta = 1^\circ$. The detection probability of the sensor is modeled as $p_{\mathrm{D}}(\boldsymbol{x}_k) = p_{\mathrm{D,max}} \exp(-\|\boldsymbol{x}'_k\|^2/450^2)$ [Reuter et al., 2014] with $p_{\mathrm{D,max}} = 0.7$ for TS1 and $p_{\mathrm{D,max}} = 0.5$ for TS2. Thus, the detection probability has its maximum of 0.7 for TS1 and 0.5 for TS2 at the ROI center and decreases towards the ROI border, where it is 0.45 for TS1 and 0.32 for TS2. The clutter PDF $f_{\mathrm{C}}(\boldsymbol{z}_k)$ is uniform (in polar coordinates) on the ROI with mean parameter $\mu_{\mathrm{C}} = 100$ for TS1 and $\mu_{\mathrm{C}} = 150$ for TS2. Note that TS2 is similar to the simulation scenario analyzed in Section 4.4 with the main exceptions of a state-dependent detection probability and a higher clutter rate (100 and 150 compared to 10 and 50). This makes TS2 even more challenging than the scenario in Section 4.4.

We compare the performance of particle implementations of the proposed LMB/P filter, the LMB filter [Reuter et al., 2017], the fast LMB filter proposed in Chapter 4, and a version of the TOMB/P filter [Williams, 2015, Kropfreiter et al., 2016] that performs recycling of Bernoulli components as proposed in [Williams, 2012]. We remark that our performance comparison does not consider algorithms with a significantly higher complexity, such as the GLMB filter [Vo and Vo, 2013, Vo et al., 2014] or the trajectory-based filters proposed in [García-Fernández et al., 2020b, Granström et al., 2018, Xia et al., 2019, García-Fernández and Svensson, 2019]. Note also that the latter filters use Gaussian representations of spatial distributions and thus presuppose a linear-Gaussian system model, which is incompatible with our nonlinear measurement model. Our performance comparison uses 1000 Monte Carlo runs for each experiment. The object trajectories for both TS1 and TS2 are randomly generated for each run according to the state-transition model described above.

The proposed LMB/P filter and the TOMB/P filter use the belief propagation (BP) algorithm of [Williams, 2015] to calculate approximations of the marginal association probabilities (cf. Eq. (5.117) and Steps 3.1 and 3.2 in Table 5.1), and the fast LMB filter of Chapter 4 uses the BP algorithm described in Section 4.2. We will therefore refer to these filters as BP-LMB/P, BP-TOMB/P, and BP-LMB, respectively. The LMB filter of [Reuter et al., 2017] is based on the Gibbs sampler and will be referred to as Gibbs-LMB. BP-LMB/P and BP-TOMB/P use 5000 particles to represent, respectively, the posterior PHD of unlabeled objects and the posterior PHD of undetected objects. Another 5000 particles are used by BP-LMB/P and BP-TOMB/P to represent newborn unlabeled objects and newborn undetected objects, respectively, but the resulting 10000 particles are reduced to 5000 particles after the update step. All filters represent the spatial PDF of each Bernoulli component by 1000 particles. BP-LMB/P, BP-LMB, and

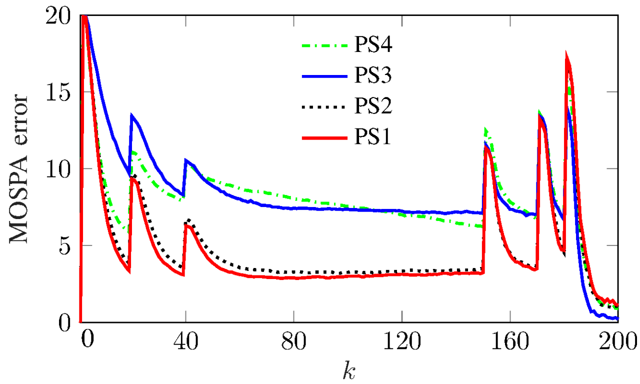

Figure 5.4: MOSPA error of BP-LMB/P versus time for TS1 using parameter settings PS1 through PS4 (defined in the text).

BP-TOMB/P use 20 BP iterations to calculate the approximate marginal probabilities. The Gibbs sampler in Gibbs-LMB uses 100 samples for TS1 and 1000 samples for TS2. All filters declare an object as detected if the existence probability of the corresponding Bernoulli component exceeds $\gamma_{\mathrm{D}} = 0.5$, and when this is the case, they calculate a sample mean approximation of (5.130) from the particle representation of the corresponding spatial PDF.

The birth statistics of all filters are established using the previous measurements $\boldsymbol{z}_{k-1}^{(m)}$, $m \in \mathcal{M}_{k-1}$. More precisely, BP-LMB/P and BP-TOMB/P choose their birth PDF as a mixture of the PDFs

$$\tilde{f}_{\mathrm{B}}^{(m)}(\boldsymbol{x}_k) \propto \int f(\boldsymbol{x}_k|\boldsymbol{x}_{k-1})\, f\big(\boldsymbol{z}_{k-1}^{(m)}|\boldsymbol{x}_{1,k-1}, \boldsymbol{x}_{2,k-1}\big)\, f_{\mathrm{v}}(\dot{x}_{1,k-1}\ \dot{x}_{2,k-1})\, \mathrm{d}\boldsymbol{x}_{k-1}\,,$$

for $m \in \mathcal{M}_{k-1}$. Gibbs-LMB creates a new Bernoulli component for each measurement $\boldsymbol{z}_{k-1}^{(m)}$, $m \in \mathcal{M}_{k-1}$, with spatial PDF $f_{\mathrm{B}}^{(l=(k,m))}(\boldsymbol{x}_k) = \tilde{f}_{\mathrm{B}}^{(m)}(\boldsymbol{x}_k)$ and BP-LMB uses the Bernoulli generation scheme proposed in Section 4.3 with the spatial PDFs $f_{\mathrm{B}}^{(l=(k,m))}(\boldsymbol{x}_k)$ in (4.40) being equal to $\tilde{f}_{\mathrm{B}}^{(m)}(\boldsymbol{x}_k)$. The mean number of newborn objects is $\mu_{\mathrm{B}} = 0.1$ for all filters. In BP-LMB/P and BP-TOMB/P, the mean number of, respectively, unlabeled objects and undetected objects is initialized as 0.01.

5.7.2 Simulation Results

In Figure 5.4, we study the performance of BP-LMB/P for TS1, using four different choices of the thresholds γ_{tr}, γ_{C}, and γ_{leg}. The figure displays the Euclidean distance based mean optimal subpattern assignment (MOSPA) metric with cutoff parameter $c = 20$ and order $p = 2$ [Schuhmacher et al., 2008] versus time k. Each curve shows a specific threshold parameter setting (PS) and was obtained by averaging over 1000 Monte Carlo runs. The PSs are defined by the values of γ_{tr}, γ_{C}, and γ_{leg} specified in Table 5.2; in particular, PS2 uses a higher value of γ_{leg}, PS3 a higher value of γ_{C}, and PS4 a higher value of γ_{tr}.

	γ_{tr}	γ_{C}	γ_{leg}
PS1	10^{-2}	10^{-10}	10^{-2}
PS2	10^{-2}	10^{-10}	10^{-1}
PS3	10^{-2}	10^{-3}	10^{-2}
PS4	10^{-1}	10^{-10}	10^{-2}

Table 5.2: Threshold parameter settings (PSs) used for TS1.

	γ_{tr}	γ_{C}	γ_{leg}	γ_{P}	γ_{T}
TS1	10^{-2}	10^{-10}	10^{-2}	10^{-3}	10^{-3}
TS2	10^{-3}	10^{-10}	10^{-3}	10^{-4}	10^{-4}

Table 5.3: Thresholds γ_{tr}, γ_{C}, and γ_{leg} used by BP-LMB/P, γ_{P} used by BP-LMB and Gibbs-LMB, and γ_{T} used by BP-TOMB/P.

One can see in Figure 5.4 that the lowest MOSPA curve is achieved for PS1, i.e., for the lowest threshold values. However, a further reduction of the thresholds would not decrease the MOSPA curves further but would result in a higher filter runtime. If γ_{leg} is increased (as in PS2), then according to Section 5.5.1, there tend to be more Bernoulli components l such that $r_k^{(l)}$ falls below γ_{leg}, and which are hence transferred from the LMB part to the Poisson part. In challenging scenarios, such as low $p_{\text{D}}(\boldsymbol{x}_k)$ and/or high clutter, it can then happen that Bernoulli components are transferred to the Poisson part even though the corresponding objects exist, and this will generally reduce the tracking performance. If γ_{C} is increased (as in PS3), then according to Section 5.4.1, this generally results in a larger number of subsets $\mathbb{L}_{k-1}^{(c)}$, which may imply that some labeled objects are no longer correctly associated with the measurements and thus the tracking performance is again reduced. Finally, if γ_{tr} is increased (as in PS4), then according to Sections 5.4.3 and 5.4.4, fewer Bernoulli components are transferred to the labeled RFS part, which may again result in a poorer tracking performance.

Therefore, for TS1, we will hereafter use the thresholds of PS1. These thresholds are shown again in Table 5.3, along with the thresholds used in TS2. In fact, for the more challenging TS2, we observed that the thresholds in Table 5.3 resulted in a better MOSPA performance; in particular, we use smaller values of γ_{tr} and γ_{leg}. Table 5.3 furthermore shows the threshold γ_{P} used by BP-LMB and Gibbs-LMB for pruning Bernoulli components and the threshold γ_{T} used by BP-TOMB/P for transferring Bernoulli components of the multi-Bernoulli part of the posterior state RFS to the Poisson part.

Figure 5.5 shows an example of the estimated object trajectories obtained with BP-LMB/P for TS1 and for TS2, along with the true trajectories. One can see that the estimated trajectories closely match the true trajectories in both scenarios.

Figure 5.6 compares the MOSPA performance of BP-LMB/P, Gibbs-LMB, BP-LMB, and BP-TOMB/P for TS1 and TS2. It is seen that for TS1, the performance of BP-LMB/P is almost identical to that of BP-LMB and BP-TOMB/P whereas the perfor-

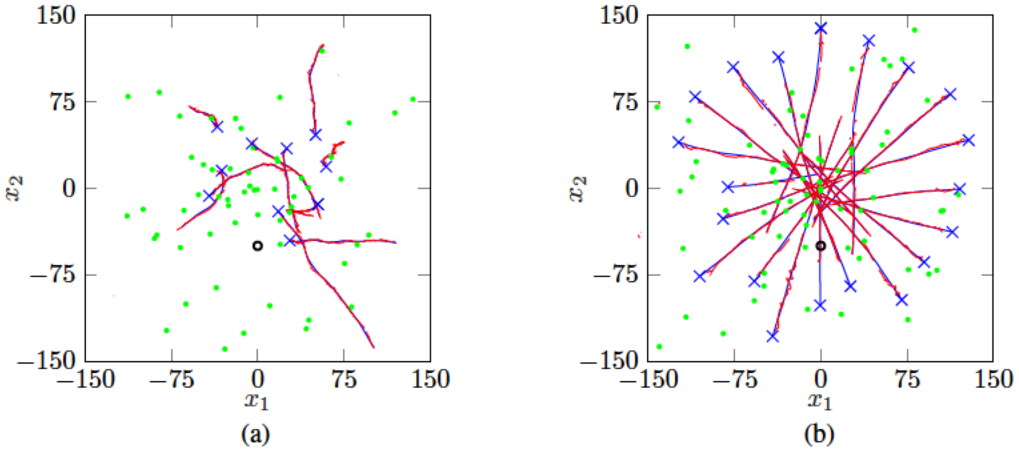

Figure 5.5: Example of the true object trajectories (represented by blue lines, starting positions indicated by blue crosses) for (a) TS1 and (b) TS2, as well as the corresponding estimates obtained with the proposed BP-LMB/P filter (represented by red lines). The position of the sensor is indicated by a black circle. The green circles show the measurements of the sensor at time $k = 100$ within the region $[-150, 150] \times [-150, 150]$.

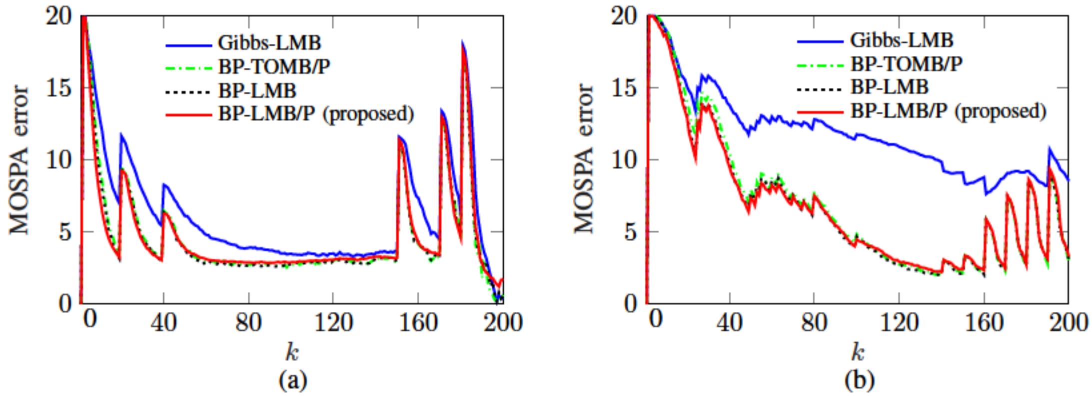

Figure 5.6: MOSPA error of the four filters versus time k for (a) TS1 and (b) TS2.

mance of Gibbs-LMB is noticeably poorer. For TS2, the results are similar except that the performance gap of Gibbs-LMB is much larger. This performance gap is due to the fact that Gibbs-LMB ignores relevant association information (cf. Section 4.4.3). The amount of relevant association information taken into account by Gibbs-LMB grows with the number of samples used in the Gibbs sampler, but this comes at the cost of a higher computational complexity. In challenging scenarios such as TS2, more association information is required to obtain good results; this explains the larger performance gap of Gibbs-LMB in that case (even though for TS2, our Gibbs-LMB implementation used ten times more samples than for TS1). Overall, these results also demonstrate the excellent performance of the BP algorithm used by BP-LMB/P, BP-LMB, and BP-TOMB/P to compute the marginal association probabilities.

In Figure 5.7, we compare BP-LMB/P, Gibbs-LMB, BP-LMB, and BP-TOMB/P for TS2, using instead of the MOSPA metric the trajectory metric proposed in [García-

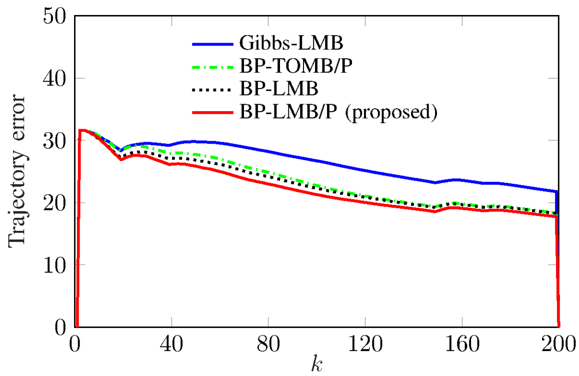

Figure 5.7: Trajectory error of the four filters versus k for TS2.

Fernández et al., 2020a] with cutoff parameter $c=20$, order $p=2$, and switching penalty $\gamma=2$. This metric can be decomposed into a "location error" (the location error of detected objects), a "false error" (caused by "false objects"), a "missed error" (caused by "missed objects"), and a "switching error." Here, false objects are detected objects that do not correspond to any object within the ground truth, whereas missed objects are objects within the ground truth that do not correspond to any detected object. Differently from the OSPA metric, the trajectory metric also takes into account the switching error caused by track switches, i.e., when a detected object is associated with different objects within the ground truth at different times. According to Figure 5.7, the trajectory metric performance of BP-LMB/P is slightly better than that of BP-LMB and BP-TOMB/P and significantly better than that of Gibbs-LMB. These results agree with our MOSPA results in Figure 5.6 (note the different y-axis scales used in the two figures). In addition, they show that BP-LMB/P also succeeds in estimating object trajectories, not just individual object states.

The four error components of the trajectory metric for TS2—i.e., location error, false error, missed error, and switching error—are shown individually in Figure 5.8. Whereas for each error component the results of BP-TOMB/P, BP-LMB, and BP-LMB/P are quite similar, those of Gibbs-LMB are partly very different. This can be explained by the fact that Gibbs-LMB ignores valuable association information and thus detects some of the objects only with a delay or not at all. As a consequence, the number of missed objects is rather large, which leads to a significantly higher missed error (Figure 5.8(c)). Furthermore, the smaller number of detected objects (compared to the other three filters) in turn implies a smaller number of false objects (Figure 5.8(b)) and also lower location and switching errors (Figures 5.8(a) and 5.8(d)).

It can also be seen that for all filters, the missed error shown in Figure 5.8(c) is much larger than the other error components (note the widely different y-axis scale used in Figure 5.8(c) compared to the other parts of Figure 5.8). Thus, the missed error dominates the overall trajectory metric, which explains why Figure 5.8(c) is similar to Figure 5.7. Furthermore, the high missed error of Gibbs-LMB (compared to the other

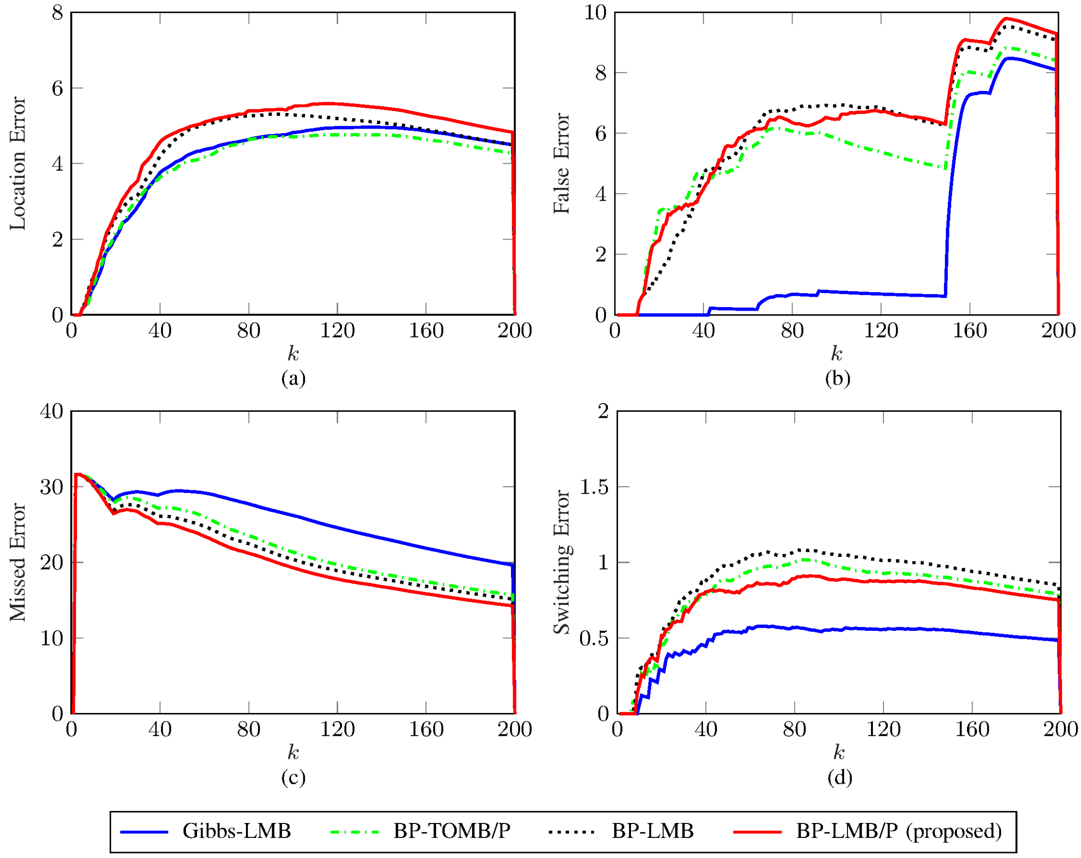

Figure 5.8: Individual components of the trajectory metric of the four filters versus k for TS2: (a) location error, (b) false error, (c) missed error, and (d) switching error.

three filters) is not compensated by the fact that the other error components are lower. The other three filters, i.e., BP-TOMB/P, BP-LMB, and BP-LMB/P, exhibit a similar performance, with BP-LMB/P performing best. The latter fact can be attributed to the proposed transfer scheme between the Poisson part and the LMB part. Indeed, these simulation results suggest that our transfer scheme, with an appropriate choice of the thresholds γ_{tr}, γ_{leg}, and γ_{C}, can result in performance advantages compared to both BP-LMB (using a pruning of Bernoulli components) and BP-TOMB/P (using a recycling of Bernoulli components). These advantages come in addition to the lower filter runtimes obtained with BP-LMB/P, as reported presently.

Table 5.4 lists the average runtime per time (k) step required by MATLAB implementations of the various filters on an Intel quad core i7-6600U CPU. Also shown is the average number of Bernoulli components per time step employed by each filter. Again, these numbers were obtained by averaging over 1000 Monte Carlo runs. One can see that BP-LMB/P achieves the lowest runtimes of all filters; furthermore, it employs the lowest numbers of Bernoulli components of all filters except Gibbs-LMB. We note that, as is demonstrated by Figure 5.6, this low complexity of BP-LMB/P does not come at the

Filter	RT-TS1	RT-TS2	NBC-TS1	NBC-TS2
BP-LMB/P (proposed)	1.33 s	5.05 s	15.21	162.82
Gibbs-LMB	5.12 s	7.94 s	9.69	34.23
BP-LMB	5.55 s	21.68 s	34.15	861.96
BP-TOMB/P	10.66 s	16.09 s	63.33	521.93

Table 5.4: Measured complexity of the four filters for TS1 and TS2. RT-TS1 and RT-TS2 designate the average runtime per time step, and NBC-TS1 and NBC-TS2 designate the average number of Bernoulli components per time step.

cost of a poorer MOSPA performance. Also, while Gibbs-LMB employs fewer Bernoulli components (especially for TS2), its MOSPA performance for TS2 is significantly poorer.

We can conclude from the results in Figures 5.6–5.8 and Table 5.4 that BP-LMB/P offers a superior performance/complexity compromise relative to the other filters. It has a significantly better performance than Gibbs-LMB (especially for TS2) and also a lower runtime. When compared to BP-LMB and BP-TOMB/P, the runtime of BP-LMB/P is much lower while its performance is almost identical. The low runtime of BP-LMB/P is a direct consequence of the fact that objects of highly unlikely existence are modeled by the Poisson RFS. The performance advantage of BP-LMB/P over Gibbs-LMB is mainly due to the fact that BP-LMB/P takes into account more association information. Gibbs-LMB ignores relevant association information, which allows it to employ fewer Bernoulli components but also results in a poorer performance. For challenging scenarios with a high number of (closely spaced) objects and/or a low detection probability and/or strong clutter, the number of samples used by the Gibbs sampler must be increased significantly to obtain an acceptable MOSPA performance, and this entails a higher complexity.

In this chapter, we proposed an efficient RFS-based multi-object tracking algorithm based on the modeling of the multi-object state by an LMB/Poisson tuple. While the presented algorithm achieves an excellent performance/complexity compromise, tracking performance can be improved by the use of multiple sensors. In the next chapter, we present a new efficient yet high-performing RFS-based distributed multi-sensor multi-object tracking algorithm.

Chapter 6

A Distributed LMB Filter Using Probabilistic Label Association

In this chapter, we propose a distributed multi-sensor LMB filter that is based on the concepts and methodologies of probabilistic label association, generalized covariance intersection (GCI), and belief propagation (BP). Current state-of-the-art distributed LMB filters use hard label associations, which can result in poor tracking performance, especially in more challenging tracking scenarios. By contrast, the proposed distributed LMB filter uses a novel GCI-based fusion method for LMB multi-object PDFs that avoids a hard association of the labeled Bernoulli components of neighboring sensors and instead uses a soft (i.e., probabilistic) association. In our approach, label association probabilities are computed and used in the fusion of the multi-object PDFs.

To develop this probabilistic association scheme, we first derive the fused posterior PDF, which is no longer of LMB form but of GLMB form and involves an inherent label association PMF. We then show that approximating this label association PMF by the product of its marginals leads to a fused posterior PDF that is again of LMB type. Next, inspired by [Williams and Lau, 2014] and the BP algorithm used in our fast LMB filter in Section 4.2, we propose a BP algorithm for fast approximate marginalization of the label association PMF. Moreover, to reduce both the communication requirements and the computational complexity of the distributed LMB filter, we develop a practical implementation of the fusion relations in which the local spatial PDFs are approximated by Gaussian PDFs. Our simulation results demonstrate that the proposed distributed LMB filter using soft label associations significantly outperforms a state-of-the-art LMB filter using hard label associations [Li et al., 2019] and can perform close to the centralized multi-sensor LMB filter based on the iterated-corrector approach [Reuter et al., 2014, Mahler, 2014].

The remainder of this chapter is organized as follows. Section 6.1 presents the basic framework of pairwise (two-sensor) LMB fusion with hard label association. Section 6.2 develops a novel formulation of pairwise fusion using probabilistic label association. Section 6.3 presents a fast approximate algorithm for probabilistic label association based on BP and proposes an efficient Gaussian implementation. Section 6.4 extends the pairwise fusion algorithm to distributed networkwide fusion in a decentralized sensor network. Section 6.5 demonstrates the performance of the proposed distributed LMB filter using probabilistic label association.

6.1 Pairwise LMB Fusion with Label Association

For distributed fusion of statistical information in sensor networks, most distributed RFS-based tracking methods use the generalized covariance intersection (GCI) technique [Clark et al., 2010], also known as exponential mixture density [Üney et al., 2013] and Kullback-Leibler average [Battistelli et al., 2015]. GCI is a suboptimal technique that fuses the local posterior PDFs of neighboring sensors. GCI fusion of LMB posterior PDFs is challenging because it is a priori unknown which labeled Bernoulli component of one sensor (representing an object) corresponds to which labeled Bernoulli component of another sensor. Current state-of-the-art distributed LMB filters are based on hard label associations [Fantacci et al., 2018,Li et al., 2019]. More precisely, in [Fantacci et al., 2018], it is assumed that all the local posterior PDFs are defined on the same set of labels, and Bernoulli components with identical labels are matched. However, this assumption is rarely satisfied in practice. In [Li et al., 2019], the labeled Bernoulli components of different sensors are matched by minimizing a "label inconsistency indicator." However, in more challenging scenarios, this can still result in a significant percentage of incorrect matching events and, thus, in a poor tracking performance.

We now start our elaboration of the probabilistic distributed LMB filter by considering "pairwise fusion" for two sensors with sensor index $s \in \{1, 2\}$. The sequences of measurements observed by these sensors up to a current time k will be denoted as $Z_{1:k}^{(1)}$ and $Z_{1:k}^{(2)}$, respectively. Furthermore, each sensor runs a local LMB filter, e.g., the proposed fast LMB filter of Chapter 4, based on its own measurement sequence. Note that the local LMB filters are not restricted to the measurement model of Section 3.2.2 and may rely on other models [Reuter et al., 2014,Beard et al., 2016]. The LMB posterior multi-object PDFs of the two sensors at time k, are denoted as $f(\tilde{X}_k|Z_{1:k}^{(1)})$ and $f(\tilde{X}_k|Z_{1:k}^{(2)})$, and are given according to (3.31) for $s \in \{1, 2\}$ as

$$f(\tilde{X}_k|Z_{1:k}^{(s)}) = \Delta(\tilde{X}_k)\, w^{(s)}\big(\mathcal{L}(\tilde{X}_k)\big) \prod_{(\boldsymbol{x}_k, l) \in \tilde{X}_k} 1_{\mathbb{L}_k^{(s)*}}(l)\, f_s^{(l)}(\boldsymbol{x}_k). \tag{6.1}$$

Recap that $\Delta(\tilde{X}_k) = 1$ if the labels of $\tilde{X}_k$ are distinct and $\Delta(\tilde{X}_k) = 0$ otherwise, and $1_{\mathbb{L}_k^{(s)*}}(l) = 1$ if $l \in \mathbb{L}_k^{(s)*}$ and $1_{\mathbb{L}_k^{(s)*}}(l) = 0$ otherwise. The weights $w^{(s)}(L)$ are given according to (3.32) as

$$w^{(s)}(L) \triangleq \left(\prod_{l\in L} 1_{\mathbb{L}^*}(l)\, r_{k,s}^{(l)}\right) \prod_{l'\in \mathbb{L}_k^{(s)*}\setminus L} \left(1-r_{k,s}^{(l')}\right), \tag{6.2}$$

for any $L \subseteq \mathbb{L}_k^{(s)}$. Here, $\mathbb{L}_k^{(s)*} \subseteq \mathbb{L}_k^{(s)}$ is the label set involved in the local posterior PDF $f(\tilde{X}_k|Z_{1:k}^{(s)})$, which is a subset of the label set $\mathbb{L}_k^{(s)}$. Different to previous sections, we now model the label by the tuple $l=(s,k',m)$, which in addition to the time of object birth k' and the measurement index m also takes into account the sensor index s. Since the label now additionally contains the sensor index s, the underlying label sets $\mathbb{L}_k^{(1)*}$ and $\mathbb{L}_k^{(2)*}$ as well as the overall label sets $\mathbb{L}_k^{(1)}$ and $\mathbb{L}_k^{(2)}$ are trivially different because s in $l=(s,k',m)$ is different for the two sensors. However, $\mathbb{L}_k^{(1)*}$ and $\mathbb{L}_k^{(2)*}$ are usually different even when some other label indexing is used. For example, they are typically different when the local LMB filters employ measurement-driven birth models and/or different strategies for pruning Bernoulli components [Buonviri et al., 2019]. Note that the local LMB posterior PDFs $f(\tilde{X}_k|Z_{1:k}^{(1)})$ and $f(\tilde{X}_k|Z_{1:k}^{(2)})$ are fully characterized by the parameter sets $\left\{\left(r_{k,1}^{(l)}, f_1^{(l)}(\boldsymbol{x}_k)\right)\right\}_{l\in\mathbb{L}_k^{(1)*}}$ and $\left\{\left(r_{k,2}^{(l)}, f_2^{(l)}(\boldsymbol{x}_k)\right)\right\}_{l\in\mathbb{L}_k^{(2)*}}$, respectively.

6.1.1 Pairwise LMB Fusion

Let us now consider "pairwise fusion" for our two sensor case, i.e., fusion of the two LMB posterior PDFs $f(\tilde{X}_k|Z_{1:k}^{(1)})$ and $f(\tilde{X}_k|Z_{1:k}^{(2)})$ into a fused posterior PDF $\tilde{f}(\tilde{X}_k|Z_{1:k}^{(1)}, Z_{1:k}^{(2)})$[1]. The GCI fusion rule is given by [Fantacci et al., 2018] according to

$$\tilde{f}(\tilde{X}_k|Z_{1:k}^{(1)}, Z_{1:k}^{(2)}) = \frac{1}{D_k}\left(f(\tilde{X}_k|Z_{1:k}^{(1)})\right)^{\omega}\left(f(\tilde{X}_k|Z_{1:k}^{(2)})\right)^{1-\omega}, \tag{6.3}$$

with $D_k \triangleq \int \left(f(\tilde{X}_k|Z_{1:k}^{(1)})\right)^{\omega}\left(f(\tilde{X}_k|Z_{1:k}^{(2)})\right)^{1-\omega}\delta\tilde{X}_k$ (here, $\int\cdot\,\delta\tilde{X}_k$ is the set integral defined in (2.21)) and some fixed $\omega\in[0,1]$. It was shown in [Fantacci et al., 2018] that if the label sets are equal, i.e., $\mathbb{L}_k^{(1)*}=\mathbb{L}_k^{(2)*}$, then $\tilde{f}(\tilde{X}_k|Z_{1:k}^{(1)}, Z_{1:k}^{(2)})$ is again an LMB PDF. However, even in that case, it is likely that some objects are described by Bernoulli components with different labels in the local LMB filters at the two sensors, and thus GCI fusion according to (6.3) involves the matching of Bernoulli components describing different objects. More precisely, suppose temporarily that $\mathbb{L}_k^{(1)*} = \mathbb{L}_k^{(2)*} =: \mathbb{L}_k^*$ and consider some label $l\in\mathbb{L}_k^*$. The corresponding spatial PDF $\tilde{f}^{(l)}(\boldsymbol{x}_k)$ belonging to the fused LMB PDF $\tilde{f}(\tilde{X}_k|Z_{1:k}^{(1)}, Z_{1:k}^{(2)})$ is calculated from the spatial PDFs $f_1^{(l)}(\boldsymbol{x}_k)$ and $f_2^{(l)}(\boldsymbol{x}_k)$ belonging to $f(\tilde{X}_k|Z_{1:k}^{(1)})$ and $f(\tilde{X}_k|Z_{1:k}^{(2)})$, respectively, as [Fantacci et al., 2018]

$$\tilde{f}^{(l)}(\boldsymbol{x}_k) = \frac{\left(f_1^{(l)}(\boldsymbol{x}_k)\right)^{\omega}\left(f_2^{(l)}(\boldsymbol{x}_k)\right)^{1-\omega}}{\int_{\mathbb{R}^{N_x}}\left(f_1^{(l)}(\boldsymbol{x}'_k)\right)^{\omega}\left(f_2^{(l)}(\boldsymbol{x}'_k)\right)^{1-\omega}\mathrm{d}\boldsymbol{x}'}.$$

[1] The tilde notation indicates the fact that $\tilde{f}(\tilde{X}_k|Z_{1:k}^{(1)}, Z_{1:k}^{(2)})$ is generally different from the true posterior PDF $f(\tilde{X}_k|Z_{1:k}^{(1)}, Z_{1:k}^{(2)})$.

However, if $f_1^{(l)}(\boldsymbol{x}_k)$ describes a different object than $f_2^{(l)}(\boldsymbol{x}_k)$, then the fused spatial PDF $\tilde{f}^{(l)}(\boldsymbol{x}_k)$ does not describe any single object, and its meaning in the fused LMB PDF $\tilde{f}(\tilde{X}_k|Z_{1:k}^{(1)}, Z_{1:k}^{(2)})$ is unclear. A similar statement can be made about the fused existence probability $\tilde{r}_k^{(l)}$ [Fantacci et al., 2018]. The matching of Bernoulli components describing different objects will generally cause $\tilde{f}(\tilde{X}_k|Z_{1:k}^{(1)}, Z_{1:k}^{(2)})$ to be very different from $f(\tilde{X}_k|Z_{1:k}^{(1)}, Z_{1:k}^{(2)})$, and in turn reduce the performance of the distributed LMB filter.

6.1.2 Label Association

In the following, we consider the practically relevant case where (consistently with our label representation $l=(s,k',m)$) all the elements of $\mathbb{L}_k^{(1)}$ are different from all the elements of $\mathbb{L}_k^{(2)}$, and thus also all the elements of $\mathbb{L}_k^{(1)*}$ are different from all the elements of $\mathbb{L}_k^{(2)*}$. In that case, $\tilde{f}(\tilde{X}_k|Z_{1:k}^{(1)}, Z_{1:k}^{(2)})$ in (6.3) is zero for any given $\tilde{X}_k$, because in the expression (6.1) of $f(\tilde{X}_k|Z_{1:k}^{(1)})$ and $f(\tilde{X}_k|Z_{1:k}^{(2)})$, $1_{\mathbb{L}_k^{(1)*}}(l)$ or $1_{\mathbb{L}_k^{(2)*}}(l)$ or both will be zero for all $l \in \mathcal{L}(\tilde{X}_k)$. Let us, for example, adopt the viewpoint of sensor 1. Let us further consider only realizations $\tilde{X}_k$ with labels $l \in \mathcal{L}(\tilde{X}_k)$, $\mathcal{L}(\tilde{X}_k) \subseteq \mathbb{L}_k^{(1)*}$. Note that other realizations $\tilde{X}_k$ with labels $l \notin \mathbb{L}_k^{(1)*}$ are irrelevant anyway because they imply $f(\tilde{X}_k|Z_{1:k}^{(1)})$. This implies that $1_{\mathbb{L}_k^{(1)*}}(l) = 1$ for all $l \in \mathbb{L}_k^{(1)*}$ and thus $f(\tilde{X}_k|Z_{1:k}^{(1)})$ is not zero for all realizations with labels $\mathcal{L}(\tilde{X}_k) \subseteq \mathbb{L}_k^{(1)*}$. However, $1_{\mathbb{L}_k^{(2)*}}(l) = 0$ for all $l \in \mathcal{L}(\tilde{X}_k)$, so that $f(\tilde{X}_k|Z_{1:k}^{(2)}) = 0$ and thus we still obtain $\tilde{f}(\tilde{X}_k|Z_{1:k}^{(1)}, Z_{1:k}^{(2)}) = 0$.

We can resolve this issue as follows: when evaluating $f(\tilde{X}_k|Z_{1:k}^{(2)})$, we first map the labels $l \in \mathcal{L}(\tilde{X}_k) \subseteq \mathbb{L}_k^{(1)*}$ to some labels $l' \in \mathbb{L}_k^{(2)*}$ so that $1_{\mathbb{L}_k^{(2)*}}(l') = 1$. We can now describe such a label mapping by a label association vector $\boldsymbol{u}_k = \big[u_k^{(l(1))} \cdots u_k^{(l(I))}\big]^{\mathrm{T}}$ of length $I = |\mathbb{L}_k^{(1)*}|$ and with entries $u_k^{(l)} \in \mathbb{L}_k^{(2)*}$ for all $l \in \mathbb{L}_k^{(1)*}$. For any $l \in \mathbb{L}_k^{(1)*}$, $u_k^{(l)} \in \mathbb{L}_k^{(2)*}$ indicates that the object with state $(\mathbf{x}_k, l)$ tracked at sensor 1 is associated with the object with state $(\mathbf{x}_k, u_k^{(l)})$ tracked at sensor 2. For a one-to-one mapping, we require that different labels at sensor 1 are associated with different labels at sensor 2, which means that all entries $u_k^{(l)}$ of $\boldsymbol{u}_k$ have to be different; this will be referred to as an admissible label association in analogy to an admissible object-measurement association in Chapters 4 and 5. The set of all admissible association vectors $\boldsymbol{u}_k$ will be denoted as $\mathcal{U}_k$. Using $\boldsymbol{u}_k$, we now modify the GCI fusion rule (6.3) according to

$$\tilde{f}^{(\boldsymbol{u}_k)}(\tilde{X}_k|Z_{1:k}^{(1)}, Z_{1:k}^{(2)}) \triangleq \frac{1}{D_k^{(\boldsymbol{u}_k)}} \big(f(\tilde{X}_k|Z_{1:k}^{(1)})\big)^{\omega} \big(f(\tilde{X}_k^{(\boldsymbol{u}_k)}|Z_{1:k}^{(2)})\big)^{1-\omega}, \tag{6.4}$$

with $D_k^{(\boldsymbol{u}_k)} \triangleq \int \big(f(\tilde{X}_k|Z_{1:k}^{(1)})\big)^{\omega} \big(f(\tilde{X}_k^{(\boldsymbol{u}_k)}|Z_{1:k}^{(2)})\big)^{1-\omega} \delta\tilde{X}_k$. Here, $\tilde{X}_k^{(\boldsymbol{u}_k)} \triangleq \big\{(\boldsymbol{x}_k^{(1)}, u_k^{(l(1))}), \ldots, (\boldsymbol{x}_k^{(n)}, u_k^{(l(n))})\big\}$ for any realization $\tilde{X}_k = \big\{(\boldsymbol{x}_k^{(1)}, l^{(1)}), \ldots, (\boldsymbol{x}_k^{(n)}, l^{(n)})\big\}$. That is, the label mapping defined by $\boldsymbol{u}_k$ changes each object label $l^{(j)} \in \mathcal{L}(\tilde{X}) \subseteq \mathbb{L}^{(1)*}$ into a label $u_k^{(l^{(j)})} \in \mathbb{L}_k^{(2)*}$, for $j = 1, \ldots, n$. Note that now, in the expression (6.1) of $f(\tilde{X}_k|Z_{1:k}^{(1)})$ and $f(\tilde{X}_k^{(\boldsymbol{u}_k)}|Z_{1:k}^{(2)})$, we have, respectively, $1_{\mathbb{L}_k^{(1)*}}(l) = 1$ and $1_{\mathbb{L}_k^{(2)*}}(u_k^{(l)}) = 1$ for all $l \in \mathcal{L}(\tilde{X}_k)$, and thus $\tilde{f}^{(\boldsymbol{u}_k)}(\tilde{X}_k|Z_{1:k}^{(1)}, Z_{1:k}^{(2)})$ is no longer zero in general.

More specifically, using the fact that $f(\tilde{X}_k|Z_{1:k}^{(1)})$ and $f(\tilde{X}_k|Z_{1:k}^{(2)})$ are both given by the LMB expression (cf. (6.1)) and that $1_{\mathbb{L}_k^{(1)*}}(l) = 1_{\mathbb{L}_k^{(2)*}}(u_k^{(l)}) = 1$ for all $l \in \mathcal{L}(\tilde{X}_k)$, the fused PDF in (6.4) becomes

$$\tilde{f}^{(\boldsymbol{u}_k)}(\tilde{X}_k|Z_{1:k}^{(1)}, Z_{1:k}^{(2)}) \propto \Delta(\tilde{X}_k)\big(w^{(1)}(\mathcal{L}(\tilde{X}_k))\big)^{\omega}\Bigg(\prod_{(\boldsymbol{x}_k,l)\in\tilde{X}_k}\big(f_1^{(l)}(\boldsymbol{x}_k)\big)^{\omega}\Bigg)$$
$$\times\,\Delta(\tilde{X}_k^{(\boldsymbol{u}_k)})\big(w^{(2)}(\mathcal{L}(\tilde{X}_k^{(\boldsymbol{u}_k)}))\big)^{1-\omega}\prod_{(\boldsymbol{x}'_k,l')\in\tilde{X}_k^{(\boldsymbol{u}_k)}}\big(f_2^{(l')}(\boldsymbol{x}'_k)\big)^{1-\omega}, \quad (6.5)$$

with (cf. (6.2))

$$w^{(1)}(\mathcal{L}(\tilde{X}_k)) \triangleq \Bigg(\prod_{l\in\mathcal{L}(\tilde{X}_k)} r_{k,1}^{(l)}\Bigg)\prod_{l'\in\mathbb{L}_k^{(1)*}\setminus\mathcal{L}(\tilde{X}_k)}\big(1-r_{k,1}^{(l')}\big), \quad (6.6)$$

$$w^{(2)}(\mathcal{L}(\tilde{X}_k^{(\boldsymbol{u}_k)})) \triangleq \Bigg(\prod_{l\in\mathcal{L}(\tilde{X}_k^{(\boldsymbol{u}_k)})} r_{k,2}^{(l)}\Bigg)\prod_{l'\in\mathbb{L}_k^{(2)*}\setminus\mathcal{L}(\tilde{X}_k^{(\boldsymbol{u}_k)})}\big(1-r_{k,2}^{(l')}\big). \quad (6.7)$$

Moreover, because $\boldsymbol{u}_k$ is an admissible label association vector, $\Delta(\tilde{X}_k^{(\boldsymbol{u}_k)})$ is equal to $\Delta(\tilde{X}_k)$. Hence, we can rewrite (6.5) as

$$\tilde{f}^{(\boldsymbol{u}_k)}(\tilde{X}_k|Z_{1:k}^{(1)}, Z_{1:k}^{(2)}) \propto \Delta(\tilde{X}_k)\big(w^{(1)}(\mathcal{L}(\tilde{X}_k))\big)^{\omega}\big(w^{(2)}(\mathcal{L}(\tilde{X}_k^{(\boldsymbol{u}_k)}))\big)^{1-\omega}$$
$$\times\prod_{(\boldsymbol{x}_k,l)\in\tilde{X}_k}\big(f_1^{(l)}(\boldsymbol{x}_k)\big)^{\omega}\big(f_2^{(u_k^{(l)})}(\boldsymbol{x}_k)\big)^{1-\omega},$$

or, more compactly,

$$\tilde{f}^{(\boldsymbol{u}_k)}(\tilde{X}_k|Z_{1:k}^{(1)}, Z_{1:k}^{(2)}) = \Delta(\tilde{X}_k)\,w_{\boldsymbol{u}_k}(\mathcal{L}(\tilde{X}_k))\prod_{(\boldsymbol{x}_k,l)\in\tilde{X}_k} f^{(l,u_k^{(l)})}(\boldsymbol{x}_k), \quad (6.8)$$

with the spatial PDFs

$$f^{(l,u_k^{(l)})}(\boldsymbol{x}_k) \triangleq \frac{1}{D_k^{(l,u_k^{(l)})}}\big(f_1^{(l)}(\boldsymbol{x}_k)\big)^{\omega}\big(f_2^{(u_k^{(l)})}(\boldsymbol{x}_k)\big)^{1-\omega} \quad (6.9)$$

and the weights $w_{\boldsymbol{u}_k}(\mathcal{L}(\tilde{X}_k))$, which are given by up to a normalization constant as

$$w_{\boldsymbol{u}_k}(\mathcal{L}(\tilde{X}_k)) \propto \big(w^{(1)}(\mathcal{L}(\tilde{X}_k))\big)^{\omega}\big(w^{(2)}(\mathcal{L}(\tilde{X}_k^{(\boldsymbol{u}_k)}))\big)^{1-\omega}\prod_{l\in\mathcal{L}(\tilde{X}_k)} D_k^{(l,u_k^{(l)})}, \quad (6.10)$$

where $D_k^{(l,u_k^{(l)})} \triangleq \int_{\mathbb{R}^{N_x}}\big(f_1^{(l)}(\boldsymbol{x}_k)\big)^{\omega}\big(f_2^{(u_k^{(l)})}(\boldsymbol{x}_k)\big)^{1-\omega}\mathrm{d}\boldsymbol{x}$. Here, the fused posterior PDF (6.8) constitutes the final fusion result for a given determinist label association vector $\boldsymbol{u}_k$.

6.2 Probabilistic Label Association

For an LMB fusion leading to good performance of the resulting distributed LMB filter, the label mapping introduced above should be such that each mapped label of sensor 1 equals the specific label of sensor 2 that describes the same object. Because the label association vector $\boldsymbol{u}_k$ defining this "correct" mapping is unknown, we hereafter model $\boldsymbol{u}_k$ as a random vector $\mathbf{u}_k$ and perform an implicit (soft, probabilistic) estimation of $\mathbf{u}_k$. We refer to this approach as probabilistic label association, by analogy to probabilistic data association used, e.g., in the fast LMB filter proposed in Chapter 4 to probabilistically associate measurements with objects.

6.2.1 Label Association Distribution

Let us define the extended label association vector $\bar{\boldsymbol{u}}_k = \big[\bar{u}_k^{(l^{(1)})} \cdots \bar{u}_k^{(l^{(I)})}\big]^{\mathrm{T}}$ of length $I = |\mathbb{L}_k^{(1)*}|$ (equal to the length of $\boldsymbol{u}_k$) with entries $\bar{u}_k^{(l)} \in \mathbb{L}_k^{(2)*} \cup \{0\}$ for $l \in \mathbb{L}_k^{(1)*}$. Here, $\bar{u}_k^{(l)} \in \mathbb{L}_k^{(2)*}$ indicates (as before) that the object with state $(\mathbf{x}_k, l)$ tracked at sensor 1 is associated with the object with state $(\mathbf{x}_k, \bar{u}_k^{(l)})$ tracked at sensor 2, and $\bar{u}_k^{(l)} = 0$ indicates that an object with label l does not exist (i.e., $(\mathbf{x}_k, l) \notin \tilde{X}_k$) according to the tracking performed at sensor 1. Note that the latter case also implies that no object with state $(\boldsymbol{x}_k, l)$ is associated with any object tracked at sensor 2. We denote by $\bar{\mathcal{U}}_k$ the set of all admissible extended association vectors $\bar{\boldsymbol{u}}_k$, i.e., of all vectors $\bar{\boldsymbol{u}}_k$ whose nonzero entries $\bar{u}_k^{(l)}$ are different. Furthermore, for any $L \subseteq \mathbb{L}_k^{(1)*}$, we define $\varphi(\bar{\boldsymbol{u}}_k, L)$ to be 1 for all admissible $\bar{\boldsymbol{u}}_k$ such that $\bar{u}_k^{(l)} \in \mathbb{L}_k^{(2)*}$ for $l \in L$ and $\bar{u}_k^{(l)} = 0$ for $l \in \mathbb{L}_k^{(1)*} \setminus L$, and to be 0 otherwise. Then, using the definitions of $w_{\boldsymbol{u}_k}(\mathcal{L}(\tilde{X}_k))$ in (6.10) and, in turn, of $w^{(1)}(\mathcal{L}(\tilde{X}_k))$ in (6.6) and $w^{(2)}(\mathcal{L}(\tilde{X}_k^{(\boldsymbol{u}_k)}))$ in (6.7), it can be shown that Eq. (6.8) can be rewritten in terms of $\bar{\boldsymbol{u}}_k$ as

$$\tilde{f}^{(\bar{\boldsymbol{u}}_k)}(\tilde{X}_k | Z_{1:k}^{(1)}, Z_{1:k}^{(2)}) = \Delta(\tilde{X}_k) \varphi(\bar{\boldsymbol{u}}_k, \mathcal{L}(\tilde{X}_k)\, w_{\bar{\boldsymbol{u}}_k} \prod_{(\boldsymbol{x}_k, l) \in \tilde{X}_k} f^{(l, \bar{u}_k^{(l)})}(\boldsymbol{x}_k). \tag{6.11}$$

Here, the weights $w_{\bar{\boldsymbol{u}}_k}$ are given up to a normalization constant by

$$w_{\bar{\boldsymbol{u}}_k} \propto \prod_{l \in \mathbb{L}_k^{(1)*}} \beta_k^{(l, \bar{u}_k^{(l)})}, \quad \bar{\boldsymbol{u}}_k \in \bar{\mathcal{U}}_k, \tag{6.12}$$

with the "label association weights"

$$\beta_k^{(l, \bar{u}_k^{(l)})} \triangleq \begin{cases} \dfrac{\big(r_{k,1}^{(l)}\big)^{\omega} \big(r_{k,2}^{(\bar{u}_k^{(l)})}\big)^{1-\omega} D_k^{(l, \bar{u}_k^{(l)})}}{\big(1 - r_{k,1}^{(\bar{u}_k^{(l)})}\big)^{1-\omega}}, & \bar{u}_k^{(l)} \in \mathbb{L}_k^{(2)*}, \\ \big(1 - r_{k,1}^{(l)}\big)^{\omega}, & \bar{u}_k^{(l)} = 0, \end{cases} \tag{6.13}$$

where $D_k^{(l,\bar{u}_k^{(l)})} \triangleq \int_{\mathbb{R}^{N_x}} \big(f_1^{(l)}(\boldsymbol{x}_k)\big)^{\omega} \big(f_2^{(\bar{u}_k^{(l)})}(\boldsymbol{x}_k)\big)^{1-\omega} \mathrm{d}\boldsymbol{x}_k$. Furthermore, the spatial PDFs $f^{(l,\bar{u}_k^{(l)})}(\boldsymbol{x}_k)$ in (6.11) are given by (6.9) with $u_k^{(l)}$ replaced by $\bar{u}_k^{(l)}$. (Note that $f^{(l,0)}(\boldsymbol{x}_k)$ does not occur in (6.11) because $\bar{u}_k^{(l)} = 0$ implies $(\boldsymbol{x}_k, l) \notin \tilde{X}_k$.) Differently from the weights $w_{\boldsymbol{u}_k}(\mathcal{L}(\tilde{X}_k))$ in our earlier expression (6.8), the weights $w_{\bar{\boldsymbol{u}}_k}$ do not depend on $\mathcal{L}(\tilde{X}_k)$; however, the factor $\varphi(\bar{\boldsymbol{u}}_k, \mathcal{L}(\tilde{X}_k))$ ensures that (6.11) is still equivalent to (6.8).

Just as $\boldsymbol{u}_k$, we hereafter consider $\bar{\boldsymbol{u}}_k$ as random (denoted $\bar{\mathbf{u}}_k$). Our probabilistic label association method is based on the idea of interpreting the weights $w_{\bar{\boldsymbol{u}}_k}$ in (6.11) and (6.12) as the probability distribution (PMF) of $\bar{\mathbf{u}}_k$. More precisely, we define the PMF of $\bar{\mathbf{u}}_k$ as

$$p(\bar{\boldsymbol{u}}_k) = \begin{cases} w_{\bar{\boldsymbol{u}}_k}, & \bar{\boldsymbol{u}}_k \in \bar{\mathcal{U}}_k, \\ 0, & \text{otherwise}, \end{cases} \tag{6.14}$$

for all $\bar{\boldsymbol{u}}_k \in (\mathbb{L}_k^{(2)*} \cup \{0\})^{|\mathbb{L}_k^{(1)*}|}$. We can then rewrite (6.11) as

$$\tilde{f}(\tilde{X}_k, \bar{\boldsymbol{u}}_k | Z_{1:k}^{(1)}, Z_{1:k}^{(2)}) = \Delta(\tilde{X}_k)\varphi(\bar{\boldsymbol{u}}_k, \mathcal{L}(\tilde{X}_k)) p(\bar{\boldsymbol{u}}_k) \prod_{(\boldsymbol{x}_k, l) \in \tilde{X}_k} f^{(l,\bar{u}_k^{(l)})}(\boldsymbol{x}_k). \tag{6.15}$$

In fact, it can be verified that integrating/summing the right-hand side of (6.15) with respect to $\tilde{X}_k$ and $\bar{\boldsymbol{u}}_k$ yields 1. Accordingly, expression (6.15) defines the joint PDF/PMF of the random variables $\tilde{\mathsf{X}}_k$ and $\bar{\mathbf{u}}_k$, whereas $\tilde{f}^{(\bar{\boldsymbol{u}}_k)}(\tilde{X}_k | Z_{1:k}^{(1)}, Z_{1:k}^{(2)})$ in (6.11) is the PDF of the random variable $\tilde{\mathsf{X}}_k$ parametrized by the nonrandom variable $\bar{\boldsymbol{u}}_k$. We can furthermore write the joint PDF/PMF of $\tilde{\mathsf{X}}_k$ and $\bar{\mathbf{u}}_k$ as $\tilde{f}(\tilde{X}_k, \bar{\boldsymbol{u}}_k | Z_{1:k}^{(1)}, Z_{1:k}^{(2)}) = \tilde{f}(\tilde{X}_k | \bar{\boldsymbol{u}}_k, Z_{1:k}^{(1)}, Z_{1:k}^{(2)}) \times p(\bar{\boldsymbol{u}}_k | Z_{1:k}^{(1)}, Z_{1:k}^{(2)})$, with the conditional fused posterior PDF

$$\tilde{f}(\tilde{X}_k | \bar{\boldsymbol{u}}_k, Z_{1:k}^{(1)}, Z_{1:k}^{(2)}) = \Delta(\tilde{X}_k)\varphi(\bar{\boldsymbol{u}}_k, \mathcal{L}(\tilde{X}_k)) \prod_{(\boldsymbol{x}_k, l) \in \tilde{X}_k} f^{(l,\bar{u}_k^{(l)})}(\boldsymbol{x}_k), \tag{6.16}$$

and $p(\bar{\boldsymbol{u}}_k | Z_{1:k}^{(1)}, Z_{1:k}^{(2)})$ given by the label association PMF $p(\bar{\boldsymbol{u}}_k | Z_{1:k}^{(1)}, Z_{1:k}^{(2)})$ in (6.14). Following this interpretation, we can obtain the unconditional fused posterior PDF, to be denoted $\tilde{f}(\tilde{X}_k | Z_{1:k}^{(1)}, Z_{1:k}^{(2)})$, as

$$\tilde{f}(\tilde{X}_k | Z_{1:k}^{(1)}, Z_{1:k}^{(2)}) = \sum_{\bar{\boldsymbol{u}}_k \in \bar{\mathcal{U}}_k} \tilde{f}(\tilde{X}_k | \bar{\boldsymbol{u}}_k, Z_{1:k}^{(1)}, Z_{1:k}^{(2)}) p(\bar{\boldsymbol{u}}_k).$$

Here, we can extend the summation set $\bar{\mathcal{U}}$ to $(\mathbb{L}_k^{(2)*} \cup \{0\})^{|\mathbb{L}_k^{(1)*}|}$, because by (6.14) there is $p(\bar{\boldsymbol{u}}_k) = 0$ for $\bar{\boldsymbol{u}}_k \in (\mathbb{L}_k^{(2)*} \cup \{0\})^{|\mathbb{L}_k^{(1)*}|} \setminus \bar{\mathcal{U}}_k$. We thus obtain, using (6.16),

$$\tilde{f}(\tilde{X}_k | Z_{1:k}^{(1)}, Z_{1:k}^{(2)}) = \Delta(\tilde{X}_k) \sum_{\bar{\boldsymbol{u}}_k \in (\mathbb{L}_k^{(2)*} \cup \{0\})^{|\mathbb{L}_k^{(1)*}|}} \varphi(\bar{\boldsymbol{u}}_k, \mathcal{L}(\tilde{X}_k)) p(\bar{\boldsymbol{u}}_k) \prod_{(\boldsymbol{x}_k, l) \in \tilde{X}_k} f^{(l,\bar{u}_k^{(l)})}(\boldsymbol{x}_k). \tag{6.17}$$

6.2.2 LMB Approximation

The PDF $\tilde{f}(\tilde{X}_k|Z^{(1)}_{1:k}, Z^{(2)}_{1:k})$ in (6.17) is no longer of LMB form (2.24); instead, it is the PDF of a GLMB RFS (cf. 2.30). Therefore, we approximate it by an LMB PDF as follows. Following the approach used in the fast LMB filter in Section 4.2, we approximate the label association PMF $p(\bar{\boldsymbol{u}}_k)$ by the product of its marginals, i.e.,

$$p(\bar{\boldsymbol{u}}_k) \approx \prod_{l\in\mathbb{L}^{(1)*}_k} p(\bar{u}^{(l)}_k), \quad \bar{\boldsymbol{u}}_k \in (\mathbb{L}^{(2)*}_k \cup \{0\})^{|\mathbb{L}^{(1)*}_k|}. \tag{6.18}$$

where

$$p(\bar{u}^{(l)}_k) = \sum_{\bar{\boldsymbol{u}}^{\sim l}_k \in (\mathbb{L}^{(2)*}\cup\{0\})^{|\mathbb{L}^{(1)*}|-1}} p(\bar{\boldsymbol{u}}_k).$$

Here, $\bar{\boldsymbol{u}}^{\sim l}_k$ denotes the vector $\bar{\boldsymbol{u}}_k$ with the lth entry, $\bar{u}^{(l)}_k$, removed. Inserting (6.18) into (6.17) yields an approximation $\tilde{\tilde{f}}(\tilde{X}_k|Z^{(1)}_{1:k}, Z^{(2)}_{1:k}) \approx \tilde{f}(\tilde{X}_k|Z^{(1)}_{1:k}, Z^{(2)}_{1:k})$ that is given by

$$\begin{aligned}&\tilde{\tilde{f}}(\tilde{X}_k|Z^{(1)}_{1:k}, Z^{(2)}_{1:k})\\ &\quad = \Delta(\tilde{X}_k) \sum_{\bar{\boldsymbol{u}}_k\in(\mathbb{L}^{(2)*}_k\cup\{0\})^{|\mathbb{L}^{(1)*}_k|}} \varphi(\bar{\boldsymbol{u}}_k, \mathcal{L}(\tilde{X}_k)) \Bigg(\prod_{l'\in\mathbb{L}^{(1)*}_k} p(\bar{u}^{(l')}_k)\Bigg) \prod_{(\boldsymbol{x}_k,l)\in\tilde{X}_k} f^{(l,\bar{u}^{(l)}_k)}(\boldsymbol{x}_k).\end{aligned}$$

Next, splitting $\prod_{l'\in\mathbb{L}^{(1)*}_k} p(\bar{u}^{(l')}_k)$ as $\big(\prod_{l'\in\mathbb{L}^{(1)*}_k\setminus\mathcal{L}(\tilde{X}_k)} p(\bar{u}^{(l')}_k)\big)\prod_{l\in\mathcal{L}(\tilde{X}_k)} p(\bar{u}^{(l)}_k)$, using $\sum_{\bar{\boldsymbol{u}}_k\in(\mathbb{L}^{(2)*}_k)^{|\mathbb{L}^{(1)*}_k|}} = \sum_{\bar{u}^{(1)}_k\in\mathbb{L}^{(2)*}_k}\cdots\sum_{\bar{u}^{|\mathbb{L}^{(1)*}_k|}_k\in\mathbb{L}^{(2)*}_k}$, and evaluating $\varphi(\bar{\boldsymbol{u}}_k, \mathcal{L}(\tilde{X}_k))$, we obtain

$$\tilde{\tilde{f}}(\tilde{X}_k|Z^{(1)}_{1:k}, Z^{(2)}_{1:k}) = \Delta(\tilde{X}_k)\Bigg(\prod_{l'\in\mathbb{L}^{(1)*}_k\setminus\mathcal{L}(\tilde{X}_k)} p(\bar{u}^{(l')}_k = 0)\Bigg) \prod_{(\boldsymbol{x}_k,l)\in\tilde{X}_k} \sum_{\bar{u}^{(l)}_k\in\mathbb{L}^{(2)*}_k} p(\bar{u}^{(l)}_k)\, f^{(l,\bar{u}^{(l)}_k)}(\boldsymbol{x}_k). \tag{6.19}$$

Comparing this expression with[2] (6.1), one can easily verify that $\tilde{\tilde{f}}(\tilde{X}_k|Z^{(1)}_{1:k}, Z^{(2)}_{1:k})$ is an LMB PDF parametrized by $\big\{\big(r^{(l)}_k, f^{(l)}(\boldsymbol{x}_k)\big)\big\}_{l\in\mathbb{L}^{(1)*}_k}$, with existence probabilities

$$r^{(l)}_k = \sum_{\bar{u}^{(l)}_k\in\mathbb{L}^{(2)*}_k} p(\bar{u}^{(l)}_k) \tag{6.20}$$

and spatial PDFs

$$f^{(l)}(\boldsymbol{x}_k) = \frac{1}{r^{(l)}_k} \sum_{\bar{u}^{(l)}_k\in\mathbb{L}^{(2)*}_k} p(\bar{u}^{(l)}_k)\, f^{(l,\bar{u}^{(l)}_k)}(\boldsymbol{x}_k), \tag{6.21}$$

[2]Note that, differently from (6.1), expression (6.19) does not include the factor $1_{\mathbb{L}^{(1)*}_k}(l)$. This is because in (6.19), $\mathcal{L}(\tilde{X}_k) \subseteq \mathbb{L}^{(1)*}_k$ and thus always $1_{\mathbb{L}^{(1)*}_k}(l) = 1$, whereas in (2.24), $\mathcal{L}(\tilde{X}_k) \subseteq \mathbb{L}_k$.

where $l \in \mathbb{L}_k^{(1)*}$. Expressions (6.20) and (6.21) complete the formulation of our proposed pairwise LMB fusion scheme using soft (probabilistic) label association. The input to this fusion scheme are the parameter sets $\big\{\big(r_{k,1}^{(l)}, f_1^{(l)}(\boldsymbol{x}_k)\big)\big\}_{l\in\mathbb{L}_k^{(1)*}}$ and $\big\{\big(r_{k,2}^{(l)}, f_2^{(l)}(\boldsymbol{x}_k)\big)\big\}_{l\in\mathbb{L}_k^{(2)*}}$, and the output is the fused Bernoulli parameter set $\big\{\big(r_k^{(l)}, f^{(l)}(\boldsymbol{x}_k)\big)\big\}_{l\in\mathbb{L}_k^{(1)*}}$, with $r_k^{(l)}$ given by (6.20) and $f^{(l)}(\boldsymbol{x}_k)$ given by (6.21). Here, $p(\bar{u}_k^{(l)})$ in (6.20), (6.21) is calculated by marginalizing $p(\bar{\boldsymbol{u}}_k)$ in (6.14), and $f^{(l,\bar{u}_k^{(l)})}(\boldsymbol{x}_k)$ in (6.21) is given by (6.9).

In a practical implementation, Bernoulli components $l \in \mathbb{L}_k^{(1)*}$ that do not have a plausible association with any Bernoulli component $l' \in \mathbb{L}_k^{(2)*}$ at sensor 2 can be excluded from the fusion procedure. The plausibility of an association can be measured by $D_k^{(l,l')} = \int_{\mathbb{R}^{N_x}} \big(f_1^{(l)}(\boldsymbol{x}_k)\big)^{\omega} \big(f_2^{(l')}(\boldsymbol{x}_k)\big)^{1-\omega} \mathrm{d}\boldsymbol{x}_k$. Thus, we do not fuse Bernoulli components $l \in \mathbb{L}_k^{(1)*}$ such that $D_k^{(l,l')} < \gamma_{\mathrm{F}}$ for all $l' \in \mathbb{L}_k^{(2)*}$, with a positive threshold γ_{F}.

6.3 Efficient Implementation

In the following section, we establish an efficient implementation of our pairwise LMB fusion algorithm. More specifically, in Section 6.3.1, we propose a BP algorithm for fast approximate marginalization of the label association PMF and, in Section 6.3.2, we present an efficient implementation based on the modeling of the spatial PDFs by Gaussians.

6.3.1 Fast BP-Based Algorithm

We now present a fast algorithm for approximate marginalization of $p(\bar{\boldsymbol{u}}_k)$. This algorithm is inspired by the BP-based algorithm for probabilistic data association used in the fast LMB filter (cf. Sections 4.2.2 and 4.2.3), which is in turn based on the BP-based algorithm in [Williams and Lau, 2014].

Inserting (6.12) into (6.14), we can express the association pmf $p(\bar{\boldsymbol{u}}_k)$ as

$$p(\bar{\boldsymbol{u}}_k) \propto \Psi(\bar{\boldsymbol{u}}_k) \prod_{l\in\mathbb{L}_k^{(1)*}} \beta_k^{(l,\bar{u}_k^{(l)})}, \quad \bar{\boldsymbol{u}}_k \in (\mathbb{L}_k^{(2)*} \cup \{0\})^{|\mathbb{L}_k^{(1)*}|}, \tag{6.22}$$

where $\Psi(\bar{\boldsymbol{u}}_k) = 1$ if $\bar{\boldsymbol{u}}_k \in \bar{\mathcal{U}}$ and $\Psi(\bar{\boldsymbol{u}}_k) = 0$ otherwise. By analogy to Section 4.2.2, we introduce the alternative label association vector $\mathbf{v}_k = \big[\mathrm{v}_k^{(l^{(1)})} \cdots \mathrm{v}_k^{(l^{(J)})}\big]^{\mathrm{T}}$ of length $J = |\mathbb{L}^{(2)*}|$ and with entries $\mathrm{v}_k^{(l)} \in \mathbb{L}_k^{(1)*} \cup \{0\}$ for $l \in \mathbb{L}_k^{(2)*}$. Here, the entry $\mathrm{v}_k^{(l)} \in \mathbb{L}_k^{(1)*}$ indicates that the object with state $(\mathbf{x}_k, l)$ tracked at sensor 2 is associated with the object with state $(\mathbf{x}_k, v_k^{(l)})$ tracked at sensor 1, and $\mathrm{v}_k^{(l)} = 0$ indicates that an object with label l does not exist according to the tracking performed at sensor 2. The latter case also implies that no object with state $(\mathbf{x}_k, l)$ is associated with any object tracked at sensor 1. Thus, $\mathbf{v}_k$ is a description of the label associations that is analogous to $\bar{\mathbf{u}}_k$ but "viewed

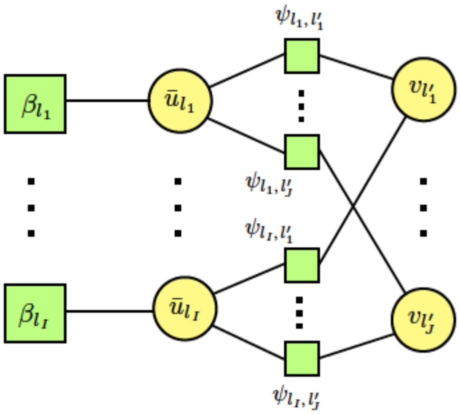

Figure 6.1: Factor graph representing the factorization of $p(\bar{\boldsymbol{u}}_k, \boldsymbol{v}_k)$ in (6.23), (6.24). Variable nodes are depicted as circles and factor nodes as squares. The shorthands $\beta_l \triangleq \beta_k^{(l,\bar{u}_k^{(l)})}$, $\bar{u}_l \triangleq \bar{u}_k^{(l)}$, $v_{l'} \triangleq v_k^{(l')}$, $\psi_{l,l'} \triangleq \psi_{l,l'}(\bar{u}_l, v_{l'})$, $I = |\mathbb{L}_k^{(1)*}|$, and $J \triangleq |\mathbb{L}_k^{(2)*}|$ are used.

from the other sensor." We can reformulate $p(\bar{\boldsymbol{u}}_k)$ in (6.22) in terms of $\bar{\boldsymbol{u}}_k$ and $\boldsymbol{v}_k$ as

$$p(\bar{\boldsymbol{u}}, \boldsymbol{v}_k) \propto \Psi(\bar{\boldsymbol{u}}_k, \boldsymbol{v}_k) \prod_{l \in \mathbb{L}_k^{(1)*}} \beta_k^{(l,\bar{u}_k^{(l)})}, \tag{6.23}$$

for $\bar{\boldsymbol{u}}_k \in (\mathbb{L}_k^{(2)*} \cup \{0\})^{|\mathbb{L}_k^{(1)*}|}$ and $\boldsymbol{v}_k \in (\mathbb{L}_k^{(1)*} \cup \{0\})^{|\mathbb{L}_k^{(2)*}|}$, with the admissibility constraint factor $\Psi(\bar{\boldsymbol{u}}_k, \boldsymbol{v}_k) \in \{0,1\}$ given by

$$\Psi(\bar{\boldsymbol{u}}_k, \boldsymbol{v}_k) = \prod_{l \in \mathbb{L}_k^{(1)*}} \prod_{l' \in \mathbb{L}_k^{(2)*}} \psi_{l,l'}(\bar{u}_k^{(l)}, v_k^{(l')}). \tag{6.24}$$

Here, $\psi_{l,l'}(\bar{u}_k^{(l)}, v_k^{(l')}) = 0$ if either $\bar{u}_k^{(l)} = l'$ and $v_k^{(l')} \neq l$ or $\bar{u}_k^{(l)} \neq l'$ and $v_k^{(l')} = l$, and $\psi_{l,l'}(\bar{u}_k^{(l)}, v_k^{(l')}) = 1$ otherwise.

The above reformulation of $p(\bar{\boldsymbol{u}}_k)$ in terms of $\bar{\boldsymbol{u}}_k$ and $\boldsymbol{v}_k$ allows us to devise an efficient algorithm for calculating accurate approximations of the marginal association probabilities $p(\bar{u}_k^{(l)})$. The factorization (6.23), (6.24) is represented by the factor graph [Kschischang et al., 2001] is shown in Figure 6.1 and equals the factor graph in Figure 4.2 used in the fast LMB filter of Section 4.2.2. Moreover, it can be shown that a derivation similar to that in the fast LMB filter presented in Sections 4.2.2 and 4.2.3 results in an efficient message passing procedure analogous to that one performed by the fast LMB filter. More precisely, in BP iteration $p \in \{1, \dots, P\}$, a message $\zeta_{l \to l'}^{[p]}$ is passed from variable node "$\bar{u}_k^{(l)}$" via factor node "$\psi_{l,l'}(\bar{u}_k^{(l)}, v_k^{(l')})$" to variable node "$v_k^{(l')}$", and a message $\nu_{l' \to l}^{[p]}$ is passed from variable node "$v_k^{(l')}$" via factor node "$\psi_{l,l'}(\bar{u}_k^{(l)}, v_k^{(l')})$" to variable node "$\bar{u}_k^{(l)}$". These messages are given by:

$$\zeta_{k,l \to l'}^{[p]} = \frac{\beta_k^{(l,l')}}{\beta_k^{(l,0)} + \sum_{\lambda \in \mathbb{L}_k^{(2)*} \setminus \{l'\}} \beta_k^{(l,\lambda)} \nu_{k,\lambda \to l}^{[p-1]}}, \tag{6.25}$$

$$\nu_{k,l'\to l}^{[p]} = \frac{1}{1+\sum_{\lambda\in\mathbb{L}_k^{(1)*}\setminus\{l\}}\zeta_{k,\lambda\to l'}^{[p]}}, \tag{6.26}$$

for all $l \in \mathbb{L}^{(1)*}$ and $l' \in \mathbb{L}^{(2)*}$. The recursion established by these two equations is initialized for $p=0$ by $\nu_{k,l'\to l}^{[0]} = 1$. After the final iteration $p=P$, approximations to the marginal association probabilities $p(\bar{u}_k^{(l)})$, $l \in \mathbb{L}^{(1)*}$ are provided by the beliefs $\tilde{p}(\bar{u}_k^{(l)})$ at the respective variable nodes "$\bar{u}_k^{(l)}$" in Figure 6.1, which are given by

$$\tilde{p}(\bar{u}_k^{(l)} = l') = \begin{cases} \beta_k^{(l,l')}\nu_{k,l'\to l}^{[P]}/C_l, & l' \in \mathbb{L}_k^{(2)*}, \\ \beta_k^{(l,l')}/C_l, & l' = 0. \end{cases} \tag{6.27}$$

Here, $C_l \triangleq \beta_k^{(l,0)} + \sum_{\lambda\in\mathbb{L}_k^{(2)*}} \beta_k^{(l,\lambda)}\nu_{k,\lambda\to l}^{[P]}$.

6.3.2 Gaussian Implementation

For a reduction of communication and computation requirements, we next assume Gaussian models for the spatial PDFs of the local LMB RFSs, i.e.,

$$f_1^{(l)}(\boldsymbol{x}_k) = \mathcal{N}\big(\boldsymbol{x}_k; \boldsymbol{\mu}_{k,1}^{(l)}, \boldsymbol{\Sigma}_{k,1}^{(l)}\big), \quad l \in \mathbb{L}_k^{(1)*},$$
$$f_2^{(l)}(\boldsymbol{x}_k) = \mathcal{N}\big(\boldsymbol{x}_k; \boldsymbol{\mu}_{k,2}^{(l)}, \boldsymbol{\Sigma}_{k,2}^{(l)}\big), \quad l \in \mathbb{L}_k^{(2)*}.$$

Accordingly, the local LMB parameter sets are now given by $\big\{\big(r_{k,s}^{(l)}, \boldsymbol{\mu}_{k,s}^{(l)}, \boldsymbol{\Sigma}_{k,s}^{(l)}\big)\big\}_{l\in\mathbb{L}_k^{(s)*}}$ for $s \in \{1,2\}$. In what follows, we will present the resulting expressions of $f^{(l,\bar{u}_k^{(l)})}(\boldsymbol{x}_k)$, $\beta_k^{(l,\bar{u}_k^{(l)})}$, and $f^{(l)}(\boldsymbol{x}_k)$, where $l \in \mathbb{L}_k^{(1)*}$.

We recall that the spatial PDF $f^{(l,\bar{u}_k^{(l)})}(\boldsymbol{x}_k)$ is calculated from $f_1^{(l)}(\boldsymbol{x}_k)$ and $f_2^{(\bar{u}_k^{(l)})}(\boldsymbol{x}_k)$ via (6.9). As was shown in [Battistelli et al., 2013], if $f_1^{(l)}(\boldsymbol{x}_k)$ and $f_2^{(\bar{u}_k^{(l)})}(\boldsymbol{x}_k)$ are Gaussian as assumed above, then $f^{(l,\bar{u}_k^{(l)})}(\boldsymbol{x}_k)$ is also Gaussian, i.e.,

$$f^{(l,\bar{u}_k^{(l)})}(\boldsymbol{x}_k) = \mathcal{N}\big(\boldsymbol{x}_k; \boldsymbol{\mu}_k^{(l,\bar{u}_k^{(l)})}, \boldsymbol{\Sigma}_k^{(l,\bar{u}_k^{(l)})}\big), \tag{6.28}$$

with mean vector $\boldsymbol{\mu}_k^{(l,\bar{u}_k^{(l)})}$ and covariance matrix $\boldsymbol{\Sigma}_k^{(l,\bar{u}_k^{(l)})}$ given by

$$\boldsymbol{\mu}_k^{(l,\bar{u}_k^{(l)})} = \boldsymbol{\Sigma}_k^{(l,\bar{u}_k^{(l)})}\big(\omega\boldsymbol{\Sigma}_{k,1}^{(l)-1}\boldsymbol{\mu}_{k,1}^{(l)} + (1-\omega)\boldsymbol{\Sigma}_{k,2}^{(\bar{u}_k^{(l)})-1}\boldsymbol{\mu}_{k,2}^{(\bar{u}_k^{(l)})}\big), \tag{6.29}$$

$$\boldsymbol{\Sigma}_k^{(l,\bar{u}_k^{(l)})} = \big(\omega\boldsymbol{\Sigma}_{k,1}^{(l)-1} + (1-\omega)\boldsymbol{\Sigma}_{k,2}^{(\bar{u}_k^{(l)})-1}\big)^{-1}. \tag{6.30}$$

It can furthermore be shown that the normalization factor $D_k^{(l,\bar{u}_k^{(l)})} = \int_{\mathbb{R}^{N_x}}\big(f_1^{(l)}(\boldsymbol{x}_k)\big)^{\omega}$

$\times \big(f_2^{(\bar{u}_k)}(\boldsymbol{x}_k)\big)^{1-\omega} \mathrm{d}\boldsymbol{x}$ occurring in (6.13) is given by

$$D_k^{(l,\bar{u}_k^{(l)})} = \gamma_k^{(l)} \kappa_k^{(\bar{u}_k^{(l)})} \mathcal{N}\Big(\boldsymbol{\mu}_{k,1}^{(l)}; \boldsymbol{\mu}_{k,2}^{(\bar{u}_k^{(l)})}, \frac{1}{\omega}\boldsymbol{\Sigma}_{k,1}^{(l)} + \frac{1}{1-\omega}\boldsymbol{\Sigma}_{k,2}^{(\bar{u}_k^{(l)})}\Big). \tag{6.31}$$

Here,

$$\gamma_k^{(l)} = \sqrt{\frac{\det\big(\frac{2\pi}{\omega}\boldsymbol{\Sigma}_{k,1}^{(l)}\big)}{\Big(\det\big(2\pi\boldsymbol{\Sigma}_{k,1}^{(l)}\big)\Big)^{\omega}}}\,, \quad \kappa_k^{(\bar{u}_k^l)} = \sqrt{\frac{\det\big(\frac{2\pi}{1-\omega}\boldsymbol{\Sigma}_{k,2}^{(\bar{u}_k^{(l)})}\big)}{\Big(\det\big(2\pi\boldsymbol{\Sigma}_{k,2}^{(\bar{u}_k^{(l)})}\big)\Big)^{1-\omega}}}\,,$$

with $\det(\cdot)$ being the determinant operator, and $\mathcal{N}\big(\boldsymbol{\mu}_{k,1}^{(l)}; \boldsymbol{\mu}_{k,2}^{(\bar{u}_k^{(l)})}, \frac{1}{\omega}\boldsymbol{\Sigma}_{k,1}^{(l)} + \frac{1}{1-\omega}\boldsymbol{\Sigma}_{k,2}^{(\bar{u}_k^{(l)})}\big)$ denotes the positive number obtained by evaluating the Gaussian PDF $\mathcal{N}\big(\boldsymbol{x}_k; \boldsymbol{\mu}_{k,2}^{(\bar{u}_k^{(l)})}, \frac{1}{\omega}\boldsymbol{\Sigma}_{k,1}^{(l)} + \frac{1}{1-\omega}\boldsymbol{\Sigma}_{k,2}^{(\bar{u}_k^{(l)})}\big)$ at $\boldsymbol{x}_k = \boldsymbol{\mu}_{k,1}^{(l)}$. An expression of the label association weight $\beta_k^{(l,\bar{u}_k^{(l)})}$ is then obtained by inserting (6.31) into (6.13).

Finally, according to (6.21) and (6.28), the fused spatial PDF $f^{(l)}(\boldsymbol{x}_k)$ is a linear combination of the PDFs $f^{(l,\bar{u}_k^{(l)})}(\boldsymbol{x}_k)$. Because of (6.28), it is actually a Gaussian mixture PDF. We next approximate this Gaussian mixture PDF by the Gaussian PDF, i.e., we consider a Gaussian approximation

$$\bar{f}^{(l)}(\boldsymbol{x}_k) = \mathcal{N}\big(\boldsymbol{x}_k; \bar{\boldsymbol{\mu}}_k^{(l)}, \bar{\boldsymbol{\Sigma}}_k^{(l)}\big), \quad l \in \mathbb{L}_k^{(1)*},$$

whose mean vector $\bar{\boldsymbol{\mu}}_k^{(l)}$ and covariance matrix $\bar{\boldsymbol{\Sigma}}_k^{(l)}$ are taken to be equal to those of $f^{(l)}(\boldsymbol{x}_k)$. Using (6.21) and (6.28), one obtains [Malladi and Speyer, 1997]

$$\bar{\boldsymbol{\mu}}_k^{(l)} = \frac{1}{r_k^{(l)}} \sum_{\bar{u}_k^{(l)} \in \mathbb{L}_k^{(2)*}} p(\bar{u}_k^{(l)})\, \boldsymbol{\mu}_k^{(l,\bar{u}_k^{(l)})}, \tag{6.32}$$

$$\bar{\boldsymbol{\Sigma}}_k^{(l)} = \frac{1}{r_k^{(l)}} \sum_{\bar{u}_k^{(l)} \in \mathbb{L}_k^{(2)*}} p(\bar{u}_k^{(l)}) \big(\boldsymbol{\Sigma}_k^{(l,\bar{u}_k^{(l)})} + (\boldsymbol{\mu}_k^{(l,\bar{u}_k^{(l)})} - \bar{\boldsymbol{\mu}}_k^{(l)})(\boldsymbol{\mu}_k^{(l,\bar{u}_k^{(l)})} - \bar{\boldsymbol{\mu}}_k^{(l)})^{\mathrm{T}}\big), \tag{6.33}$$

for $l \in \mathbb{L}_k^{(1)*}$. Here, $r_k^{(l)}$ is given by (6.20), $p(\bar{u}_k^{(l)})$ is the marginal label association probability (cf. (6.18)), and $\boldsymbol{\mu}_k^{(l,\bar{u}_k^{(l)})}$ and $\boldsymbol{\Sigma}_k^{(l,\bar{u}_k^{(l)})}$ are given by (6.29) and (6.30), respectively. Within this Gaussian approximation, the fused Bernoulli parameter set is $\big\{\big(r_k^{(l)}, \bar{\boldsymbol{\mu}}_k^{(l)}, \bar{\boldsymbol{\Sigma}}_k^{(l)}\big)\big\}_{l\in\mathbb{L}_k^{(1)*}}$. We note that in the final algorithm (cf. Section 6.4), $p(\bar{u}_k^{(l)})$ is approximated by the belief $\tilde{p}(\bar{u}_k^{(l)})$ in (6.27).

6.4 The Proposed Distributed LMB Filter

In the formulation of our pairwise fusion method, we used sensor $s=1$ as a "reference sensor" for fusing the posterior PDFs of sensors $s=1$ and $s=2$. As a consequence, the fused quantities $r_k^{(l)}$, $p(\bar{u}_k^{(l)})$, $\bar{\boldsymbol{\mu}}_k^{(l)}$, $\bar{\boldsymbol{\Sigma}}_k^{(l)}$, and $\bar{f}^{(l)}(\boldsymbol{x}_k)$ are defined for $l \in \mathbb{L}_k^{(1)*}$, i.e., the underlying label set is $\mathbb{L}_k^{(1)*}$. In a distributed implementation, each sensor $s \in \{1,2\}$ runs its own instance of the pairwise fusion method, using its own label set $\mathbb{L}_k^{(s)*}$ as the reference label set. This implies that the fused LMB parameter sets calculated at the two sensors will be different. Let $\big\{\big(\bar{r}_{k,s}^{(l)}, \bar{\boldsymbol{\mu}}_{k,s}^{(l)}, \bar{\boldsymbol{\Sigma}}_{k,s}^{(l)}\big)\big\}_{l\in\mathbb{L}_k^{(s)*}}$ denote the fused LMB parameter set calculated at sensor $s \in \{1,2\}$; this should not be confused with the original local LMB parameter set $\big\{\big(r_{k,s}^{(l)}, \boldsymbol{\mu}_{k,s}^{(l)}, \boldsymbol{\Sigma}_{k,s}^{(l)}\big)\big\}_{l\in\mathbb{L}_k^{(s)*}}$.

The proposed fusion algorithm (still considering pairwise fusion) is now obtained by replacing in (6.20), (6.32), and (6.33) the marginal association PMFs $p(\bar{u}_k^{(l)})$ by the beliefs $\tilde{p}(\bar{u}_k^{(l)})$ given by (6.27). The fused LMB parameter set of sensor $s \in \{1,2\}$ using this additional approximation will be denoted by $\big\{\big(\tilde{r}_{k,s}^{(l)}, \tilde{\boldsymbol{\mu}}_{k,s}^{(l)}, \tilde{\boldsymbol{\Sigma}}_{k,s}^{(l)}\big)\big\}_{l\in\mathbb{L}_k^{(s)*}}$. Note that calculation of this fused LMB parameter set at sensor s presupposes that the original local LMB parameter set of the respective other sensor is available at sensor s. This means that each sensor s has to transmit its local LMB parameter set $\big\{\big(r_{k,s}^{(l)}, \boldsymbol{\mu}_{k,s}^{(l)}, \boldsymbol{\Sigma}_{k,s}^{(l)}\big)\big\}_{l\in\mathbb{L}_k^{(s)*}}$ to its fusion partner.

So far, we considered the pairwise fusion of the local LMB parameter sets of two sensors. This pairwise fusion can be used to achieve networkwide fusion in a connected network of $S \geq 2$ sensors $s \in \{1,\dots,S\}$ via the following iterative procedure consisting of $i=1,\dots,I$ iterations [Battistelli et al., 2013]. Let $N_s \subseteq \{1,\dots,S\}\setminus\{s\}$ denote the set of "neighbors" of sensor s, i.e., the set of sensors with which sensor s is able to communicate. In the first iteration, i.e, $i=1$, each sensor s transmits its local LMB parameter set $\big\{\big(r_{k,s}^{(l)}, \boldsymbol{\mu}_{k,s}^{(l)}, \boldsymbol{\Sigma}_{k,s}^{(l)}\big)\big\}_{l\in\mathbb{L}_k^{(s)*}}$ to its neighbors $s' \in N_s$. Then, each sensor s performs pairwise fusion sequentially (recursively) with each of the LMB parameter sets it received from its neighbors, in an arbitrary order. That is, the local LMB parameter set is fused with that of an arbitrary sensor $s' \in N_s$, the LMB parameter set resulting from this pairwise fusion is fused with that of an arbitrary sensor $s'' \in N_s\setminus\{s'\}$, etc. Let $\big\{\big(\tilde{r}_{k,s}^{(l,1)}, \tilde{\boldsymbol{\mu}}_{k,s}^{(l,1)}, \tilde{\boldsymbol{\Sigma}}_{k,s}^{(l,1)}\big)\big\}_{l\in\mathbb{L}_k^{(s)*}}$—the superscript "1" indicates the first, i.e, $i=1$, iteration—denote the LMB parameter set resulting from this sequence of $|N_s|$ successive pairwise fusion steps. In the second iteration, the sequence of $|N_s|$ pairwise fusion steps is repeated but with $\big\{\big(\tilde{r}_{k,s}^{(l,1)}, \tilde{\boldsymbol{\mu}}_{k,s}^{(l,1)}, \tilde{\boldsymbol{\Sigma}}_{k,s}^{(l,1)}\big)\big\}_{l\in\mathbb{L}_k^{(s)*}}$ substituted for the original local LMB parameter set $\big\{\big(r_{k,s}^{(l)}, \boldsymbol{\mu}_{k,s}^{(l)}, \boldsymbol{\Sigma}_{k,s}^{(l)}\big)\big\}_{l\in\mathbb{L}_k^{(s)*}}$ and the fusion results of the other sensors substituted for their original local LMB parameter sets; this requires another round of parameter transmissions between neighboring sensors. An analogous sequence of $|N_s|$ pairwise fusions is performed at each sensor also in each of the subsequent $I-1$ iteration. The proposed networkwide fusion algorithm is summarized in Table 6.1.

As an alternative to this recursive algorithm, a gossip algorithm [Dimakis et al., 2010]

Table 6.1: Proposed distributed LMB filter algorithm with soft label association—recursion at time $k \geq 1$ and at sensor $s \in \{1, \ldots, S\}$

Input: LMB parameter set $\{(r_{k,s}^{(l)}, \boldsymbol{\mu}_{k,s}^{(l)}, \boldsymbol{\Sigma}_{k,s}^{(l)})\}_{l \in \mathbb{L}_k^{(s)*}}$ of sensor s.

Output: Fused LMB parameter set $\{(\bar{r}_{k,s}^{(l)}, \bar{\boldsymbol{\mu}}_{k,s}^{(l)}, \bar{\boldsymbol{\Sigma}}_{k,s}^{(l)})\}_{l \in \mathbb{L}_k^{(s)*}}$.

Operations:

1) Initialize $\{(\tilde{r}_{k,s}^{(l,1)}, \tilde{\boldsymbol{\mu}}_{k,s}^{(l,1)}, \tilde{\boldsymbol{\Sigma}}_{k,s}^{(l,1)})\}_{l \in \mathbb{L}_k^{(s)*}} = \{(r_{k,s}^{(l)}, \boldsymbol{\mu}_{k,s}^{(l)}, \boldsymbol{\Sigma}_{k,s}^{(l)})\}_{l \in \mathbb{L}_k^{(s)*}}$.

Execute the following steps for all $i = 1, \ldots, I$ iterations:

2) Receive LMB parameter sets $\{(\tilde{r}_{k,s'}^{(l,i)}, \tilde{\boldsymbol{\mu}}_{k,s'}^{(l,i)}, \tilde{\boldsymbol{\Sigma}}_{k,s'}^{(l,i)})\}_{l \in \mathbb{L}_k^{(s')*}}$ from all neighboring sensors $s' \in N_s$.

3) Perform pairwise LMB fusion of sensor s with all neighboring sensors $s' \in N_s' = N_s$ according to:

   - Select LMB fusion sets as $\{(r_{k,1}^{(l)}, \boldsymbol{\mu}_{k,1}^{(l)}, \boldsymbol{\Sigma}_{k,1}^{(l)})\}_{l \in \mathbb{L}_k^{(1)*}} = \{(\tilde{r}_{k,s}^{(l,i)}, \tilde{\boldsymbol{\mu}}_{k,s}^{(l,i)}, \tilde{\boldsymbol{\Sigma}}_{k,s}^{(l,i)})\}_{l \in \mathbb{L}_k^{(s)*}}$ and $\{(r_{k,2}^{(l)}, \boldsymbol{\mu}_{k,2}^{(l)}, \boldsymbol{\Sigma}_{k,2}^{(l)})\}_{l \in \mathbb{L}_k^{(2)*}} = \{(\tilde{r}_{k,s'}^{(l,i)}, \tilde{\boldsymbol{\mu}}_{k,s'}^{(l,i)}, \tilde{\boldsymbol{\Sigma}}_{k,s'}^{(l,i)})\}_{l \in \mathbb{L}_k^{(s')*}}$ with s' randomly chosen from N_s'.

   Perform pairwise fusion of $\{(r_{k,1}^{(l)}, \boldsymbol{\mu}_{k,1}^{(l)}, \boldsymbol{\Sigma}_{k,1}^{(l)})\}_{l \in \mathbb{L}_k^{(1)*}}$ and $\{(r_{k,2}^{(l)}, \boldsymbol{\mu}_{k,2}^{(l)}, \boldsymbol{\Sigma}_{k,2}^{(l)})\}_{l \in \mathbb{L}_k^{(2)*}}$ according to:

   - For $l \in \mathbb{L}_k^{(1)*}$, calculate the label association weights $\beta_k^{(l,\bar{u}_k^{(l)})}$ according to (6.13) using (6.31) and mean $\boldsymbol{\mu}_k^{(l,\bar{u}_k^{(l)})}$ and covariance $\boldsymbol{\Sigma}_k^{(l,\bar{u}_k^{(l)})})$ parametrizing the spatial PDFs $f^{(l,\bar{u}_k^{(l)})}(\boldsymbol{x}_k)$ according to (6.29) and (6.30), respectively.
   - For $l \in \mathbb{L}_k^{(1)*}$, calculate the approximate marginal association probabilities $\tilde{p}(\bar{u}_k^{(l)})$ according to (6.27) by iteratively computing $\zeta_{k,l\to l'}^{[p]}$ according to (6.25) and $\nu_{k,l'\to l}^{[p]}$ according to (6.26) for $p = 1, ..., P$.
   - For $l \in \mathbb{L}_k^{(1)*}$, calculate the fused existence probability $r_k^{(l)}$ according to (6.20) and the fused mean $\bar{\boldsymbol{\mu}}_k^{(l)}$ and Covariance $\bar{\boldsymbol{\Sigma}}_k^{(l)}$ according to (6.32) and (6.33), respectively, with $p(\bar{u}_k^{(l)})$ replaced $\tilde{p}(\bar{u}_k^{(l)})$.
   - Remove s' from N_s', set $\{(\tilde{r}_{k,s}^{(l,i)}, \tilde{\boldsymbol{\mu}}_{k,s}^{(l,i)}, \tilde{\boldsymbol{\Sigma}}_{k,s}^{(l,i)})\}_{l \in \mathbb{L}_k^{(s)*}} = \{(r_k^{(l)}, \bar{\boldsymbol{\mu}}_k^{(l)}, \bar{\boldsymbol{\Sigma}}_k^{(l)})\}_{l \in \mathbb{L}_k^{(1)*}}$, and go back to the first bullet point unless $N_s' = \emptyset$.

4) Transmit $\{(\tilde{r}_{k,s}^{(l,i)}, \tilde{\boldsymbol{\mu}}_{k,s}^{(l,i)}, \tilde{\boldsymbol{\Sigma}}_{k,s}^{(l,i)})\}_{l \in \mathbb{L}_k^{(s)*}}$ to all neighboring sensors $s' \in N_s$ and go back to point 2) unless $i = I$.

may be used. In each iteration of the gossip algorithm, the current LMB parameter sets of randomly chosen pairs of communicating sensors are fused. This is initialized by the original local LMB parameter sets.

6.5 Numerical Study

In the following, we present a simulation study analyzing the performance of the proposed distributed LMB filter. More precisely, we describe the underlying simulation scenario in Section 6.5.1 and present the obtained results in Section 6.5.2.

6.5.1 Simulation Setup

We consider two simulation scenarios, briefly referred to as SC1 and SC2, which are inspired by [Fantacci et al., 2018] and the simulations conducted in Section 5.7. In both scenarios, the region of interest (ROI) is $[-150, 150] \times [-150, 150]$. We simulated ten (SC1) and twenty (SC2) objects during 200 time steps. The object trajectories were randomly chosen in each simulation run. The objects appear at various times before time step 40 (SC1) or 90 (SC2) and at randomly chosen positions in the area $[-50, 50] \times [-50, 50]$, and they disappear at various times after time step 150. The object states consist of two-dimensional position and velocity, i.e., $\mathsf{x}_k = [\mathsf{x}_{k,1}\ \mathsf{x}_{k,2}\ \dot{\mathsf{x}}_{k,1}\ \dot{\mathsf{x}}_{k,2}]^{\mathrm{T}}$. They evolve according to the nearly constant velocity motion model [Bar-Shalom et al., 2002, Sec. 6.3.2]

$$\mathsf{x}_k = \boldsymbol{A}\mathsf{x}_{k-1} + \boldsymbol{W}\mathsf{u}_k ,$$

where $\boldsymbol{A} \in \mathbb{R}^{4\times4}$ and $\boldsymbol{W} \in \mathbb{R}^{4\times2}$ are chosen as in [Bar-Shalom et al., 2002] and $\mathsf{u}_k \sim \mathcal{N}(\mathbf{0}, \sigma_u^2 \mathbf{I}_2)$ with $\sigma_u^2 = 10^{-3}$ is an iid sequence of 2D Gaussian random vectors. A realization of the object trajectories for SC1 is shown in Figure 6.2(a).

There are two sensors in SC1 and five in SC2. The sensor positions are $\boldsymbol{p}^{(1)} = [-50\ \ 0]^{\mathrm{T}}$ and $\boldsymbol{p}^{(2)} = [50\ \ 0]^{\mathrm{T}}$ and, in SC2, additionally $\boldsymbol{p}^{(3)} = [0\ \ 0]^{\mathrm{T}}$, $\boldsymbol{p}^{(4)} = [0\ \ 50]^{\mathrm{T}}$, and $\boldsymbol{p}^{(5)} = [0\ \ -50]^{\mathrm{T}}$. The communication links between the sensors are shown in Figure 6.2. The object-generated measurements conform to the nonlinear range-bearing measurement model

$$\mathsf{z}_k = \big[\rho(\mathsf{x}_k)\ \ \phi(\mathsf{x}_k)\big]^{\mathrm{T}} + \mathsf{v}_k .$$

Here, $\rho(\mathsf{x}_k) \triangleq \|\mathsf{x}'_k - \boldsymbol{p}^{(s)}\|$, where $\mathsf{x}'_k \triangleq [\mathsf{x}_{k,1}\ \mathsf{x}_{k,2}]^{\mathrm{T}}$ denotes the object position and $\boldsymbol{p}^{(s)} = [p_1^{(s)}\ p_2^{(s)}]^{\mathrm{T}}$ the position of sensor s, and $\phi(\boldsymbol{x}_k) \triangleq \tan^{-1}\Big(\frac{\mathsf{x}_{k,2} - p_2^{(s)}}{\mathsf{x}_{k,1} - p_1^{(s)}}\Big)$. Furthermore, v_k is iid Gaussian measurement noise with independent entries with standard deviations $\sigma_\rho = 2$ and $\sigma_\phi = 1°$. The detection probability is chosen as 0.7 on the entire ROI. The clutter measurements are distributed uniformly on the ROI (in polar coordinates), with mean number equal to 10 (SC1) or 50 (SC2).

We consider a distributed LMB filter, briefly referred to as S-DLMB, that employs the proposed fusion algorithm with probabilistic (soft) label association using the BP and

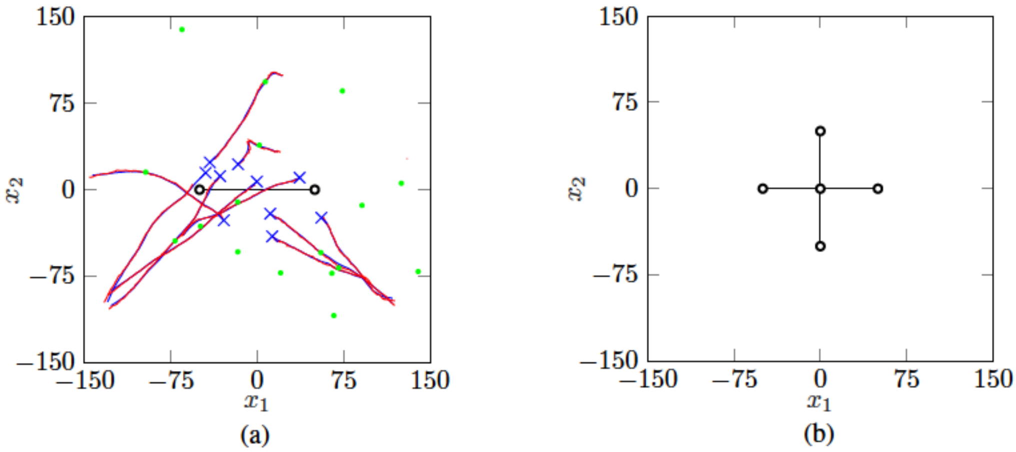

Figure 6.2: (a) Example of the object trajectories (represented by blue lines, starting positions indicated by blue crosses) in simulation scenario SC1, as well as the corresponding estimates obtained with the proposed S-DLMB filter (represented by red lines). The positions of the two sensors are indicated by black circles. The green bullets show the measurements of the second sensor at time $k = 100$. (b) Sensors and communication links in simulation scenario SC2.

Gaussian approximations described in Sections 6.3.1 and 6.3.2, respectively. For SC2 (five sensors), S-DLMB uses the iterative networkwise extension of the algorithm (described in Section 6.4) with five fusion iterations. We compare the performance of S-DLMB with that of the distributed LMB filter proposed in [Li et al., 2019], which uses GCI fusion with a hard label association algorithm and will be referred to as H-DLMB.[3] Furthermore, we also consider a centralized multisensor LMB filter, referred to as CLMB, that is based on the iterated-corrector scheme [Reuter et al., 2014, Mahler, 2014]. CLMB and the local LMB filters involved in S-DLMB and H-DLMB use a particle implementation of the fast LMB filter proposed in Chapter 4. In all filters, each spatial PDF is represented by 500 particles, and Bernoulli components with an existence probability below 10^{-3} are pruned after each filter update step. In S-DLMB and H-DLMB, the particle representation of each spatial PDF is further approximated by a Gaussian PDF after each filter update step, with the Gaussian parameters given by the sample mean and sample covariance of the particles. Then, S-DLMB executes the fusion algorithm described in Section 6.3.2 and H-DLMB the fusion algorithm described in [Li et al., 2019]. The fusion parameter ω is 0.5 in both cases. After the fusion step, 500 particles are drawn from the fused Gaussian PDF, and the local LMB filters execute the next filtering step. The threshold γ_{F} used in S-DLMB as described in Section 6.2.2, and also used in a similar way in H-DLMB, is

[3]We do not show the results of the distributed LMB filter proposed in [Fantacci et al., 2018], because the LMB fusion performed by that filter uses the same label set for all the sensors, i.e., $\mathbb{L}_k^{(s)*} = \mathbb{L}_k^*$ for all s, and always matches Bernoulli components with equal labels. This is not compatible with our label indexing system, which always describes an object by different labels at different sensors. However, we note that with any other label indexing system, too, there is a high probability that an object is described by different labels at different sensors. This will generally result in a poor tracking performance of filters matching Bernoulli components with equal labels.

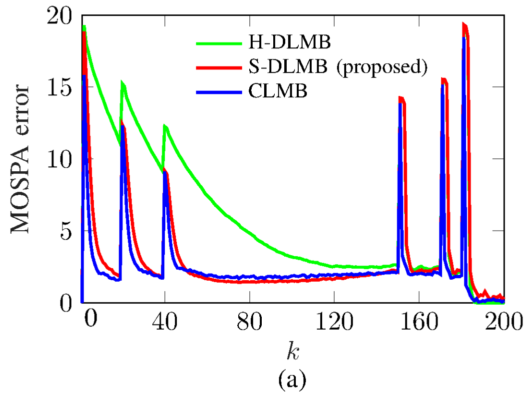

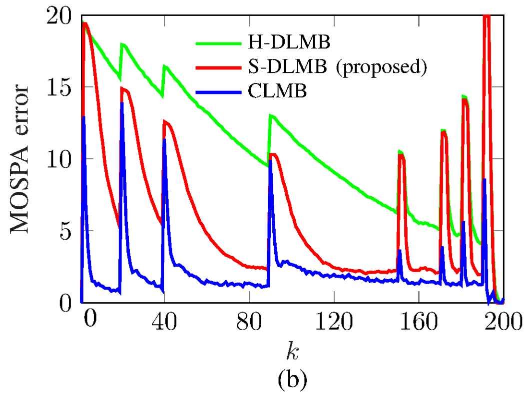

Figure 6.3: MOSPA error versus time k for (a) SC1 and (b) SC2.

Filter	SC1	SC2
S-DLMB (proposed)	0.1072 s	2.2554 s
H-DLMB	0.0470 s	0.6682 s
CLMB	0.0186 s	0.4428 s

Table 6.2: Measured average runtime per time step.

10^{-20}. The remaining simulation parameters equal those in Section 4.4.1.

6.5.2 Simulation Results

Figure 6.2(a) shows an example of the realization of the true object trajectories for SC1. Also shown are the corresponding estimated trajectories obtained with S-DLMB at the second sensor (with position $\boldsymbol{p}^{(2)} = [50 \;\; 0]^{\mathrm{T}}$); those obtained at the first sensor are similar. One can see that the estimated trajectories closely match the true trajectories.

For a quantitative assessment and comparison of the performance of the three filters, we computed the mean Euclidean distance based optimal subpattern assignment (MOSPA) metric [Schuhmacher et al., 2008] with cutoff parameter $c = 20$, order $p = 2$, and averaging over 1000 simulation runs and all the sensors. Figure 6.3 shows the results for SC1 and SC2. The peaks in Figure 6.3 correspond to object appearance and disappearance; note that several objects can appear or disappear at the same time. It is seen that S-DLMB almost always significantly outperforms H-DLMB; furthermore, it performs similarly to CLMB in SC1 and poorer than CLMB in SC2. These results show that the proposed soft label association fusion is a significant improvement over the hard label association fusion employed by H-DLMB, and the resulting LMB filter performance can come close to the performance of the centralized LMB filter based on the iterated-corrector approach.

Table 6.2 shows the average runtime per time (k) step of MATLAB implementations of S-DLMB, H-DLMB, and CLMB executed on an Intel quad core i7-6600U CPU. One can see that S-DLMB has the highest complexity, followed by H-DLMB and CLMB.

However, we note that the lower complexity of H-DLMB (compared to S-DLMB) comes at the cost of a significantly poorer MOSPA performance.

The communication requirements of S-DLMB and H-DLMB are generally similar. Indeed, for both S-DLMB and H-DLMB, in each fusion iteration, each local LMB filter broadcasts to its neighbors one set of Gaussian parameters per Bernoulli component.

Chapter 7

Conclusion

This thesis proposed three high-performing and efficient random finite set (RFS) based methods for multi-object tracking. A cornerstone of these methods is the labeled multi-Bernoulli (LMB) RFS, which is an instance of a labeled RFS. The LMB RFS inherently provides track continuity, i.e., the consistent association of the state estimates corresponding to the same object over consecutive time steps. Furthermore, the proposed methods use the framework of belief propagation (BP) for efficient probabilistic data association or label association. This methodological approach is shown experimentally to result in an attractive tracking accuracy/complexity compromise. In the following, the contributions of this thesis will be reviewed in more detail.

7.1 Summary of Contributions

Our first contribution was a new fast LMB filter using BP for probabilistic data association. The derivation of this filter was based on a new derivation of the original LMB filter in which the posterior GLMB PDF is formulated in terms of a joint object-measurement association PMF. We showed that the approximation of this PMF by the product of its marginals leads to an approximate posterior PDF that is again of LMB form. We then developed a BP-based algorithm for fast marginalization. The resulting fast LMB filter has a computational complexity that scales only linearly in the number of Bernoulli components and in the number of measurements. We also proposed an efficient scheme for generating Bernoulli components using the approximate marginal association probabilities provided by the BP algorithm. Finally, we presented a complexity analysis for the proposed fast LMB filter algorithm as well as numerical results demonstrating its excellent tracking performance in comparison to the Gibbs sampler-based LMB filter [Reuter et al., 2017] and the BP-based TOMB/P filter [Williams, 2015]. The Gibbs sampler-based LMB filter discards valuable association information through a pruning of GLMB components. This can lead to a reduced tracking performance in challenging scenarios, e.g., scenarios with many closely spaced objects and/or a low detection probability. By contrast, the proposed BP-based LMB filter does not rely on a pruning of GLMB components. The BP-based TOMB/P filter [Williams, 2015] models undetected objects by a Poisson RFS. In the considered scenarios, this resulted in an increased computational complexity but did not improve the tracking performance.

A second contribution of this thesis was an RFS-based tracking algorithm, referred to as LMB/P filter, that improves on the fast LMB filter of Chapter 4 in scenarios with a high number of objects and/or clutter measurements. In the LMB/P filter, for the first time, the multi-object state is modeled as the tuple of an LMB RFS and a Poisson RFS, i.e., as the combination of a labeled and an unlabeled RFS. After proposing a new general system model for tuples of labeled/unlabeled RFSs, we derived the prediction step and the exact update step for the LMB/Poisson tuple state model. Next, we applied several approximations and modifications to the exact update step, including the partitioning of label and measurement sets, the pruning of implausible object-measurement associations, and the transfer of certain unlabeled objects to labeled objects and vice versa. As a result, the LMB/P filter uses the LMB RFS to track objects that are likely to exist and the Poisson RFS to track objects that are unlikely to exist. The latter fact leads to a large complexity reduction, especially in challenging scenarios with a high number of objects and/or clutter measurements. Our experimental results for a challenging simulation scenario with a high number of clutter measurements demonstrated the excellent performance and low complexity of the LMB/P filter. More precisely, in comparison to the fast BP-based LMB filter of Chapter 5, the BP-based TOMB/P filter with recycling [Williams, 2012], and the Gibbs sampler-based LMB filter [Reuter et al., 2017], the BP-based implementation of the LMB/P filter achieved the lowest computational complexity, while the tracking accuracy was comparable to that of the fast BP-based LMB filter of Chapter 5 and the BP-based TOMB/P filter with recycling and significantly better than that of the Gibbs sampler-based LMB filter.

Finally, we proposed a distributed multi-sensor LMB filtering algorithm based on probabilistic label association, generalized covariance intersection (GCI), and BP. The proposed algorithm uses a soft (i.e., probabilistic) association of Bernoulli components and thereby improves on current state-of-the-art distributed LMB filters, which are based on hard label association. Especially in challenging scenarios, hard label association may associate "wrong" Bernoulli components of neighboring sensors and thus may lead to a poor tracking performance. We first derived the fused posterior PDF for the two-sensor case using GCI-based fusion with hard label association. Here, the label association was described by a label association vector that associates the labeled Bernoulli components of one sensor with those of the other sensor. Then, the fused posterior PDF based on soft label association was derived by modeling the association vector by a random vector. This PDF was found to no longer be an LMB PDF but a GLMB PDF involving an inherent label association PMF. We then showed that the approximation of the label association PMF by the product of its marginals results in an approximated posterior

PDF that is again of LMB form. Inspired by the algorithm in [Williams and Lau, 2014] and the BP algorithm for probabilistic data association used in our fast LMB filter in Chapter 4, we proposed a BP-based algorithm for fast approximate marginalization of the label association PMF. We also developed a practical implementation of our fusion algorithm with reduced computational complexity and communication requirements by using Gaussian approximations of the spatial PDFs involved in the local LMB posterior PDFs. Finally, we obtained a networkwide fusion algorithm by iteratively applying the proposed two-sensor fusion scheme between each sensor and all its neighboring sensors. Simulation experiments demonstrated the excellent performance of the proposed distributed LMB filter. More specifically, we observed that our method significantly outperforms a state-of-the-art distributed LMB filter using hard label association [Li et al., 2019] and performs similarly to the centralized multi-sensor LMB filter based on the iterated-corrector approach.

7.2 Future Research

The development of efficient and high-performing RFS-based multi-object tracking algorithms is an area of active research. In the following, we suggest some possible extensions of our work.

- The fast LMB filter proposed in Chapter 4 constitutes a single-sensor solution to the multi-object tracking problem and can be extended to the multi-sensor case. A trivial and computationally simple multi-sensor extension would be given by the iterated-corrector approach, in which the update step is executed for each sensor measurement separately and sequentially. An update step that uses all the sensor measurements jointly can be expected to lead to a higher tracking accuracy but would require the solution of a multi-dimensional association problem. We conjecture that the BP approach to probabilistic data association described in Section 4.2 can be extended to the multi-sensor case. A similar multi-sensor extension can also be envisioned for the single-sensor multi-object tracking algorithm proposed in Chapter 5.

- The distributed GCI-based LMB filter proposed in Chapter 6 is based on the fusion of two LMB posterior PDFs using probabilistic label association. On the other hand, the efficient multi-object tracking method proposed in Chapter 5 employs an LMB/Poisson posterior PDF. It would be interesting to derive a distributed LMB/Poisson multi-object tracking method by applying the GCI fusion technique combined with BP-based probabilistic label association to two LMB/Poisson posterior PDFs.

- While the GCI fusion rule corresponds to the geometric average of the involved local posterior PDFs [Üney et al., 2013], another fusion rule corresponds to the arithmetic average of the local posterior PDFs [Li et al., 2020]. Current state-of-the-art distributed LMB filters based on the arithmetic average fusion rule use a hard label association scheme [Gao et al., 2020]. We can combine our concept of soft label association proposed in Chapter 6 with the arithmetic average fusion rule in order to derive a distributed LMB filter using arithmetic average fusion with soft label association.

Appendix

In Table 7.1, we present an algorithm for constructing the partitionings (5.93) and (5.94). This algorithm is further explained in the following. In Step 1, the sets $\mathcal{M}_k(l) \subseteq \mathcal{M}_k$ comprise the indices of all those measurements whose association with the object with state $(\mathbf{x}_k, l)$ is plausible. (Note that the $\mathcal{M}_k(l)$ for different $l \in \mathbb{L}^*_{k-1}$ are not necessarily disjoint.) Then, after an initialization step in Step 2, we perform the iterative procedure constituted by Step 3, which generates label subsets $\mathbb{L}^{(c)}_{k-1} \subseteq \mathbb{L}^*_{k-1}$, $c \in \{1, \ldots, C\}$ and corresponding measurement index subsets $\mathcal{M}^{(c)}_k \subseteq \mathcal{M}_k$, $c \in \{1, \ldots, C\}$.

The generation of these subsets is done such that for each $c \in \{1, \ldots, C\}$, the association of an object state $(\mathbf{x}_k, l)$, $l \in \mathbb{L}^{(c)}_{k-1}$ with a measurement index m is plausible for $m \in \mathcal{M}^{(c)}_k$ and implausible for $m \in \mathcal{M}^{(c')}_k$ with $c' \neq c$. This is achieved by doing the following for each $l^{(j)} \in \mathbb{L}^*_{k-1}$: In Step 3.1, we determine the subset $\mathcal{C}'$ of those indices $c \in \{1, \ldots, C\}$ for which the measurement index subsets $\mathcal{M}^{(c)}_k \subseteq \mathcal{M}_k$ have some elements in common with $\mathcal{M}_k(l^{(j)})$, i.e., with the measurement indices corresponding to object state $(\mathbf{x}_k, l^{(j)})$; this expresses the fact that the association between object state $(\mathbf{x}_k, l^{(j)})$ and some measurement indices from $\bigcup_{c' \in \mathcal{C}'} \mathcal{M}^{(c')}_k$ is plausible. If none of the $\mathcal{M}^{(c)}_k$ has an element in common with $\mathcal{M}_k(l^{(j)})$, i.e., if the association between object state $(\mathbf{x}_k, l^{(j)})$ with any measurement index $m \in \bigcup_{c \in \{1,\ldots,C\}} \mathcal{M}^{(c)}_k$ is implausible, then $\mathcal{C}'$ is empty. In that case, C is incremented by 1, and a new label subset and a new measurement index subset are created as $\mathbb{L}^{(C)}_{k-1} = \{l^{(j)}\}$ and $\mathcal{M}^{(C)}_k = \mathcal{M}_k(l^{(j)})$, respectively (see Step 3.2). Otherwise, i.e., if $|\mathcal{C}'| \geq 1$, we merge all the label subsets $\mathbb{L}^{(c')}_{k-1}$ with $c' \in \mathcal{C}'$ as well as the considered label $l^{(j)}$ into one common label subset $\mathbb{L}^{(c)}_{k-1}$, and we merge all the corresponding measurement index subsets $\mathcal{M}^{(c')}_k$, $c' \in \mathcal{C}'$ as well as $\mathcal{M}_k(l^{(j)})$ into one common measurement index subset $\mathcal{M}^{(c)}_k$ (see Step 3.2, first bullet item). Here, the index c is picked arbitrarily from $\mathcal{C}'$. Next, we perform a reindexing such that the index values in $\mathcal{C}'' \triangleq (\{1, \ldots, C\} \setminus \mathcal{C}') \cup \{c\}$ become $1, 2, \ldots, |\mathcal{C}''|$. Furthermore, we update C as $C = |\mathcal{C}''|$, so that the new set of subset indices is given by $\{1, \ldots, C\}$ (see Step 3.2, second and third bullet items). Subsequently, Steps 3.1 and 3.2 are repeated for the next $l^{(j)} \in \mathbb{L}^*_{k-1}$ (if available).

The final number C of subsets $\mathbb{L}^{(c)}_{k-1}$, $c \in \{1, \ldots, C\}$ is determined by this iterative procedure. Finally, in Step 4, the measurement indices $m \in \mathcal{M}_k$ that are not part of any subset $\mathcal{M}^{(c)}_k$ are collected in $\mathcal{M}^{\text{res}}_k$. We note that a larger threshold γ_{C} used in the

Table 7.1: Algorithm for constructing the partitionings (5.93) and (5.94)

Input: Label set $\mathbb{L}^*_{k-1} = \{l^{(1)}, \ldots, l^{(|\mathbb{L}^*_{k-1}|)}\}$; measurement index set $\mathcal{M}_k$; threshold γ_C.

Output: Number of subsets C, label subsets $\mathbb{L}^{(c)}_{k-1}$, $c \in \{1, \ldots, C\}$; measurement index subsets $\mathcal{M}^{(c)}_k$, $c \in \{1, \ldots, C\}$ and $\mathcal{M}^{\mathrm{res}}_k$.

Operations:

1) For each $l \in \mathbb{L}^*_{k-1}$, determine $\mathcal{M}_k(l) \subseteq \mathcal{M}_k$ as the subset of all measurement indices $m \in \mathcal{M}_k$ for which $\beta^{(l,m)}_k \geq \gamma_C$.
2) Initialization: Set $C = 1$, $\mathbb{L}^{(1)}_{k-1} = \{l^{(1)}\}$, and $\mathcal{M}^{(1)}_k = \mathcal{M}_k(l^{(1)})$.
3) Iteration: For $j = 2, \ldots, |\mathbb{L}^*_{k-1}|$, do the following:
   - 3.1) Determine $\mathcal{C}' \subseteq \{1, \ldots, C\}$ as the set of all $c \in \{1, \ldots, C\}$ for which $\mathcal{M}^{(c)}_k \cap \mathcal{M}_k(l^{(j)}) \neq \emptyset$.
   - 3.2) If $\mathcal{C}' = \emptyset$, then increment C by one and set $\mathbb{L}^{(C)}_{k-1} = \{l^{(j)}\}$ and $\mathcal{M}^{(C)}_k = \mathcal{M}_k(l^{(j)})$; else do the following:
     - Select an arbitrary $c \in \mathcal{C}'$ and set $\mathbb{L}^{(c)}_{k-1} = \{l^{(j)}\} \cup \bigcup_{c' \in \mathcal{C}'} \mathbb{L}^{(c')}_{k-1}$ and $\mathcal{M}^{(c)}_k = \mathcal{M}_k(l^{(j)}) \cup \bigcup_{c' \in \mathcal{C}'} \mathcal{M}^{(c')}_k$.
     - Set $\mathcal{C}'' = (\{1, \ldots, C\} \setminus \mathcal{C}') \cup \{c\}$ and $C = |\mathcal{C}''|$.
     - Perform a reindexing whereby the indices contained in $\mathcal{C}''$ are replaced by the new indices $1, 2, \ldots, C$.
4) Set $\mathcal{M}^{\mathrm{res}}_k = \mathcal{M}_k \setminus \bigcup_{c \in \mathcal{C}} \mathcal{M}^{(c)}_k$.

definition of the sets $\mathcal{M}_k(l)$ in Step 1 tends to result in smaller subsets $\mathcal{M}_k(l)$, $\mathbb{L}^{(c)}_{k-1}$, and $\mathcal{M}^{(c)}_k$, a larger residual set $\mathcal{M}^{\mathrm{res}}_k$, a larger number C of subsets $\mathbb{L}^{(c)}_{k-1}$ and $\mathcal{M}^{(c)}_k$, and a higher probability of $\mathcal{C}'$ being empty.

Bibliography

[Adrian, 1991] Adrian, R. J. (1991). Particle-imaging techniques for experimental fluid mechanics. *Annu. Rev. Fluid Mech.*, 23(1):261–304.

[Anderson and Moore, 1979] Anderson, B. and Moore, J. B. (1979). *Optimal Filtering*. Prentice Hall, Englewood Cliffs, NJ.

[Arulampalam et al., 2002] Arulampalam, M. S., Maskell, S., Gordon, N., and Clapp, T. (2002). A tutorial on particle filters for online nonlinear/non-Gaussian Bayesian tracking. *IEEE Signal Process. Mag.*, 50(2):174–188.

[Bar-Shalom, 1974] Bar-Shalom, Y. (1974). Extension of the probabilistic data association filter in multi-target tracking. In *Proc. Symp. Nonlinear Estimation Theory Appl.*, San Diego, CA, USA.

[Bar-Shalom et al., 2002] Bar-Shalom, Y., Li, X.-R., and Kirubarajan, T. (2002). *Estimation with Applications to Tracking and Navigation*. Wiley, New York, NY, USA.

[Bar-Shalom et al., 2011] Bar-Shalom, Y., Willett, P. K., and Tian, X. (2011). *Tracking and Data Fusion: A Handbook of Algorithms*. Yaakov Bar-Shalom, Storrs, CT, USA.

[Bartoletti et al., 2014] Bartoletti, S., Conti, A., Giorgetti, A., and Win, M. Z. (2014). Sensor radar networks for indoor tracking. *IEEE Wireless Commun. Lett.*, 3(2):157–160.

[Battistelli et al., 2013] Battistelli, G., Chisci, L., Fantacci, C., Farina, A., and Graziano, A. (2013). Consensus CPHD filter for distributed multitarget tracking. *IEEE J. Sel. Top. Signal Process.*, 7(3):508–520.

[Battistelli et al., 2015] Battistelli, G., Chisci, L., Fantacci, C., Farina, A., and Vo, B.-N. (2015). Average Kullback-Leibler divergence for random finite sets. In *Proc. FUSION-15*, pages 1359–1366, Washington, DC, USA.

[Beard et al., 2016] Beard, M., Reuter, S., Granström, K., Vo, B.-T., Vo, B.-N., and Scheel, A. (2016). Multiple extended target tracking with labeled random finite sets. *IEEE Trans. Signal Process.*, 64(7):1638–1653.

[Blackman, 2004] Blackman, S. S. (2004). Multiple hypothesis tracking for multiple target tracking. *IEEE Trans. Aerosp. Electron. Syst.*, 19:5–18.

[Bullo et al., 2009] Bullo, F., Cortes, J., and Martinez, S. (2009). *Distributed Control of Robotic Networks: A Mathematical Approach to Motion Coordination Algorithms*. Princeton University Press, Princeton, NJ.

[Buonviri et al., 2019] Buonviri, A., York, M., LeGrand, K., and Meub, J. (2019). Survey of challenges in labeled random finite set distributed multi-sensor multi-object tracking. In *Proc. AEROCONF-19*, pages 1–12, Big Sky, MT, USA.

[Challa et al., 2011] Challa, S., Morelande, M. R., Musicki, D., and Evans, R. (2011). *Fundamentals of Object Tracking*. Cambridge University Press, Cambridge, UK.

[Clark et al., 2010] Clark, D., Julier, S., Mahler, R. P. S., and Ristić, B. (2010). Robust multi-object sensor fusion with unknown correlations. In *Proc. SSPD-10*, pages 1–5, London, UK.

[Cox and Hingorani, 1996] Cox, I. J. and Hingorani, S. L. (1996). An efficient implementation of Reid's multiple hypothesis tracking algorithm and its evaluation for the purpose of visual tracking. *IEEE Trans. Pattern Anal. Mach. Intell.*, 18(2):138–150.

[Daley and Vere-Jones, 2002] Daley, D. J. and Vere-Jones, D. (2002). *An Introduction to the Theory of Point Processes: Volume I: Elementary Theory and Methods*. Springer, New York, NY, USA.

[Daley and Vere-Jones, 2007] Daley, D. J. and Vere-Jones, D. (2007). *An Introduction to the Theory of Point Processes: Volume II: General Theory and Structure*. Springer, New York, NY, USA.

[Dimakis et al., 2010] Dimakis, A. G., Kar, S., Moura, J. M. F., Rabbat, M. G., and Scaglione, A. (2010). Gossip algorithms for distributed signal processing. *Proc. IEEE*, 98(11):1847–1864.

[Eppstein, 1998] Eppstein, D. (1998). Finding the k shortes paths. *SIAM J. Comput.*, 28(2):652 – 673.

[Fantacci et al., 2018] Fantacci, C., Vo, B.-N., Vo, B.-T., Battistelli, G., and Chisci, L. (2018). Robust fusion for multisensor multiobject tracking. *IEEE Signal Process. Lett.*, 25(5):640–644.

[Ferri et al., 2017] Ferri, G. et al. (2017). Cooperative robotic networks for underwater surveillance: An overview. *IET Radar Sonar Navig.*, 11(12):1740–1761.

[Fortmann et al., 1983] Fortmann, T. E., Bar-Shalom, Y., and Scheffe, M. (1983). Sonar tracking of multiple targets using joint probabilistic data association. *IEEE J. Ocean. Eng.*, 8(3):173–184.

[Gaglione et al., 2020] Gaglione, D., Soldi, G., Meyer, F., Hlawatsch, F., Braca, P., Farina, A., and Win, M. Z. (2020). Bayesian information fusion and multitarget tracking for maritime situational awareness. *IET Radar Sonar Navig.*, 14(12):1845–1857.

[Gao et al., 2020] Gao, L., Battistelli, G., and Chisci, L. (2020). Fusion of labeled RFS densities with minimum information loss. *IEEE Trans. Signal Process.*, 68:5855–5868.

[García-Fernández et al., 2020a] García-Fernández, Á. F., Rahmathullah, A. S., and Svensson, L. (2020a). A metric on the space of finite sets of trajectories for evaluation of multi-target tracking algorithms. *IEEE Trans. Signal Process.*, 68:3917–3928.

[García-Fernández and Svensson, 2019] García-Fernández, Á. F. and Svensson, L. (2019). Trajectory PHD and CPHD filters. *IEEE Trans. Signal Process.*, 67(22):5702–5714.

[García-Fernández et al., 2020b] García-Fernández, Á. F., Svensson, L., and Morelande, M. R. (2020b). Multiple target tracking based on sets of trajectories. *IEEE Trans. Aerosp. Electron. Syst.*, 56(3):1685–1707.

[García-Fernández and Vo, 2015] García-Fernández, Á. F. and Vo, B.-N. (2015). Derivation of the PHD and CPHD filters based on direct Kullback-Leibler divergence minimization. *IEEE Trans. Signal Process.*, 63(21):5812–5820.

[García-Fernández et al., 2018] García-Fernández, Á. F., Williams, J. L., Granström, K., and Svensson, L. (2018). Poisson multi-Bernoulli mixture filter: Direct derivation and implementation. *IEEE Trans. Aerosp. Electron. Syst.*, 54(4):1883–1901.

[Genovesio et al., 2006] Genovesio, A., Liedl, T., Emiliani, V., Parak, W. J., Coppey-Moisan, M., and Olivo-Marin, J. C. (2006). Multiple particle tracking in 3-D+t microscopy: Method and application to the tracking of endocytosed quantum dots. *IEEE Trans. Image Process.*, 15(5):1062–1070.

[Goodman et al., 1997] Goodman, I., Mahler, R. P. S., and Nguyen, H. (1997). *Mathematics of Data Fusion.* Kluwe Academic Publishers, Boston, MA, USA.

[Granström et al., 2018] Granström, K., Svensson, L., Xia, Y., Williams, J., and García-Femández, A. F. (2018). Poisson multi-Bernoulli mixture trackers: Continuity through random finite sets of trajectories. In *Proc. FUSION-18*, pages 973–981, Cambridge, UK.

[Ho and Lee, 1964] Ho, Y. and Lee, R. (1964). A Bayesian approach to problems in stochastic estimation and control. *IEEE Trans. Autom. Control*, 9(4):333–339.

[Hu et al., 2012] Hu, G., Tay, W. P., and Wen, Y. (2012). Cloud robotics: Architecture, challenges and applications. *IEEE Netw.*, 26(3):21–28.

[Jonker and A, 1987] Jonker, R. and A, V. (1987). A shortest augmenting path algorithm for dense and sparse linear assignment problems. *Comput.*, 38(11):325–340.

[Julier and Uhlmann, 2004] Julier, S. J. and Uhlmann, J. K. (2004). Unscented filtering and nonlinear estimation. *Proc. IEEE*, 92(3):401–422.

[Kalman, 1960] Kalman, R. E. (1960). A new approach to linear filtering and prediction problems. *J. Basic Eng.*, 82(1):35–45.

[Kropfreiter et al., 2016] Kropfreiter, T., Meyer, F., and Hlawatsch, F. (2016). Sequential Monte Carlo implementation of the track-oriented marginal multi-Bernoulli/Poisson filter. In *Proc. FUSION-16*, pages 972–979, Heidelberg, Germany.

[Kschischang et al., 2001] Kschischang, F. R., Frey, B. J., and Loeliger, H.-A. (2001). Factor graphs and the sum-product algorithm. *IEEE Trans. Inf. Theory*, 47(2):498–519.

[Kurien, 1990] Kurien, T. (1990). Issues in the design of practical multitarget tracking algorithms. In Bar-Shalom, Y., editor, *Multitarget-Multisensor Tracking: Advanced Applications*, pages 43–83. Artech-House, Norwood, MA.

[Levinson et al., 2011] Levinson, J. et al. (2011). Towards fully autonomous driving: Systems and algorithms. In *Proc. IEEE IV 2011*, pages 163–168, Baden-Baden, Germany.

[Li et al., 2019] Li, S., Battistelli, G., Chisci, L., Yi, W., Wang, B., and Kong, L. (2019). Computationally efficient multi-agent multi-object tracking with labeled random finite sets. *IEEE Trans. Signal Process.*, 67(1):260–275.

[Li et al., 2020] Li, T., Wang, X., Liang, Y., and Pan, Q. (2020). On arithmetic average fusion and its application for distributed multi-Bernoulli multitarget tracking. *IEEE Trans. Signal Process.*, 68:2883–2896.

[Lu et al., 2018] Lu, Q., Bar-Shalom, Y., Willett, P., Granström, K., Ben-Dov, R., and Milgrom, B. (2018). Tracking initially unresolved thrusting objects using an optical sensor. *IEEE Trans. Aerosp. Electron. Syst.*, 54(2):794–807.

[Mahler, 2003] Mahler, R. P. S. (2003). Multitarget Bayes filtering via first-order multitarget moments. *IEEE Trans. Aerosp. Electron. Syst.*, 39(4):1152–1178.

[Mahler, 2007a] Mahler, R. P. S. (2007a). PHD filters of higher order in target number. *IEEE Trans. Aerosp. Electron. Syst.*, 43(4):1523–1543.

[Mahler, 2007b] Mahler, R. P. S. (2007b). *Statistical Multisource-Multitarget Information Fusion*. Artech House, Boston, MA, USA.

[Mahler, 2014] Mahler, R. P. S. (2014). *Advances in Statistical Multisource-Multitarget Information Fusion*. Artech House, Boston, MA, USA.

[Malladi and Speyer, 1997] Malladi, D. P. and Speyer, J. L. (1997). A new approach to multiple model adaptive estimation. In *Proc. CDC-97*, volume 4, pages 3460–3467, San Diego, CA, USA.

[Maška et al., 2014] Maška, M. et al. (2014). A benchmark for comparison of cell tracking algorithms. *Bioinformatics*, 30(11):1609–1617.

[Meyer et al., 2017] Meyer, F., Braca, P., Willett, P., and Hlawatsch, F. (2017). A scalable algorithm for tracking an unknown number of targets using multiple sensors. *IEEE Trans. Signal Process.*, 65(13):3478–3493.

[Meyer et al., 2018] Meyer, F., Kropfreiter, T., Williams, J. L., Lau, R. A., Hlawatsch, F., Braca, P., and Win, M. Z. (2018). Message passing algorithms for scalable multitarget tracking. *Proc. IEEE*, 106(2):221–259.

[Morefield, 1977] Morefield, C. (1977). Application of 0-1 integer programming to multitarget tracking problems. *IEEE Trans. Autom. Control*, 22(3):302–312.

[Musicki and Evans, 2004] Musicki, D. and Evans, R. (2004). Joint integrated probabilistic data association: JIPDA. *IEEE Trans. Aerosp. Electron. Syst.*, 40(3):1093–1099.

[Musicki et al., 1994] Musicki, D., Evans, R., and Stankovic, S. (1994). Integrated probabilistic data association. *IEEE Trans. Autom. Control*, 39(6):1237–1241.

[Patole et al., 2017] Patole, S. M., Torlak, M., Wang, D., and Ali, M. (2017). Automotive radars: A review of signal processing techniques. *IEEE Signal Process. Mag.*, 34(2):22–35.

[Pattipati et al., 1992] Pattipati, K., Deb, S., Bar-Shalom, Y., and Washburn, R. (1992). A new relaxation algorithm and passive sensor data association. *IEEE Trans. Autom. Control*, 37(2):198–213.

[Rasmussen and Hager, 2001] Rasmussen, C. and Hager, G. D. (2001). Probabilistic data association methods for tracking complex visual objects. *IEEE Trans. Pattern Anal. Mach. Intell.*, 23(6):560–576.

[Reid, 1979] Reid, D. B. (1979). An algorithm for tracking multiple targets. *IEEE Trans. Autom. Control*, 24(6):843–854.

[Reuter et al., 2017] Reuter, S., Danzer, A., Stübler, M., Scheel, A., and Granström, K. (2017). A fast implementation of the labeled multi-Bernoulli filter using Gibbs sampling. In *Proc. IVS-17*, pages 765–772, Los Angeles, CA, USA.

[Reuter et al., 2014] Reuter, S., Vo, B.-T., Vo, B.-N., and Dietmayer, K. (2014). The labeled multi-Bernoulli filter. *IEEE Trans. Signal Process.*, 62(12):3246–3260.

[Ristic et al., 2013] Ristic, B., Vo, B.-T., Vo, B.-N., and Farina, A. (2013). A Tutorial on Bernoulli Filters: Theory, Implementation and Applications. *IEEE Trans. Signal Process.*, 61(13):3406–3430.

[Schuhmacher et al., 2008] Schuhmacher, D., Vo, B.-T., and Vo, B.-N. (2008). A consistent metric for performance evaluation of multi-object filters. *IEEE Trans. Signal Process.*, 56(8):3447–3457.

[Shen and Molisch, 2014] Shen, J. and Molisch, A. F. (2014). Estimating multiple target locations in multi-path environments. *IEEE Trans. Wireless Commun.*, 13(8):4547–4559.

[Svensson and Morelande, 2014] Svensson, L. and Morelande, M. (2014). Target tracking based on estimation of sets of trajectories. In *Proc. FUSION-14*, pages 1–8, Salamanca, Spain.

[Urmson et al., 2008] Urmson, C. et al. (2008). Autonomous driving in urban environments: Boss and the urban challenge. *J. Field Robot.*, 25(8):425–466.

[Vermaak et al., 2005] Vermaak, J., Godsill, S. J., and Perez, P. (2005). Monte Carlo filtering for multi target tracking and data association. *IEEE Trans. Aerosp. Electron. Syst.*, 41(1):309–332.

[Vo and Ma, 2006] Vo, B.-N. and Ma, W.-K. (2006). The gaussian mixture probability hypothesis density filter. *IEEE Trans. Signal Process.*, 54(11):4091–4104.

[Vo et al., 2015] Vo, B.-N., Mallick, M., Bar-Shalom, Y., Coraluppi, S., Osborne, R., Mahler, R., and Vo, B.-T. (2015). Multitarget tracking. In *Wiley Encyclopedia of Electrical and Electronics Engineering*. Wiley, New York, NY, USA.

[Vo et al., 2005] Vo, B.-N., Singh, S., and Doucet, A. (2005). Sequential Monte Carlo methods for multitarget filtering with random finite sets. *IEEE Trans. Aerosp. Electron. Syst.*, 41(4):1224–1245.

[Vo et al., 2017] Vo, B.-N., Vo, B.-T., and Hoang, H. G. (2017). An efficient implementation of the generalized labeled multi-Bernoulli filter. *IEEE Trans. Signal Process.*, 65(8):1975–1987.

[Vo et al., 2014] Vo, B.-N., Vo, B.-T., and Phung, D. (2014). Labeled random finite sets and the Bayes multi-target tracking filter. *IEEE Trans. Signal Process.*, 62(24):6554–6567.

[Vo and Vo, 2013] Vo, B.-T. and Vo, B.-N. (2013). Labeled random finite sets and multi-object conjugate priors. *IEEE Trans. Signal Process.*, 61(13):3460–3475.

[Vo et al., 2009] Vo, B.-T., Vo, B.-N., and Cantoni, A. (2009). The cardinality balanced multi-target multi-Bernoulli filter and its implementations. *IEEE Trans. Signal Process.*, 57(2):409–423.

[Williams, 2011] Williams, J. L. (2011). Experiments with graphical model implementations of multiple target multiple Bernoulli filters. In *Proc. IEEE ISSNIP-11*, pages 532–537, Adelaide, Australia.

[Williams, 2012] Williams, J. L. (2012). Hybrid Poisson and multi-Bernoulli filters. In *Proc. FUSION-12*, pages 1103–1110, Singapore.

[Williams, 2015] Williams, J. L. (2015). Marginal multi-Bernoulli filters: RFS derivation of MHT, JIPDA, and association-based MeMBer. *IEEE Trans. Aerosp. Electron. Syst.*, 51(3):1664–1687.

[Williams and Lau, 2014] Williams, J. L. and Lau, R. (2014). Approximate evaluation of marginal association probabilities with belief propagation. *IEEE Trans. Aerosp. Electron. Syst.*, 50(4):2942–2959.

[Williams and Lau, 2010] Williams, J. L. and Lau, R. A. (2010). Data association by loopy belief propagation. In *Proc. FUSION-10*, pages 1–8, Edinburgh, UK.

[Witrisal et al., 2016] Witrisal, K., Meissner, P., Leitinger, E., Shen, Y., Gustafson, C., Tufvesson, F., Haneda, K., Dardari, D., Molisch, A. F., Conti, A., and Win, M. Z. (2016). High-accuracy localization for assisted living: 5G systems will turn multipath channels from foe to friend. *IEEE Signal Process. Mag.*, 33(2):59–70.

[Xia et al., 2019] Xia, Á. F. G.-F. Y., Granström, K., Svensson, L., and Williams, J. L. (2019). Gaussian implementation of the multi-Bernoulli mixture filter. In *Proc. FUSION-19*, pages 1–8, Ottawa,ON, Canada.

[Xia et al., 2019] Xia, Y., Granström, K., Svensson, L., García-Femández, A. F., and Williams, J. L. (2019). Multiscan implementation of the trajectory Poisson multi-Bernouli mixture filter. *J. Adv. Inf. Fusion*, 14(2):213–235.

[Üney et al., 2013] Üney, M., Clark, D., and Julier, S. J. (2013). Distributed fusion of PHD filters via exponential mixture densities. *IEEE J. Sel. Top. Signal Process.*, 7(3):521–531.